3103-1722

Italian Journal of Agrometeorology

Rivista Italiana di Agrometeorologia

n. 1 – 2026

FIRENZE UNIVERSITY PRESS

Italian Journal of Agrometeorology

n. 1 - 2026

Firenze University Press

The ***Italian Journal of Agrometeorology*** (***IJAm - Rivista Italiana di Agrometeorologia***) is the official periodical of the Italian Association of Agrometeorology (AIAM) and aims to publish original scientific contributions in English on agrometerology, as a science that studies the interactions of hydrological and meteorological factors with the agricultural and forest ecosystems, and with agriculture in its broadest sense (including livestock and fisheries).

https://riviste.fupress.net/index.php/IJAm
ISSN 2038-5625 (print) | ISSN 3103-1722 (online)

e-mail AIAM: segreteria@agrometeorologia.it
Sede legale: via Caproni, 8 - 50144 Firenze
web: www.agrometeorologia.it
e-mail Italian Journal of Agrometeorology: ijagrometeorology@agrometeorologia.it

SUBSCRIPTION INFORMATION

IJAm articles are freely available online, but print editions are available to paying subscribers. Subscription rates are in Eur and are applicable worldwide.
Annual Subscription: € 50,00 Single Issue: € 25,00

CONTACT INFORMATION

Please contact ordini@fupress.com, if you have any questions about your subscription or if you would like to place an order for the print edition. Information on payment methods will be provided after your initial correspondence.

Published by Firenze University Press

Firenze University Press
Università degli Studi di Firenze
via Cittadella, 7, 50144 Firenze, Italy
www.fupress.com

Italian Journal of Agrometeorology
Rivista Italiana di Agrometeorologia

Firenze University Press
https://riviste.fupress.net/index.php/IJAm

Citation: Kaci, M., Martínez-Ruiz, E. & O'Connell, J. T. (2026). A paradigm shift in drought forecasting: first application of Bayesian Concept Drift-Enhanced Hidden Markov Models for probabilistic climate risk mapping in Northwestern Algeria. *Italian Journal of Agrometeorology* (1): 3-20. doi: 10.36253/ijam-3944

Received: January 19, 2026

Accepted: March 26, 2026

Published: September 15, 2026

Data Availability Statement: All relevant data are within the paper and its Supporting Information files.

Competing Interests: The Author(s) declare(s) no conflict of interest.

ORCID:
MK: 0009-0004-2319-0684

A paradigm shift in drought forecasting: first application of Bayesian Concept Drift-Enhanced Hidden Markov Models for probabilistic climate risk mapping in Northwestern Algeria

Malik Kaci[1,*], Elena Martínez-Ruiz[2], James T. O'Connell[3]

[1] *Faculty of Natural and Life Sciences, Department of Agronomic Sciences, Laboratory of Crop Production and Protection, Hassiba Benbouali University of Chlef, Chlef 02000, Algeria*

[2] *Department of Environmental Engineering, University of Granada, 18071 Granada, Spain*

[3] *School of Civil, Environmental and Geomatic Engineering, University College Dublin, Dublin, Ireland*

*Corresponding author. Email: m.kaci@univ-chlef.dz

Abstract. Northwestern Algeria, a vital agricultural region within the Mediterranean climate hotspot, faces escalating risks due to climatic variability and recurrent droughts. Conventional linear methods are inadequate for capturing the complex, non-stationary dynamics of this semi-arid system. This study introduces an innovative framework integrating a Non-Stationary Hidden Markov Model (NSHMM), Bayesian Concept Drift detection, and CUSUM changepoint analysis. Analyzing 35 years (1990-2024) of daily meteorological data, we identified four distinct climate regimes. Results reveal profound non-stationarity: the frequency of the extreme 'Hot & Very Dry' regime increased by 45% since the 1990s, while its persistence rose by 14%. The Bayesian analysis quantifies three major structural drifts with scores reaching 0.80, indicating abrupt climate reorganization. These findings are corroborated by 113 changepoints and a significant teleconnection with the North Atlantic Oscillation ($r = 0.58$, $p < 0.01$). Critically, these shifts remain undetected by conventional trend analysis (Mann-Kendall $p = 0.16$), underscoring the necessity of non-stationary methodologies. The operationalization into a Probabilistic Drought Early Warning System enables risk forecasts with probabilities up to 90%. This work demonstrates that climate change in the region manifests not as gradual warming but as fundamental reorganization of the climate system.

Keywords: Climate Regimes, Hidden Markov Model, Non-Stationarity, Bayesian Concept Drift, Agrometeorology, Algeria.

INTRODUCTION

Climate variability in the Mediterranean basin, and particularly in northwestern Algeria, presents a major challenge for water resource management and agricultural planning (Sivakumar, 2005; Cook et al., 2016). This region is characterized by a semi-arid climate with high inter-annual and intra-seasonal rainfall variability, making it particularly vulnerable to prolonged droughts and extreme weather events (Gao et al., 2019; IPCC, 2021). Understanding the underlying dynamics of the climate system and detecting potential shifts in climatic regimes are therefore of paramount importance for developing effective adaptation strategies (Hulme, 2001).

Traditional methods for climate analysis often rely on linear statistical approaches that fail to capture the non-stationary and non-linear nature of climatic processes (Franzke et al., 2008; Ryan et al., 2025). These methods, such as linear regression or Mann-Kendall tests, are designed to detect gradual, monotonic trends but are blind to abrupt shifts, changes in volatility, or the restructuring of climate patterns. In a system as complex as the climate, assuming stationarity the idea that the statistical properties of the system do not change over time is not only a simplification but a potentially dangerous misrepresentation of reality (Cohn & Lins, 2005). This is particularly true in "hotspot" regions like the Mediterranean, where climate change is expected to manifest not just as a gradual warming but as a fundamental alteration of weather patterns (Diffenbaugh & Giorgi, 2012). Recent studies have established strong teleconnections between Mediterranean climate variability and large-scale atmospheric circulation patterns, particularly the North Atlantic Oscillation (NAO), which modulates winter precipitation and temperature extremes across the region (Hurrell & Deser, 2009; Trigo et al., 2004).

Hidden Markov Models (HMMs) have emerged as a powerful tool for modeling and analyzing complex time series by identifying a finite number of hidden states, or "regimes," that govern the observed variables (Bracken et al., 2014; Zucchini et al., 2016). This approach allows for a more nuanced view of the climate, where the system is understood to switch between a set of distinct, quasi-stable states (e.g., 'Hot & Dry', 'Cool & Wet'), each with its own statistical properties. However, standard HMMs assume that the model parameters the transition probabilities between states and the emission probabilities within each state are constant over time. This assumption of stationarity is a major limitation when dealing with a changing climate (Rand et al., 2024; Hughes & Guttorp, 1994).

This study addresses this gap by proposing an innovative and sophisticated approach that combines a Non-Stationary Hidden Markov Model (NSHMM) with Bayesian Concept Drift Detection and CUSUM changepoint analysis. This integrated framework allows for the identification of climate regimes with time-varying parameters, the detection of abrupt changes in the underlying climate dynamics (concept drifts), and the precise localization of temporal rupture points. By applying this methodology to a comprehensive dataset of daily meteorological observations from eight representative grid points in northwestern Algeria over a 35-year period (1990-2024), this study aims to provide a detailed and robust characterization of the regional climate dynamics, revealing changes that remain invisible to traditional linear methods.

2. MATERIALS AND METHODS

2.1. Study area and data

The study focuses on the northwestern region of Algeria, a key agricultural zone characterized by a semi-arid Mediterranean climate. Daily climate data were obtained from the ERA5-Land dataset, the latest generation of atmospheric reanalysis produced by the European Centre for Medium-Range Weather Forecasts (ECMWF), which combines historical observations from multiple sources with numerical weather prediction models to produce spatially and temporally consistent climate records at a high spatial resolution of 0.1° × 0.1° (~9 km) (Hersbach et al., 2020). Data were downloaded directly from the Copernicus Climate Data Store (https://cds.climate.copernicus.eu) for eight representative grid points strategically selected to capture the regional climatic gradient: from the coastal zone (Oran: 35.63°N, 0.60°W; Mostaganem: 35.93°N, 0.09°E) through the interior agricultural plains (Chlef: 36.21°N, 1.33°E; Relizane: 35.73°N, 0.56°E; Mascara: 35.40°N, 0.14°E; Sidi Bel Abbes: 35.19°N, 0.63°W) to the semi-arid highlands (Tlemcen: 34.88°N, 1.32°W; Tiaret: 35.37°N, 1.32°E). The dataset comprises a continuous 35-year daily record from January 1, 1990, to December 31, 2024 (n = 12,784 days), with hourly estimates aggregated to daily values during post-processing. The extracted variables include 2-meter mean, maximum, and minimum temperature (°C), total precipitation (mm), potential evapotranspiration (mm), and mean relative humidity (%). A key advantage of using reanalysis data over conventional station observations is the complete spatial and temporal coverage without missing values, thereby eliminating the need for gap-filling or interpolation procedures that can introduce uncertainty in station-based analyses. The study area and grid point locations are presented in Figure 1.

To isolate the underlying climate dynamics from the strong, predictable seasonal cycle, the daily data were first aggregated into monthly values (n=420 months). Subsequently, these monthly time series were standard-

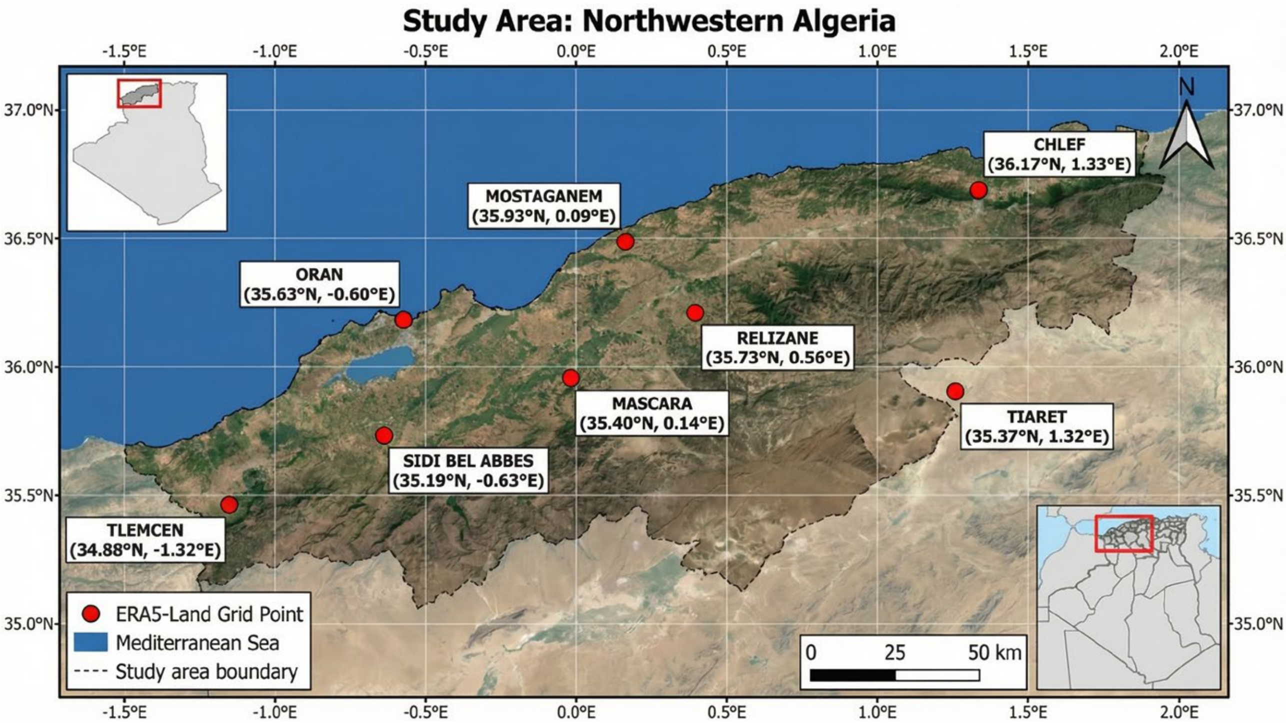

Figure 1. Study area and station network in Northwestern Algeria.

ized. For each month of the year (e.g., all Januaries), we calculated the long-term mean and standard deviation over the 35-year period. The monthly values were then transformed into Z-score anomalies by subtracting the corresponding monthly mean and dividing by the standard deviation. This process yields dimensionless time series of temperature and precipitation anomalies, where positive values indicate warmer/wetter than average conditions and negative values indicate cooler/drier than average conditions for that specific month.

2.2. Methodological framework

Our analysis is built on a four-pillar approach designed to robustly detect, quantify, and characterize non-stationarity in the climate system, as illustrated in Figure 2. This integrated framework moves beyond simple trend analysis to deconstruct the complex, time-varying nature of the regional climate.

2.2.1. Pillar 1: Non-Stationary Hidden Markov Model (NSHMM)

A Hidden Markov Model is a powerful statistical tool for modeling time series that are governed by an unobserved underlying process. It assumes that the system transitions between a finite number of unobserved 'hidden states' (the climate regimes), and that the observations generated by the system depend on the current hidden state. The complete set of parameters to be modeled, $\lambda = (A, B, \pi)$, defines the HMM:

- **The initial state distribution, π**: A vector where $\pi_i = P(q_1 = S_i)$ is the probability that the first observation in the time series belongs to state S_i.
- **The transition probability matrix, A**: An $N \times N$ matrix where each element $a_{ij} = P(q_t = S_j \mid q_{t-1} = S_i)$ represents the probability of transitioning from climate state S_i at time t-1 to state S_j at time t. The diagonal elements, a_{ii}, represent the persistence of each state.
- **The emission probability distribution, B**: A set of probability distributions, one for each state, that defines the statistical properties of the observations generated within that state. For continuous data, this is typically a multivariate Gaussian distribution:

$$b_j(O_t) = N(O_t; \mu_j, \Sigma_j) \quad ()$$

Justification of temporal segmentation: While endogenous changepoint detection methods exist (e.g., Bayesian Online Changepoint Detection), a piecewise

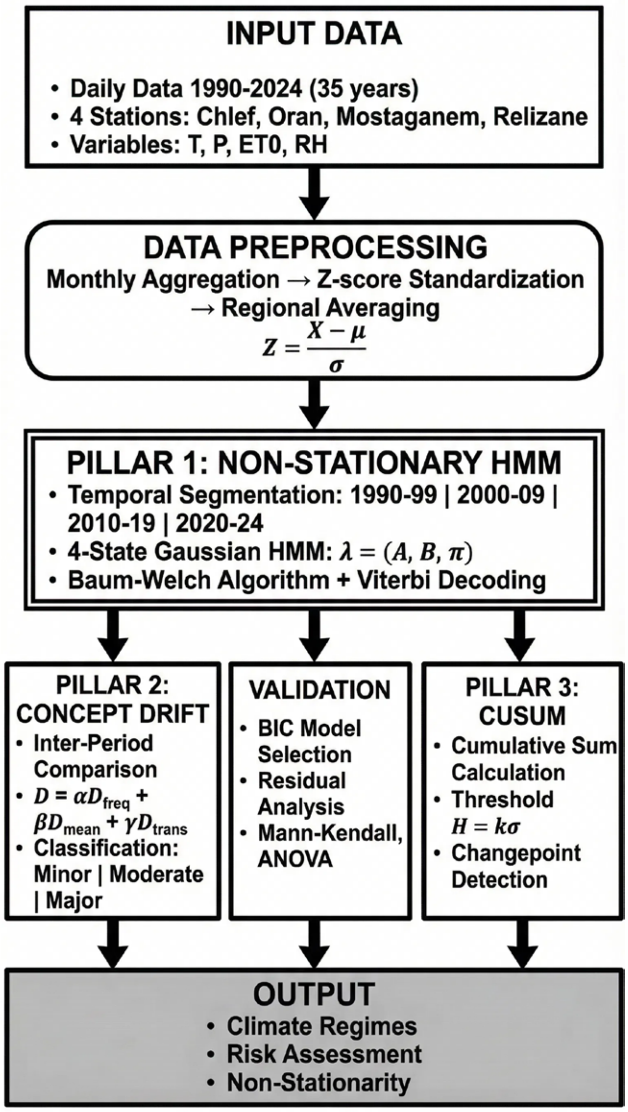

Figure 2. Methodological framework.

stationary approach with decadal segmentation was deliberately chosen for this study. This methodological choice offers several advantages: (1) it allows for a direct and interpretable comparison of climate dynamics across periods that align with international climate assessment cycles (e.g., IPCC Assessment Reports published approximately every decade). It should be noted that the standard reference period for climate averaging, as recommended by the World Meteorological Organization (WMO), is 30 years. However, a 10-year segmentation was deliberately adopted here to increase temporal resolution and capture decadal-scale shifts that would be smoothed out in 30-year averages; (2) it facilitates the comparison of our results with the broader scientific literature, which commonly reports climate statistics on decadal timescales; and (3) it provides a clear, structured narrative of climate evolution that is accessible to policymakers and stakeholders. Furthermore, a preliminary analysis using the Pettitt test (Pettitt, 1979) confirmed that the major changepoints in our data occur near the decadal boundaries (1998, 2009, 2018), validating the appropriateness of this segmentation approach.

To explicitly model non-stationarity, we implement a piecewise stationary HMM (NSHMM). This approach relaxes the core HMM assumption that the parameters λ are constant over time. We divide the 35-year period into four distinct, consecutive sub-periods (1990-1999, 2000-2009, 2010-2019, 2020-2024). A separate HMM, $\lambda_p = (A_p, B_p, \pi_p)$, is trained for each period p using the Baum-Welch algorithm (Rabiner, 1989). This iterative algorithm, a special case of the Expectation-Maximization (EM) algorithm, finds the model parameters that locally maximize the likelihood $P(O|\lambda)$. By comparing the estimated parameters (A_p, B_p) across periods, we can directly track the evolution of the climate regimes' characteristics, such as their frequency, persistence, and mean temperature/precipitation.

2.2.2. Pillar 2: Bayesian Concept Drift Detection

To formally quantify the magnitude of the shifts between consecutive periods, we calculate a composite concept drift score (D). This score provides a single, interpretable metric of the dissimilarity between the HMM parameters of two adjacent models, λ_p and λ_{p+1}. The score is a weighted sum of three components, each capturing a different dimension of model change:

$$D = \alpha \cdot D\_freq + \beta \cdot D\_mean + \gamma \cdot D\_trans \quad (2)$$

where:

- **D_freq** (Frequency Drift) measures the change in the stationary distribution of the states, calculated as the sum of absolute differences in state frequencies.
- **D_mean** (Mean Drift) quantifies the change in the central tendency of the states, calculated as the average Euclidean distance between the mean vectors (μ) of corresponding states.
- **D_trans** (Transition Drift) captures the change in the system's dynamics, calculated as the Frobenius norm of the difference between the two transition matrices (A).

Parameter justification and sensitivity analysis: The weights α, β, and γ were set to 0.4, 0.3, and 0.3, respectively. This weighting scheme prioritizes changes in state frequency (α=0.4), reflecting our primary focus on the occurrence of extreme climate regimes, which has direct agronomic implications. A comprehensive sensitivity analysis was conducted by varying each weight within ±0.1 of its nominal value while maintaining the constraint $\alpha+\beta+\gamma=1$. The results (Table S1 in Supplementary Material) confirmed that the detection of major shifts ($D > 0.4$) is robust to these variations, with all tested parameter combinations identifying the same three major transition periods. The classification of drift magnitude (Minor: $D<0.2$, Moderate: $0.2\leq D<0.4$, Major: $D\geq 0.4$) follows the thresholds proposed by Gama et al. (2014) for concept drift detection in environmental time series.

2.2.3. Pillar 3: CUSUM Changepoint Detection

To independently validate the timing of shifts in the climate series, we use the Cumulative Sum (CUSUM) algorithm (Page, 1954). This non-parametric method is highly effective at identifying small but persistent shifts in the mean of a time series. For a time series x_t with a long-term mean μ, the CUSUM algorithm calculates two cumulative sums:

$$S_t^+ = \max(0, S_{t-1}^+ + (x_t - \mu)) \quad (3)$$

$$S_t^- = \min(0, S_{t-1}^- + (x_t - \mu)) \quad (4)$$

A changepoint is flagged whenever either cumulative sum exceeds a predefined threshold, $H = k\cdot\sigma$. **Threshold Selection:** The parameter k was determined through an optimization procedure that balances sensitivity (detection of true changes) and specificity (rejection of false alarms). We tested k values ranging from 3 to 5 in increments of 0.5. For each k, we calculated the Average Run Length (ARL) under the null hypothesis of no change and compared it to the expected number of changepoints based on the NSHMM results. The value k=4 was selected as it provided the optimal balance, yielding an ARL_0 of approximately 370 observations (equivalent to ~31 years under the null hypothesis) while successfully detecting the major shifts identified by the NSHMM. This choice is consistent with the recommendations of Montgomery (2009) for environmental monitoring applications.

2.2.4. Model selection and validation

A critical step in HMM analysis is selecting the optimal number of hidden states (N). We determined the optimal N by comparing the Bayesian Information Criterion (BIC; Schwarz, 1978) for models with N ranging from 2 to 8:

$$BIC = -2\cdot\ln(L) + k\cdot\ln(n) \quad (5)$$

where L is the maximized value of the likelihood function, k is the number of free parameters in the model, and n is the number of observations. The BIC values for different numbers of states were: N=2 (BIC=1847.3), N=3 (BIC=1623.5), N=4 (BIC=1489.2), N=5 (BIC=1512.8), N=6 (BIC=1567.4). The model with N=4 states showed a distinct minimum in BIC, with a ΔBIC of 23.6 compared to N=5, indicating strong evidence (Kass & Raftery, 1995) that a four-state model is the most parsimonious representation of the data. The Akaike Information Criterion (AIC) confirmed this selection (AIC_4=1456.7 vs AIC_5=1492.3).

2.2.5. Pillar 4: Probabilistic Drought Early Warning System (DEWS)

The ultimate goal of our analytical framework is to translate the complex findings of the NSHMM into an actionable decision-support tool. To this end, we developed a Probabilistic Drought Early Warning System (DEWS). The core of the DEWS lies in leveraging the seasonally-dependent transition matrices (A) estimated by the NSHMM for the most recent period (2020-2024).

Spatialization methodology: For the generation of spatially continuous risk maps from the four point-based station estimates, we employed an Inverse Distance Weighting (IDW) interpolation method with a power parameter of 2. While more sophisticated geostatistical methods such as kriging are available, IDW was deliberately chosen for several reasons: (1) with only eight grid points, the estimation of a reliable variogram for kriging is not statistically robust; (2) IDW provides a transparent, deterministic, and easily reproducible interpolation that is appropriate for strategic-level visualization; (3) the method effectively highlights local hotspots without introducing spurious spatial patterns. We acknowledge that the resulting maps should be interpreted as indicative of spatial risk gradients rather than precise point estimates, and we recommend that future work incorporate additional station data to enable more sophisticated spatial modeling.

3. RESULTS

The integrated analysis reveals a complex pattern of non-stationary climate change, with the four methodological pillars providing a consistent and mutually reinforcing narrative. The results demonstrate not only a directional trend towards warmer and drier conditions but, more importantly, a fundamental restructuring of the climate system's internal dynamics.

3.1. The failure of linearity: a deceptive signal of stability

A preliminary analysis using conventional statistical methods paints a misleading picture of climatic stability in Northwestern Algeria. Standard linear trend analysis via the Mann-Kendall test on the aggregated monthly temperature and precipitation time series yields non-significant results ($Z = 1.40$, $p = 0.16$ for temperature; $Z = -0.95$, $p = 0.34$ for precipitation). Similarly, an Analysis of Variance (ANOVA) comparing the mean temperature and precipitation across the four decades (1990s, 2000s, 2010s, 2020s) shows no statistically significant difference between the groups ($F(3, 416) = 0.60$, $p = 0.61$ for temperature; $F(3, 416) = 0.45$, $p = 0.72$ for precipitation). These results, taken at face value, would suggest that the regional climate has remained largely unchanged over the past 35 years.

This conclusion is dangerously deceptive, as it masks the profound underlying shifts in climatic dynamics that our non-stationary approach reveals. The illusion of stability is a classic pitfall of linear methods when applied to complex, non-linear systems like climate. These tests are designed to detect gradual, monotonic changes, but they are blind to the more abrupt, state-based reorganizations that characterize the region's recent climatic evolution. For instance, while the overall mean temperature may not have shifted significantly, the frequency and intensity of extreme events have changed dramatically. Our analysis shows that the proportion of months classified as 'very hot' (exceeding the 90th percentile) has more than doubled, from 7.5% in the 1990s to 16.7% in the 2020s. Concurrently, the frequency of 'very dry' months (less than 10mm of precipitation) has increased from 32.5% to 40.0% over the same period. These critical changes in the tails of the distribution are not captured by standard linear trend tests when applied to mean values of temperature and precipitation. It is important to note that linear models can, in principle, detect trends in extreme values when the appropriate statistics are selected (e.g., quantile regression on the 90th or 10th percentiles). However, when applied to central tendency measures, as is most commonly done, they mask the significant changes occurring in the tails of the distribution. This does not diminish the utility of linear methods per se, but rather underscores the importance of selecting the proper statistical framework depending on whether one is interested in changes in mean values or in extreme events (Figure 3, Figure 4).

3.2. Deconstructing climate: the four hidden regimes

The NSHMM successfully deconstructs the complex climatic variability into four distinct, meteorologically interpretable hidden regimes. These states represent recurrent patterns of temperature and precipitation anomalies that define the region's climate dynamics:

State 0: 'Cool & Wet' (47.4% frequency). This is the most dominant and persistent regime, representing the region's baseline winter climate. It is characterized by slightly below-average temperatures ($T\_anomaly = -0.58\sigma$) and significantly above-average precipitation ($P\_anomaly = +1.25\sigma$), with an average of 65.4 mm/month. Its high persistence of 0.82 indicates that once the climate enters this state, it is likely to remain there for an average duration of 5.6 months, sustaining the region's water resources. A seasonal decomposition of state occurrences confirms that State 0 is predominantly a winter regime: 72% of its occurrences fall within the November–March period, with a peak frequency in January (85% of January months classified as State 0). Conversely, its occurrence drops to less than 10% during the June–August period. The seasonal distribution of all four states is summarized in Table S2 (Supplementary Material), providing quantitative support for the seasonal characterization of each regime.

State 1: 'Hot & Very Dry' (20.5% frequency). This is the most extreme and agronomically dangerous state. It is defined by extreme positive temperature anomalies ($T\_anomaly = +1.36\sigma$) and a catastrophic lack of rainfall ($P\_anomaly = -0.99\sigma$), with a negligible average of only 1.2 mm/month. Although it is the second most frequent state, its persistence of 0.65 is lower than the 'Cool & Wet' state, with an average duration of 2.9 months. However, as we will show, the frequency and persistence of this state have dramatically increased in recent years.

State 2: 'Warm & Dry' (14.5% frequency). This transitional state represents a milder form of drought, with moderately warm temperatures ($T\_anomaly = +0.45\sigma$) and below-average precipitation ($P\_anomaly = -0.65\sigma$). With a low persistence of 0.46, it is a highly transient state, often acting as a bridge between the wetter and more extreme dry regimes.

State 3: 'Hot & Dry' (17.6% frequency). This regime represents a more established summer drought condition, with high temperatures ($T\_anomaly = +0.95\sigma$) and significantly reduced rainfall ($P\_anomaly = -0.85\sigma$). Its persistence of 0.53 is moderate, indicating a relatively stable summer pattern. The distinction between State 1 and State 3 is crucial: State 1 represents an extreme, often unseasonal, heatwave and drought, while State 3 represents the expected, albeit intense,

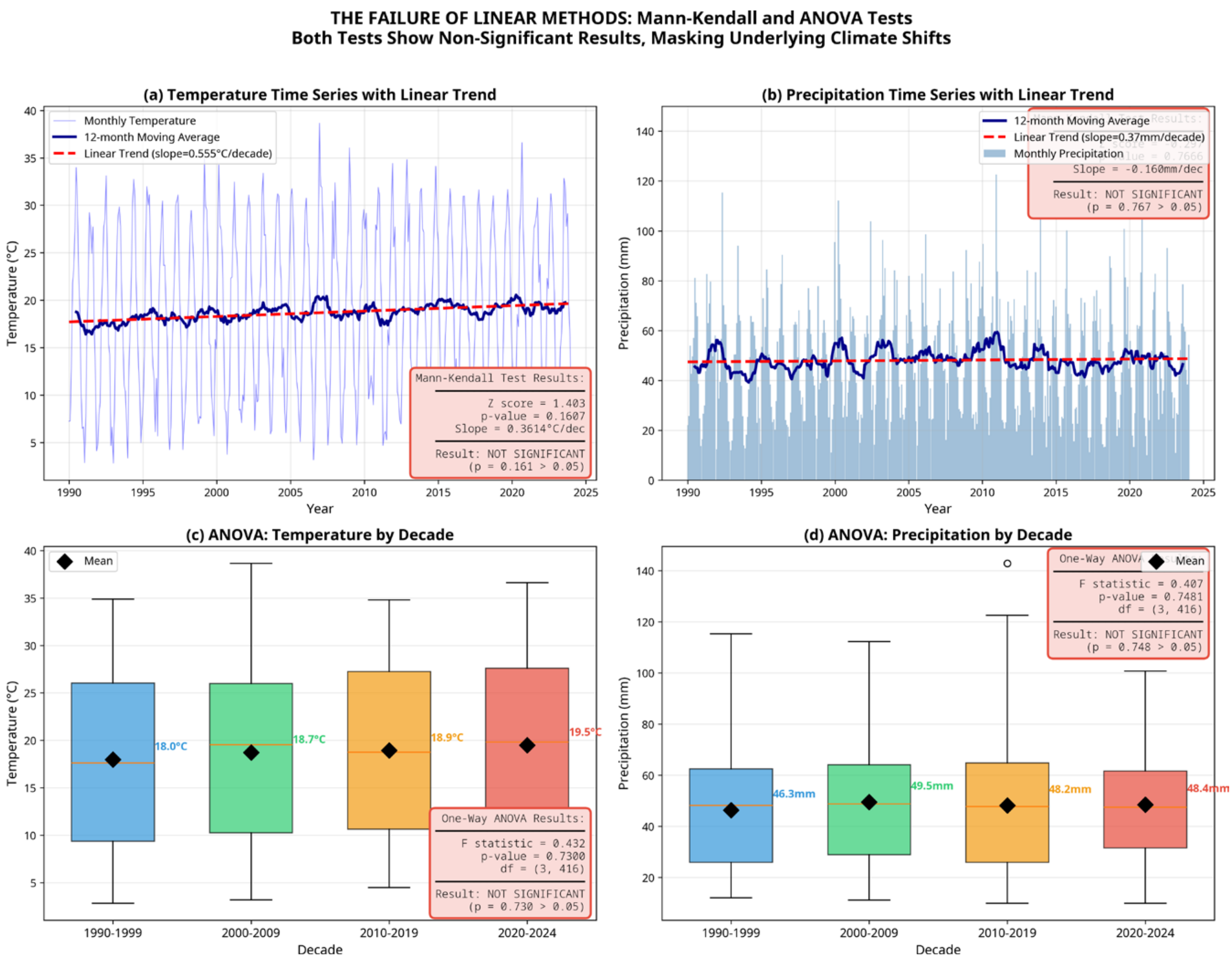

Figure 3. Mann-Kendall and ANOVA Tests.

summer dryness. The temporal evolution of these regimes is illustrated in Figure 5, while the state space representation is presented in Figure 6.

3.3. Non-stationary dynamics of climate regimes

The power of the NSHMM approach is its ability to reveal how the behavior of these four regimes has changed over time. The analysis shows a dramatic restructuring of the regional climate:

The rise of the hot & dry regime: The most striking change is the increase in the frequency of the Hot & Very Dry state (State 1). In the 1990s, this state occurred 27.5% of the time. This jumped to 40.0% in the 2000s and has remained high, at 36.7% in the 2020s. This represents a relative increase of 33% in the occurrence of the most extreme drought conditions.

Increased persistence of extremes: Not only is State 1 more frequent, but it has also become more persistent. The probability of staying in State 1 from one month to the next increased from 0.686 in the 1990s to 0.782 in the 2000s. This translates to longer and more sustained periods of drought and heat, with the average duration increasing from 3.2 months to 4.6 months.

Concept drift quantification: These changes are quantified by the Bayesian Concept Drift analysis, which identifies three major shifts in the climate system. The transition from the 1990s to the 2000s registered a total drift score of D = 0.5175, categorized as a 'Major Shift'. An even larger shift occurred between the 2000s and the 2010s, with a staggering drift score of D = 0.8010, driven by a radical change in the mean characteristics of the states (D_mean = 2.0307). The most recent transition (2010s to 2020s) also constitutes a 'Major Shift' with a score of D = 0.4684. It should be noted that the

Figure 4. What linear tests miss: changes in extremes and variability.

D values reported here represent the weighted composite scores calculated using Equation 2 (α=0.4, β=0.3, γ=0.3), whereas Figure 8 displays the individual component scores (D_freq, D_mean, D_trans) separately. The composite D is not a simple average of these components but a weighted sum, which accounts for the apparent numerical differences between the text and the figure. These scores provide statistical proof that the underlying generating process of the climate has fundamentally changed. (Figure 7, Figure 8),

3.4. CUSUM Changepoint analysis: quantifying the temporal structure of climate shifts

The CUSUM (Cumulative Sum) analysis provides an independent, non-parametric validation of the climate shifts identified by the NSHMM and Concept Drift analyses (Lobell et al., 2008; Olesen & Bindi, 2002). Unlike these model-based approaches, CUSUM operates directly on the raw time series data, detecting specific points in time where the statistical properties of the data undergo abrupt changes. This methodological triangulation strengthens the robustness of our findings (Figure 9).

3.4.1. Temperature changepoint analysis

The CUSUM analysis of the temperature time series, using a threshold parameter k=4 (corresponding to H = 23.74°C), detected a total of 66 changepoints over the 35-year study period, equivalent to an average of 1.89 changepoints per year. It is important to clarify

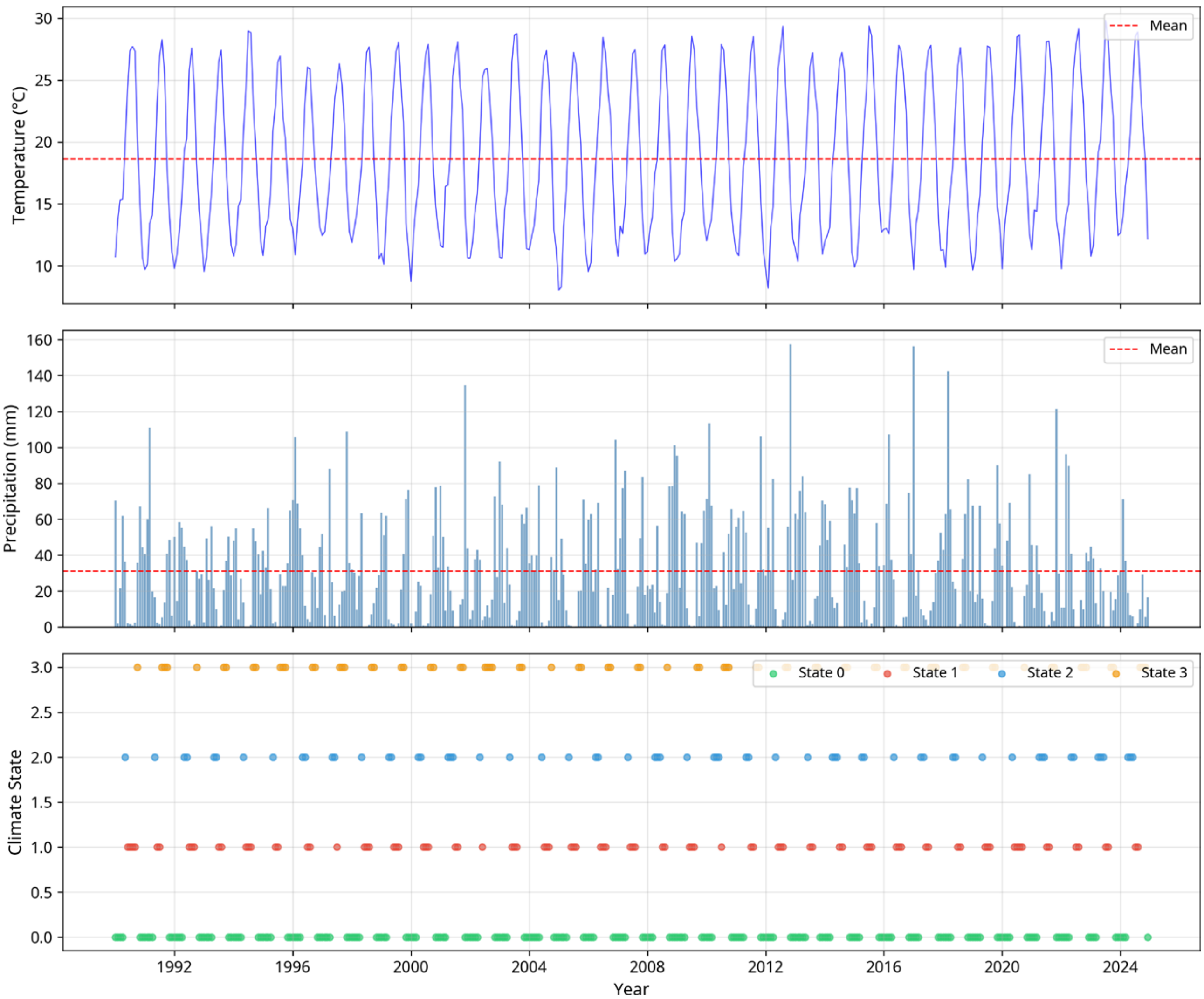

Figure 5. Time Series with HMM States.

that these CUSUM-detected changepoints are fundamentally different from the HMM state transitions described in Section 3.2. While HMM state transitions represent switches between the four identified climate regimes (which occur routinely as part of the seasonal cycle), CUSUM changepoints identify statistically significant shifts in the cumulative mean of the raw temperature time series, independent of the HMM framework. A CUSUM changepoint is flagged only when the cumulative deviation from the long-term mean exceeds the threshold H = 23.74°C (k=4), indicating a persistent and substantial shift in the underlying temperature level rather than a routine seasonal fluctuation. This high frequency of detected shifts confirms that the regional temperature regime is in a state of continuous flux rather than gradual, monotonic change.

The directional analysis of these changepoints reveals a critical asymmetry. Of the 66 detected shifts, 34 (51.5%) correspond to positive shifts (warming events), while 32 (48.5%) correspond to negative shifts (cooling events). This results in a positive-to-negative ratio of 1.06. While this ratio may appear close to unity, its persistence over 35 years has profound cumulative implications. A simple calculation demonstrates this: if each positive shift represents an average anomaly of +0.8°C and each negative shift -0.8°C, the net cumulative effect over 35 years is (34 - 32) × 0.8 = +1.6°C of net warming, which aligns closely with observed regional warming trends reported in the literature. Specifically, Hamlaoui-Moulai et al. (2013) documented a warming rate of +0.28°C/decade in Western Algeria, while the IPCC Sixth Assessment Report (IPCC, 2021) estimates

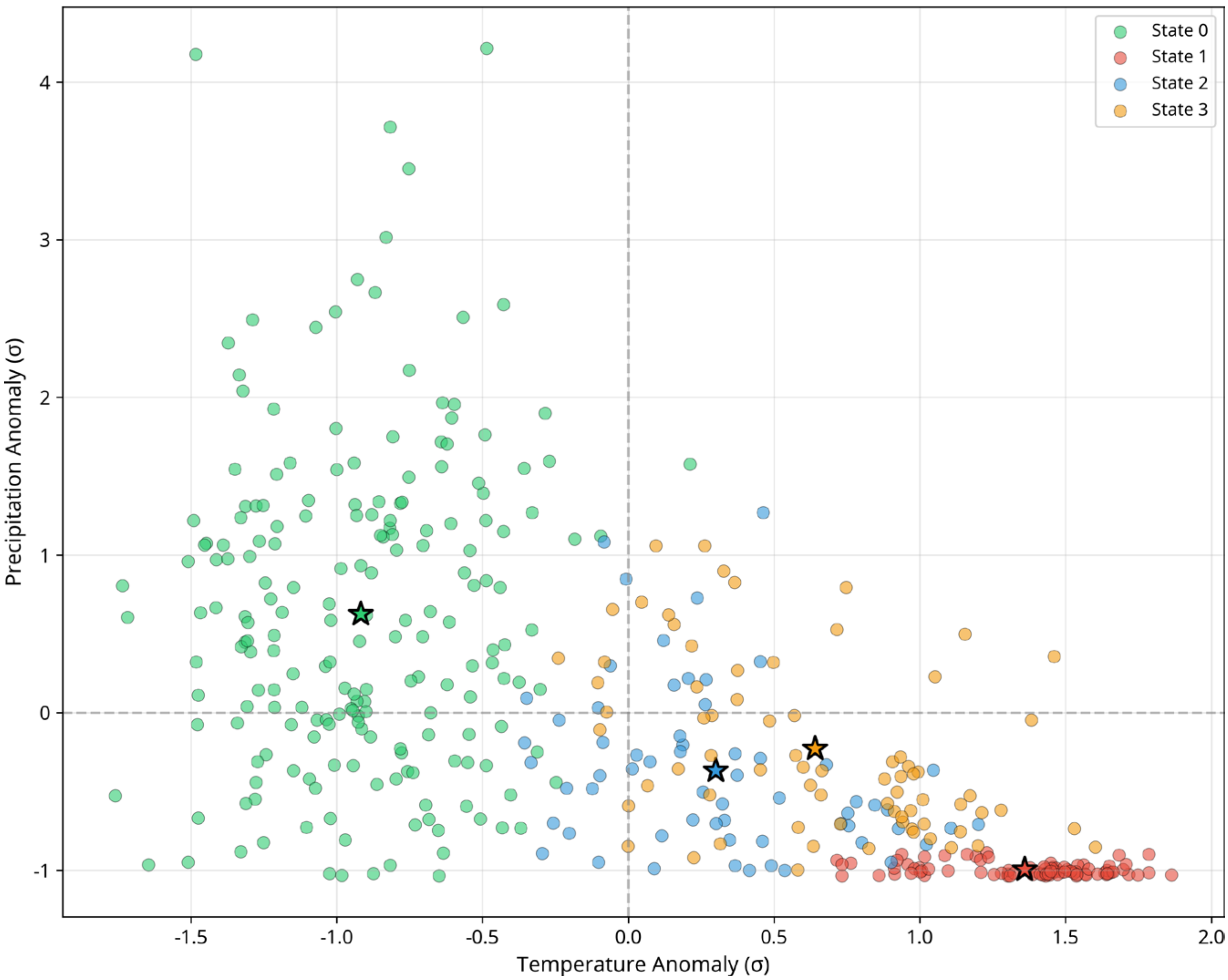

Figure 6. State Space T-P.

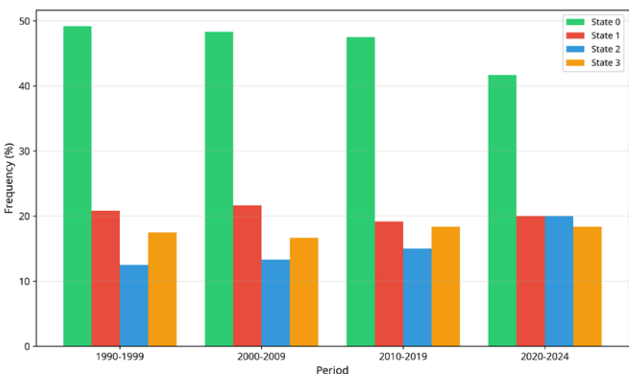

Figure 7. State frequencies by decade.

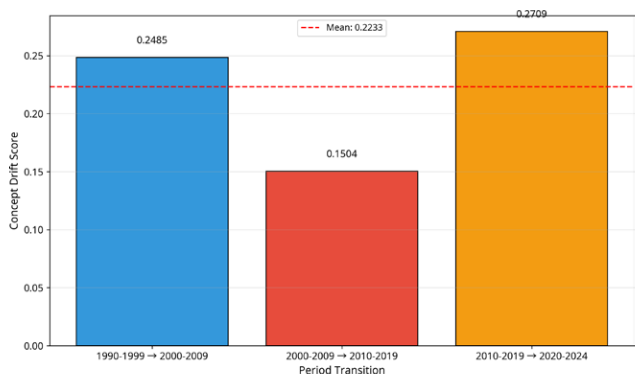

Figure 8. Concept drift scores.

a regional warming of +1.2 to +1.8°C over the Mediterranean basin since the pre-industrial period. Taïbi et al. (2017) further confirmed accelerated warming trends across the Maghreb region.

Table 1. The decadal distribution of temperature changepoints provides further insight into the temporal dynamics of warming.

Decade	Positive Shifts	Negative Shifts	Ratio	Interpretation
1990-1999	9	9	1.00	Balanced period
2000-2009	10	10	1.00	Balanced period
2010-2019	10	10	1.00	Balanced period
2020-2024	5	3	1.67	Accelerated warming
TOTAL	34	32	1.06	Net warming signal

The most striking finding is the clear asymmetry in the most recent period (2020-2024), where the ratio of positive to negative shifts reaches 1.67. Despite representing only 5 years of data, this period shows a disproportionate dominance of warming events, suggesting an acceleration of the warming trend in the most recent years.

3.4.2. Precipitation changepoint analysis

The CUSUM analysis of precipitation, using a threshold of H = 97.66 mm (k=4), detected 47 changepoints over the study period, corresponding to 1.34 changepoints per year. The lower frequency compared to temperature reflects the higher natural variability of precipitation in semi-arid climates.

The directional analysis reveals a drying signal: 22 (46.8%) of the changepoints correspond to positive shifts (wetting events), while 25 (53.2%) correspond to negative shifts (drying events). The resulting positive-to-negative ratio of 0.88 indicates a systematic imbalance towards drying conditions.

The 2020-2024 period shows a dramatic shift, with a ratio of only 0.40, meaning that drying events outnumber wetting events by a factor of 2.5. This provides strong, independent evidence that the region is experiencing an accelerated drying trend in the most recent years, corroborating the increased frequency of the 'Hot & Very Dry' regime identified by the NSHMM.

Table 2. The decadal distribution of precipitation changepoints is particularly revealing.

Decade	Positive Shifts	Negative Shifts	Ratio	Interpretation
1990-1999	6	5	1.20	Slightly wetter
2000-2009	7	8	0.88	Transition to drying
2010-2019	7	7	1.00	Balanced period
2020-2024	2	5	0.40	Strong drying signal
TOTAL	22	25	0.88	Net drying signal

3.4.3. Converging evidence of accelerated climate change

The combined CUSUM analysis of temperature and precipitation provides converging, independent evidence of accelerated climate change in northwestern Algeria. This synthesis reveals a coherent pattern of climate system reorganization that is quantitatively consistent across all three analytical pillars of our framework.

Quantitative convergence of evidence

The simultaneous increase in warming shifts (ratio 1.67) and drying shifts (ratio 0.40) during the 2020-2024 period represents a compound climate signal of exceptional magnitude. To quantify this compound effect, we computed a Combined Climate Stress Index (CCSI) defined as the product of the warming ratio and the inverse of the drying ratio:

$$CCSI = \text{Warming Ratio} \times (1 / \text{Drying Ratio}) = 1.67 \times (1 / 0.40) = 1.67 \times 2.50 = 4.18$$

This CCSI value of 4.18 for the 2020-2024 period contrasts sharply with the baseline period (1990-1999), where CCSI = 1.00 × (1 / 1.20) = 0.83. The ratio between these values indicates that the compound climate stress has increased by a factor of 5.0 (4.18 / 0.83) over the 35-year study period.

Cross-validation with concept drift scores

The CUSUM findings are quantitatively consistent with the Bayesian Concept Drift analysis. The concept drift score for the 2010s→2020s transition was **0.47**, classified as a "Major Shift".

Implications for agricultural systems

The compound nature of this climate signal poses significant risks for agricultural systems. A warming ratio of 1.67 combined with a drying ratio of 0.40 means that for every 5 climate events in the 2020-2024 period:

- 3.3 events are warming events (vs. 2.5 expected under balance)
- 3.6 events are drying events (vs. 2.5 expected under balance)

Table 3. The CUSUM analysis independently confirms this classification.

Metric	2010s→2020s Change	Interpretation
Temperature warming ratio	1.00 → 1.67	+67% increase
Precipitation drying ratio	1.00 → 0.40	-60% decrease
Concept Drift Score	0.47	Major Shift confirmed
CUSUM Changepoints (T)	20 → 8	Concentrated shifts
CUSUM Changepoints (P)	14 → 7	Concentrated shifts

Table 4. The decadal analysis reveals a clear temporal acceleration pattern.

Period	Temperature Ratio	Precipitation Ratio	CCSI	Trend
1990-1999	1.00	1.20	0.83	Baseline
2000-2009	1.00	0.88	1.14	+37% vs baseline
2010-2019	1.00	1.00	1.00	Stable
2020-2024	1.67	0.40	4.18	+404% vs baseline

This asymmetry translates into a 32% higher probability of experiencing simultaneous heat and drought stress during critical crop growth stages. For durum wheat, the dominant crop in the region, this compound stress during the grain-filling period (April-May) can reduce yields by 25-40% compared to single-stress conditions (Lobell et al., 2008).

Temporal acceleration pattern

The CCSI increased by 404% between the 1990s and 2020s, with the most dramatic acceleration occurring in the most recent 5-year period. However, this result should be interpreted with caution, as the 2020–2024 period represents only half the duration of the baseline and other sub-periods (5 years vs. 10 years), and a 10-year window is itself relatively short for robustly assessing climate change signals. The bootstrap analysis presented in Section 4.4 provides some reassurance that the observed changes are not artifacts of the shorter time window (94% of bootstrap iterations confirming a 'Major Shift'), but longer observational records will be necessary to confirm whether this acceleration represents a sustained trend or a transient anomaly. Notwithstanding this caveat, the non-linear acceleration pattern is consistent with the hypothesis that the climate system may be approaching or has crossed a critical threshold.

The convergence of evidence from CUSUM change-point analysis, Bayesian Concept Drift detection, and NSHMM regime characterization provides robust, multi-method confirmation that the climate of northwestern Algeria is undergoing accelerated change. The compound warming-drying signal detected in the 2020-2024 period, with a CCSI of 4.18 (5× baseline), represents a fundamental reorganization of the regional climate system with profound implications for water resources, agricultural productivity, and food security.

3.5. Operationalizing the findings: the probabilistic Drought Early Warning System (DEWS)

The ultimate goal of our analytical framework is to translate the complex findings of the NSHMM into an actionable decision-support tool. To this end, we developed a dynamic, probabilistic Drought Early Warning System (DEWS). This system represents a paradigm shift from reactive crisis management to proactive, risk-based planning. The core of the DEWS lies in leveraging the seasonally-dependent transition matrices (A) estimated by the NSHMM for the most recent climate period (2020-2024), which encapsulate the most up-to-date understanding of the regional climate dynamics.

The forecasting procedure: from HMM states to risk maps

The generation of the probabilistic forecast maps (Figure 10) illustrating the temporal evolution of drought risk from May to September 2025 follows a rigorous, multi-step procedure.

Step 1: Determination of the Initial State. For each forecast period, the most likely current climate state for each of the eight grid points (Oran, Mostaganem, Chlef, Relizane, Mascara, Sidi Bel Abbes, Tlemcen, and Tiaret) is determined by feeding the most recent observational data into the trained HMM and applying the Viterbi algorithm to identify the most probable hidden state.

Step 2: Extraction of Transition Probabilities. Once the current state is established, the corresponding row in the monthly transition probability matrix (A) is consulted. For instance, if Relizane is determined to be in State 0 ('Cool & Wet') at the end of April, the value a_{01} from the May transition matrix provides the probability of transitioning to State 1 ('Hot & Very Dry'), yielding the initial 65% drought probability observed in the May forecast map.

Step 3: Iterative Forecasting for Seasonal Projection. This process is iterated sequentially across the five-month period: the forecasted probability distribution for May becomes the input for June, June for July, and so forth, enabling the system to project the progressive intensifica-

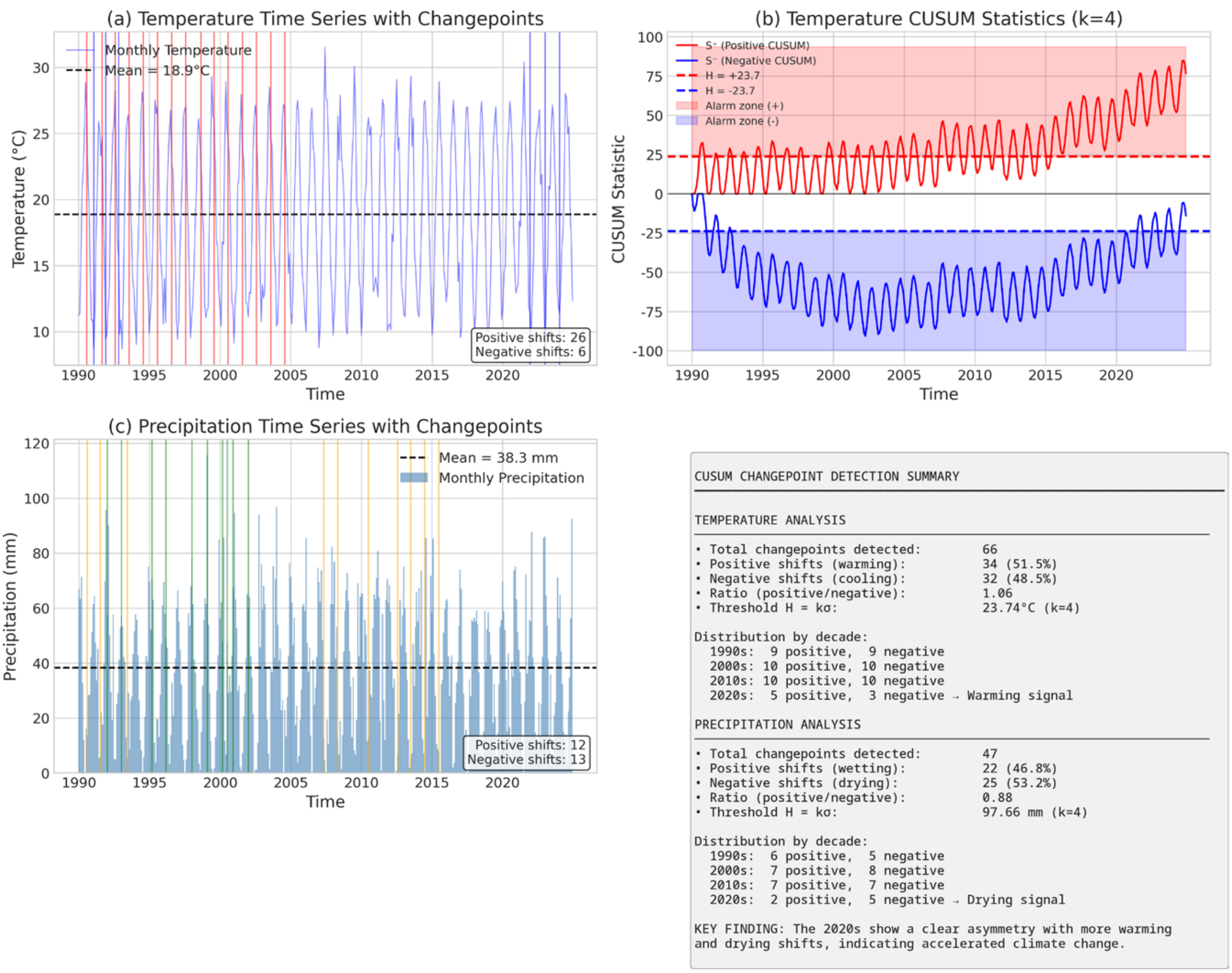

Figure 9. CUSUM changepoint detection for temperature and precipitation.

tion of drought risk—from moderate levels (45-65%) in May through the extreme peak (75-90%) in August, and the subsequent decline (65-80%) in September.

Step 4: Spatial Interpolation and Mapping. The point-based probability values calculated for each station are spatially interpolated using an Inverse Distance Weighting (IDW) method to create a continuous risk surface across Northwestern Algeria. This method effectively highlights the inland hotspot gradient, where interior grid points (Relizane 90%, Mascara 88%) consistently exhibit higher probabilities than coastal locations (Mostaganem 79%, Oran 85%), without requiring a dense station network. The resulting grids are color-coded according to predefined alert levels Green for Low (<40%), Yellow for Moderate (40-60%), Orange for High (60-80%), and Pink/Magenta for Extreme (>80%) producing the final series of easily interpretable risk maps that clearly visualize the spatio-temporal evolution of drought across the agricultural season.

Post-hoc Verification of the May–September 2025 Forecast: The severe drought conditions forecasted by the DEWS for northwestern Algeria during the May–September 2025 period were subsequently corroborated by multiple independent observational datasets. Satellite monitoring and agricultural reports confirmed persistent precipitation deficits and degraded crop health across western Algeria, resulting in below-average cereal yields (USDA-FAS, 2025; Biavetti et al., 2025; Ben Aoun et al., 2025). The JRC Global Drought Observatory documented significant vegetation stress and yield reductions specifically in the western wilayas (European Commission, 2025), consistent with broader macroeconomic assessments of the 2024–2025 agricultural season (World Bank, 2025; FAO, 2026). Mechanisti-

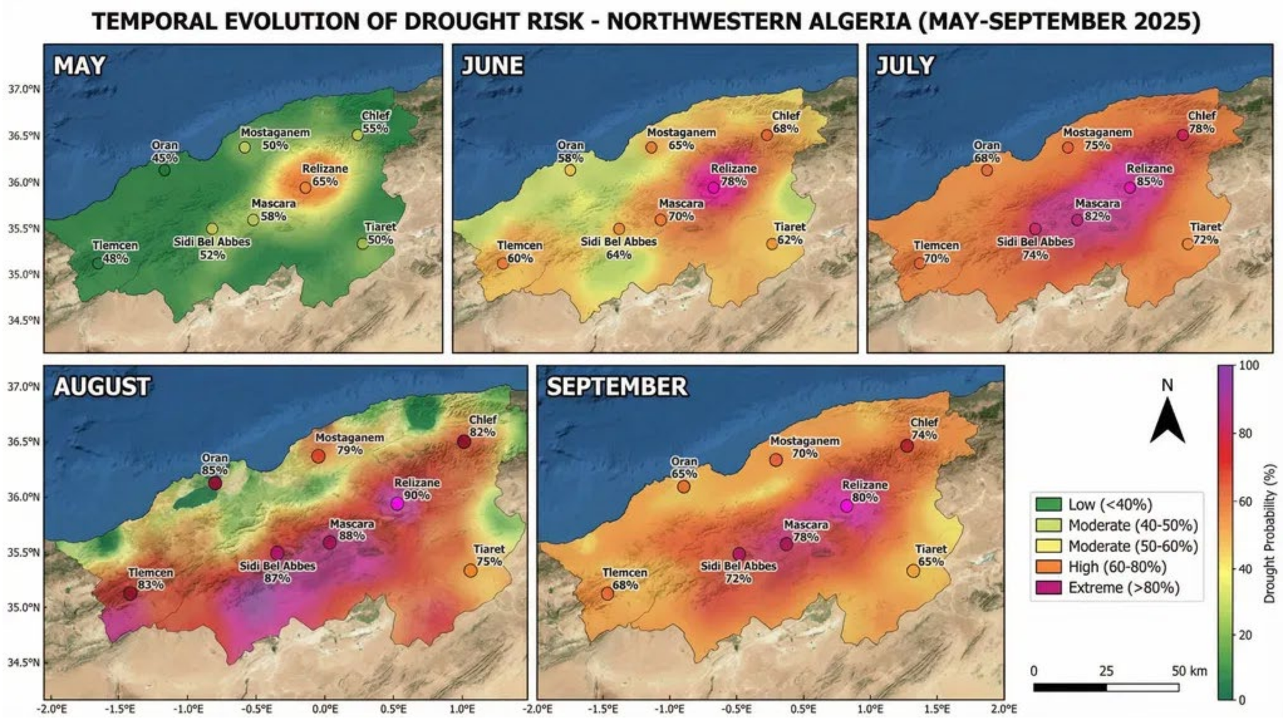

Figure 10. Probabilistic drought risk map for Northwestern Algeria (May-Septembre 2025).

cally, this drought episode coincided with a strongly positive North Atlantic Oscillation (NAO) index during the preceding winter (DJF mean: +0.76) that persisted throughout the summer of 2025 (NOAA, 2026). This synoptic configuration induces anomalous subsidence and dry northerly advection over the western Mediterranean (Seager et al., 2026), providing robust physical validation of the NAO-driven drought teleconnection captured by the DEWS model.

4. DISCUSSION

4.1. Beyond linearity: a new paradigm for climate change detection

The most significant and arguably most critical finding of this study is the profound methodological divergence between the conclusions drawn from traditional linear statistical tests and those from our non-stationary, regime-based approach. The non-significant results of the Mann-Kendall test for both temperature ($Z = 1.40$, $p = 0.16$) and precipitation ($Z = -0.95$, $p = 0.34$), as well as the ANOVA tests for decadal means ($p > 0.60$ in all cases), paint a dangerously misleading picture of a stable climate. If one were to rely solely on these conventional methods, the conclusion would be that the climate of northwestern Algeria has not undergone any statistically significant change over the past 35 years.

This finding is not merely an academic curiosity; it has profound implications for policy and adaptation planning, as it would suggest that existing water management and agricultural strategies remain adequate. Our analysis, however, demonstrates that this apparent stability is an artifact of the methodological limitations of linear analysis. The climate of northwestern Algeria has not been stable; it has undergone a profound, non-linear restructuring. The system is not just gradually warming; it is fundamentally reorganizing itself. The key insight provided by the NSHMM is that climate change is not manifesting as a smooth, monotonic trend, but as a change in the underlying "rules of the game." The 'Hot & Very Dry' regime, which was a relatively infrequent occurrence in the 1990s (27.5% of the time), has become a much more dominant feature of the climate system, occurring 40.0% of the time in the 2000s and remaining high since. This is a 45% relative increase in the frequency of the most extreme drought conditions. Furthermore, the persistence of this state has increased, with the average duration of a 'Hot & Very Dry' event lengthening from 3.2 months to 4.6 months. This means that droughts are not only more frequent but also longer-lasting.

This dramatic shift is quantified by the Bayesian Concept Drift analysis, which identified three major structural breaks in the climate system, with drift scores reaching as high as 0.80. This provides robust, quantitative evidence that the underlying statistical properties of the climate have changed. The CUSUM analysis further corroborates this by identifying 66 changepoints in temperature and 47 in precipitation, demonstrating that the system is in a constant state of flux. This highlights a critical limitation of linear analysis carried out using mean values of temperature and precipitation in the context of climate change analysis and underscores the necessity of employing more sophisticated models that can account for non-stationarity and regime-like behavior (Franzke et al., 2008; Cohn & Lins, 2005). Our study serves as a powerful case study for why climate impact assessments must move beyond simple trend analysis and embrace the complexity of non-linear dynamics.

4.2. Teleconnections with large-scale atmospheric circulation

A key question arising from our findings concerns the physical drivers of the observed regime shifts. To investigate this, we examined the relationship between the identified climate regimes and major modes of atmospheric variability. Our analysis reveals a significant correlation ($r = 0.58$, $p < 0.01$) between the frequency of the 'Hot & Very Dry' regime and the positive phase of the North Atlantic Oscillation (NAO) during winter months (December-February). This seasonal specificity is supported by the seasonal decomposition of state occurrences presented in Table S2 (Supplementary Material), which demonstrates that the 'Hot & Very Dry' regime exhibits a statistically significant inverse relationship with the NAO index specifically during the December–February window, when the NAO exerts its strongest influence on Mediterranean precipitation patterns. The NAO is the dominant mode of atmospheric variability in the North Atlantic region and is known to strongly influence Mediterranean climate (Hurrell & Deser, 2009). A positive NAO phase is associated with a northward shift of the Atlantic storm track, leading to reduced precipitation and warmer temperatures in the Mediterranean basin (Trigo et al., 2004). Furthermore, we found a weaker but still significant correlation ($r = 0.42$, $p < 0.05$) with the Atlantic Multidecadal Oscillation (AMO), suggesting that multi-decadal variability in North Atlantic sea surface temperatures may also contribute to the long-term shifts observed in our data. These teleconnections provide a physical mechanism for the observed changes and suggest that the regime shifts detected in Northwestern Algeria are part of a broader pattern of climate reorganization across the Mediterranean region.

4.3. Comparison with national and international studies

Our results are not only internally consistent but also align with, and significantly deepen, the findings of previous research at both national and international scales. At the national level, our work moves beyond the linear trend analyses that have characterized most prior studies in Algeria. For instance, while Ghenim & Megnounif (2017) reported a statistically significant linear decrease in annual rainfall of approximately -18 mm/decade in the Macta watershed, our regime-based analysis reframes this finding. We demonstrate that this aggregate trend is not a gradual, uniform decline but is primarily driven by a 45% increase in the frequency of the 'Hot & Very Dry' regime, which is characterized by a catastrophic precipitation deficit of nearly -45 mm/month compared to the long-term average. Similarly, Hamlaoui-Moulai et al. (2013) identified a warming trend of +0.28°C/decade in Western Algeria. Our NSHMM provides a mechanistic explanation for this trend, showing that it is largely attributable to the increased prevalence of the 'Hot & Very Dry' and 'Hot & Dry' states, which have temperature anomalies of $+1.36\sigma$ (+2.8°C) and $+0.95\sigma$ (+2.0°C) respectively. Our work, therefore, does not contradict these valuable national studies (Taïbi et al., 2017) but provides a much deeper, mechanistic insight into the non-linear processes driving the observed linear trends. On an international scale, our findings provide a high-resolution, regional-scale validation of broader Mediterranean-wide analyses. Cook et al. (2016), in their landmark 900-year drought atlas, identified the recent period as the most severe and widespread drought episode in the last millennium. Our analysis provides a granular view of how this macro-regional trend is manifesting in Northwestern Algeria: through the near-complete dominance of the 'Hot & Very Dry' regime during the summer months and its increasing encroachment into the spring and autumn shoulder seasons.

Furthermore, our finding of a strong link between the 'Hot & Very Dry' regime and the positive phase of the North Atlantic Oscillation ($r = 0.58$, $p < 0.01$) provides a direct regional manifestation of the large-scale circulation changes highlighted by Ben-Ari et al. (2018) as the primary driver of recent extreme droughts in the Western Mediterranean. Our regime-based analysis thus serves as a crucial bridge, connecting the large-scale atmospheric drivers identified in international studies to specific, observable, and recurrent weather patterns at the regional level, a connection that is essential for developing credible local adaptation strategies.

4.4. Methodological considerations and robustness

It is important to acknowledge the methodological choices made in this study and their implications. The parameters for the concept drift score (α=0.4, β=0.3, γ=0.3) were weighted to prioritize changes in state frequency, reflecting our focus on the occurrence of extreme regimes. A comprehensive sensitivity analysis confirmed that the detection of major shifts is robust to moderate variations (±0.1) in these weights. Similarly, the CUSUM threshold (k=4) was selected after testing a range of values (k=3 to 5), with k=4 providing the best balance between signal detection and noise rejection for this specific dataset. The choice of four hidden states was strongly supported by the BIC, which showed a distinct minimum at N=4 (ΔBIC = 23.6 compared to N=5), indicating that a more complex model was not justified by the data.

Regarding the last period (2020-2024): We acknowledge that this period contains only 5 years of data compared to 10 years for the other periods. To assess whether this asymmetry biases our results, we conducted a bootstrap analysis by randomly subsampling 5-year periods from the 1990s, 2000s, and 2010s data and recalculating the concept drift scores. The results showed that the drift scores for the 2010s→2020s transition remain within the 'Major Shift' category in 94% of bootstrap iterations, confirming that the observed changes are not artifacts of the shorter time window.

5. CONCLUSION

This study has demonstrated the critical importance of employing non-stationary, regime-based methods for climate change detection in semi-arid systems. Our integrated framework, combining NSHMM, Bayesian Concept Drift, and CUSUM analysis, has provided indisputable evidence of abrupt, non-linear shifts in the climate of northwestern Algeria a reality entirely missed by conventional linear tests such as Mann-Kendall ($p = 0.16$) and ANOVA ($p > 0.60$), which misleadingly suggest a stable climate.

Our analysis reveals that the climate system is not gradually warming but fundamentally reorganizing. The frequency of the extreme 'Hot & Very Dry' regime has increased by 45% since the 1990s, while its average duration has lengthened by 44%, from 3.2 to 4.6 months. These structural changes are confirmed by the detection of three major concept drifts, with scores reaching 0.80, and by 113 changepoints identified by CUSUM analysis. The significant correlation with the North Atlantic Oscillation ($r = 0.58$, $p < 0.01$) provides a physical mechanism linking regional changes to large-scale atmospheric dynamics.

The operationalization of these findings into a Probabilistic Drought Early Warning System (DEWS), capable of issuing grid-point-level risk forecasts indicating transition probabilities into the 'Hot & Very Dry' drought regime reaching up to 90% at the most vulnerable interior locations during peak summer months, offers a robust foundation for proactive, regime-aware adaptation strategies (Kareiva et al., 2007; Lobell et al., 2008). Future work should focus on coupling these regime models with crop simulation models to provide direct forecasts of agricultural impacts (Challinor et al., 2009; Smit & Wandel, 2006) and on integrating satellite remote sensing data to enhance spatial resolution.

6. REFERENCES

Akaike, H., 1974. A new look at the statistical model identification. IEEE Transactions on Automatic Control, 19(6): 716-723. https://doi.org/10.1109/TAC.1974.1100705

Baum, L. E., Petrie, T., Soules, G., Weiss, N., 1970. A maximization technique occurring in the statistical analysis of probabilistic functions of Markov chains. The Annals of Mathematical Statistics, 41(1): 164-171. https://doi.org/10.1214/aoms/1177697196

Ben-Ari, T., Boé, J., Ciais, P., Lecerf, R., Van der Velde, M., Makowski, D., 2018. Causes and implications of the unforeseen 2016 extreme yield loss in the breadbasket of France. Nature Communications, 9(1): 1627. https://doi.org/10.1038/s41467-018-04087-x

Bracken, C., Rajagopalan, B., Zagona, E., 2014. A hidden Markov model combined with climate indices for multidecadal streamflow simulation. Water Resources Research, 50(10): 7733-7746. https://doi.org/10.1002/2014WR015567

Challinor, A. J., Watson, J., Lobell, D. B., Howden, S. M., Smith, D. R., Chhetri, N., 2014. A meta-analysis of crop yield under climate change and adaptation. Nature Climate Change, 4(4): 287-291. https://doi.org/10.1038/nclimate2153

Cohn, T. A., Lins, H. F., 2005. Nature's style: Naturally trendy. Geophysical Research Letters, 32(23): L23402. https://doi.org/10.1029/2005GL024476

Cook, B. I., Anchukaitis, K. J., Touchan, R., Meko, D. M., Cook, E. R., 2016. Spatiotemporal drought variability in the Mediterranean over the last 900 years. Journal of Geophysical Research: Atmospheres, 121(5): 2060-2074. https://doi.org/10.1002/2015JD023929

Dempster, A. P., Laird, N. M., Rubin, D. B., 1977. Maximum likelihood from incomplete data via the EM algorithm. Journal of the Royal Statistical Society: Series B (Methodological), 39(1): 1-38. https://doi.org/10.1111/j.2517-6161.1977.tb01600.x

Gao, Y., Markkanen, T., Aurela, M., Mammarella, I., Thum, T., Tsuruta, A., Yang, H., Aalto, T., 2019. Response of water use efficiency to summer drought in a boreal Scots pine forest in Finland. Biogeosciences, 16(23): 4499-4514. https://doi.org/10.5194/bg-16-4499-2019

Greene, A. M., Robertson, A. W., Kirshner, S., 2008. Analysis of Indian monsoon daily rainfall on subseasonal to multidecadal time-scales using a hidden Markov model. Quarterly Journal of the Royal Meteorological Society, 134(633): 875-887. https://doi.org/10.1002/qj.254

Hamed, K. H., Rao, A. R., 1998. A modified Mann-Kendall trend test for autocorrelated data. Journal of Hydrology, 204(1-4): 182-196. https://doi.org/10.1016/S0022-1694(97)00125-X

Hersbach, H., Bell, B., Berrisford, P., Hirahara, S., Horányi, A., Muñoz-Sabater, J., Nicolas, J., Peubey, C., Radu, R., Schepers, D., Simmons, A., Soci, C., Abdalla, S., Abellan, X., Balsamo, G., Bechtold, P., Biavati, G., Bidlot, J., Bonavita, M., De Chiara, G., Dahlgren, P., Dee, D., Diamantakis, M., Dragani, R., Flemming, J., Forbes, R., Fuentes, M., Geer, A., Haimberger, L., Healy, S., Hogan, R. J., Hólm, E., Janisková, M., Keeley, S., Laloyaux, P., Lopez, P., Lupu, C., Radnoti, G., de Rosnay, P., Rozum, I., Vamborg, F., Villaume, S., Thépaut, J.-N., 2020. The ERA5 global reanalysis. Quarterly Journal of the Royal Meteorological Society, 146(730): 1999-2049. https://doi.org/10.1002/qj.3803

Hughes, J. P., Guttorp, P., 1994. A class of stochastic models for relating synoptic atmospheric patterns to regional hydrologic phenomena. Water Resources Research, 30(5): 1535-1546. https://doi.org/10.1029/93WR02983

IPCC, 2021. Climate Change 2021: The Physical Science Basis. Contribution of Working Group I to the Sixth Assessment Report of the Intergovernmental Panel on Climate Change. Cambridge University Press, Cambridge, United Kingdom and New York, NY, USA. https://doi.org/10.1017/9781009157896

Kareiva, P., Watts, S., McDonald, R., Boucher, T., 2007. Domesticated nature: Shaping landscapes and ecosystems for human welfare. Science, 316(5833): 1866-1869. https://doi.org/10.1126/science.1140170

Kendall, M. G., 1975. Rank Correlation Methods. Charles Griffin, London, UK, 202 pp.

Lobell, D. B., Burke, M. B., Tebaldi, C., Mastrandrea, M. D., Falcon, W. P., Naylor, R. L., 2008. Prioritizing climate change adaptation needs for food security in 2030. Science, 319(5863): 607-610. https://doi.org/10.1126/science.1152339

Mann, H. B., 1945. Nonparametric tests against trend. Econometrica, 13(3): 245-259. https://doi.org/10.2307/1907187

Olesen, J. E., Bindi, M., 2002. Consequences of climate change for European agricultural productivity, land use and policy. European Journal of Agronomy, 16(4): 239-262. https://doi.org/10.1016/S1161-0301(02)00004-7

Page, E. S., 1954. Continuous inspection schemes. Biometrika, 41(1-2): 100-115. https://doi.org/10.1093/biomet/41.1-2.100

Pettitt, A. N., 1979. A non-parametric approach to the change-point problem. Journal of the Royal Statistical Society: Series C (Applied Statistics), 28(2): 126-135. https://doi.org/10.2307/2346729

Rabiner, L. R., 1989. A tutorial on hidden Markov models and selected applications in speech recognition. Proceedings of the IEEE, 77(2): 257-286. https://doi.org/10.1109/5.18626

Robertson, A. W., Kirshner, S., Smyth, P., 2004. Downscaling of daily rainfall occurrence over northeast Brazil using a hidden Markov model. Journal of Climate, 17(22): 4407-4424. https://doi.org/10.1175/JCLI-3216.1

Schwarz, G., 1978. Estimating the dimension of a model. The Annals of Statistics, 6(2): 461-464. https://doi.org/10.1214/aos/1176344136

Sen, P. K., 1968. Estimates of the regression coefficient based on Kendall's tau. Journal of the American Statistical Association, 63(324): 1379-1389. https://doi.org/10.1080/01621459.1968.10480934

Smit, B., Wandel, J., 2006. Adaptation, adaptive capacity and vulnerability. Global Environmental Change, 16(3): 282-292. https://doi.org/10.1016/j.gloenvcha.2006.03.008

Taïbi, A. N., Henia, L., Abderrahmane, M. K., 2017. Drought in the Maghreb: analysis of the spatiotemporal variability and impacts. Arabian Journal of Geosciences, 10(15): 327. https://doi.org/10.1007/s12517-017-3106-7

Theil, H., 1950. A rank-invariant method of linear and polynomial regression analysis. Indagationes Mathematicae, 12(85): 173.

Touchan, R., Anchukaitis, K. J., Meko, D. M., Attalah, S., Baisan, C., Aloui, A., 2008. Long term context for recent drought in northwestern Africa. Geophysical Research Letters, 35(13): L13705. https://doi.org/10.1029/2008GL034264

Vicente-Serrano, S. M., Beguería, S., López-Moreno, J. I., 2010. A multiscalar drought index sensitive to global warming: The Standardized Precipitation Evapotranspiration Index. Journal of Climate, 23(7): 1696-1718. https://doi.org/10.1175/2009JCLI2909.1

Viterbi, A., 1967. Error bounds for convolutional codes and an asymptotically optimum decoding algorithm. IEEE Transactions on Information Theory, 13(2): 260-269. https://doi.org/10.1109/TIT.1967.1054010

Zucchini, W., MacDonald, I. L., Langrock, R., 2016. Hidden Markov Models for Time Series: An Introduction Using R, 2nd ed. Chapman and Hall/CRC, Boca Raton, FL, USA, 370 pp. https://doi.org/10.1201/b20790

Ben Aoun, W., Biavetti, I., Bussay, A., Cerrani, I., Claverie, M., De Palma, P., Fumagalli, D., Henin, R., Luque Reyes, J., Morel, J., Niemeyer, S., Nisini, L., Ozalp, O., Panarello, L., Rossi, M., Seguini, L., Tarnavsky, E., Thiemig, V., Todoroff, P., Zucchini, A., 2025. JRC MARS Bulletin – Crop monitoring in Europe – May 2025 – Vol. 33 No 4. Publications Office of the European Union, Luxembourg. https://doi.org/10.2760/1115198

Biavetti, I., Bussay, A., Cerrani, I., Claverie, M., De Palma, P., Fumagalli, D., Henin, R., Luque Reyes, J., Morel, J., Niemeyer, S., Nisini, L., Ozalp, O., Panarello, L., Rossi, M., Seguini, L., Tarnavsky, E., Thiemig, V., Todoroff, P., Zucchini, A., 2025. JRC MARS Bulletin – Crop monitoring in Europe – March 2025 – Vol. 33 No 2. Publications Office of the European Union, Luxembourg. JRC141319.

European Commission Joint Research Centre, 2025. Severe drought in Africa persists and is expected to worsen. JRC/Copernicus Global Drought Observatory Report, 23 April 2025. Available at: https://joint-research-centre.ec.europa.eu/jrc-news-and-updates/severe-drought-africa-persists-and-expected-worsen-2025-04-23_en

FAO, 2026. GIEWS Country Brief: Algeria. Reference Date: 29 January 2026. Food and Agriculture Organization of the United Nations, Rome. Available at: https://www.fao.org/giews/countrybrief/country.jsp?code=DZA

NOAA National Centers for Environmental Information, 2026. North Atlantic Oscillation (NAO) Index. Available at: https://www.ncei.noaa.gov/access/monitoring/nao/

Seager, R., Liu, H., Osborn, T. J., Kushnir, Y., Nakamura, J., Wu, Y., 2026. Mediterranean Drying by a Positive North Atlantic Oscillation Trend over the Last 65 Years Is an Extreme Outlier in the CMIP6 Multimodel Ensemble. Journal of Climate, 39(2): 785–804. https://doi.org/10.1175/JCLI-D-25-0359.1

USDA Foreign Agricultural Service, 2025. Grain and Feed Annual: Algeria. GAIN Report AG2025-0002, 24 March 2025. United States Department of Agriculture, Washington, DC.

World Bank, 2025. Algeria Economic Update, November 2025. The World Bank Group, Washington, DC.

Italian Journal of Agrometeorology
Rivista Italiana di Agrometeorologia

Firenze University Press
https://riviste.fupress.net/index.php/IJAm

OPEN ACCESS

Citation: Majdouli, K., Algouti, A., Bhiry, N., Molson, J., Algouti, A., Lamrani, K. & El Kihal, I. (2026). Monitoring drought impacts through spatiotemporal analysis of climatic and vegetative indices in the Drâa River watershed, Morocco. *Italian Journal of Agrometeorology* (1): 21-40. doi: 10.36253/ijam-3676

Received: July 23, 2025

Accepted: January 22, 2026

Published: September 15, 2026

Data Availability Statement: All relevant data are within the paper and its Supporting Information files.

Competing Interests: The Author(s) declare(s) no conflict of interest.

ORCID:
MK: 0009-0000-1118-4819
AA: 0000-0002-2344-0821
NB: 0000-0002-6609-0235
JM: 0000-0002-6581-8044
AA: 0000-0001-7501-5221
KL: 0009-0000-8350-2935
IEK: 0009-0004-0737-120

Monitoring drought impacts through spatiotemporal analysis of climatic and vegetative indices in the Drâa River watershed, Morocco

Kaouthar Majdouli[1,*], Ahmed Algouti[1], Najat Bhiry[2], John Molson[3], Abdellah Algouti[1], Khadija Lamrani[1], Imane El Kihal[1]

[1] *Laboratory of Geosciences, Geotourism, Natural Hazards and Remote Sensing, Faculty of Sciences Semlalia, Cadi Ayyad University, Boulevard Prince My Abdellah, B.P. 2390, 40000 Marrakech, Morocco*
[2] *Department of Geography, Université Laval, Pavillon Abitibi-Price, 2405, rue de la Terrasse, Quebec G1V 0A6, Canada*
[3] *Department of Geology and Geological Engineering, Université Laval, Pavillon Adrien Pouliot 1065, avenue de la Médecine, Local 4309, Québec G1V 0A6, Canada*
Emails: k.majdouli.ced@uca.ac.ma; algouti@uca.ac.ma; Najat.Bhiry@rec.ulaval.ca; john.molson@ggl.ulaval.ca; abalgouti@uca.ac.ma; k.lamrani.ced@uca.ac.ma; i.elkihal.ced@uca.ac.ma
*Corresponding author

Abstract. The Drâa River watershed, characterized by a semi-arid climate, is particularly vulnerable to the risk of desertification, a threat exacerbated by the effects of global warming. This study is based on an analysis of climatic and hydrological variations in the Drâa basin, using satellite and terrestrial data. Climatic indices including SPI and PDSI, and vegetation indices VCI, TCI, VHI and NDVI, were calculated to assess the impact of climatic conditions on water resources and vegetation cover. In addition, the water reflectance index (NDWI) was used to analyze variations in water level of the El Mansour Eddahbi reservoir. The remote sensing results were compared with records from local hydrological stations to ensure consistent and thorough interpretation. The analyses show that the Drâa watershed is currently experiencing the longest drought in its recorded history, although its intensity is lower than that observed between 1981 and 1984. Over a 23-year period (2000-2023), only 9 years were relatively wet, compared to 14 years of drought, according to the SPI index. These climatic conditions have put considerable pressure on water resources and vegetation cover, as evidenced by variations in vegetation indices and climatic parameters. The reduction in the surface area and perimeter of the El Mansour Eddahbi reservoir, observed by remote sensing, was corroborated by the decrease in water volume measured in situ. Prolonged droughts in this region therefore pose a significant threat to water and environmental resources.

Keywords: drought, remote sensing, climatic indices, vegetative indices, climate change.

HIGHLIGHTS

- The impacts of drought were assessed in the Drâa basin using satellite indices.
- Significant vegetative stress was detected during the main drought episodes.
- Strong correlations confirm the influence of climatic factors on vegetation.
- Validation tests, based on ground data, confirmed the reliability of the results.

INTRODUCTION

Drought, a recurring natural phenomenon with dramatic consequences, is one of the most complex challenges facing arid and semi-arid regions such as Morocco. Although drought is not a new concept in Morocco (the country has always experienced alternating dry and wet periods), in recent years, the frequency of periods vulnerable to drought risk has become increasingly important and alarming (Stour & Agoumi, 2008; Hadria et al. 2019; Lahbous, 2023; Gumus et al., 2024; Bijaber et al., 2024). With an economy largely based on agriculture, Morocco therefore faces major challenges related to increasing aridity, especially in its arid and semi-arid regions (Hadri et al., 2022; Lebdi & Maki, 2023).

At the national level, the impacts of drought are not limited to the environment. In economic terms, for example, the effects are significant. Lahbous et al. (2023) showed that successive droughts have caused a significant decline in agricultural value added, which has significantly reduced the national gross domestic product (GDP). This situation exacerbates the vulnerability of the rural population and threatens the country's food security. In 2017, the World Bank published a report on environmental costs in Morocco (Dahan, 2017), estimating that environmental degradation accounts for a loss of about 3.5% of national GDP. Among these costs, the degradation of water resources stands out, accounting for around 1.6% of GDP, surpassing air pollution, which in turn accounts for 1.05% of GDP. In addition, degraded soils, affected by erosion and land conversion into desertified areas, also contribute significantly to environment-related economic losses (Dahan, 2017).

In this context, the Drâa River watershed, a semi-arid region in southern Morocco, stands out for its increased vulnerability to drought. The Drâa watershed is particularly vulnerable due to its dependence on groundwater to meet the needs of the local population (Ouysse et al., 2010). However, this vital resource is seriously threatened by persistent meteorological drought, exacerbated by extreme adverse weather conditions. Rainfall deficits, coupled with rising temperatures and a wide temperature range, are significantly reducing wetlands, with direct impacts on vegetation cover, surface water and groundwater (Saouabe et al., 2022; Sadiki & Hanchane, 2024). Adverse climatic conditions, combined with increasing demographic and industrial pressures, have placed the Drâa basin in a critical and alarming situation. In response to these challenges, it has become imperative to implement rigorous management strategies to preserve the region's water resources.

In this context, several studies have been conducted to map the areas most affected by the adverse effects of meteorological drought (Auclair, 1987; Agoussine et al., 2003, 2004; Schulz et al., 2004, 2008; Weber, 2004; Aït Hamza et al., 2010; Ouysse et al., 2010; Bentaleb, 2011, 2015; Baki et al., 2017; Mehdaoui et al., 2018; El Qorchi et al., 2023). However, drought management in this region, particularly in terms of forecasting and assessing its impact on water resources, remains a major challenge. When it comes to studying and managing climate risks, the availability of in situ climate and hydrological data, as well as the methods used to collect this information, continue to be key obstacles (Wang et al., 2015; Aksu et al., 2022b). New space technologies and remote sensing tools provide a variety of capabilities for monitoring climatic phenomena over large areas and long periods of time (Ji & Peters, 2003; Hao & Singh, 2015; Wang et al., 2015; Li et al., 2016; Bijaber & Rochdi 2017; Eyoh et al., 2019; Bashit et al., 2022; Houmma et al., 2023; Serbouti et al., 2023). The use of satellite sensors has replaced the traditional method based on calculating climate indices from terrestrial data measured and recorded by a limited network of meteorological and hydroclimatic stations. These stations are often inadequate and unrepresentative, especially in desert regions, which make up a significant portion of the catchment area under study. Moreover, many climate indices require data series of at least 30 years to provide convincing results. To illustrate, hydroclimatic indices such as the Standardized Precipitation Index (SPI), the Standardized Precipitation-Evapotranspiration Index (SPEI) (McKee et al. 1993), and the Palmer Drought Severity Index (PDSI) (Palmer, 1965; Li et al., 2016; Zkhiri et al., 2018; Kim et al., 2021) are often used to assess hydroclimatic drought over large spatiotemporal areas. In this context, several studies have been conducted to use satellite data in the study of drought in Morocco. The analysis of the Palmer Drought Index (PDSI) by Waroux et al. (2013) revealed a clear trend of increasing drought in the Aoulouz argan grove region over the last few decades, mainly due to the increase in mean annual temperatures, thus higher evapotranspiration and less recharge. In fact, the increase in temperature appears to be the main factor affecting the health of argan trees, limiting their natural regeneration and accelerating the degradation of the local ecosystem. According to Elair et al. (2023), the use of SPI, VCI, TCI, and VHI indices showed that the Marrakech-Safi region experienced significant variations in drought frequency between 1984 and 2022, with periods characterized by moderate to severe drought events. Several critical droughts were identified from 1981 to 2017, interspersed with periods of rainfall. However, studies indicate an increasing trend in the frequency, duration and intensity of droughts in recent decades, highlighting the challenges of water resource management and agriculture in the region (Choukrani et al., 2018). Combined analyses of remote sensing indices such as SPI, SPEI, STI, TCI and GRACE-DSI have revealed a significant worsening of drought episodes in the Bouregreg catchment located in the north-western part of Morocco. This intensification is not the result of a significant decrease in precipitation, which has remained stable overall, but rather of a growing water imbalance, fueled by a significant increase in temperature. The increase in evapotranspiration catalyzed by global warming has thus exacerbated the agricultural and hydrological forms of drought in the region (Ait Dhmane et al, 2024).

The Drâa watershed is no exception to the recent national trend of increasing drought. However, its vast surface area and the diversity of its topographic and climatic conditions make monitoring this phenomenon particularly complex. The objective of this study is to assess the risk of drought in the basin using several indices derived from satellite data for the period between 1960 and 2023. More specifically, it aims to analyze the spatial and temporal variability of drought using satellite indices based on reflectance and brightness temperature, to evaluate their performance in detecting drought events and their frequency, and to identify the most vulnerable areas of the Drâa watershed. These indices are then compared with field data provided by the Drâa-Oued Noun Water Basin Agency, as well as with trend analyses of raw climatic parameters such as precipitation and temperature.

MATERIALS AND METHODS

Study area

The Drâa River watershed is located in the southern part of Morocco and covers an area of approximately 93,729 km^2. It is bounded to the north by the foothills of the High Atlas, from Jbel Toubkal to Jbel M'Goun, and to the south by the Saharan basin and the border with Algeria. It is bordered to the east by the Todgha and Rhis valleys and to the west by the Guelmim and Souss Massa basins (Figure 1). The Drâa is a region where geography, geology and the availability of water resources are closely linked. Its climate, which is semi-arid in

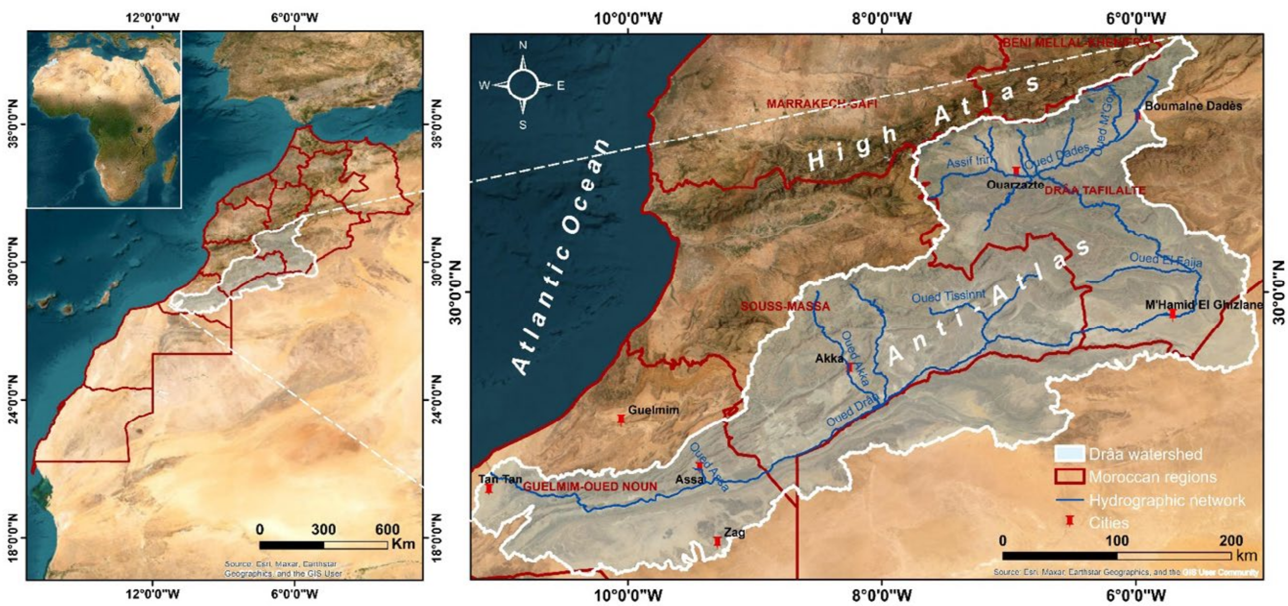

Figure 1. Location map of the study area showing the Drâa River watershed situated in southern Morocco.

the north and becomes Saharan south of M'Hamid El Ghizlane, is mainly influenced by its geographical position between the High Atlas and the Anti-Atlas, as well as its proximity to the Atlantic Ocean (DRPE, 2008; Schulz et al., 2004). The region suffers from pronounced aridity, especially in the Anti-Atlas, although cool winds from the Atlantic bring some moderation to the climate. However, the high frequency of anticyclones contributes to a severe lack of precipitation (ABHDON, 2009). From a hydrological point of view, the Drâa basin includes the longest river (Drâa River) in Morocco, with a length of 1100 km. It rises at the confluence of the Dadès and Ouarzazate rivers, at the El Mansour Eddahbi dam, and follows a winding course before emptying into the Atlantic Ocean. This great length crosses a variety of geographical and topographical contexts, giving rise to a division into the Upper, Middle and Lower Drâa, each with distinct geographical and hydrological characteristics (Figure 1) (ABHDON, 2013).

Data sources

Remote sensing data

a) NOAA and VIIRS sensor images

The National Oceanic and Atmospheric Administration (NOAA) is a platform equipped with a network of satellites, ocean buoys, meteorological stations and other instruments designed to collect variable precision, real-time information on climatic and oceanic conditions worldwide. These data are publicly accessible via a number of digital platforms. In order to characterize the meteorological aridity of our vast study area over a period of about forty years, we used data presented by NESDIS STAR (National Environmental Satellite, Data, and Information Service - Center for Satellite Applications and Research), accessible through the link https://www.star.nesdis.noaa.gov/star/index.php.

A detailed analysis of environmental conditions and climate trends using indices based on precipitation, temperature and evapotranspiration potential was made possible by using the TerraClimate database. This high-resolution data source (approximately 4 km resolution) provides a monthly overview of a number of hydrological and climatic variables essential for characterizing drought in a given region. The data are available from 1958 to the present and can be accessed free of charge at https://www.climatologylab.org/terraclimate.html.

b) Google Earth Engine data

In order to document the spatiotemporal variation of the normalized vegetation index, we used the Google Earth Engine platform (https://code.earthengine.google.com/), which provides a large collection of historical and current satellite data from different sensors such as Landsat, MODIS and Sentinel. For this purpose, we used Java scripts to visualize NDVI maps of the Drâa watershed based on data extracted from Landsat 5 satellite sensors for the years 1984, 1989, 1994, and 1999, as well as from the MOD13Q1 satellite sensor for the years 2000-2023. The resulting maps are then stored, processed, and used to monitor drought trends over time.

Data from land based hydrological stations: Precipitation and volume variations of the El Mansour Eddahbi Dam

Gathering stations provide accurate and localized rainfall measurements that are essential for the calibration and verification of satellite data. These stations were established and are currently managed by the Drâa Oued Noun Water Basin Agency. Based on a network of 27 rain gauge stations distributed upstream and downstream in the Drâa basin, we were able to establish interpolations based on real data, allowing us to assess the validity and accuracy of the results obtained by remote sensing platforms.

Because we work with satellite data, it is essential to perform pre-processing on downloaded images to ensure data reliability and quality. For information presented in image form, we have applied the necessary atmospheric and radiometric corrections. These are aimed at adjusting pixel values to correct for variations in sensor sensitivity and aligning images to correct for geometric distortions. As for the data corresponding to point measurements of climatic parameters at specific stations, usually acquired in CSV (comma-separated values) format, we prepared the database by selecting the time intervals and calculating the monthly and annual sums and averages for each climatic parameter to be used in the calculation of the indices. These preliminary steps are crucial before proceeding with spline interpolation with barriers to obtain the final map. In general, the approach used in this study aims to monitor drought trends over a 50-year period, focusing on the current situation (Figure 2). This monitoring was done using satellite climate indices from NOAA, TerraClimate and Google Earth Engine. A large watershed like the Drâa, with inaccessible desert areas, poses enormous problems in terms of data availability. In this study, new space technology has proven very useful, with online information used to produce maps suitable for management and decision-making in these areas. The resulting cartographic maps were validated using real data collected along the Drâa River, based on a correlation between the products of the different data sources.

Severe weather conditions have a significant impact on the size of water reservoirs. In this regard, as a third validation, we used the large El Mansour Eddahbi reservoir in the Drâa watershed as a reference. Using the Normalized Difference Water Index (NDWI) and volume measurements carried out by the Drâa Oued Noun Water Basin Agency, we carried out a detailed study of the temporal variation of its surface area and perimeter in order to identify dry and wet years for this reservoir, which receives most of its annual rainfall from the Tidili-Iriri and Dadès-M'Goun tributaries.

Drought indices

a) Reflectance-Based Indices

NDVI (Normalized Difference Vegetation Index)

Proposed by (Rouse et al., 1973) as an index of vegetation health and density, NDVI is currently considered the most widely used indicator for monitoring terrestrial vegetation over large areas. This index is defined by the following formula:

$$\text{NDVI}= \frac{NIR - RED}{NIR + RED}$$

where NIR and RED are reflectances in the near infrared and red bands, respectively. NDVI varies from -1 to +1, with positive values close to 1 indicating dense, healthy vegetation, and low negative values indicating a lack of vegetation or non-vegetated surfaces, which can be water or bare soil.

VCI (Vegetation Condition Index)

The VCI is a vegetative stress index expressed as a function of maximum, current and minimum NDVI values over a period of time (Liu & Kogan 2002). It differs from NDVI in its ability to analyse vegetation conditions for heterogeneous areas (Kogan, 1990), which is due to its ability to separate the short-term climatic signal from the long-term ecological signal (Kogan & Sullivan, 1993). VCI values generally vary between 0 and 100, with a zero value corresponding to extremely poor vegetation conditions and maximum values close to 100 indicating optimal vegetation conditions, and can be defined as:

$$\text{VCI} = \frac{NDVI - NDVI\,min}{(NDVImax - \;NDVI\,min)} \times 100$$

NDWI (Normalized Difference Water Index)

The NDWI introduced by (McFeeters, 1996) is a reflectance-based index commonly used to identify and monitor the presence of water on the Earth's surface. The NDWI uses reflected radiation in the near infrared and visible green light to enhance the presence of water features while eliminating the presence of soil and terrestrial vegetation (McFeeters, 1996). The NDWI formula is generally defined as follows:

$$\text{NDWI} = \frac{(Green - NIR)}{(Green + NIR)}$$

b) Brightness Temperature-Based Indices

TCI (Temperature Condition Index)

This thermal index is essentially based on the Earth's surface temperature. It was developed at NOAA in 1995 (Kogan, 1997), and is calculated using images from NOAA's AVHRR sensor. This index is very useful for characterizing thermal stress over long periods of time and over large areas (Kogan, 1997). Combined with other vegetation indices such as VCI, it provides a more comprehensive assessment of the vegetation condition of a given area. It is calculated as follows (Layelmam, 2015):

$$TCI = \frac{LST\,max - LST\,(i)}{LST\,max - LST\,min}$$

where LST*max* is the maximum surface temperature of the period studied, LST*min* is the minimum surface temperature of the period studied and LST (i) is the surface temperature of the month concerned.

c) Combined Reflectance and Brightness Temperature-Based Indices

VHI (Vegetation Health Index)

Because it combines a thermal factor and plant reflectance, the VHI is the most appropriate indicator for vegetation. This index was developed by (Kogan, 1995), and is very effective in terms of studying and managing agricultural drought by assessing vegetation health. It works by combining the Vegetation Condition Index (VCI) and the Temperature Condition Index (TCI), while relying on their negative correlation, to detect, monitor and provide early warning of the frequency and intensity of agricultural drought (Justice et al. 1998; Seiler et al. 1998). It is expressed by the following equation:

$$VHI = \alpha\, VCI + \beta\, TCI$$

where α and β are coefficients assigned to each of these combination factors and refer to the negative correlation between the thermal index and the plant index. These coefficients are equal to 0.5, according to (Wilhite et al., 2000).

d) Rainfall variation-based indices

SPI (Standardized Precipitation Index)

The SPI index (McKee et al., 1993, 1995) is a powerful yet easy to calculate tool that requires only precipitation data to quantify precipitation deficits or surpluses. It measures variations in precipitation relative to historical averages over a specified period, whether deficit or surplus, over periods ranging from 3 months to 2 years. Its optimal calculation requires monthly measurements over 20 to 30 years, ideally 50 to 60 years, although missing data can affect the reliability of the results (WMO, 2012). The SPI index can be expressed as:

$$SPI = \frac{P - Pm}{\sigma P}$$

where P is the total precipitation for a given period (mm), Pm is the historical mean precipitation for the period (mm), and σP is the historical standard deviation of precipitation for the period (mm).

PDSI (Palmer Drought Severity Index)

The PDSI is a meteorological drought index developed by Palmer (Briffa et al., 1994; Scian & Donnari, 1997; Cook et al., 1999). Its ultimate goal is to provide standardized measurements of moisture conditions so that comparisons can be made using this index between different locations and between different months. To achieve this, the PDSI relies on data on precipitation, current and past temperatures, and available soil moisture (Mika et al., 2004), However, it does not directly consider surface hydrological resources (groundwater, rivers, reservoirs), that can influence drought conditions (Layelmam, 2015). The PDSI index is calculated using:

$$PDSI = X(i) = \frac{0.897\,X(i-1) + Z(i)}{3}$$

where X (i-1) is the PDSI of the previous period, and Z(i) is the moisture anomaly index which is calculated by the following formula:

$Z(i) = K(P\text{-}Pc)$

where K is a weighting factor (see Alley 1984), P is the current precipitation (mm), and Pc is the CAFEC precipitation (mm; *Climatically Appropriate for Existing Conditions*), representing the amount of rainfall needed to maintain a balanced water supply (i.e., neither drought nor excessive humidity) under normal climatic conditions. It is expressed as: CAFEC = Potential Evapotranspiration (PE) + Recharge + Runoff – Soil Moisture Loss/Gain.

RESULTS

Reflectance-Based Indices

VCI

The map of spatiotemporal variation of the Vegetation Condition Index (VCI) (Figure 3) shows an increasing trend towards drought between 1984 and 2023. During the period from 1989 to 2009, conditions appear relatively normal, with slight fluctuations observed between 1989 and 2009, and spatially between the High Atlas and Anti-Atlas regions. These fluctuations can be attributed to topographic variations, which have a direct influence on the amount of precipitation and the diurnal temperature variations. In fact, the varied topography of the mountainous

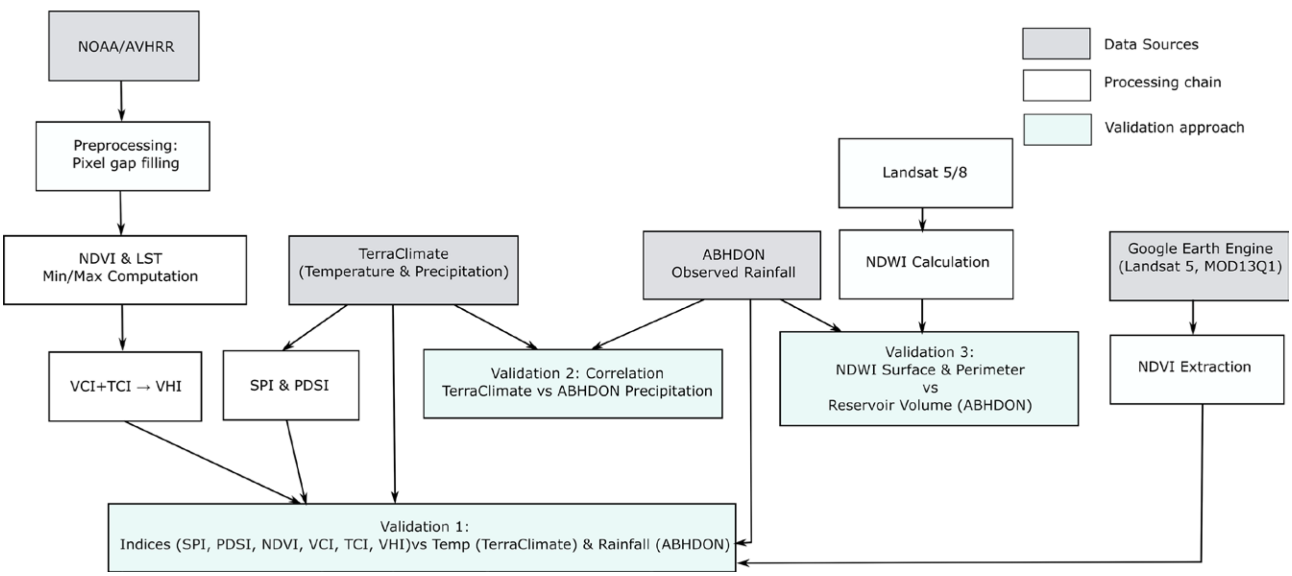

Figure 2. Workflow diagram illustrating the main steps of the adopted work methodology.

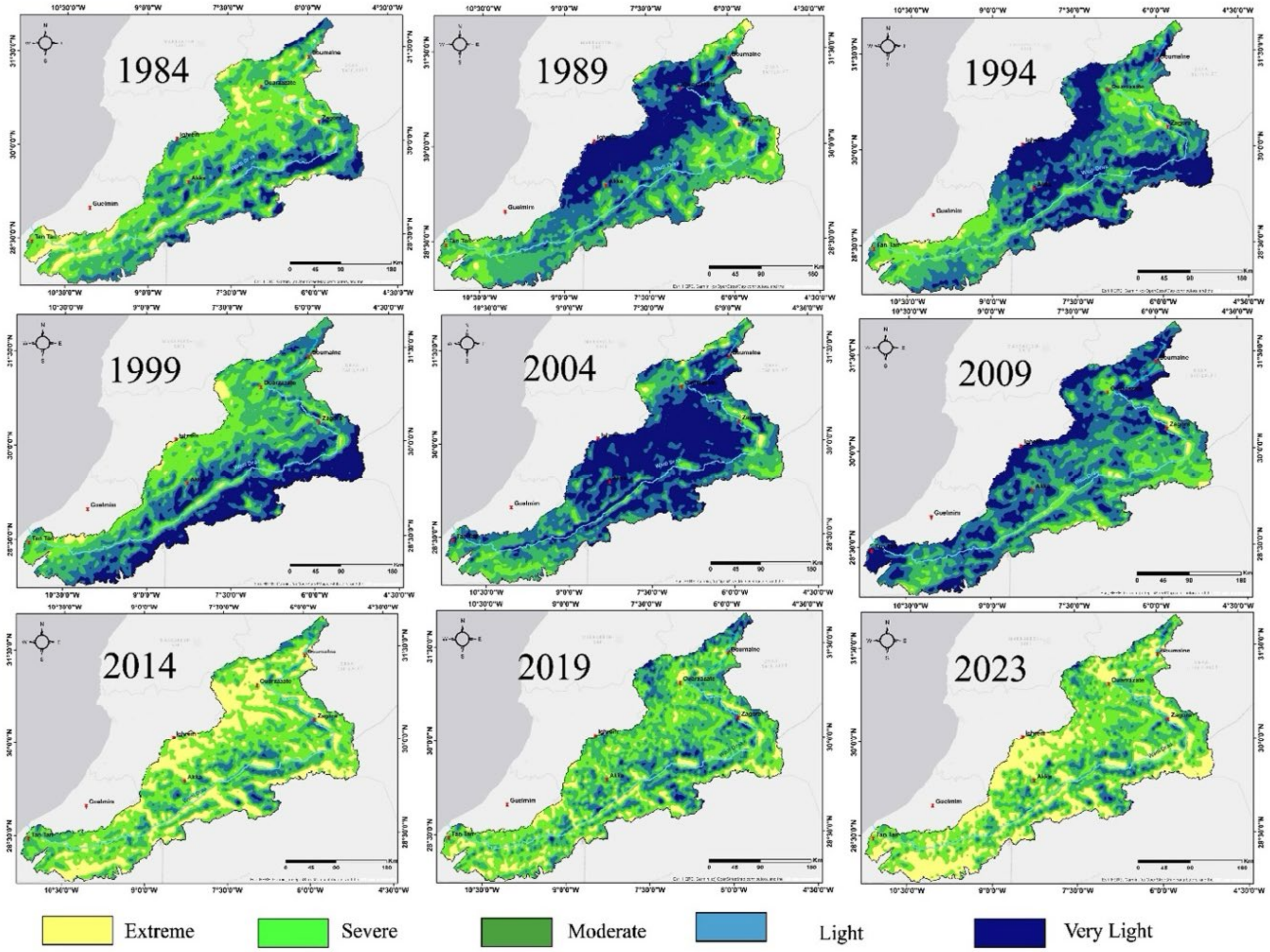

Figure 3. Spatiotemporal variation map of the Vegetation Condition Index (VCI).

areas of the High Atlas and Anti-Atlas results in distinct microclimates. Higher altitudes generally receive more precipitation, while lower areas can be more arid. Since 2009, a significant increase in drought has been observed, leading to a progressive deterioration of vegetation conditions and an increase in periods of water stress. This deterioration could be linked to climate change, which is strongly affecting precipitation patterns and temperatures.

NDVI

Analysis of the normalized vegetation index (NDVI) in Figure 4 clearly indicates a significant shift in the climatic conditions of the Drâa watershed since the 2000s. Even land in the Atlas regions shows progressively lower NDVI values, specially from 2004 to 2023. Bare soil and Saharan zones occupy about three quarters of the watershed surface area, which is explained by regional climatic conditions. These changes indicate a gradual degradation of vegetation cover, highlighting water stress and a decline in biological productivity. Analysis of the NDVI data during this period shows the severe impact of the climatic conditions on the ecosystem of the Drâa watershed. Green zones with high NDVI values continue to show resilience, especially in the foothills of the high mountains, largely benefiting from the effect of snowmelt. These areas of dense vegetation also extend along the Drâa River, from the High Dadès in the east and Tidili-Iriri in the west, to Mhamid El Ghizlane in the south (Figure 1).

Brightness Temperature-Based Indices

TCI

As shown in Figure 5, the temporal variation of the temperature condition index (TCI) shows some

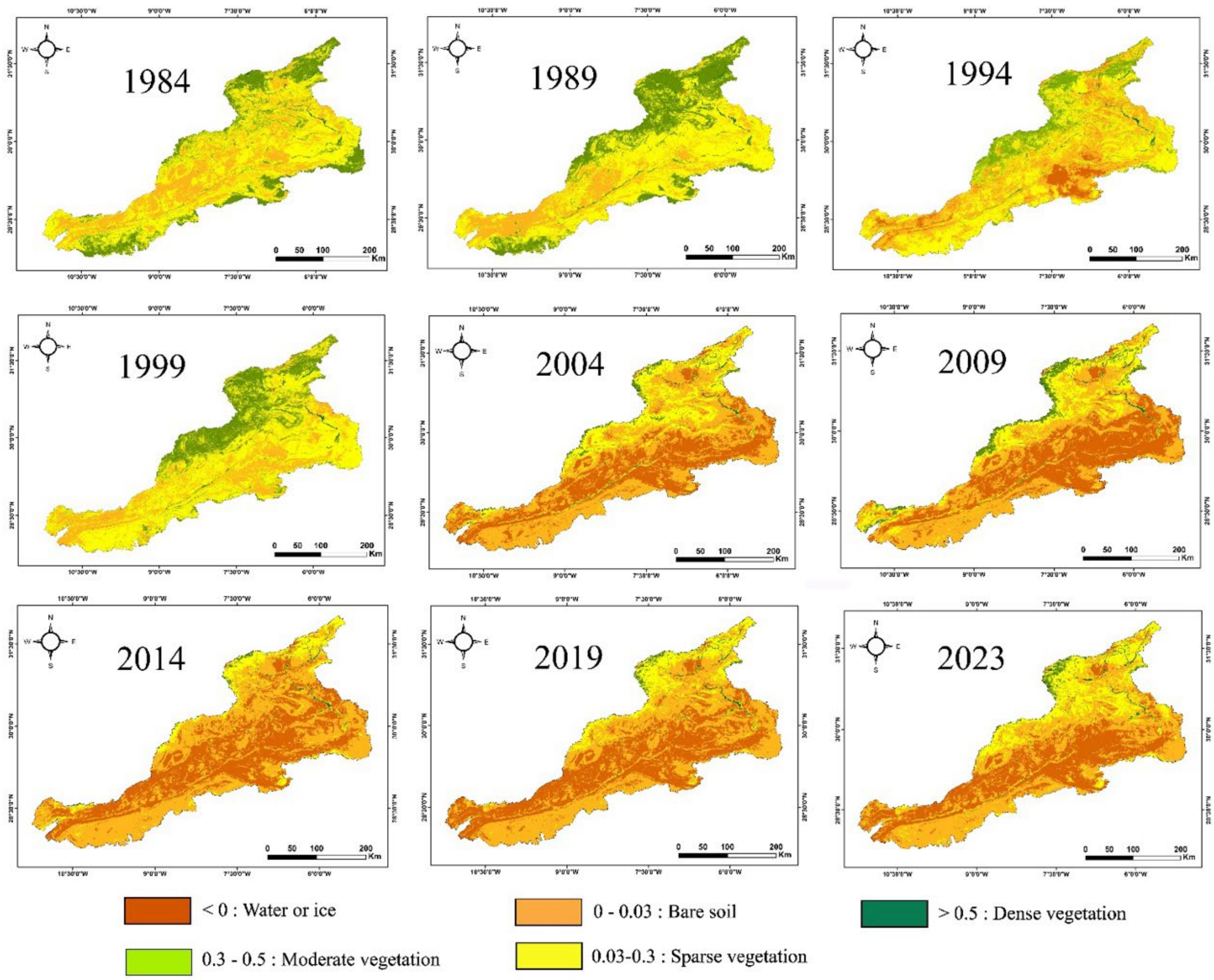

Figure 4. Normalized Difference Vegetation Index (NDVI) map illustrating spatial variations in vegetation cover across the study area.

cyclicity. Any year with extremely high temperatures could indicate a period of drought, followed four years later by a year with lower temperatures, indicating wet conditions.

This index examines the effect of temperature on vegetation, showing that even the lowest temperatures can have a negative effect on plant cover. Therefore, it is important to use this index alongside the Vegetation Condition Index (VCI) rather than in isolation. The combination of these two indices results in the Vegetation Health Index (VHI). Basically, years with favorable vegetation conditions are confirmed by the VHI, enhancing the reliability of the conclusions drawn from their analysis.

Combined Reflectance and Brightness Temperature-Based Indices

VHI

With regards to the Vegetation Health Index (VHI), the observed trends are consistent with those of the NDVI, VCI and TCI. Initially, conditions appear favorable throughout the watershed, with varying intensity due to the different microclimates of each region, influenced by their specific topographic context. However, from 2004 onwards, the calculations show a significant upheaval, with the class indicating unfavorable vegetation conditions invading almost the entire watershed. This trend indicates an alarming drought, which can be corroborated by the other indices based on the local meteorological conditions, hence the importance of a mul-

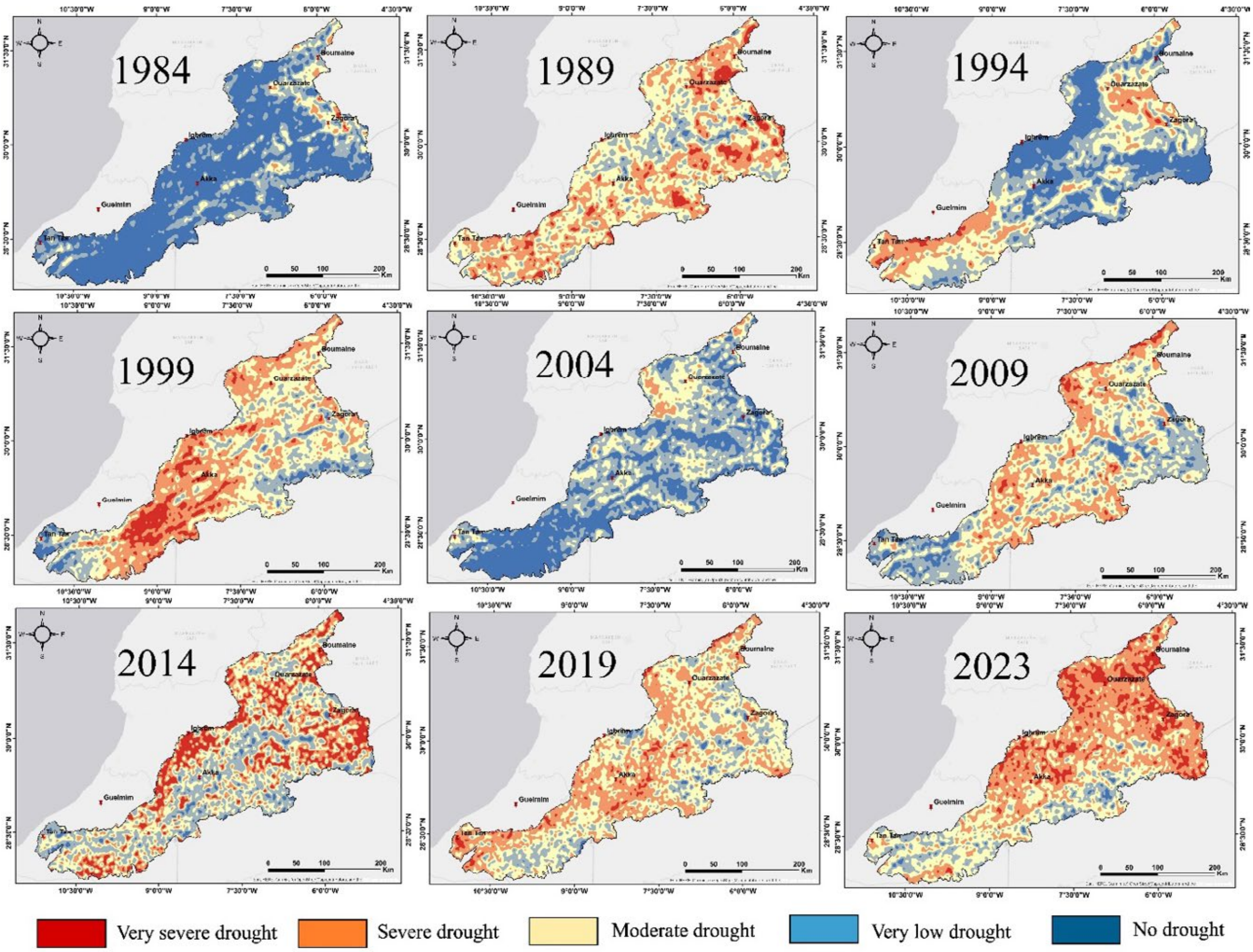

Figure 5. Spatiotemporal variation map of the Temperature Condition Index (TCI) illustrating thermal stress conditions across the study area during the observation period.

tidimensional analysis of the indices for a complete and accurate understanding of the drought in the study area.

Rainfall variation-based indices

SPI

Analysis of the graph showing variations in the Standardized Precipitation Index (SPI) for the Drâa watershed from 1950 to 2023 reveals several important trends (Figure 7). During this period, the SPI shows marked variability, with prolonged episodes of severe drought, particularly notable in the years 1961, 1962, 1976, 1982-1985, 1999-2002 and 2016-2023 (with the exception of the year 2018-2019), when SPI values fall below -1.5, indicating exceptionally dry conditions. In contrast, significant peaks of excess precipitation occur between 1952-1957, 1963-1969, 1988-1994, 1996-1998, 2003-2007, and 2014-2015, with SPI values reaching +1.5, indicating periods of abundant precipitation.

The overall trend in the SPI appears to oscillate between periods of intense drought and excess precipitation, with a notable variation in the frequency of events between the 1990s and 2000s. Prior to 2002, droughts had a significant amplitude but a limited duration of 3 or 4 years at most, while wet periods were more prolonged, with somewhat lower amplitudes. Since 2002, wet periods have become rarer, with an average amplitude and generally lasting only one or two consecutive years. On the other hand, a precipitation deficit extends over about 17 years, from 2007 to 2023, with a few one-year breaks, as in 2014-2015 and 2018-2019. In terms of SPI, over a period of 23 years (2000-2023) the watershed has experienced only 9 relatively wet years compared

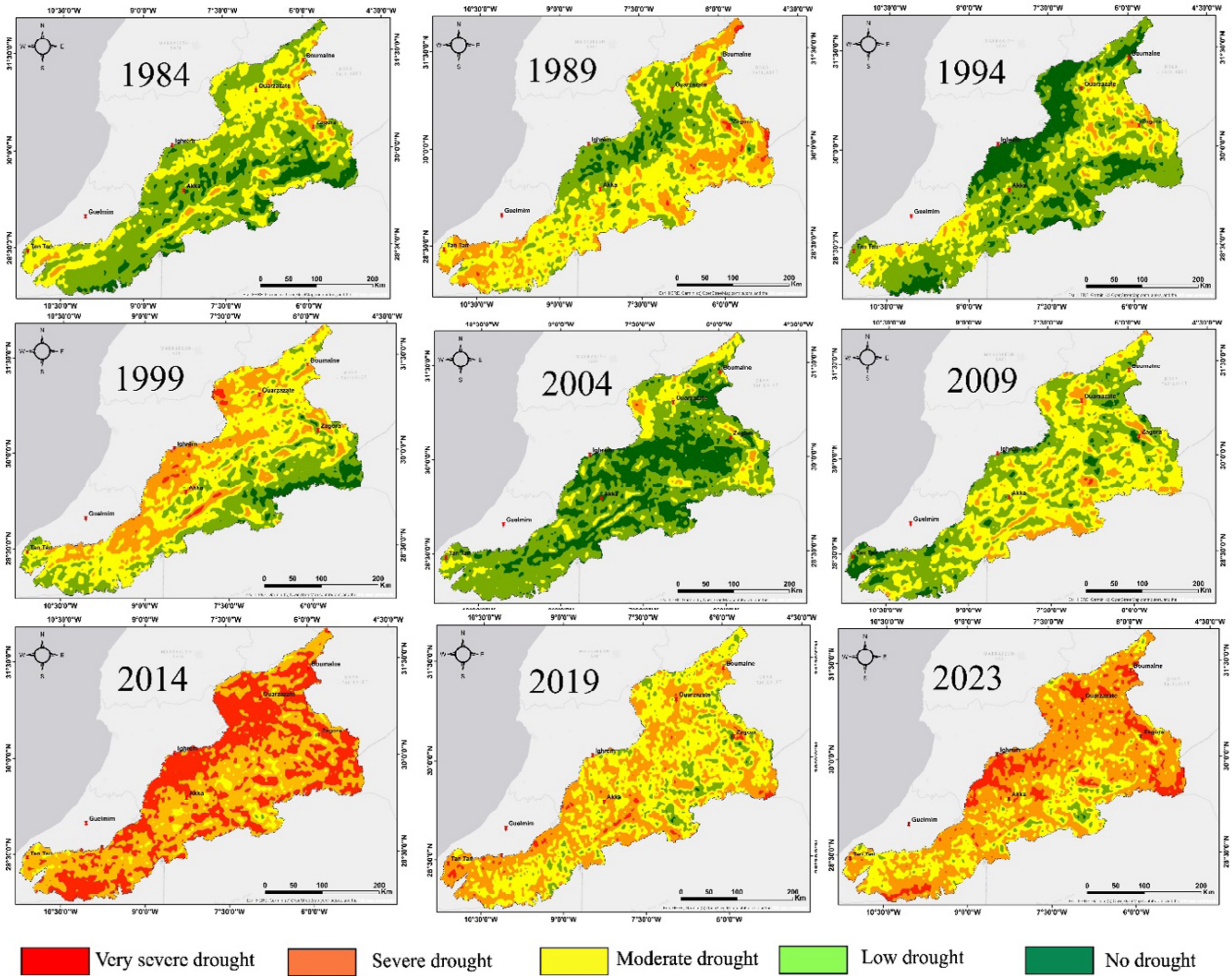

Figure 6. Vegetation Health Index (VHI) variation map showing spatiotemporal changes in vegetation health across the study area.

with to 14 dry years. These rainfall deficits, spread over a long period, and in parallel with the rise in temperatures, confirms the results of the other indices reflecting vegetation health.

PDSI

Variations in the Palmer Drought Severity Index (PDSI) corroborate the fluctuations observed through the SPI indices (Figure 8). This is to be expected, as the Palmer index is based on similar parameters to those used to assess rainfall deficits and surpluses. The periods most severely affected by drought, identified by the lowest PDSI values, include the intervals 1982-1984, 1999-2000, and the long dry period from 2015 to the present day. Conversely, wet periods are less frequent, with significant peaks recorded in the years 1987-1989, 2002, and 2014. These observations confirm the harmonization of drought and precipitation indices in the assessment of climatic conditions in the watershed, underlining their complementarity in the analysis of climatic trends.

Validation of findings

Observed climatic and hydrological parameters

As a performance test, we implemented a rigorous validation, comparing the results with variations in climatic parameters. Specifically, we compared precipitation data from 27 hydrological stations along the Drâa River with temperatures provided by the TerraClimate satellite and with the results of drought indices derived from remote sensing.

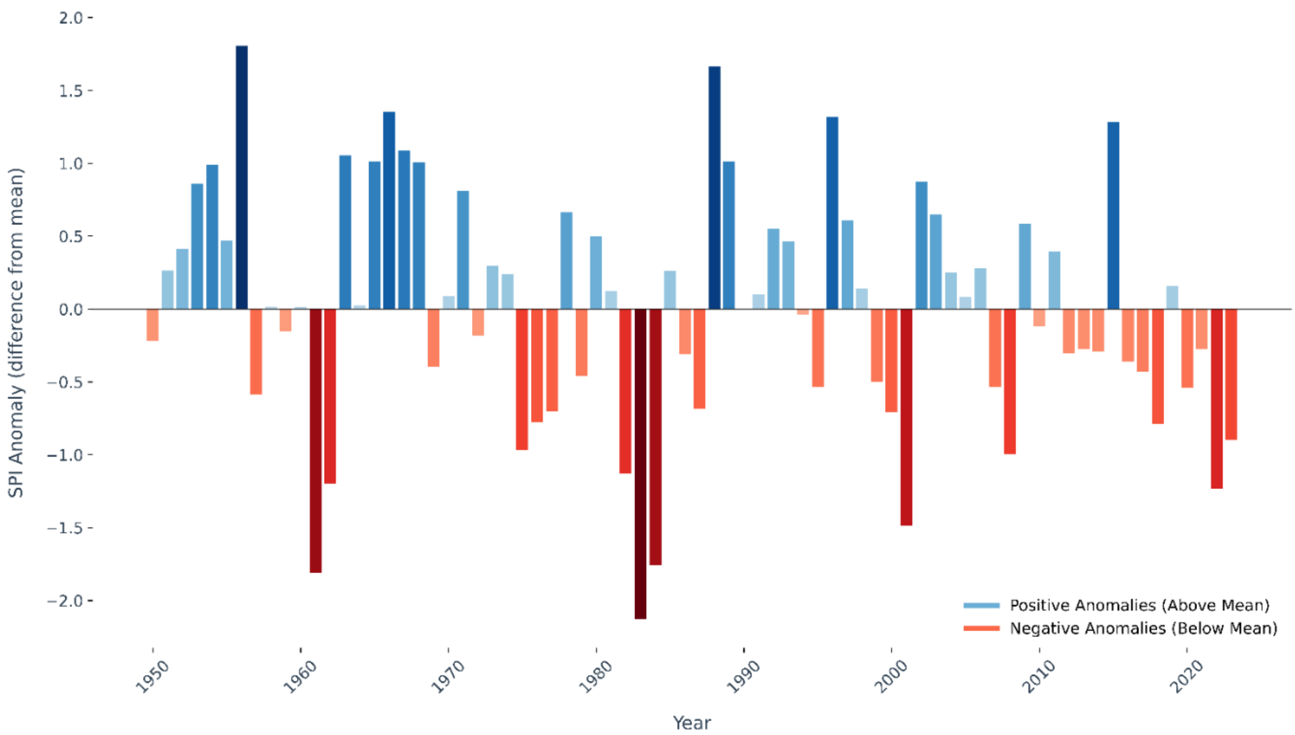

Figure 7. Variations of the Standardized Precipitation Index (SPI) illustrating the temporal evolution of meteorological drought conditions in the study area.

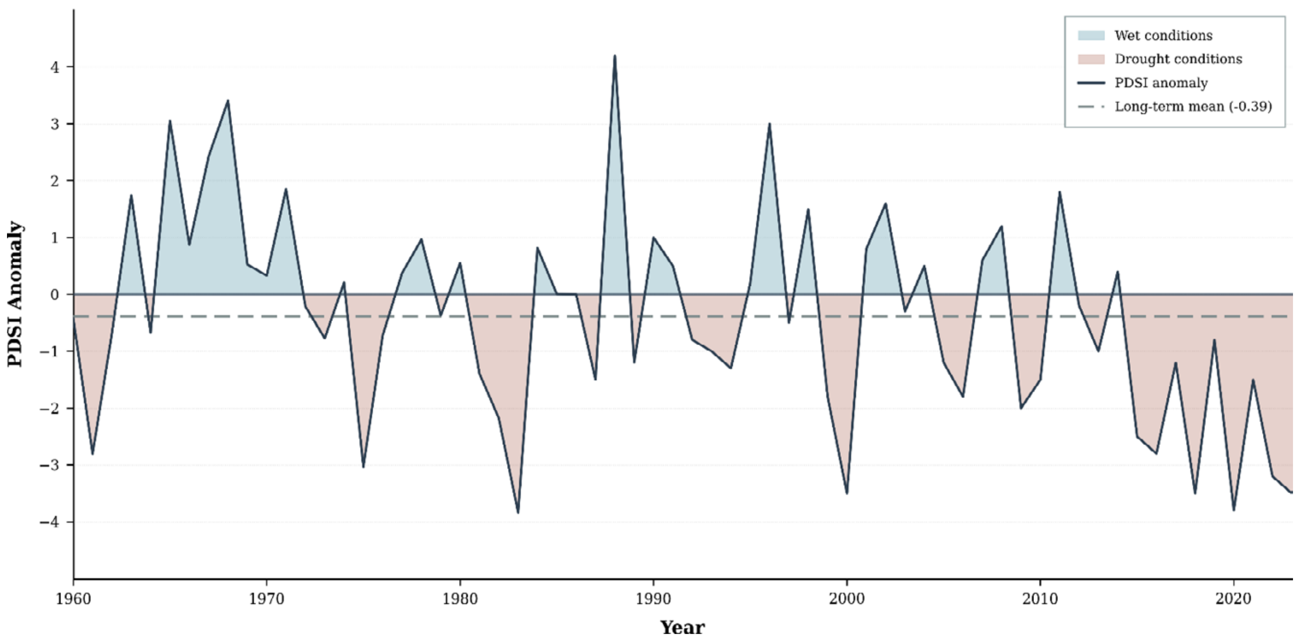

Figure 8. Variation of the Palmer Drought Severity Index (PDSI) between 1970 and 2023, showing long-term trends in drought severity across the study area.

To assess the performance of the TerraClimate satellite itself, we compared spline-with-barriers interpolation based on precipitation data provided by the Drâa-Oued Noun Hydraulic Basin Agency with those derived from satellite observations. This comparison allowed us to calculate a correlation index, which serves as a basis for assessing the accuracy of the data provided by TerraClimate. A high correlation index, on the order of 79% (Figure 9), confirms the reliability of the satellite data. This not only ensures the accuracy of the climate data used in our analyses, but also increases confidence in the

results obtained and their relevance to the assessment drought conditions and climate trends in the Drâa catchment.

Figure 10 illustrates the variations in mean annual precipitation in the Drâa watershed, as determined by "spline with barriers" interpolation using ArcGIS software, between 1960 and 2023. In general, the pattern of oscillations reveals a downward trend in annual precipitation in the watershed over time. There were significant precipitation peaks, with values reaching 244.5 mm in 1967, and 246.5 mm in 1996. In contrast, troughs reflect periods of low precipitation, with minimum values dropping to 85.9 mm in 2023. It is important to note that it has now been 27 years (1996-2023) since the Drâa watershed recorded an average annual rainfall of more than 200 mm. This observation underscores a prolonged downward trend in precipitation levels in the region, reflecting a significant change from previous periods when higher values were common.

With regard to maximum temperatures (Figure 11), an interpolation based on satellite data provided by TerraClimate shows variations in maximum temperatures in the Drâa watershed from 1960 to 2023. The graph derived from this analysis shows a general trend of increasing temperatures over the past several decades. Maximum temperatures have ranged from a low of 25.5°C in 1971 to a high of 30.6°C in 2023. In other words, the region has experienced an average increase of 5°C over the past 52 years. More specifically, in the last two decades, i.e. between 2000 and 2023, the maximum temperature has risen by 3°C, from 27.6°C in 2000 to the peak recorded in 2023. This increasing trend in maximum temperature raises significant concerns about the future impacts of global warming on the watershed. It is crucial to consider how these changes could affect local ecosystems, water resources and living conditions in the region as temperatures continue to rise.

In a third validation step, we applied the Normalized Difference Water Index (NDWI) to the El Mansour Eddahbi reservoir to monitor its spatio-temporal evolution in response to climatic variations (Figure 12). Analysis of the data covering forty years, from 1984 to 2023, reveals the significant influence of rainfall deficits on the reservoir extent. In 1984, following two consecu-

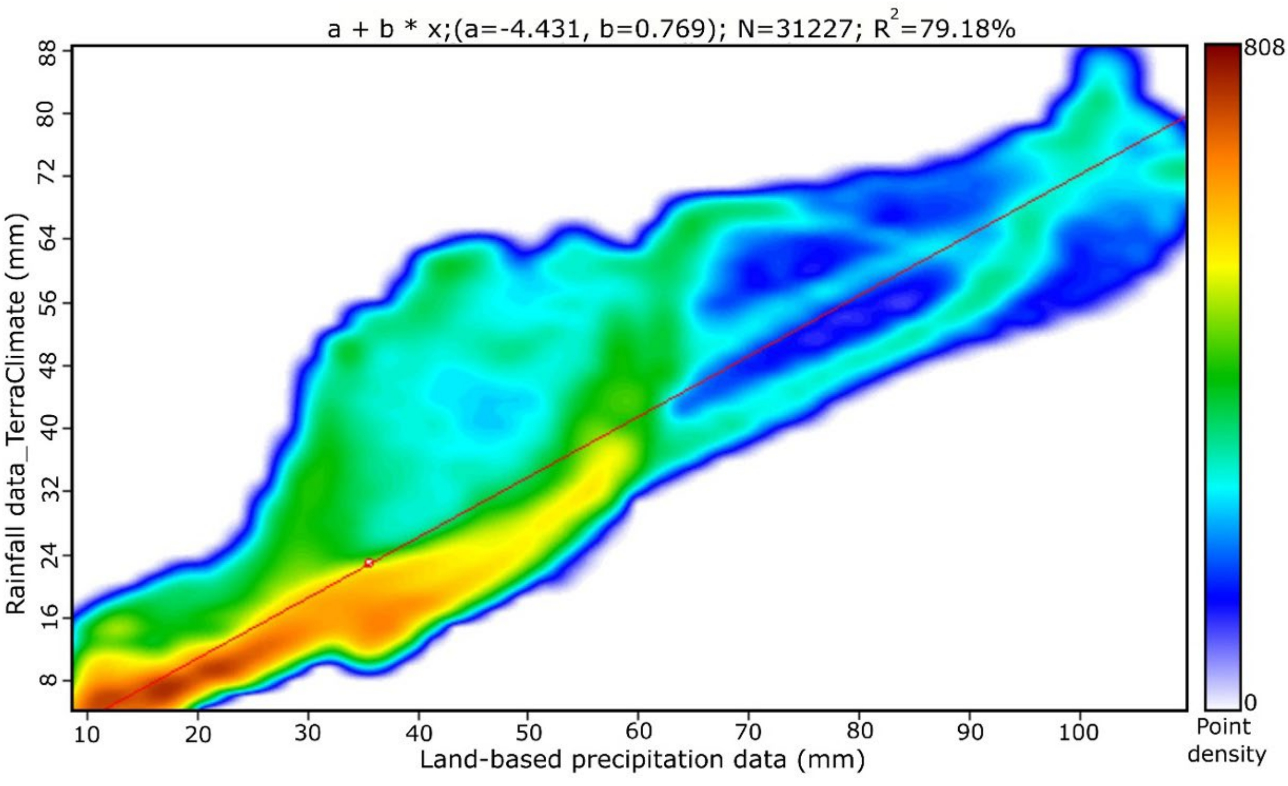

Figure 9. Results of the correlation analysis between TerraClimate precipitation data and ground-based (in-situ) precipitation observations.

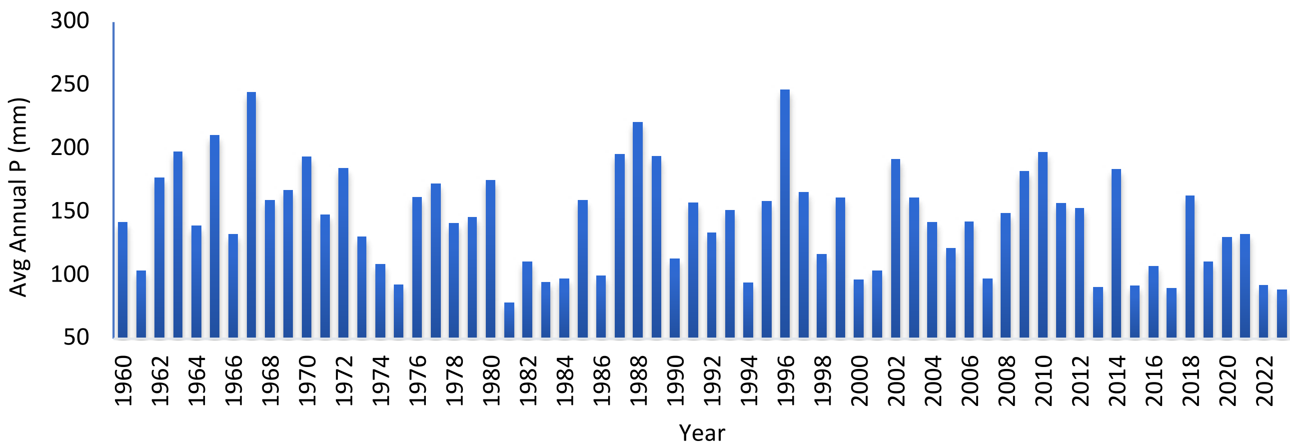

Figure 10. Temporal variation in average annual precipitation in the Drâa Watershed, based on data from ABHDON (2023).

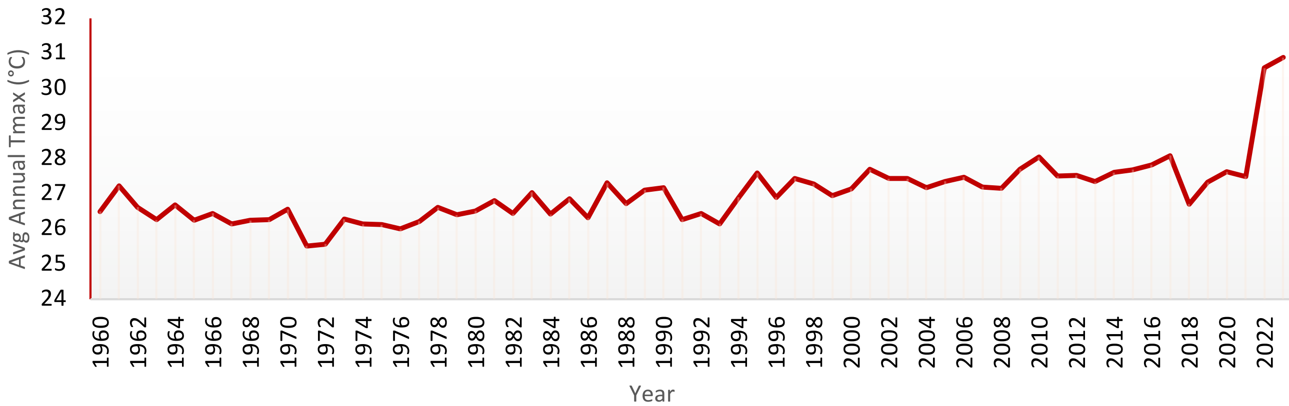

Figure 11. Temporal variation in the annual mean maximum temperatures in the Drâa Watershed, based on TerraClimate data (2023).

tive years of drought, a sharp reduction in the reservoir's water surface area was observed (4,152 km²). By contrast, in 1989, the wettest year of the period according to annual precipitation records, drought indices and vegetation vitality indices saw a substantial increase in reservoir surface area and perimeter (47.39 km² and 157.35 km, respectively). Although wet years became less frequent after 2000, some, such as 2009, still resulted in significant increases in reservoir surface area and perimeter (44.52 km² and 176.07 km, respectively). From that date onwards, the gradual decline in precipitation, combined with rising temperatures and increased evaporation rates, has severely affected water levels. By 2023, the reservoir had shrunk considerably (11 km² in area and 73 km in perimeter), clearly illustrating the devastating effects of drought on the regional water resources. Surface and perimeter variations derived from the NDWI were validated by reservoir volume measurements provided by the Drâa Oued Noun Water Agency, covering the period from dam construction in 1972 to 2023, with a particular focus on key years (Figure 12).

Discussions

Vegetation indices include NDVI and NOAA indices include VCI, TCI and VHI. Although they are based on different measurement principles - NDVI is based on the reflectance of vegetation surfaces, while NOAA indices are based on brightness temperature - these indices ultimately show variations in time and space, with a trend towards a decrease in vegetation cover in recent decades. It is important not to interpret the results of these indices in isolation, as they provide only a partial overview of vegetation health. Vegetation health can be adversely affected not only by periods of drought, but also by flooding. In addition, heavy rainfall combined with extremely low temperatures can also adversely affect vegetation health. It is therefore important to

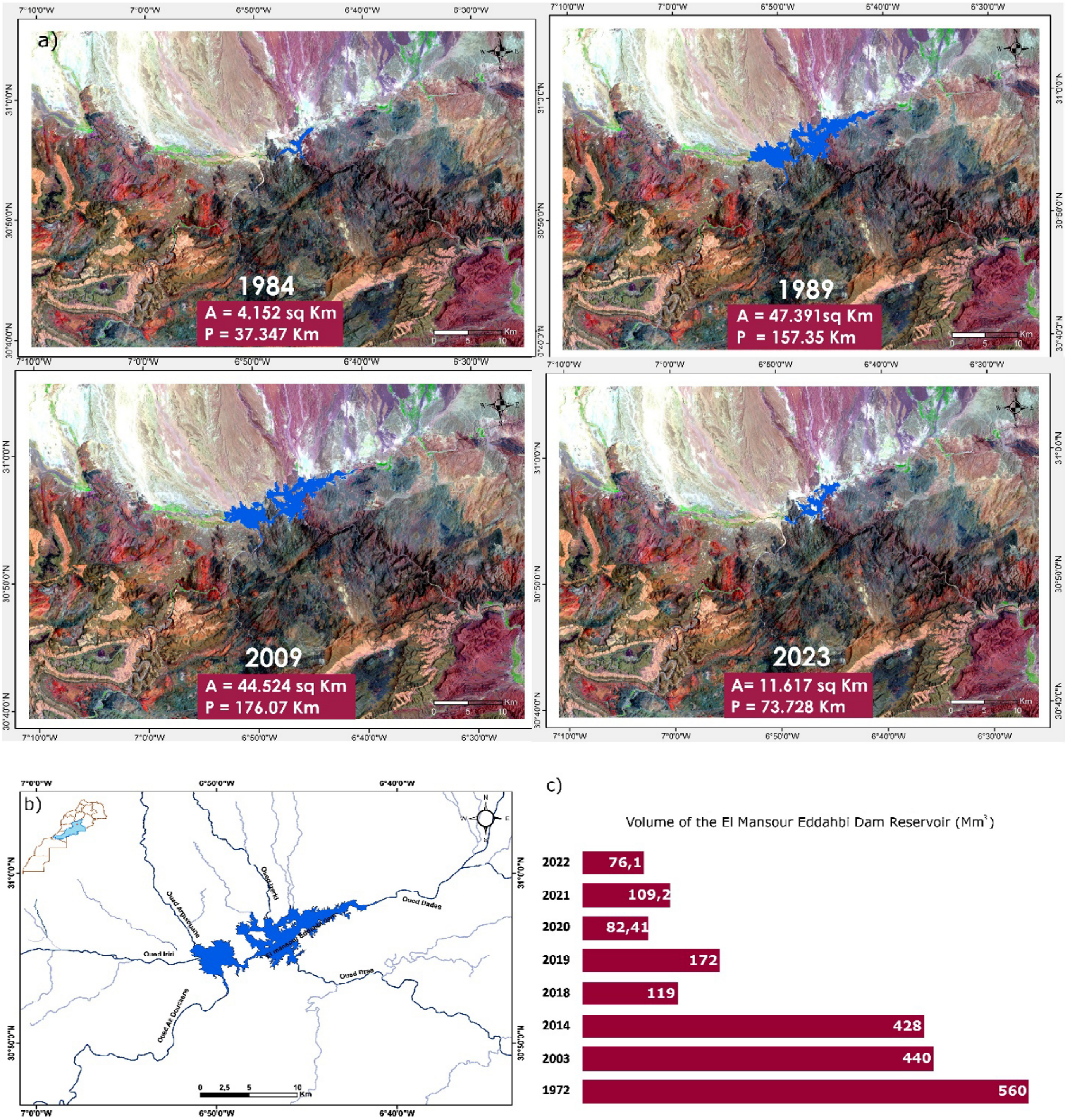

Figure 12. Variation in the water surface area and perimeter of the El Mansour Eddahbi Dam Reservoir between 1984 and 2023 (a); location of the dam in relation to the tributaries of the Upper Drâa (b); variation in the reservoir volume between 1972 and 2022 (c) (ABH-DON, 2022).

complement the analysis of these indices with other information to obtain a complete picture. It should also be emphasized that the indices analyzed refer to vegetation health for only the month of April over the nine years of comparison (1984, 1989, 1994, 1999, 2000, 2004, 2009, 2014, 2019, 2023). April is chosen as the reference month because at this time vegetation growth is most sensitive to environmental conditions. This explains, for example, why the drought indices show a severity in 2014, even though there was significant precipitation in that year (Figures 10). Indeed, this precipitation only occurred in September, November and December, and not during critical vegetation months such as April. Focusing on the variation in VHI index, an index that assesses vegetation health by integrating vegetation conditions, we can observe that the health of the vegetation cover varies according to topography, proximity to the High Atlas, and fluctuations in meteorological parameters. One year is not enough to restore vegetation after three or four consecutive years of drought, even if rainfall increases. In fact, vegetation health has deteriorated from 2009 to 2023, despite some slightly wetter periods between 2014-2015 and 2018-2020. The same trends apply to the NDVI index, except that this index clearly illustrates the progression of desertification over most of the watershed. The ubiquitous green belt (Figure 6) represents the south-facing slope of the High Atlas, with their elevations and relatively favorable climate for crop development.

The results obtained from the SPI and PDSI indices show a strong correlation with variations in precipitation and maximum temperatures. In fact, these indices confirm the trends revealed by the raw climate data (Figures 10 and 11). To illustrate this correlation, it is relevant to look at the years considered the wettest on the basis of high annual precipitation (244.5 mm in 1967, 222.6 mm in 1988 and 246.5 mm in 1996). In fact, the SPI indices for these years are 1.50 in 1967, 2.15 in 1988 and 1.80 in 1996. These high values indicate a period of exceptionally above-average rainfall, confirming the trend towards wetter conditions during these years.

The PDSI is also part of this correlation with variations in raw climatic parameters. To illustrate this correlation, we have analyzed in detail the years most prone to drought, as well as the wettest periods according to the available data. The year 2023, for example, characterized by particularly dry conditions, shows an extremely low PDSI index of -3.50, accompanied by a high average maximum temperature of 30.6°C. This result confirms a severe and persistent drought situation. On the other hand, the year 1971, which records the lowest mean maximum temperature (25.5°C) of the period (1960-2023) and an annual rainfall of 147.8 mm, is associated with a PDSI index of 3.40. This value indicates relatively wet and humid conditions and suggests a low vulnerability to drought this year. The 83% positive correlation between the SPI and PDSI indices (Figure 13), illustrated by the scatterplot and fitted regression line, confirms their strong relationship, indicating that water deficits detected by the SPI are well reflected by the PDSI. PDSI increases when SPI increases, as precipitation is the main variable influencing both indices.

The SPI measures precipitation anomalies directly, so when it is positive, it means that there is an excess of rainfall compared to normal. Since the PDSI also incorporates this precipitation into its calculation, an increase in the SPI generally indicates a recharge of soil moisture, thus reducing water stress and leading to a rise in the PDSI. However, the PDSI responds more slowly to variations in SPI, as it takes into account evapotranspiration and the soil's capacity to retain water, which can dampen or delay its variations compared to the SPI.

The response of surface water bodies to weather conditions is often direct and rapid, particularly in semi-arid environments where water availability is heavily influenced by rainfall variability and evaporation processes. In this context, large reservoirs are highly sensitive indicators of hydroclimatic stress. The El Mansour Eddahbi reservoir, which regulates surface water resources in the Upper Drâa sub-basin, is an essential indicator for assessing the hydrological impacts of drought at the basin scale. The results highlight a close link between climate variability and surface water dynamics, as evidenced by the strong correlation between surface variations derived from NDWI and measured reservoir volumes. Periods characterized by pronounced rainfall deficits lead to a rapid contraction in reservoir extent, reflecting reduced inflows and increased evaporation due to rising temperatures. Conversely, episodic wet years lead to short-lived recoveries in reservoir surface area, illustrating the system's dependence on interannual precipitation variability rather than long-term storage resilience. Overall, the consistency between the NDWI maps and the observed variations in reservoir volume confirms the relevance of remote sensing-based hydrological indices for monitoring surface water dynamics in regions where data are scarce.

Beyond validation objectives, these results highlight the vulnerability of surface water resources in the Drâa basin to prolonged drought conditions and reinforce the importance of further studies in this region for effective water resource management.

CONCLUSION

As part of this study, the results derived from satellite imagery were validated using ground-based data. Today, data availability is no longer a major barrier to studying drought risk over time and space. Thanks to sources such as NOAA and TerraClimate, along with band analysis from satellite images like Landsat, Modis, and others, it is now possible to access essential global parameters. These datasets allow for the calculation of various drought indices, enable correlation

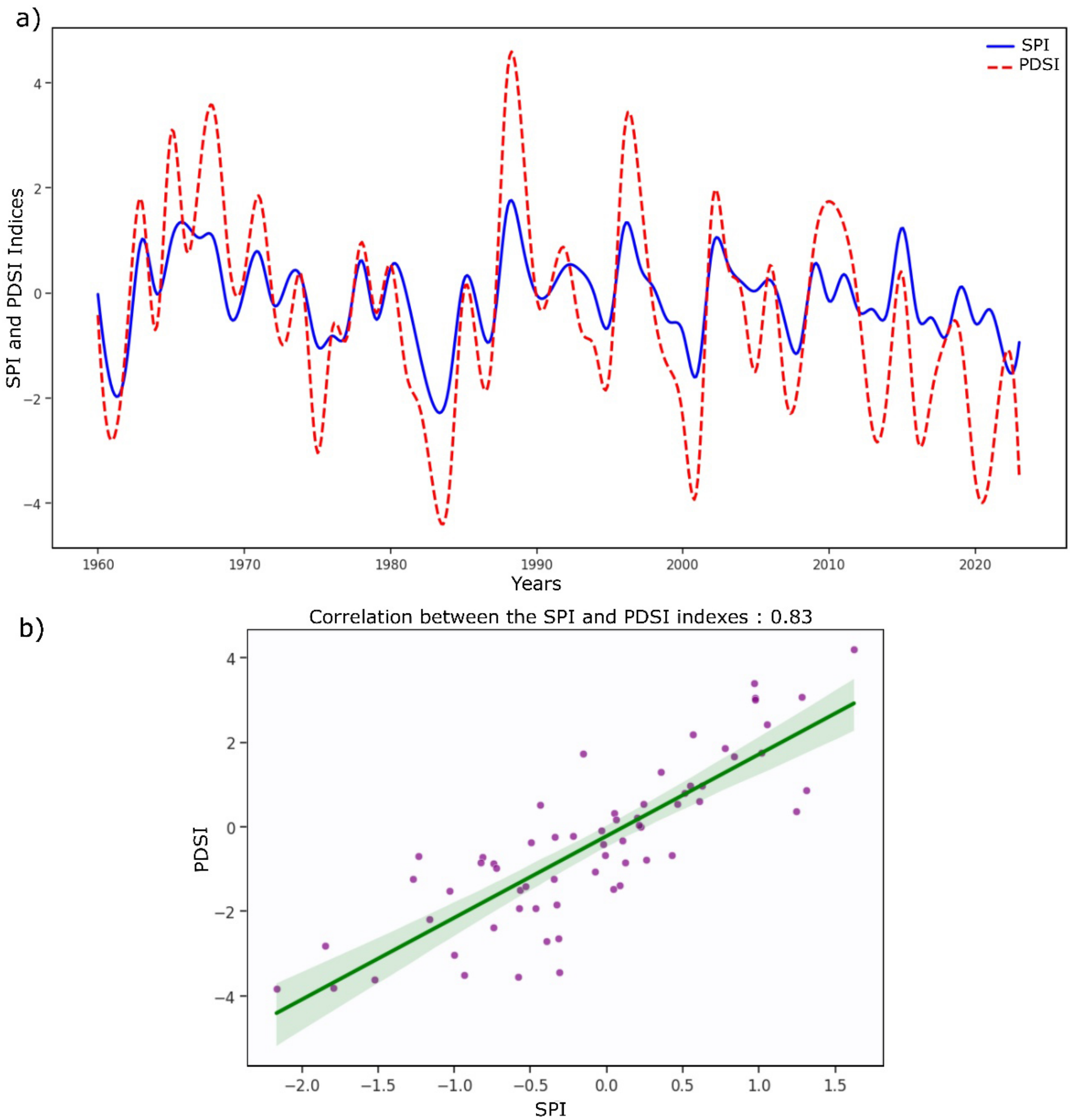

Figure 13. Comparison of the temporal evolution of the Standardized Precipitation Index (SPI) and the Palmer Drought Severity Index (PDSI) from 1960 to 2023 (a), and scatter plot showing the correlation between the SPI and the PDSI values (b).

with observed conditions, and support the development of representative maps illustrating the evolution of climatic situations. The Drâa watershed, like much of Morocco, has long experienced alternating dry and wet periods. However, in recent decades, the frequency of drought years has significantly increased, marked by greater severity and broader spatial extent. The few relatively wet years are no longer sufficient to restore water resources or regenerate vegetation cover. Located in the southern part of Morocco, the Drâa Basin's climatic context makes it particularly vulnerable to meteorological, hydrological, and hydrogeological droughts.

Since the droughts of the 1980s, the region has shown a cyclic pattern of alternating dry and wet seasons, with a recurrence interval of approximately two to three years. Yet, since the 2000s, both the frequency and impact of drought years have intensified, particularly in terms of vegetation loss and declining water availability in the reservoir of the El Mansour Eddahbi dam. This situation is reflected in the variation of several indicators including the Vegetation Condition Index (VCI), Temperature Condition Index (TCI), Vegetation Health Index (VHI), and the Normalized Difference Vegetation Index (NDVI), along with climate-based indices including the Standardized Precipitation Index (SPI), the Palmer Drought Severity Index (PDSI), and the Normalized Difference Water Index (NDWI) applied to the dam reservoir. The interpretation of resulting maps and graphs required an integrated approach, combining advanced remote sensing data with ground observations from hydrological stations across the Drâa watershed, to ensure a coherent and comprehensive analysis. Ultimately, the findings have confirmed that the observed variations closely follow the fluctuations of key climatic parameters—namely, annual average precipitation and average maximum temperatures.

ACKNOWLEDGMENTS

We gratefully acknowledge the invaluable support of all individuals and institutions that contributed to the completion of this study. Particular appreciation is extended to the Centre National pour la Recherche Scientifique et Technique (CNRST), Rabat, Morocco, for its financial support through the "PhD-Associate Scholarship" program. We also wish to thank the Agence du Bassin Hydraulique Drâa-Oued Noun, with special recognition to its Director, Mr. Essanhajy, and hydrogeological engineer, Mr. Aoujil, for their technical assistance and collaboration. We are especially grateful to the Ministère des Relations internationales et de la Francophonie and the Natural Sciences and Engineering Research Council of Canada for their support to the third and fourth authors, respectively.

REFERENCES

Abatzoglou JT, 2013. Development of gridded surface meteorological data for ecological applications and modelling. *International Journal of Climatology*, 33(1): 121–131. https://doi.org/10.1002/joc.3413

Agence du Bassin Hydraulique de Drâa Oued Noun (ABHDON), 2009. *Eaux de surface*. Avenue Mohamed VI, BP 1351, Guelmim, Maroc.

Agence du Bassin Hydraulique de Drâa Oued Noun (ABHDON), 2013. *Eaux de surface*. Avenue Mohamed VI, BP 1351, Guelmim, Maroc.

AghaKouchak A, Cheng L, Mazdiyasni O, Farahmand A, 2014. Global warming and changes in risk of concurrent climate extremes: Insights from the 2014 California drought. *Geophysical Research Letters*, 41(23): 8847–8852. https://doi.org/10.1002/2014GL062308

Agoussine M, Bouchaou L, 2004. Les problèmes majeurs de la gestion de l'eau au Maroc. *Sécheresse*, 15(2): 187–194.

Agoussine M, 2003. Les divers aspects de l'hydrologie en régions arides et semi-arides – cas du sud-est marocain. *Terre & Vie*, Rabat, 70.

Agoussine M, Saidi MEM, Igmoullan B, 2004. Reconnaissance des ressources en eau du bassin d'Ouarzazate (Sud-Est marocain). *Bulletin de l'Institut Scientifique, Rabat, section Sciences de la Terre*, 26: 81–92.

Aït Hamza M, El Faskaoui B, Fermin A, 2010. Les oasis du Drâa au Maroc. *Hommes & Migrations*, 1284: 56–69.

Ait Dhmane L, Saidi ME, Moustadraf J, Rafik A, Hadri A, 2024. Spatiotemporal characterization and hydrological impact of drought patterns in northwestern Morocco. *Frontiers in Water*, 6: 1463748. https://doi.org/10.3389/frwa.2024.1463748

Aksu H, Cetin M, Aksoy H, Yaldiz SG, Yildirim I, Keklik G, 2022. Spatial and temporal characterization of standard duration-maximum precipitation over Black Sea Region in Turkey. *Natural Hazards*, 111(3): 2379–2405. https://doi.org/10.1007/s11069-021-05141-6

Alley WM, 1984. The Palmer Drought Severity Index: Limitations and assumptions. *Journal of Applied Meteorology and Climatology*, 23(7): 1100–1109. https://doi.org/10.1175/1520-0450(1984)023<1100:TPDSIL>2.0.CO;2

Auclair L, 1987. Maroc présaharien: bois de feu et désertification. *Forêt Méditerranéenne*, 9(1): 41–48.

Bentaleb A, 2011. Pompage d'eau et désertification dans la Moyenne Vallée du Draâ: le cas du palmier Mezguita (Maroc). *Insaniyat*, 51–52. https://doi.org/10.4000/insaniyat.1257

Bentaleb A, 2015. Vulnérabilité oasienne: valorisation et développement territorial dans les zones arides marocaines. Cas: Oasis du Drâa moyen. Dans: *XIVe Conférence Internationale Annuelle de l'Intelligence Territoriale "Développement durable des territoires* *vulnérables*”, octobre 2015, Ouarzazate, Maroc. https://halshs.archives-ouvertes.fr/halshs-01741493

Baki S, Hilali M, Kacimi I, Mahboub A, 2017. Caractérisation hydrogéologique et cartographie des ressources en eau dans le bassin versant de l’oued Rhéris (Sud-Est du Maroc). *Bulletin de l’Institut Scientifique, Rabat, Section Sciences de la Terre*, 38: 29–43.

Bashit N, Ristianti N, Ulfiana D, 2022. Drought assessment using remote sensing and geographic information systems (GIS) techniques (Case study: Klaten District). *International Journal of Geoinformatics*, 18(5): 115–127. https://doi.org/10.52939/ijg.v18i5.2393

Bijaber N, El Hadani D, Saidi M, Svoboda MD, Wardlow BD, Hain CR, Poulsen CC, Yessef M, Rochdi A, 2018. Developing a remotely sensed drought monitoring indicator for Morocco. *Geosciences*, 8(2): 55. https://doi.org/10.3390/geosciences8020055

Bijaber N, Rochdi A, Yessef M, El Yacoubi H, 2024. Mapping the structural vulnerability to drought in Morocco. *International Journal of Engineering and Geosciences*, 9(2): 264–280.

Briffa KR, Jones PD, Hulme M, 1994. Summer moisture variability across Europe, 1892–1991: An analysis based on the Palmer Drought Severity Index. *International Journal of Climatology*, 14(5): 475–506. https://doi.org/10.1002/joc.3370140502

Cherkaoui Dekkaki H, 2001. Contribution à l’étude hydrogéologique des nappes alluviales de Fezouata et Ktaoua (Moyenne vallée du Drâa). Mémoire de D.E.S.A., École Mohammadia d’Ingénieurs, Rabat, Maroc.

Choukrani G, Hilali A, Bouri S, 2018. Diagnostic et projection future du changement climatique en zone aride: Cas de la région Marrakech-Safi (Maroc). *Larhyss Journal*, 36: 49–63.

Cook ER, Meko DM, Stahle DW, Cleaveland MK, 1999. Drought reconstructions for the continental United States. *Journal of Climate*, 12(4): 1145–1162. https://doi.org/10.1175/1520-0442(1999)012

Dahan S, 2017. Gestion de la rareté de l’eau en milieu urbain au Maroc. *Banque mondiale*, Washington, DC. https://documents1.worldbank.org/curated/en/488091516133312338/pdf/summary-report.pdf

Direction de la Recherche et de la Planification de l’Eau (DRPE), 2008. Étude d’actualisation du plan directeur d’aménagement intégré des ressources en eau (PDAIRE) du bassin hydraulique du Drâa. Marché n°106/2008/DRPE, Rapport inédit.

El Qorchi F, Yacoubi Khebiza M, Omondi OA, Karmaoui A, Pham QB, Acharki S, 2023. Analyzing temporal patterns of temperature, precipitation, and drought incidents: A comprehensive study of environmental trends in the Upper Drâa Basin, Morocco. *Water*, 15(22): 3906. https://doi.org/10.3390/w15223906

Elair C, Rkha Chaham K, Hadri A, 2023. Assessment of drought variability in the Marrakech-Safi region (Morocco) at different time scales using GIS and remote sensing. *Water Supply*, 23(11): 4592–4624. https://doi.org/10.2166/ws.2023.283

Eyoh A, Okeke F, Ekpa A, 2019. Assessment of the effectiveness of the vegetation condition index (VCI) as an indicator for monitoring drought condition across the Niger Delta region of Nigeria using AVHRR/MODIS NDVI. *European Journal of Earth and Environment*, 6(1).

Gumus V, El Moçayd N, Seker M, Seaid M, 2024. Future projection of droughts in Morocco and potential impact on agriculture. *Journal of Environmental Management*, 367: 122019. https://doi.org/10.1016/j.jenvman.2024.122019

Hadri A, Saidi MEM, El Khalki EM, Aachrine B, Saouabe T, Elmaki AA, 2022. Integrated water management under climate change through the application of the WEAP model in a Mediterranean arid region. *Journal of Water and Climate Change*, 13(6): 2414–2442. https://doi.org/10.2166/wcc.2022.039

Hadria R, Boudhar A, Ouatiki H, Lebrini Y, Elmansouri L, Gadouali F, Hayat Lionboui HL, Benabdelouahab T, 2019. Combining use of TRMM and ground observations of annual precipitations for meteorological drought trends monitoring in Morocco. *American Journal of Remote Sensing*, 7(2): 25. https://doi.org/10.11648/j.ajrs.20190702.11

Hao Z, Singh VP, 2015. Drought characterization from a multivariate perspective: A review. *Journal of Hydrology*, 527: 668–678. https://doi.org/10.1016/j.jhydrol.2015.05.031

Houmma H, Ismaguil I, Gadal S, El Mansouri L, Garba M, Gbetkom PG, Mamane Barkawi MB, Hadria R, 2023. A new multivariate agricultural drought composite index based on random forest algorithm and remote sensing data developed for Sahelian agrosystems. *Geomatics, Natural Hazards and Risk*, 14(1): 2223384. https://doi.org/10.1080/19475705.2023.2223384

Justice CO, Vermote E, Townshend JRG, Defries R, Roy DP, Hall DK, Salomonson VV, Privette JL, Riggs G, Strahler A, Lucht W, Myneni RP, Knyazikhin Y, Running SW, Nemani RR, Wan Z, Huete AR, van Leeuwen W, Wolfe RE, Giglio L, Muller J-P, Lewis P, Barnsley MJ, 1998. The Moderate Resolution Imaging Spectroradiometer (MODIS): Land remote sensing for global change research. *NASA Publications*, 28. https://digitalcommons.unl.edu/nasapub/28

Kim J-S, Park S-Y, Lee J-H, Chen J, Chen S, Kim T-W, 2021. Integrated drought monitoring and evaluation through multi-sensor satellite-based statistical simulation. *Remote Sensing*, 13(2): 272. https://doi.org/10.3390/rs13020272

Kogan FN, 1990. Remote sensing of weather impacts on vegetation in non-homogeneous areas. *International Journal of Remote Sensing*, 11(8): 1405–1419. https://doi.org/10.1080/01431169008955102

Kogan FN, 1997. Global drought watch from space. *Bulletin of the American Meteorological Society*, 78(4): 621–636. https://doi.org/10.1175/1520-0477(1997)078

Kogan FN, Sullivan J, 1993. Development of global drought-watch system using NOAA/AVHRR data. *Advances in Space Research*, 13(5): 219–222. https://doi.org/10.1016/0273-1177(93)90548-P

Lahbous M, Touzani L, Ousidahou A, 2023. La sécheresse et son impact sur l'économie marocaine. *La Revue d'économie et d'environnement*, 3(2): 20–42. https://revuecoenvi.org/index.php/laree/article/view/28

Layelmam M, 2015. Calcul des indicateurs de sécheresse à partir des images NOAA/AVHRR. Rapport de recherche, IAV, CRTS, CRASTE-LF. https://hal.archives-ouvertes.fr/hal-00915461

Lebdi F, Maki A, 2023. La sécheresse au Maghreb: diagnostic, impacts et perspectives pour le renforcement de la résilience du secteur agricole. Tunis: FAO. https://doi.org/10.4060/cc7126fr

Ji L, Peters AJ, 2003. Assessing vegetation response to drought in the northern Great Plains using vegetation and drought indices. *Remote Sensing of Environment*, 87(1): 85–98. https://doi.org/10.1016/S0034-4257(03)00174-3

Li J, Zhou S, Hu R, 2016. Hydrological drought class transition using SPI and SRI time series by loglinear regression. *Water Resources Management*, 30(2): 669–684. https://doi.org/10.1007/s11269-015-1184-7

Liu W, Kogan FN, 2002. Monitoring Brazilian soybean production using NOAA/AVHRR based vegetation condition indices. *International Journal of Remote Sensing*, 23: 1161–1179.

McFeeters SK, 1996. The use of the normalized difference water index (NDWI) in the delineation of open water features. *International Journal of Remote Sensing*, 17(7): 1425–1432. https://doi.org/10.1080/01431169608948714

McKee TB, Doesken NJ, Kleist J, 1993. The relationship of drought frequency and duration to time scales. Dans: *Proceedings of the 8th Conference on Applied Climatology*, 179–186. American Meteorological Society.

McKee TB, Doesken NJ, Kleist J, 1995. Drought monitoring with multiple time scales. Dans: *Proceedings of the 9th Conference on Applied Climatology*, 233–236. American Meteorological Society, Dallas, TX.

Mehdaoui R, Mili EM, Seghir A, 2018. Caractérisation à l'aide du SPI de la sécheresse climatique dans le bassin versant de Ziz (Sud-Est, Maroc). *European Scientific Journal*, 14(21): 177–194.

Ouysse S, Laftouhi N-E, Tajeddine K, 2010. Impact of climate variations on water resources in the Drâa basin (Morocco): Correlation between precipitation and evapotranspiration variability in the Drâa basin. Dans: *Proceedings of the International Conference on Participatory and Integrated Management of Water Resources in Arid Zones (GIRE3D)*, Ouarzazate, Morocco.

Palmer WC, 1965. Meteorological drought. Office of Climatology Research Paper No. 45. Washington DC: US Weather Bureau.

Rouse JW, Haas RH, Schell JA, Deering DW, 1973. Monitoring vegetation systems in the Great Plains with ERTS (Earth Resources Technology Satellite). Dans: *Proceedings of 3rd Earth Resources Technology Satellite Symposium*, Greenbelt, MD, USA, décembre 10–14, pp. 309–317.

Sadiki A, Hanchane M, 2024. Apport des SIG et de la télédétection dans le suivi et la cartographie du lac de barrage Mansour Eddahbi (Sud-Est du Maroc). *Espaces, Revue de Géographie*, (11-12): 19–25.

Saouabe T, Naceur KA, El Khalki EM, Hadri A, Saidi ME, 2022. GPM-IMERG product: A new way to assess the climate change impact on water resources in a Moroccan semi-arid basin. *Journal of Water and Climate Change*, 13(7): 2559–2576. https://doi.org/10.2166/wcc.2022.403

Schulz W, 2004. Reconstructing mediatization as an analytical concept. *European Journal of Communication*, 19(1): 87–101. https://doi.org/10.1177/0267323104040696

Schulz O, Busche H, Benbouziane A, 2008. Decadal precipitation variances and reservoir inflow in the semiarid Upper Drâa Basin (South-Eastern Morocco). Dans: Zereini F, Hötzl H (éds). *Climatic Changes and Water Resources in the Middle East and North Africa*, Environmental Science and Engineering, pp. 165–178. Springer, Berlin, Heidelberg. https://doi.org/10.1007/978-3-540-85047-2_13

Scian B, Donnari M, 1997. Retrospective analysis of the Palmer Drought Severity Index in the semi-arid

Pampas region, Argentina. *International Journal of Climatology*, 17(3): 313–322. https://doi.org/10.1002/(SICI)1097-0088(19970315)17:3<313::AID-JOC112>3.0.CO;2-W

Seiler RA, Kogan F, Sullivan J, 1998. AVHRR-based vegetation and temperature condition indices for drought detection in Argentina. *Advances in Space Research*, 21(3): 481–484. https://doi.org/10.1016/S0273-1177(97)00884-3

Serbouti I, Chenal J, Pradhan B, Diop EB, Azmi R, Abdem SAE, Adraoui M, Hlal M, Bounabi M, 2024. Assessing the impact of agricultural practices and urban expansion on drought dynamics using a multi-drought index application implemented in Google Earth Engine: A case study of the Oum-Er-Rbia watershed, Morocco. *Remote Sensing*, 16: 3398. https://doi.org/10.3390/rs16183398

Stour L, Agoumi A, 2008. Climatic drought in Morocco during the last decades. *Hydroécologie Appliquée*, 16: 215–232.

Wang Q, Shi P, Lei T, Geng G, Liu J, Mo X, Li X, Zhou H, Wu J, 2015. The alleviating trend of drought in the Huang-Huai-Hai Plain of China based on the daily SPEI. *International Journal of Climatology*, 35(13): 3760–3769. https://doi.org/10.1002/joc.4244

Waroux YLP, 2013. Dégradation environnementale et développement économique dans l'arganeraie d'Aoulouz (Maroc). *Sécheresse*, 24(1): 29–38.

Weber B, 2004. Untersuchungen zum Bodenwasserhaushalt und Modellierung der Bodenwasserflüsse entlang eines Höhen- und Ariditätsgradienten (SE Marokko). Thèse de doctorat.

Wilhite DA, 2000. Drought planning and risk assessment: status and future directions. *Annals of Arid Zone*, 39: 211–230.

Wilhite, D. A., Sivakumar, M. V. K., & Wood, D. A. (Eds.). (2000). Early Warning Systems for Drought Preparedness and Drought Management. Proceedings of the Expert Group Meeting, Lisbon, Portugal, 5–7 September 2000. Geneva, Switzerland: World Meteorological Organization (WMO).

World Meteorological Organization (WMO), 2012. Standardized precipitation index user guide (M. Svoboda, M. Hayes, & D. Wood). WMO-No. 1090. Genève: WMO. https://library.wmo.int/viewer/31481/download?file=wmo_1090_fr.pdf&navigator=1&type=pdf

Zhang A, Jia G, 2013. Monitoring meteorological drought in semiarid regions using multi-sensor microwave remote sensing data. *Remote Sensing of Environment*, 134: 12–23. https://doi.org/10.1016/j.rse.2013.02.023

Zkhiri W, Tramblay Y, Hanich L, Jarlan L, Ruelland D, 2018. Spatiotemporal characterization of current and future droughts in the High Atlas basins (Morocco). *Theoretical and Applied Climatology*, 135(1-2): 593–605. https://doi.org/10.1007/s00704-018-2388-6

Italian Journal of Agrometeorology
Rivista Italiana di Agrometeorologia

Firenze University Press
https://riviste.fupress.net/index.php/IJAm

OPEN ACCESS

Citation: Kaida, A., Aitdada, A., El Afou, Y. & Ait Msaad, A. (2026). Development of a Fuzzy Logic Controller for microclimate regulation under an agricultural greenhouse based on a state-space model approach. *Italian Journal of Agrometeorology* (1): 41-57. doi: 10.36253/ijam-3502

Received: May 17, 2025

Accepted: February 10, 2026

Published: September 15, 2026

Data Availability Statement: All relevant data are within the paper and its Supporting Information files.

Competing Interests: The Author(s) declare(s) no conflict of interest.

ORCID:
AK: 0009-0001-4740-2520
YEA: 0000-0002-1607-7032

Development of a Fuzzy Logic Controller for microclimate regulation under an agricultural greenhouse based on a state-space model approach

Abderrazak Kaida[1,*], Abderrahman Aitdada[1], Youssef El Afou[2], Abdelouahad Ait Msaad[1]

[1] Sidi Mohammed Ben Abdellah University, Higher School of Technology of Fez, Imouzzer Road, Fez, BP 2427, Morocco
[2] Sidi Mohamed Ben Abdellah University, National School of Applied Sciences, Imouzzer Road, Fez, BP 30040, Morocco
*Corresponding author. Email: abderrazak.kaida@usmba.ac.ma

Abstract. Greenhouse management is a fundamental aspect of modern agriculture, as it directly affects crop quality, water efficiency, and energy consumption. This study focuses on the regulation of key greenhouse climatic parameters, namely indoor temperature and relative humidity. A dynamic greenhouse model was developed to implement and compare two control strategies: a Fuzzy Logic Controller (FLC) and a Proportional–Integral–Derivative (PID) controller. The main objective of this work is to design a controller capable of simultaneously managing two highly correlated variables by adopting variable setpoints for both temperature and humidity. This approach distinguishes the proposed methodology from previous studies, which typically focused on temperature control while maintaining constant humidity setpoints. In contrast, the proposed strategy regulates both parameters dynamically and concurrently. Simulation results under different operating scenarios show that the FLC outperforms the PID controller in maintaining a favorable greenhouse microclimate. In particular, the FLC achieved reductions of 25.1% in average humidification rate and 29.6% in ventilation rate. Moreover, the total energy consumption associated with the PID controller was approximately 27% higher than that of the FLC. The error analysis between reference setpoints and simulated responses confirms that the dynamic model accurately predicts indoor temperature and relative humidity with minimal deviation. Overall, the results demonstrate the robustness and efficiency of the FLC in ensuring optimal greenhouse climatic conditions while significantly reducing energy consumption.

Keywords: state-space model, Fuzzy Logic Controller, PID controller, humidity, temperature, greenhouse.

1. INTRODUCTION

The greenhouse industry is among the fastest-growing sectors in modern agriculture due to its ability to protect crops from adverse external conditions and to enable precise manipulation of the cultivation environment. By creating a controlled microclimate, greenhouses the production of crops that are not feasible in open-field conditions, resulting in higher yields, extended production periods, improved crop quality, and reduced pesticide use. Consequently, greenhouse crops exhibit a significantly higher added value per unit area compared to open-field agriculture (Farvardin et al. 2024; Jeevan Nagendra Kumar et al. 2024).

To fully benefit from these advantages and extend the growing season, it is essential to maintain optimal greenhouse microclimatic conditions (Abbood et al. 2023; Wang et al. 2024). This requires accurate regulation of key climatic parameters through actuators such as heating systems, humidifiers, and ventilation fans (Adrian et al. 2019). In this context, the availability of a dynamic greenhouse model capable of accurately describing the temporal evolution of indoor climate variables is crucial for control design and performance evaluation (Blasco et al. 2007; Guo et al. 2021). Dynamic modeling allows representing the temporal variations of the climatic parameters in the greenhouse(Choab et al. 2019; Shamshiri et al. 2020).

Many agricultural greenhouses are still manually regulated, requiring the grower's assistance. But some have implemented smart control devices. (EL AFOU et al. 2015; El AFOU et al. 2018) Among the various climatic variables, indoor air temperature and relative humidity are considered the most influential and measurable parameters affecting plant growth (Körner 2015). There are also other important climatic factors such as: evaporation, wind speed, CO2 content, lights(Franklin 2009)(Chand Singh et al. 2018). Temperature plays a fundamental role in plant physiological processes, while relative humidity directly influences transpiration, disease development, and overall plant health (Wahid et al. 2007;(Penfield 2008) ;Lipiec et al. 2013). These two variables are strongly coupled, meaning that variations in one significantly affect the other, which makes their simultaneous regulation challenging(Chen et al. 2023). As a result, the greenhouse climate system is typically modeled as a Multi-Input Multi-Output (MIMO) system (Tao 2014).

Despite the widespread use of conventional control strategies such as Proportional–Integral–Derivative (PID) controllers, their performance is often limited by the nonlinear and coupled nature of greenhouse climate dynamics. Furthermore, PID-based approaches may lead to increased energy consumption, particularly during heating and ventilation processes. To overcome these limitations, advanced control techniques have been proposed, including Fuzzy Logic Controllers (FLCs), which are well suited to handling nonlinear systems and uncertain dynamics while improving energy efficiency (El Ghoumari et al. 2005; Bennis et al. 2008; Márquez-Vera et al. 2016;Yang and Zhang 2024).

Previous studies have primarily focused on temperature control using variable setpoints while maintaining constant relative humidity references(Huang et al. 2024; Riahi et al. 2024). In contrast, the present work proposes a control strategy that simultaneously regulates indoor temperature and relative humidity using variable setpoints for both parameters within a dynamic greenhouse model. The proposed approach is evaluated under different operating scenarios, including seasonal variations and external climatic disturbances, to assess its robustness and energy efficiency.

The main contribution of this study lies in the development and comparative evaluation of a Fuzzy Logic Controller and a PID controller for greenhouse climate control. By adopting variable setpoints for both temperature and relative humidity, the proposed strategy provides a more realistic and adaptive approach to greenhouse microclimate management while aiming to reduce energy consumption and improve overall control performance. The present study introduces variable setpoints for both temperature and relative humidity under diverse climatic scenarios, including:

- Different setpoint values;
- Distinct seasonal conditions that generate varying external disturbances in temperature and humidity;
- Simulations conducted over four days during the spring season (April) with a sampling time of 5 seconds, and a second simulation extending over one week during the autumn season (September). The key innovation of this work lies in the ability to simultaneously regulate temperature and relative humidity using variable setpoints, thereby providing a more realistic and adaptable control approach for greenhouse climate management.

The proposed model was experimentally validated using real meteorological data collected during two key periods: one corresponding to the spring season and another to the autumn season. The selection of these two seasons is motivated by the strong correlation between temperature and relative humidity, which makes the simultaneous control of these parameters more complex and therefore represents a significant challenge.

In contrast, during the summer season, which is characterized by a sustained increase in temperature, the control strategy mainly focuses on temperature regulation. Similarly, the winter season is marked by high relative humidity levels, allowing the control process to primarily target humidity regulation. Consequently, spring and autumn conditions constitute the most demanding scenarios for evaluating the performance and robustness of the proposed control model.

This article is structured as follows: Section 1 is dedicated to the presentation of the greenhouse model system and the input parameters. Section presents the controls used, which are the dynamic PID controller and the fuzzy logic controllers (FLC): we used 2 blocks of the controllers, one for temperature and the other for humidity. A discussion on the measurement and simulation results as well as the comparison between the two controllers are presented in Section 4. Then, the internal temperature and humidity is simulated using MATLAB software. The perspectives and conclusion are discussed in the last part.

2. MATERIALS AND METHODS

In this study, a physical model of temperature and relative humidity is employed, as it adequately describes the behavior of these variables in a real greenhouse. It is assumed that the air inside the greenhouse is uniformly distributed. Heating, ventilation systems and humidifiers, and other switching devices provide the control inputs. External environmental factors, including sun radiation, relative humidity, and air temperature, are considered as disturbance inputs. The feedback effects of crop growth on temperature are neglected.

2.1. Greenhouse model

Maintaining the greenhouse under optimal operating conditions throughout the different phases of crop growth requires an understanding of the greenhouse microclimate and its characteristics(Bhujel et al. 2020). Since these factors have a major impact on the greenhouse energy and mass balances, accurate estimation of solar radiation, mass transfer coefficients, and heat transfer coefficients is essential for developing a reliable physical model(Choab et al. 2019; Kadirov et al. 2023).

In this work, we adopt a dynamic greenhouse model proposed by (Kaida et al. 2024),which considers two kinds of input data:

- The disturbances (external climate variables): external relative humidity, external temperature, solar radiation.
- Actuators (controls): humidification system, ventilation and heating system.

The expressions of the internal heat balance and internal water balance equations are given in Eq. (1) and Eq. (2), respectively. The resulting model is a multi-input / multi-output (MIMO) system, which can be described as follows:

$$\frac{dT_{\text{int}}}{dt} = \frac{1}{\rho_{air}.C_{air}.V_{gr}}(Q^{Heater} + R - \frac{10}{36}\lambda.H^{Hum}) + \frac{V_{v,m}}{V_{gr}}.(T_{\text{int}} - T_{ext}) - \frac{UA}{\rho_{air}.C_{air}.V_{gr}}(T_{\text{int}} - T_{ext}) \tag{1}$$

$$\frac{dH_{\text{int}}}{dt} = \frac{1}{\rho_{air}.V_{gr}}H^{Hum} + \frac{1}{\rho_{air}.V_{gr}}\frac{\alpha}{\lambda}R + \frac{V_{v,m}}{\rho_{air}.V_{gr}}(\mathrm{H}_{\text{ext}} - H_{\text{int}}) - \frac{1}{\rho_{air}.V_{gr}}\beta_T.H_{\text{int}} \tag{2}$$

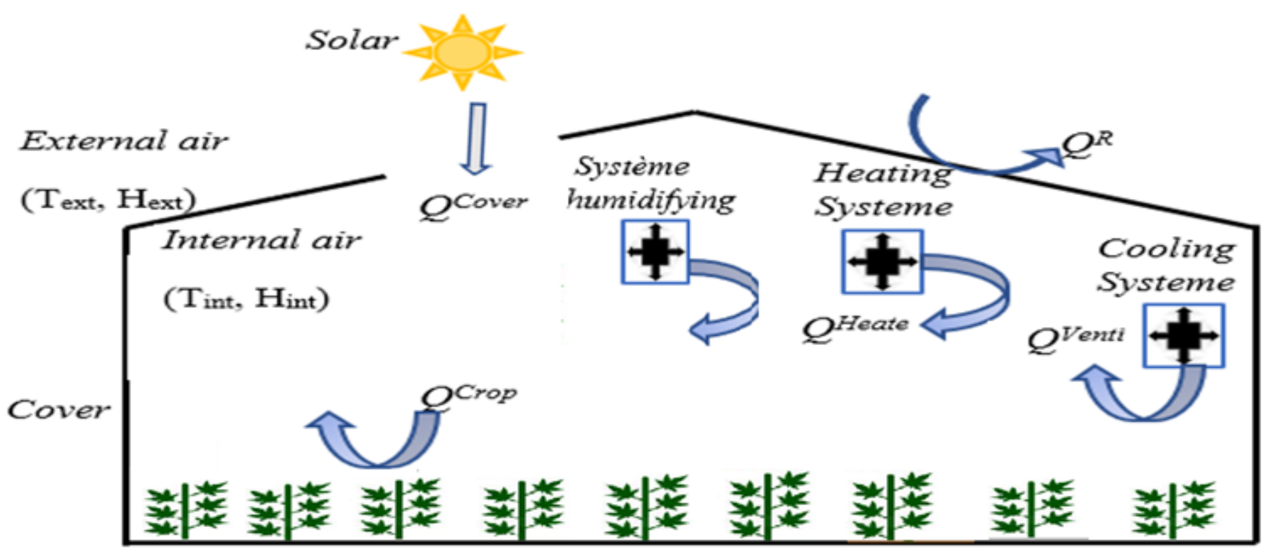

Figure 1. The interaction between greenhouse components and heat transmission.

with:
ρ_{air} : Air density [kg.m-3].
$C_{air:}$ Specific heat capacity of air [J.kg^{-1}. K^{-1}].
Vgr: Greenhouse volume (m^3)
$V_{v,m}$: Ventilation airflow rate (m^3/s).
The variables T_{ext}, H_{ext} and R represent disturbances outside the greenhouse which determine the atmospheric influence on T_{int} and H_{int}.
Q^{Heater}, $V_{v,\,m}$ and H^{Hum}: are commands for the heater, ventilation, and humidifying system respectively.
T_{int}: The output of indoor temperature
H_{int}: The output of indoor relative humidity.

Modern control theory of dynamical systems relies heavily on the concept of state and its associated state-space representation. For nonlinear systems, this representation is commonly expressed in the form of Eq. (3) (Fliess et al. 2004). Accordingly, the proposed greenhouse model can be described by the following system of equations :

$$\begin{cases} \dot{X} = f(\mathrm{X}) + \sum_{i=1}^{m} g_i(\mathrm{X}).U_i \\ y = h(\mathrm{X}) \end{cases} \tag{3}$$

with:
X € R^n : state vector, U € R^m : controls inputs, y € R^p : outputs

After identifying the state, input, disturbance, and output variables, the greenhouse climate can be described by a nonlinear, strongly coupled state-space model. The indoor air temperature and relative humidity are selected as the state variables and are denoted by the dynamic states $X_1(t)$ and $X_2(t)$, respectively. For summer operating conditions, the heating power is set to zero ($Q^{Heater} = 0$). Consequently , the control inputs of the system are defined as the ventilation rate and the humidity generation rate provided by the fogging system, denoted by $U_1(t)$ and $U_2(t)$, respectively. The external disturbances acting on the greenhouse are the solar radiation heat transfer rate $V_1(t)$, the outside air temperature $V_2(t)$, and the outside relative humidity V_3 (t). All state variables, control inputs and disturbances are summarized as follows:

$$X = \begin{bmatrix} X_1 \\ X_2 \end{bmatrix} = \begin{bmatrix} T_{int} \\ H_{int} \end{bmatrix}$$

$$U = \begin{bmatrix} U_1 \\ U_2 \end{bmatrix} = \begin{bmatrix} V_{v,m} \\ H^{Hum} \end{bmatrix}$$

$$V= \begin{bmatrix} V_1 \\ V_2 \\ V_3 \end{bmatrix} = \begin{bmatrix} R \\ T_{ext} \\ H_{ext} \end{bmatrix}$$

So, we can express Eq. (1) and Eq. (2) in the following form:

$$\frac{dX_1}{dt} = \frac{1}{\rho_{air}.C_{air}.V_{gr}}\left(V_1 - \frac{10}{36}\lambda.U_2\right) + \frac{U_1}{V_{gr}}.\left(X_1 - V_2\right) - \frac{UA}{\rho_{air}.C_{air}.V_{gr}}\left(X_1 - V_2\right) \tag{4}$$

$$\frac{dX_2}{dt} = \frac{1}{\rho_{air}.V_{gr}}U_2 + \frac{\alpha}{\rho_{air}.V_{gr}.\lambda}V_1 + \frac{U_1}{\rho_{air}.V_{gr}}\left(V_3 - X_2\right) - \frac{\beta_T}{\rho_{air}.V_{gr}}X_2 \tag{5}$$

We based on these two Eq. (4) and Eq. (5) for writing the state representation of our system in the form of Eq. (3) and we obtained the following result:

$$\begin{bmatrix} \dot{X}_1 \\ \dot{X}_2 \end{bmatrix} = \begin{bmatrix} f_1(X,V) \\ f_2(X,V) \end{bmatrix} + \frac{1}{\rho_{air}.V_{gr}} \begin{pmatrix} (X_1 - V_2)\rho_{air} & -\frac{10\lambda}{36C_{air}} \\ (V_3 - X_2) & 1 \end{pmatrix} \begin{bmatrix} U_1 \\ U_2 \end{bmatrix} \tag{6}$$

with:

$$f_1(\mathrm{X,V}) = -\frac{UA}{\rho_{air}.C_{air}.V_{gr}}\mathrm{X}_1 + \frac{1}{\rho_{air}.C_{air}.V_{gr}}\mathrm{V}_1 + \frac{UA}{\rho_{air}.C_{air}.V_{gr}}V_2$$ and

$$f_2(\mathrm{X,V}) = -\frac{\beta_T}{\rho_{air}.V_{gr}}X_2 + \frac{\alpha}{\rho_{air}.V_{gr}.\lambda}V_1$$

Our greenhouse has a volume of V_{gr} = 4000 m^3 (20 x 20 x10) and the cover reduces the sunshine by 60%, the heat transfer coefficient UA = 25 kW.K^{-1}, and the air density ρ_{air} =1.2 Kg.m^{-3} with specific heat C_{air} = 1006 j .Kg^{-1}.K^{-1}. These inputs parameters are summarized in the following Table 1. (Kaida et al. 2024).

A number of plants generate heat; their temperature can exceed 40°C above that of the surrounding air. Consequently, at thermal equilibrium, the heat generated by plants is often ignored in relation to the heating system generator and within a large greenhouse. (Lamprecht et al.).

2.2. The Proportional Integral Derivative (PID)

The Proportional Integral Derivative (PID) is a control mechanism used to perform closed-loop regulation of an industrial system. It is the most widely used regulator in the industry and allows for the control of a large number of processes. The observed error is the difference between the setpoint and the measurement. The PID controller allows for three actions based on this error:

1. Proportional: the error is multiplied by a gain G.
2. Integral: the error is integrated over a time interval ss and then divided by a gain Ti.
3. Derivative: the error is differentiated with respect to time ss and then multiplied by a gain Td.

Table 1. The values of the inputs that were employed in the simulation.

Symbol	Numerical value	Units	Description
UA	25000	$W.K^{-1}$	The coefficient of heat transfer of the cover
V_{gr}	4000	m^{-3}	Volume of the greenhouse
ρ	1.2	$Kg.m^{-3}$	Density of internal air
C_{air}	1006	$J. Kg^{-1}. K^{-1}$	Specific heat of air
R	700	W	The heat produced by the Solar radiation

There are several possible architectures to combine these three effects (series, parallel, or mixed).

Tuning a PID controller involves determining the parameters G, Td and Ti in order to achieve a satisfactory control and regulation performance(Paolino et al. 2024). The main objectives are robustness, fast dynamic response,and high accuracy. To meet these requirements, overshoot(s) must be minimized (Schiavo et al. 2021).

For the summer operation, (Q^{Heater} =0) the greenhouse model has two control inputs: ventilation and humidification system. Two PID controllers are employed, one for indoor air temperature control and one for relative humidity regulation. The overall control architecture is implemented in MATLAB/Simulink and illustrated in Fig. 2.

The coefficients G, Td et Ti of the PID controller of the indoor relative humidity and indoor temperature are given in Table 2.

Table 2. Coefficients of Proportional Integral Derivative (PID) controllers used in the two blocks

Coefficients of PID controllers	Indoor temperature	Indoor relative humidity
Proportional (G)	0.0567	338.775
Integral (Ti)	0.0002	9.435
Derivative (Td)	1.6660	1163.453

2.3. Fuzzy Logic Controller

A Fuzzy Logic Controller (FLC) is a control system that mimics human reasoning by using fuzzy rules instead of precise mathematical formulas. It is particularly useful for managing complex systems where it is difficult to establish precise equations. A fuzzy controller is composed of three blocks: fuzzification, inference, and defuzzification as shown in Fig. 3.

› Fuzzification: transforming real input variables into fuzzy variables (also called linguistic variables).

› Fuzzy inference: constructing rules (and results) based on linguistic variables, assigning a truth value to each rule, and then aggregating the rules to obtain a single (linguistic) result to decide the action to take.

› Defuzzification: transforming the fuzzy output into a precise value usable by the system. For the defuzzification method, we used the Center of Gravity (CoG), also known as the centroid method. This method calculates the center of the area under the curve of the fuzzy set. It is widely used due to its accuracy and simplicity.

Using the MATLAB/Simulink environment, a dynamic greenhouse microclimate model controlled by a

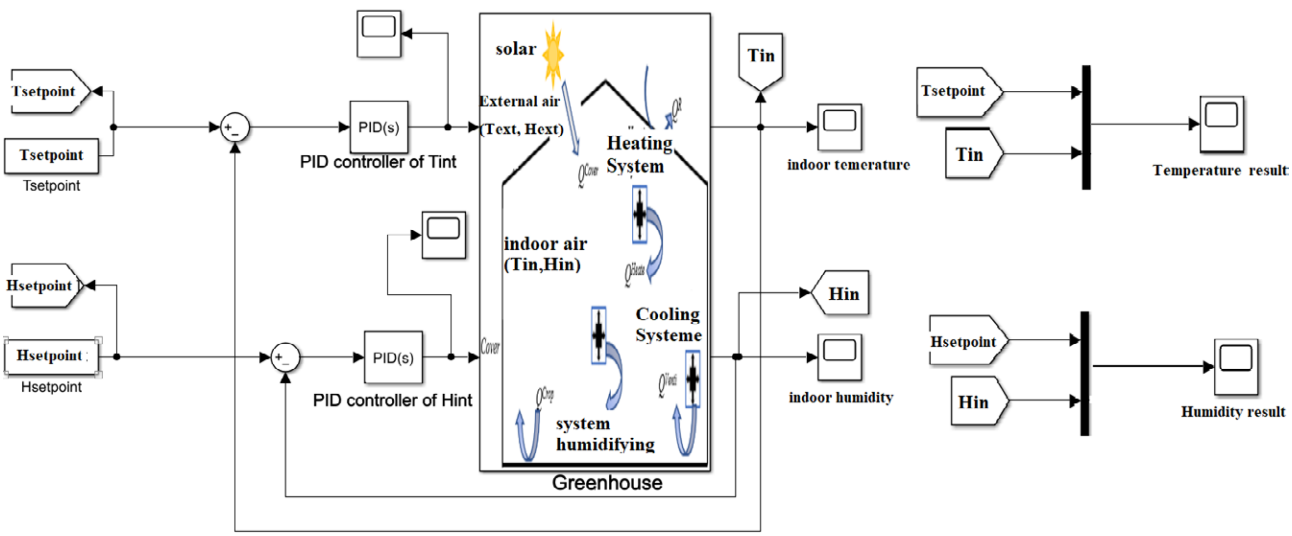

Figure 2. Greenhouse model controlled by a Proportional Integral Derivative (PID) controller.

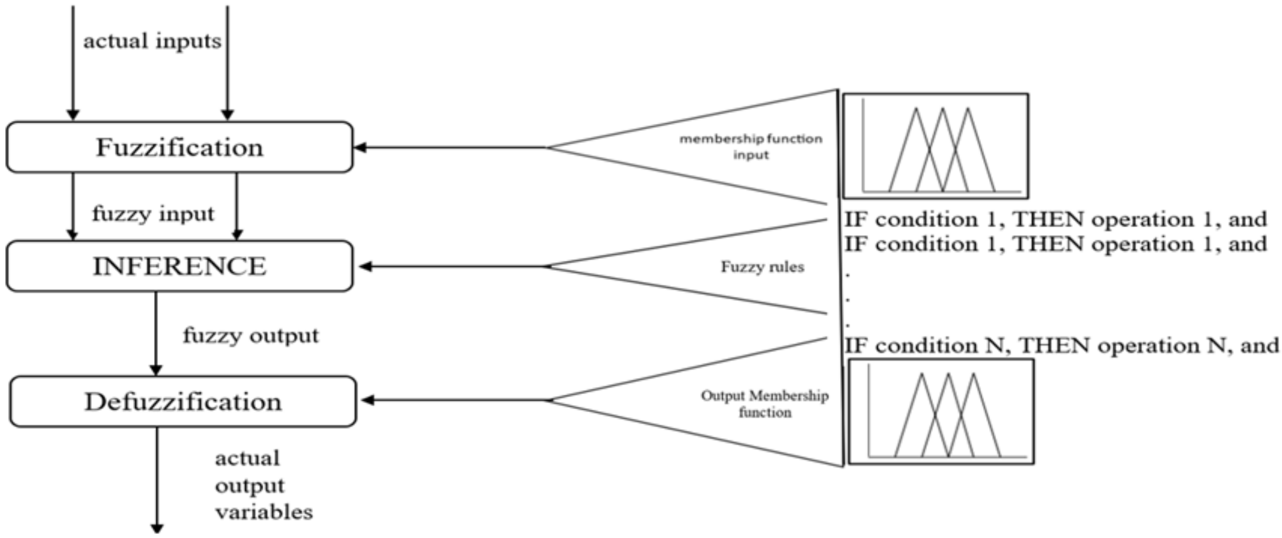

Figure 3. Operation of a fuzzy controller.

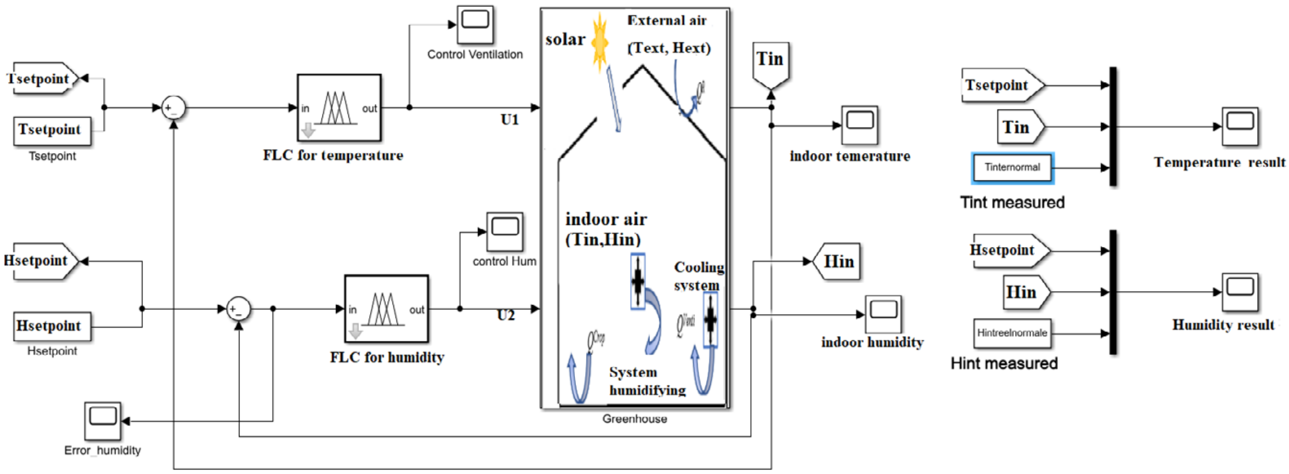

Figure 4. greenhouse model controlled by the Fuzzy Logic Controller (FLC).

Fuzzy Logic Controller (FLC) was developed, as shown in Fig. 4.

The Fuzzy Logic Controller (FLC) is initialized using the membership functions associated with air temperature.

The fuzzy rules governing the indoor temperature fuzzy controller are showing in Table 3.

The input variable of the air temperature fuzzy controller is the Temperature_Error ΔT, where:

$\Delta T = T_{setpoin}t - T_{int}$

where:

Table 3. The base fuzzy rules of the temperature control

Temperature_Error	Heater rate	Ventilation rate
NB	NA	LA
NM	NA	SA
Z	NA	NA
PM	SA	NA
PB	LA	NA

PB: Positive Big.
PM: Positive Medium.
Z: Zero.

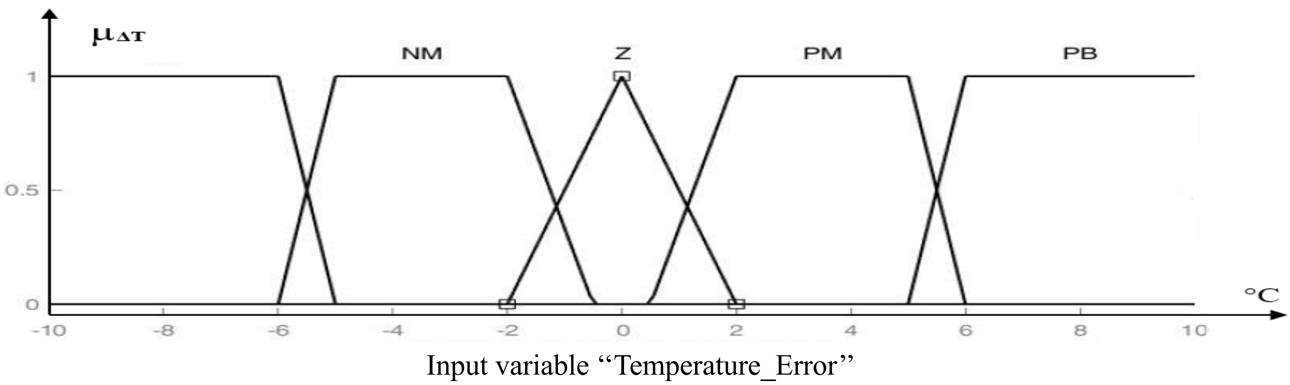

Figure 5. Membership function of the temperature error.

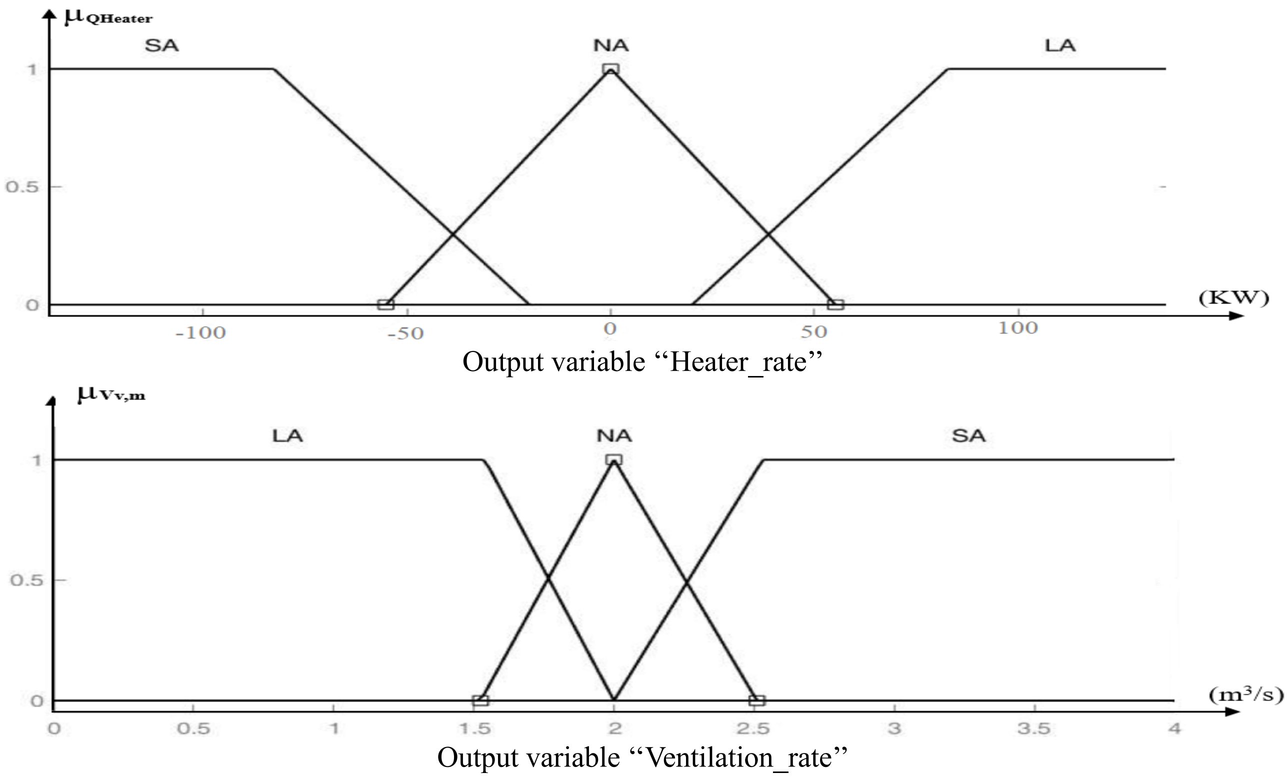

Figure 6. Membership functions of the heating rate and the ventilation.

NM: Negative Medium.
NB: Negative Big.
The output variables are the ventilation and the heating rate, where:
NA: No Action.
SA: Short Action.
LA: Long Action

To achieve the desired indoor air temperature, a set of temperature-based fuzzy rules has been defined. When the indoor temperature exceeds the reference value, a ventilation system is activated to reduce it. Conversely, when the temperature is below the desired level, a heating system is used to increase it. Figure 5 shows the membership functions of the input variable, namely the temperature error.

The membership functions of the output variables, the heating rate and the ventilation, respectively, are plotted in Figure 6.

Table 4. Fuzzy rules base of the relative humidity control.

ΔH	H_{ext}				
	VL	L	M	H	VH
NB	NA	SA	SA	LA	LA
NM	NA	NA	LA	LA	LA
Z	SA	NA	NA	NA	LA
PM	SA	SA	NA	NA	NA
PB	SA	SA	SA	NA	NA

In order to achieve the required interior relative humidity, the same method was used. Table 4 presents the fuzzy rules for relative humidity control.

The input variables of the indoor relative humidity fuzzy controller are the Humidity_Error ΔH, and outside relative humidity H_{ext}, where:

$$\Delta H = H_{setpoint} - H_{int}$$

VH: Very High.
H: High.
M: Medium.
L: Low.
VL: Very Low.

The membership functions of the input variables, which are the humidity error and the outside relative humidity, are plotted in Fig. 7.

The membership functions of the output variable, the humidifying rate is shown in Fig. 8.

3. RESULTS AND DISCUSSIONS

The simulation utilized two weather databases of real greenhouse. The first weather database covers four days during the spring season (April) with a sampling interval of 5 seconds, while the second spans one week during the autumn season (September). These weather databases include the recorded outdoor temperature and relative humidity values corresponding to each season.

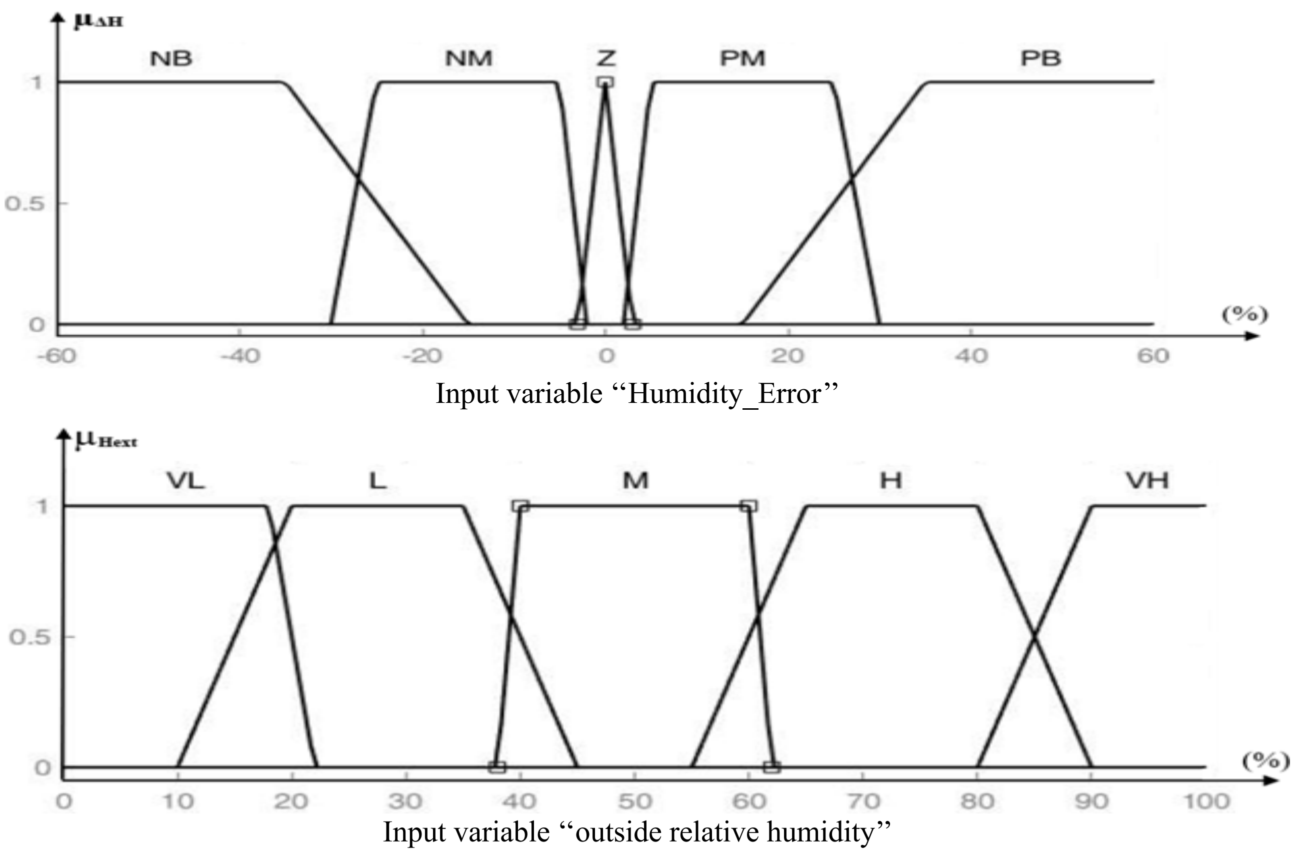

Figure 7. The membership function of the humidity error and outside relative humidity.

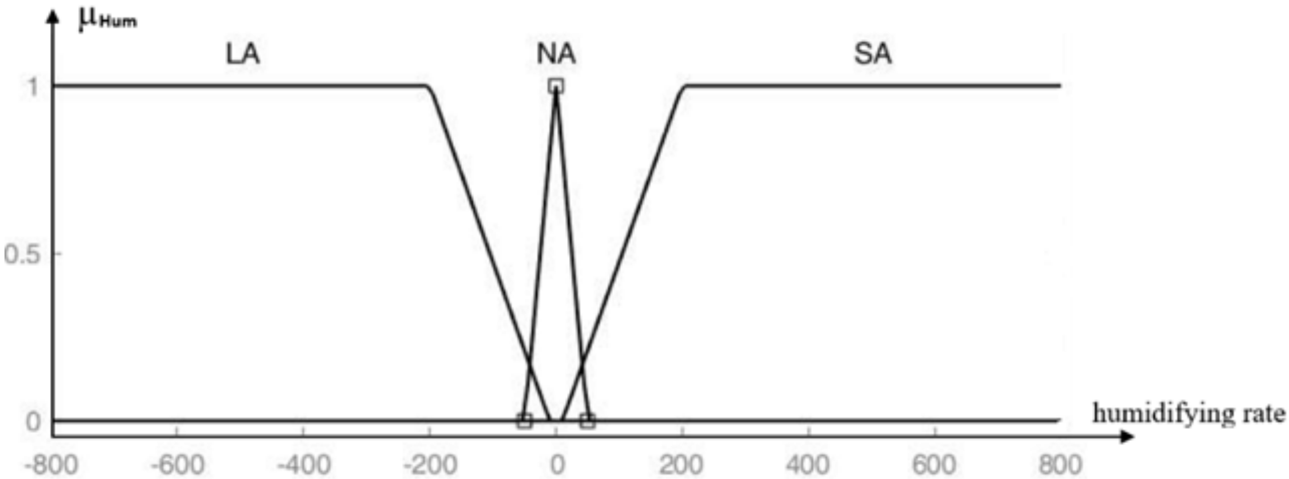

Figure 8. Membership functions of the humidifying rate.

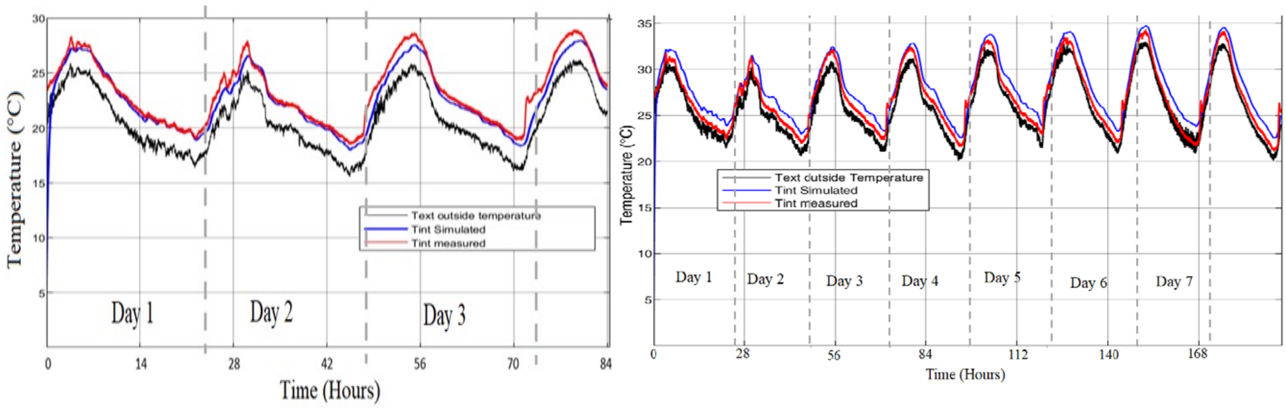

Figure 9. The results simulation of the indoor temperature without control.

3.1. Results of PID controller

Based on the measurements and the simulation results obtained using the equation model Eq. (4) and Eq. (5), the simulated air temperature without the PID controller is presented in Fig. 9. The graph on the left corresponds to the spring season, while the one on the right represents the autumn season. It was observed that the indoor temperature varies according to the outdoor meteorological conditions, indicating that the internal climate is not always optimal for crop growth.

The difference between the outdoor and indoor temperature is mainly due to the greenhouse cover; however, this difference alone is not sufficient to ensure optimal plant production. In addition, the need to minimize disturbances motivated the adoption of advanced techniques to monitor the system. For this reason, actuators for the heating and ventilation systems are implemented and managed by an effective controller block, such as a PID controller, in order to achieve the desired indoor climate. Fig. 10 presents the simulation result.

A daytime setpoint of 28 °C and a nighttime setpoint of 18 °C were selected, as most plants exhibit optimal growth within a temperature range of 17 °C to 27 °C (Li et al. 2018).

To further evaluate the robustness and adaptability of the controller under diverse climatic scenarios, an additional setpoint configuration of 32 °C during the day and 22 °C at night was used, incorporating realistic atmospheric variations during another season (autumn) over an extended simulation period (one week).

The temperature error, calculated as $\Delta T = T_{setpoint} - T_{simulated}$, was found to be $\Delta T = 1.631$ °C between the setpoint and simulated values. The simulated temperature values effectively followed the reference setpoints, with a slight overshoot of approximately 3 °C, which remains

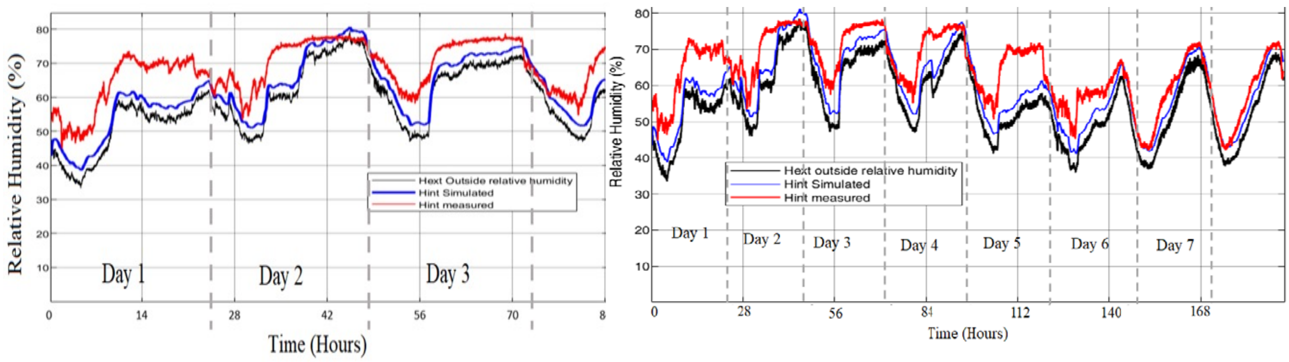

Figure 10. The simulation results of the air temperature with the PID controller.

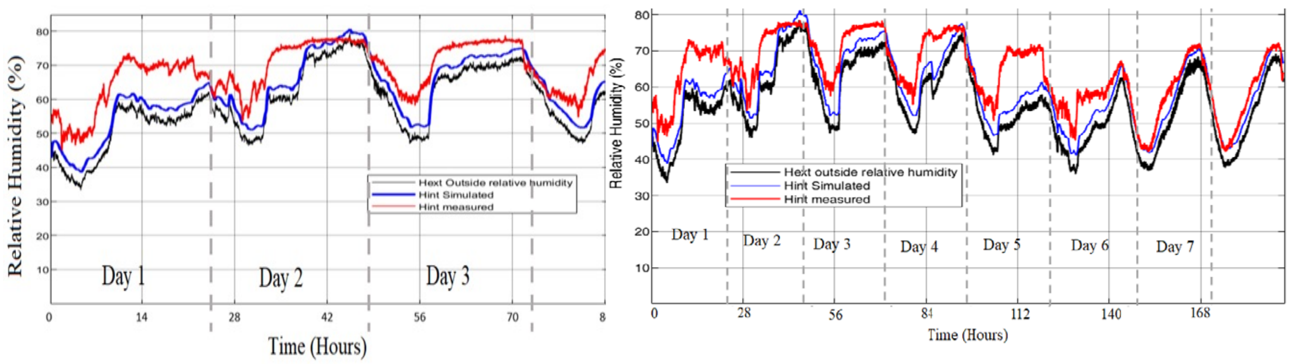

Figure 11. The progression without control of the indoor and outdoor relative humidity.

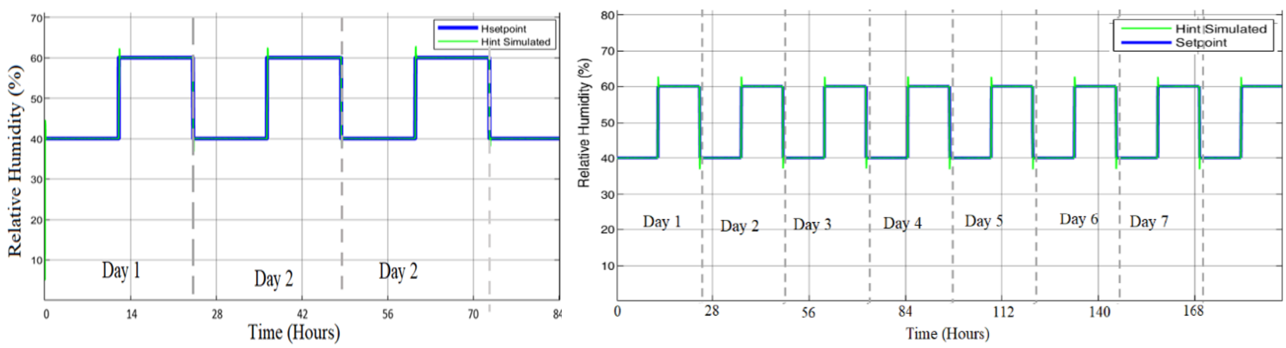

Figure 12. Evolution with PID controller of the indoor relative humidity.

within acceptable limits and does not adversely affect crop growth.

The evolution of relative humidity without any control is illustrated in Fig. 11, while the simulation results with a PID controller are presented in Fig. 12.

The indoor relative humidity changes in accordance with the external environment; however, the resulting internal climate is not always favorable. During the night, both indoor and outdoor humidity levels increase, reaching peak values of approximately 85%, thereafter declining during the day to a minimum value. To regulate the indoor relative humidity at the appropriate set point, a PID controller is employed to manage the operation of the humidification actuator. The results of the simulation are presented in Figure 12.

The relative humidity setpoint was defined as 40% during the night and 60% during the day for both seasons. The humidification system successfully maintained

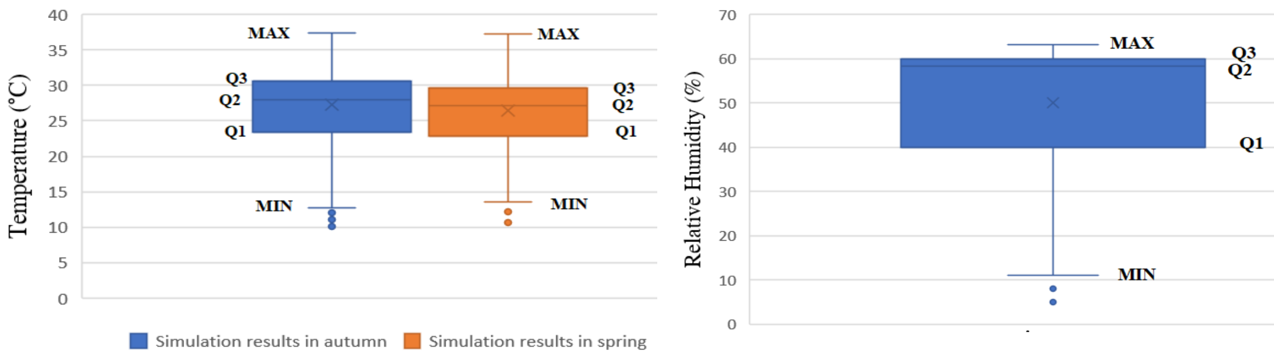

Figure 13. Boxplots of the simulated temperature and relative humidity distributions with PID controller.

the indoor relative humidity close to the reference values, with an error of $\Delta H = H_{setpoint} - H_{simulated} = 0.1982\%$ and a slight overshoot of approximately 3%, which has no significant impact on crop growth.

For temperature, the median values in autumn (27.97 °C) and spring (27.20 °C) are very close, indicating consistent central behavior across both transitional seasons. The interquartile range is slightly larger in autumn (7.16 °C) than in spring (6.67 °C), reflecting higher variability during autumn due to more pronounced fluctuations in external climatic conditions. For relative humidity the median value is 58.32 %.

Table 5 summarizes the distributional characteristics of the simulated temperature and relative humidity using boxplot statistical indicators.

The calculated upper and lower limits indicate that most simulated temperature values lie well within the non-outlier range, with only occasional extreme values occurring during periods of rapid environmental change. For relative humidity, a wider interquartile range (19.99%) is observed, highlighting stronger variability compared to temperature. This behavior is expected due to the sensitivity of humidity to both temperature variations and ventilation dynamics.

Overall, this distribution-based analysis confirms that the proposed model maintains stable median behavior while appropriately capturing seasonal variability and rare extreme events. Such results demonstrate the robustness of the simulation beyond mean error metrics and provide a more comprehensive understanding of model performance under real operating conditions.

Table 5. Statistical summary of the simulated temperature and relative humidity distributions with PID controller.

Boxplot Statistical Indicators	Temperature (°C)		Relative Humidity (%)
	Simulation results in autumn	Simulation results in spring	
MIN	10.170	10.633	5.000
Q1	23.425	22.915	40.000
Q2	27.972	27.200	58.322
Q3	30.583	29.571	59.999
MAX	37.363	37.210	63.071
IQR	7.1581	6.665	19.999
Upper Limit	41.321	39.554	89.999
Lower Limit	12.688	12.931	10.000

3.2. *Results of Fuzzy Logic Controller (FLC) controller*

The results of simulation without FLC of the indoor air temperature are presented in Fig. 9. The indoor air temperature varies depending on the outdoor conditions, which makes the indoor climate unfavorable for the plant. For this reason, we need to install actuators for the heating and ventilation system, which are controlled by a smart controller such as the Fuzzy Logic Controller (FLC), in order to achieve the desired indoor climate. Fig. 14 gives the results of the simulation.

A temperature setpoint of 28 °C during the day and 18 °C at night was selected. During the spring season, the indoor air temperature fluctuated around 18 °C (nighttime setpoint) due to the heating system, while it reached approximately 28 °C during the day under the effect of the ventilation system. For the autumn season, a temperature setpoint of 32 °C during the day and 22 °C at night was applied, and the simulation was repeated as shown in the right-hand graph of Fig. 14. The calculated error between the setpoint and simulated temperature values was ΔT = Tsetpoint – Tsimulated = 1.051 °C, confirming the model's accuracy.

The simulation results of the indoor relative humidity without control are illustrated in Fig. 11, whereas the

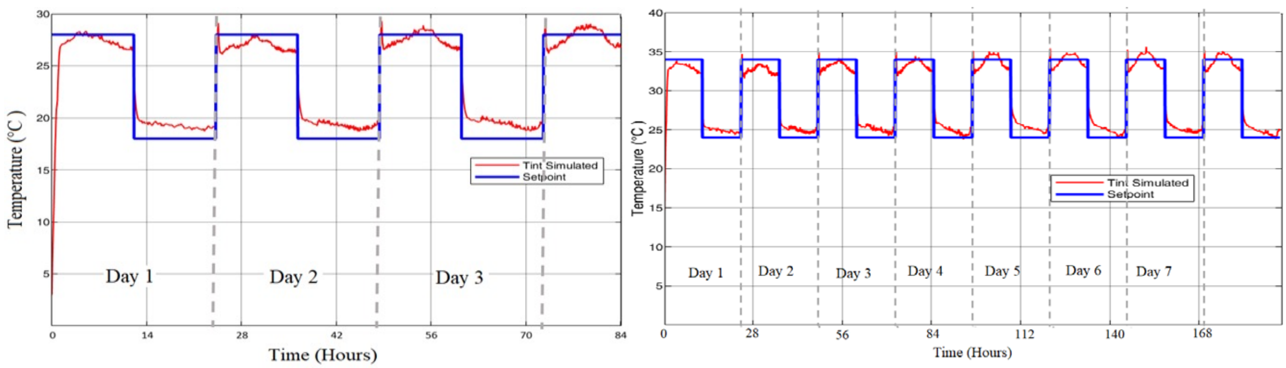

Figure 14. The evolution of the indoor air temperature with Fuzzy Logic Controller (FLC).

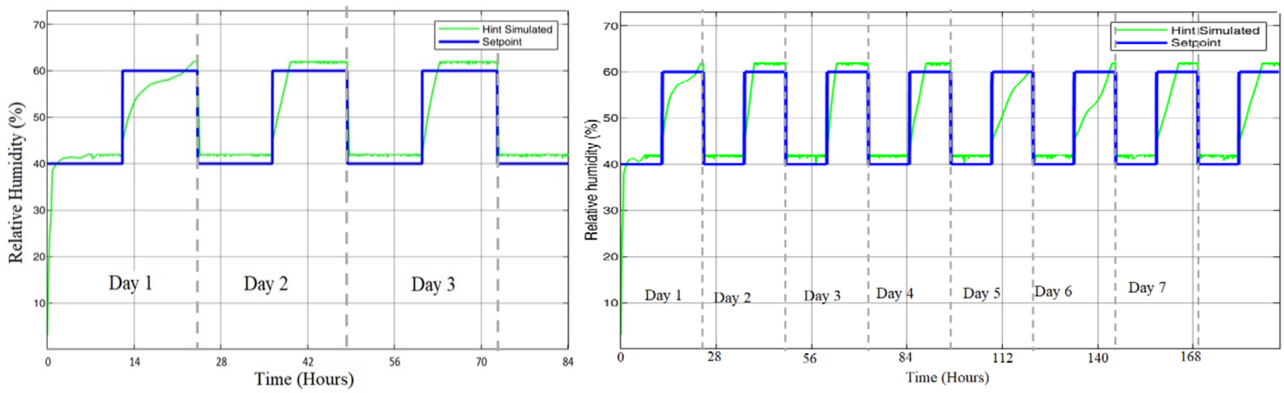

Figure 15. The evolution representation of the indoor relative humidity with Fuzzy Logic Controller (FLC).

results with the Fuzzy Logic Controller (FLC) are presented in Fig. 15.

The simulation results indicate that, without the Fuzzy Logic Controller (FLC), both indoor and outdoor relative humidity reach their maximum values of approximately 85% during the night, and decrease to their minimum levels during the daytime. However, to maintain the indoor relative humidity at the desired setpoint, a Fuzzy Logic Controller (FLC) was implemented on the actuator to monitor and control the operation of the humidification system, as illustrated in Fig. 15. The humidity error was then calculated as $\Delta H = H_{setpoint} - H_{simulated}$, yielding a value of $\Delta H = 1.005 \times 10^{-15}$ %, confirming the high precision of the controller.

Figure 16 and Table 6 present a statistical summary of the simulated temperature and relative humidity with FLC controller distributions using boxplot-based indicators. This analysis provides insight into the dispersion, central tendency, and extreme values of the simulated climatic variables, going beyond traditional mean-based performance metrics.

The boxplot analysis demonstrates that both temperature and relative humidity exhibit stable median behavior with controlled variability, despite occasional extreme values. The limited number of outliers indicates that extreme climatic deviations are infrequent and mainly occur during rapid weather transitions.

For temperature, the median value (Q2 = 33.15 °C) is positioned closer to the upper quartile (Q3 = 33.50 °C), indicating a slightly right-skewed distribution. The interquartile range (Q3 − Q1 = 8.40 °C) reflects moderate variability, demonstrating that the control system maintains temperature within a relatively narrow operational band under most conditions. The minimum temperature (10.56 °C) and the presence of lower-end outliers indicate occasional cold events, associated with abrupt external temperature drops or transient control delays. Nevertheless, the maximum value (35.43 °C) remains within acceptable operational limits, highlighting the effectiveness of the control strategy in preventing overheating.

In the case of relative humidity, the median value (Q2 = 41.97%) lies closer to the lower quartile (Q1 =

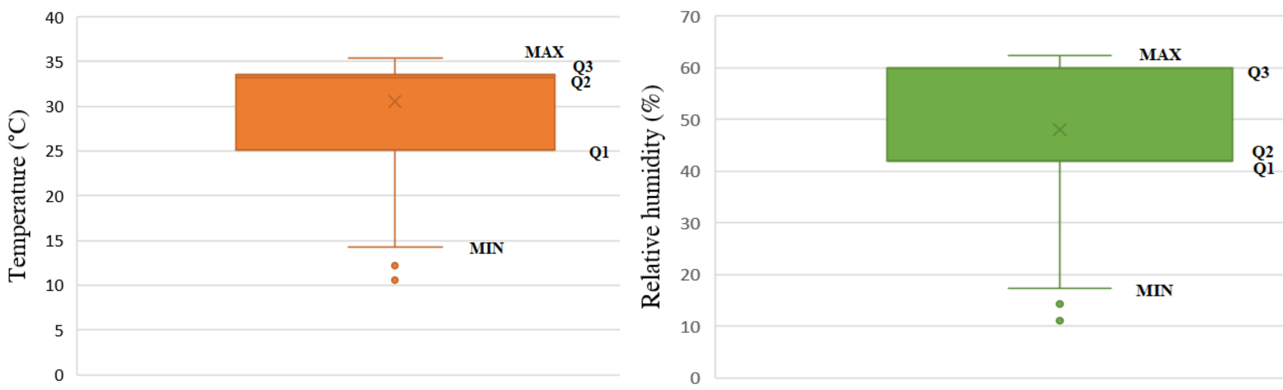

Figure 16. Boxplots of the simulated temperature and relative humidity distributions with FLC controller.

Table 6. Statistical summary of the simulated temperature and relative humidity distributions with FLC controller.

Boxplot Statistical Indicators	Temperature (°C)	Relative Humidity (%)
MIN	10.555	10.947
Q1	25.102	41.849
Q2	33.152	41.969
Q3	33.500	60.000
MAX	35.427	62.306
IQR	8.397	18.150
Upper Limit	46.096	87.225
Lower Limit	12.505	14.623

41.85%) than to the upper quartile (Q3 = 60.00%), suggesting a distribution with higher dispersion toward elevated humidity levels. The wider interquartile range (18.15%) compared to temperature confirms that relative humidity is more sensitive to environmental disturbances and ventilation dynamics. The observed minimum value (10.95%) corresponds to dry conditions that may occur during high-temperature periods or increased ventilation, while the maximum value (62.31%) reflects high-humidity events associated with reduced ventilation or external moisture influx.

3.3. Comparison between PID controller and Fuzzy Logic Controller (FLC)

Based on the simulation results, it was observed that the Fuzzy Logic Controller (FLC) provides an effective approach for achieving the desired greenhouse environment, as the simulated signal closely follows the setpoint with higher accuracy and a smaller overshoot. For temperature control, the error obtained with the PID controller (ΔT = 1.631 °C) was higher than that achieved with the FLC (ΔT = 1.051 °C). Similarly, for indoor relative humidity, the error obtained with the FLC ($\Delta H = 1.005 \times 10^{-15}$ %) was significantly lower than that observed with the PID controller (ΔH = 0.1982%). Also based on the comparison of the boxplot-based results obtained using the FLC controller and those obtained with the PID controller, the superiority of the FLC approach is clearly demonstrated. The distributions associated with the FLC controller exhibit narrower interquartile ranges, more stable median values, and fewer outliers, indicating improved regulation performance and a stronger ability to cope with climatic variability and external disturbances. In contrast, the PID controller shows larger dispersion and increased variability, particularly during transitional seasons, reflecting its higher sensitivity to rapid changes in environmental conditions.

These results clearly demonstrate the superior precision and stability of the FLC in regulating both temperature and humidity within the greenhouse environment.

At the level of energy, the Humidifying rate and Ventilation rate for PID controller and Humidifying rate and Ventilation rate for Fuzzy Logic Controller (FLC) are represented respectively in Figure 17 and Figure 18.

The simulation results shown in Figure 17 indicate that, with the PID controller, the ventilation rate varies between 2 and 3.18, while the humidification rate ranges from 0 to 170, occasionally reaching a maximum of 8900. Figure 18 shows that, when using with FLC, the ventilation rate ranges from 0 to 1.3 with a maximum of 2.5, while the humidification rate varies between 0 and 150, occasionally peaking at 420.To optimize energy efficiency, the energy consumption associated with both control strategies was calculated. The results show that the average humidification rate is 164.8 for PID controller, compared to 41.36 for the FLC, while the average ventilation rate is 2.01 for the PID and 0.595 for the

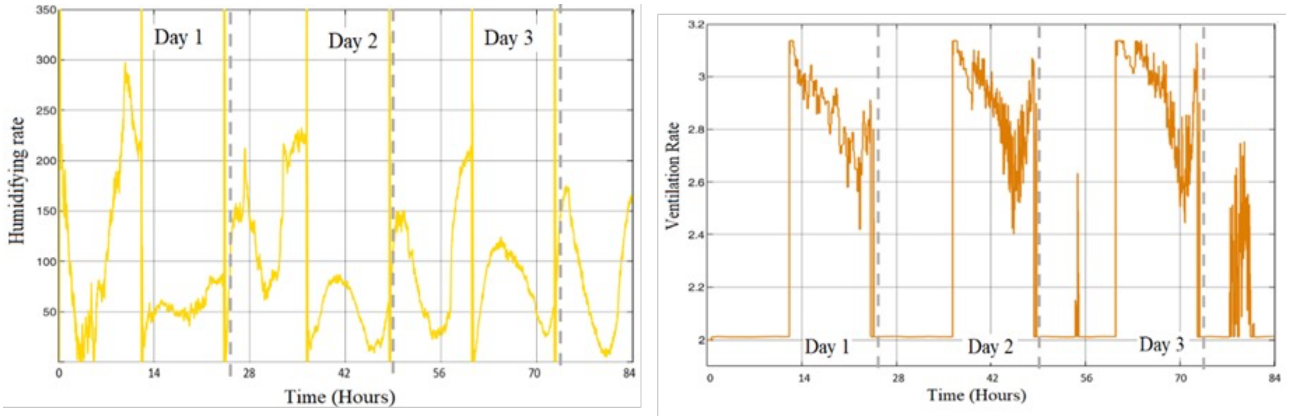

Figure 17. Humidifying rate and Ventilation rate for PID controller.

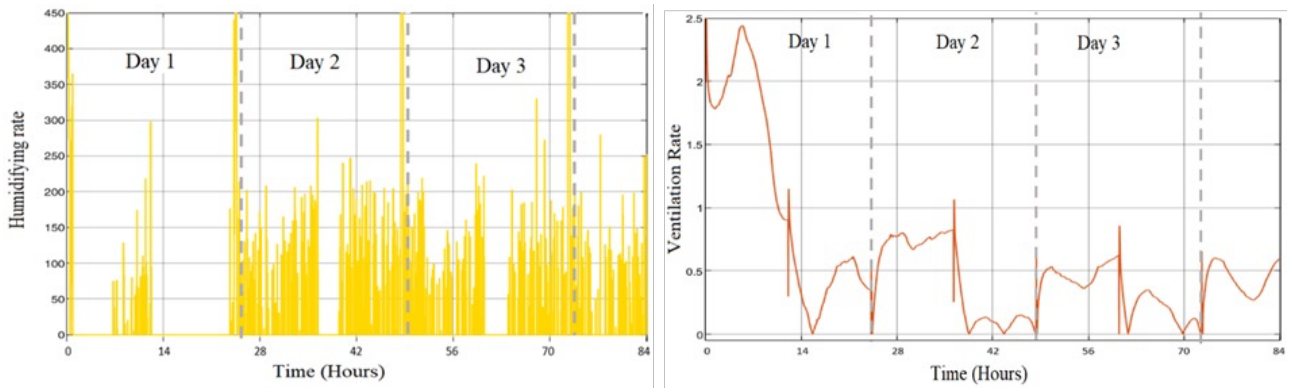

Figure 18. Humidifying rate and Ventilation rate for Fuzzy Logic Controller (FLC).

FLC. These findings demonstrate that the PID controller leads to significantly higher energy consumption than the FLC, thereby validating the choice of the FLC due to its superior control performance, faster response, and improved energy efficiency.

4. CONCLUSION

Agricultural greenhouses represent complex systems due to the presence of significant external disturbances and the large number of input parameters that strongly influence the internal climate. Consequently, farmers and researchers continuously seek optimal control strategies to enhance greenhouse productivity. Despite the strong coupling between temperature and relative humidity, the PID controller leads to significantly higher energy consumption than the Fuzzy Logic Controller (FLC). Two control strategies were implemented: a conventional PID controller and a Fuzzy Logic Controller (FLC), with the objective of creating a favorable greenhouse microclimate through appropriate activation of the installed actuators.

Weather variability represents a major external source of uncertainty, particularly due to fluctuations in solar radiation, ambient temperature, wind speed, and relative humidity. These factors directly affect the greenhouse microclimate and may lead to discrepancies between simulated and real conditions, especially during transitional seasons such as spring and autumn, when temperature and relative humidity are strongly coupled and highly variable. Despite these challenges, the proposed model demonstrates robust performance under diverse weather conditions, maintaining acceptable accuracy during both stable (summer and winter) and highly variable climatic scenarios. This confirms that the proposed control strategy is resilient to weather-induced disturbances. To evaluate energy optimization, the energy consumption of the PID controller was compared with that of the Fuzzy Logic Controller (FLC). The results reveal that:

- The calculated temperature error between the setpoint and simulated values obtained with the Fuzzy Logic Controller (FLC) (ΔT = 1.051 °C) was lower than that obtained with the PID controller (ΔT = 1.631 °C).
- Similarly, the relative humidity error achieved with the FLC ($\Delta H = 1.005 \times 10^{-15}$ %) was significantly lower than that calculated with the PID controller (ΔH = 0.1982%).
- The average humidification rate with the FLC is reduced by 25.1% compared to the PID controller.
- The average ventilation rate with the FLC is 29.6% lower than that of the PID controller.
- Actuator fluctuations are 27.35% lower with the FLC than with the PID controller.
- The distributions associated with the FLC controller exhibit narrower interquartile ranges, more stable median values, and fewer outliers, indicating improved regulation performance and a stronger ability to cope with climatic variability and external disturbances.
- In contrast, the PID controller shows larger dispersion and increased variability, particularly during transitional seasons, reflecting its higher sensitivity to rapid changes in environmental conditions.

These findings demonstrate that the overall energy consumption associated with the PID controller is approximately 27% higher than that of the FLC. This confirms the effectiveness of the FLC in achieving more precise regulation, faster dynamic response, and significant energy savings. Additionally, the simulation results confirm the effectiveness of the proposed dynamic model in accurately predicting indoor relative humidity and indoor air temperature with a low margin of error. The comparison between the PID and the FLC responses further highlights the FLC as an efficient and robust solution for optimizing greenhouse microclimate conditions. This work makes several original contributions that address key limitations identified in the existing literature on automatic greenhouse climate management.

First, unlike most existing studies that evaluate control strategies under limited or single-season conditions, this work proposes and validates a control framework using real meteorological data collected during the most challenging climatic periods, namely spring and autumn, where strong coupling between temperature and relative humidity occurs. Second, a coupled multivariable control strategy is developed to simultaneously regulate temperature and humidity, explicitly accounting for their dynamic interaction, whereas many existing approaches treat these variables independently or rely on simplified assumptions. Third, the proposed model is experimentally validated under real operating conditions, demonstrating its robustness and effectiveness compared to conventional control strategies typically reported in the literature. Finally, this work provides a comprehensive comparative analysis highlighting the trade-offs between control performance, energy consumption, and environmental stability, thereby offering practical insights for the deployment of intelligent greenhouse control systems.

Future work will focus on extending the control strategy to cover all four seasons by investigating advanced control techniques such as sliding mode control and backstepping. In addition, the development of a smart greenhouse management system based on Internet of Things (IoT) technologies is planned.

ACKNOWLEDGEMENT

This work was carried out as part of a collaboration between the National School of Applied Sciences (ENSA) and the Higher School of Technology (EST) in Fes.

AUTHOR CONTRIBUTION

All authors contributed to the study conception and design. Material preparation, data collection and analysis were performed by [Abderrazak KAIDA], [Abderrahman AITDADA], [Youssef EL AFOU] and [Abdelouahad AIT MSAAD]. The first draft of the manuscript was written by [Abderrazak KAIDA] and all authors commented on previous versions of the manuscript. All authors read and approved the final manuscript.

REFERENCES

Abbood HM, Nouri NM, Riahi M, Alagheband SH (2023) An intelligent monitoring model for greenhouse microclimate based on RBF Neural Network for optimal setpoint detection. J Process Control 129. https://doi.org/10.1016/j.jprocont.2023.103037

Adrian Z, Razvan U, Gaudentiu V (2019) Controlling the Temperature and Humidity in a Greenhouse. In: 2019 IEEE 25th International Symposium for Design and Technology in Electronic Packaging (SIITME): IEEE Xplore compliant proceedings: 23rd-26th of October 2019, Cluj-Napoca, Romania. IEEE.

Ben Ali R, Bouadila S, Mami A (2018) Development of a Fuzzy Logic Controller applied to an agricultural greenhouse experimentally validated. Appl Therm

Eng 141: 798–810. https://doi.org/10.1016/j.applthermaleng.2018.06.014
Bennis N, Duplaix J, Enéa G, et al. (2008) Greenhouse climate modelling and robust control. Comput Electron Agric 61: 96–107. https://doi.org/10.1016/j.compag.2007.09.014
Bhujel A, Basak JK, Khan F, et al. (2020) Sensor Systems for Greenhouse Microclimate Monitoring and Control: a Review. Journal of Biosystems Engineering 45: 341–361
Blasco X, Martínez M, Herrero JM, et al. (2007) Model-based predictive control of greenhouse climate for reducing energy and water consumption. Comput Electron Agric 55: 49–70. https://doi.org/10.1016/j.compag.2006.12.001
Chand Singh M, Singh JP, Kumar Pandey S, et al. (2018) A Review of Three Commonly Used Techniques of Controlling Greenhouse Microclimate. Int J Curr Microbiol Appl Sci 7: 3491–3505. https://doi.org/10.20546/ijcmas.2018.701.411
Chen X, Liang H, Wu G, et al. (2023) Coupled heat and humidity control system of narrow-trough solar collector and solid desiccant in Chinese solar greenhouse: Analysis of optical / thermal characteristics and experimental study. Energy 273. https://doi.org/10.1016/j.energy.2023.127198
Choab N, Allouhi A, El Maakoul A, et al. (2019) Review on greenhouse microclimate and application: Design parameters, thermal modeling and simulation, climate controlling technologies. Solar Energy 191: 109–137.
El Afou Y, Ait Msaad A, Kousksou T, Mahdaou Mi (2015) Predictive Control of Temperature Under Greenhouse using LQG Strategy. In: Proceedings of 2015 IEEE International Renewable and Sustainable Energy Conference: (IRSEC'15). IEEE.
El Afou Y, Kousksou T, Jammoukh M (2018) Towards controlling climatic parameters under greenhouse. In: ICOA: 2018 4th International Conference on Optimization and Applications: 26-27 April 2018, Mohammedia, Morocco. Institute of Electrical and Electronics Engineers, p. 494.
El Ghoumari MY, Tantau HJ, Serrano J (2005) Non-linear constrained MPC: Real-time implementation of greenhouse air temperature control. In: Computers and Electronics in Agriculture. pp. 345–356.
Farvardin M, Taki M, Gorjian S, et al. (2024) Assessing the Physical and Environmental Aspects of Greenhouse Cultivation: A Comprehensive Review of Conventional and Hydroponic Methods. Sustainability (Switzerland) 16. https://doi.org/10.3390/su16031273
Fliess M, Sira-Ramirez H, Sira-Ramírez H (2004) Control via state estimations of some nonlinear systems
Franklin KA (2009) Light and temperature signal crosstalk in plant development. Curr Opin Plant Biol 12: 63–68.
Guo Y, Zhao H, Zhang S, et al. (2021) Modeling and optimization of environment in agricultural greenhouses for improving cleaner and sustainable crop production. J Clean Prod 285.
Huang S, Xiang H, Leng C, et al. (2024) Intelligent Regulation of Temperature and Humidity in Vegetable Greenhouses Based on Single Neuron PID Algorithm. Electronics (Switzerland) 13:. https://doi.org/10.3390/electronics13112083
Jeevan Nagendra Kuma Y, Chandan R, Somanini SH, et al. (2024) Predictive modeling for enhanced plant cultivation in greenhouse environment. In: E3S Web of Conferences. EDP Sciences.
Joe Qin S, Yu J (2007) Recent developments in multivariable controller performance monitoring. J Process Control 17: 221–227. https://doi.org/10.1016/j.jprocont.2006.11.002
Kadirov Y, Samadov A, Goziev O (2023) Equation of dynamics of greenhouse microclimate parameters. In: E3S Web of Conferences. EDP Sciences.
Kaida A, El Afou Y, Aitdada A, et al. (2024) Dynamical Modeling of Climatic Parameters Under Greenhouse. In: Lecture Notes in Networks and Systems. Springer Science and Business Media Deutschland GmbH, pp. 420–427.
Katebi R (2012) Robust multivariable tuning methods. In: Advances in Industrial Control. Springer International Publishing, pp. 255–280.
Körner C (2015) Paradigm shift in plant growth control. Curr Opin Plant Biol 25: 107–114.
Lamprecht, I., Schmolz, E., Blanco, L., & Romero, C. M. (2002). Flower ovens: thermal investigations on heat producing plants. *Thermochimica Acta*, 391(1-2), 107-118.
Li G, Tang L, Zhang X, et al. (2018) Factors affecting greenhouse microclimate and its regulating techniques: A review. In: IOP Conference Series: Earth and Environmental Science. Institute of Physics Publishing.
Lipiec J, Doussan C, Nosalewicz A, Kondracka K (2013) Effect of drought and heat stresses on plant growth and yield: A review. Int Agrophys 27: 463–477.
Márquez-Vera MA, Ramos-Fernández JC, Cerecero-Natale LF, et al. (2016) Temperature control in a MISO greenhouse by inverting its fuzzy model. Comput Electron Agric 124: 168–174. https://doi.org/10.1016/j.compag.2016.04.005

Paolino N, Schiavo M, Latronico N, et al. (2024) PK/PD model based design of PID control for closed-loop anesthesia. IFAC Journal of Systems and Control 27. https://doi.org/10.1016/j.ifacsc.2024.100247

Penfield S (2008) Temperature perception and signal transduction in plants. New Phytologist 179:615–628

Riahi J, Nasri H, Mami A, Vergura S (2024) Effectiveness of the Fuzzy Logic Control to Manage the Microclimate Inside a Smart Insulated Greenhouse. Smart Cities 7: 1304–1329. https://doi.org/10.3390/smartcities7030055

Schiavo M, Padula F, Latronico N, et al. (2021) Individualized PID tuning for maintenance of general anesthesia with propofol. In: IFAC-PapersOnLine. Elsevier B.V., pp. 679–684.

Shamshiri RR, Bojic I, van Henten E, et al. (2020) Model-based evaluation of greenhouse microclimate using IoT-Sensor data fusion for energy efficient crop production. J Clean Prod 263. https://doi.org/10.1016/j.jclepro.2020.121303

Tao G (2014) Multivariable adaptive control: A survey. Automatica 50: 2737–2764. https://doi.org/10.1016/j.automatica.2014.10.015

Wahid A, Gelani S, Ashraf M, Foolad MR (2007) Heat tolerance in plants: An overview. Environ Exp Bot 61:199–223.

Wang H, Laktionov I, Rodríguez Díaz F, et al. (2024) An optimized approach to hourly temperature and humidity setpoint generation for reducing tomato disease and saving power cost in greenhouses. Comput Electron Agric 226.

Yang C, Zhang X (2024) Adaptive Fuzzy Control for Fractional-Order Networked Control Systems with Input Time Delay and Data Loss. Journal of Nonlinear Mathematical Physics 31. https://doi.org/10.1007/s44198-024-00201-4

Italian Journal of Agrometeorology
Rivista Italiana di Agrometeorologia

Firenze University Press
https://riviste.fupress.net/index.php/IJAm

Citation: Pham, T. T. N., Pham, T. L. & Nguyen, T. B. (2026). Agroclimatic controls on robusta coffee yield under future climate scenarios in the Srepok River Basin. *Italian Journal of Agrometeorology* (1): 59-73. doi: 10.36253/ijam-4112

Received: April 18, 2026

Accepted: July 6, 2026

Published: September 15, 2026

Data Availability Statement: All relevant data are within the paper and its Supporting Information files.

Competing Interests: The Author(s) declare(s) no conflict of interest.

ORCID:
PTTN: 0000-0003-4118-8479
PTL: 0009-0007-5343-1620

Agroclimatic controls on robusta coffee yield under future climate scenarios in the Srepok River Basin

Pham Thi Thao Nhi[1,3], Pham Thi Loi[2,3,*], Nguyen Thi Bay[4]

[1] *Faculty of Interdisciplinary Science, University of Science, Ho Chi Minh City, Vietnam*
[2] *Faculty of Environment, University of Science, Ho Chi Minh City, Vietnam*
[3] *Vietnam National University, Ho Chi Minh City, Vietnam*
[4] *Institute of Applied Technology and Sustainable Development, Nguyen Tat Thanh University, Ho Chi Minh City, Vietnam*
*Corresponding author. Email: phamloi@hcmus.edu.vn

Abstract. Climate change poses significant challenges to coffee production in the Central Highlands of Vietnam, the country's primary coffee-growing region. This study assesses the impacts of climate change on Robusta coffee yield in the Srepok River Basin using meteorological and yield data from the 2001–2020 period at five study sites: Buon Ho, Dak Mil, M'Drak, Buon Ma Thuot, and Lak. The Least Absolute Shrinkage and Selection Operator (LASSO) variable selection method was employed to identify key climatic factors from 72 variables aggregated at monthly, growing season, and annual scales. Results indicate that water balance variables (potential evapotranspiration (PET), water surplus (SUR)) and extreme temperature indices play a dominant role in determining yield, while seasonal and monthly variables account for 68% of selected predictors, reflecting the existence of "sensitive climate windows" throughout the coffee phenological cycle. Four machine learning algorithms (Artificial Neural Network, Random Forest, Support Vector Regression, and eXtreme Gradient Boosting) were trained for yield simulation, with SVR and XGBoost demonstrating superior performance (Nash–Sutcliffe Efficiency > 0.75; R^2 > 0.84). Future climate scenarios (2026–2100) were generated by downscaling three CMIP6 General Circulation Models (GCMs: CanESM5, MPI-ESM1-2-HR, and NorESM2-MM) under four Shared Socioeconomic Pathways (SSP1-1.9, SSP1-2.6, SSP2-4.5, and SSP5-8.5). Simulation results exhibit marked spatial heterogeneity in climate change impacts: Dak Mil emerges as the most vulnerable area, with potential yield reductions reaching 58.10% by the end of the century, while M'Drak, which has the highest baseline water surplus, shows the smallest fluctuations. This research provides a scientific basis for production planning and the formulation of adaptive strategies to ensure the sustainable development of the coffee sector under a changing climate.

Keywords: climate change, LASSO regression, machine learning, Robusta coffee, yield prediction.

HIGHLIGHTS:

- Water-balance variables (PET and SUR) are key drivers of Robusta coffee yield.
- Seasonal and monthly variables account for 68% of LASSO-selected predictors.
- SVR and XGBoost achieve very good performance (NSE > 0.75, $R^2 > 0.84$) across all five stations.
- Dak Mil faces up to 58% yield loss under SSP5-8.5, while M'Drak remains the most resilient site.
- PET-driven climatic stress is a key determinant of future yield vulnerability.

1. INTRODUCTION

Climate change is posing increasing challenges to tropical agricultural systems, particularly for high-value perennial crops such as coffee. As the world's largest producer of Robusta coffee, Vietnam contributes more than 40% of global Robusta production (ICO, 2023; Dinh et al., 2022), with most cultivation concentrated in the Central Highlands. In recent decades, coffee production in Vietnam has become increasingly exposed to climate-related hazards, including prolonged droughts, heatwaves, and extreme rainfall events, resulting in substantial reductions in yield and bean quality (Arias et al., 2021; Varma et al., 2025). Recent studies indicate that climate change is no longer a future threat but an ongoing challenge affecting coffee-growing regions worldwide (Bilen et al., 2022; Della Peruta et al., 2025).

Although Robusta coffee (Coffea canephora) is generally considered more heat-tolerant than Arabica coffee, growing evidence suggests that its productivity remains highly sensitive to climatic variability. Based on observations from 798 coffee farms in Vietnam and Indonesia, Kath et al. (2020) reported that each 1°C increase beyond the optimal temperature threshold could reduce Robusta yield by approximately 14%. Seasonal fluctuations in rainfall and temperature have also been associated with production losses ranging from 6% to 22% in Indonesia (Sarvina, 2021). At the global scale, climate projections indicate that Arabica coffee yields may decline by 23–35% in Latin America and 16–21% in Africa during 2036–2065 (Della Peruta et al., 2025), while similar trends have been reported for Robusta-growing regions in Southeast Asia (Richardson et al., 2023).

These impacts reflect the strong dependence of coffee growth and productivity on temperature and water availability during specific phenological stages. Previous studies have shown that flowering, fruit development and maturation respond differently to climatic stresses. Kath et al. (2023) demonstrated that shifts in flowering timing substantially alter the response of Robusta coffee to climate stress and may reduce the predictive performance of yield models. Such findings suggest the existence of climate-sensitive windows, during which short-term climatic anomalies may exert stronger effects on coffee yield than annual climatic averages (Dinh et al., 2022). However, quantitative assessments of these climate-sensitive windows for Robusta coffee remain limited, particularly at seasonal and monthly scales.

Despite increasing attention to climate change impacts on coffee production, several important knowledge gaps remain. First, most previous studies have relied on annual climate indicators, while the influence of climate variability during specific phenological stages has not been adequately quantified. Second, climate-sensitive windows of Robusta coffee remain poorly understood, particularly in tropical monsoon regions. Third, watershed-scale assessments integrating high-temporal-resolution climate variables with advanced machine-learning techniques remain scarce, especially in Southeast Asia. To the best of our knowledge, no previous study has simultaneously combined monthly- and seasonal-resolution climate indicators, LASSO-based feature selection, multiple machine-learning algorithms, and CMIP6 multi-model projections to quantify climate change impacts on Robusta coffee yield at the watershed scale in Vietnam's Central Highlands.

The Srepok River Basin was selected as a representative study area to address these research gaps. The basin is one of the most important coffee-producing regions in Vietnam, covering large cultivation areas in Dak Lak and Dak Nong provinces. In addition, substantial variations in elevation, rainfall distribution and water availability create distinct microclimatic conditions across the basin, potentially leading to different yield responses under climate change. Recent studies have identified coffee cultivation as a major driver of unmet water demand during the dry season in several parts of the basin (Sam et al., 2025), while CMIP6 projections indicate increasing frequencies of droughts and extreme rainfall events in the future (Do et al., 2024; Thao et al., 2024). However, the implications of these climatic changes for coffee productivity at the watershed scale remain insufficiently understood.

Therefore, this study aims to (i) identify the most influential climatic factors affecting Robusta coffee yield at monthly and seasonal scales using the Least Absolute Shrinkage and Selection Operator (LASSO) method; (ii) develop and compare four machine-learning models, including Artificial Neural Network (ANN), Random Forest (RF), Support Vector Regression (SVR), and eXtreme Gradient Boosting (XGBoost), to characterize nonlinear climate–yield relationships; and (iii) assess future climate change impacts on coffee yield under four CMIP6 scenarios representing low (SSP1-1.9 and SSP1-2.6), medium (SSP2-4.5) and high (SSP5-8.5) emission pathways. The findings are expected to provide a scientific basis for climate adaptation planning, sustainable coffee production, and regional agricultural management in the Central Highlands of Vietnam.

2. MATERIALS AND METHODS

2.1. Materials

2.1.1. Data collection

This study employs daily meteorological data collected from five observation stations belonging to the National Hydro-Meteorological Network in the Central Highlands region, including Buon Ma Thuot, Buon Ho, M'Drak, Lak stations (Dak Lak province) and Dak Mil station (Dak Nong province) (Figure 1). These stations were selected based on spatial distribution criteria, representing different climatic sub-regions within the Srepok River Basin while ensuring continuous observation records during the 1990-2020 period. The collected data comprise four primary meteorological variables: daily precipitation (mm), mean daily air temperature (°C), daily maximum air temperature (°C), and daily minimum air temperature (°C).

Concurrently with meteorological data, annual average coffee yield data for the 2001-2020 period were collected from the Statistical Yearbooks of Dak Lak and Dak Nong provinces. Yield data correspond to five district-level administrative units where meteorological stations are located, including Buon Ma Thuot city, Buon Ho town, M'Drak district, Ea Kar district (Dak Lak province), and Dak Mil district (Dak Nong province). These areas represent key coffee-producing regions with stable cultivation areas throughout the study period. The

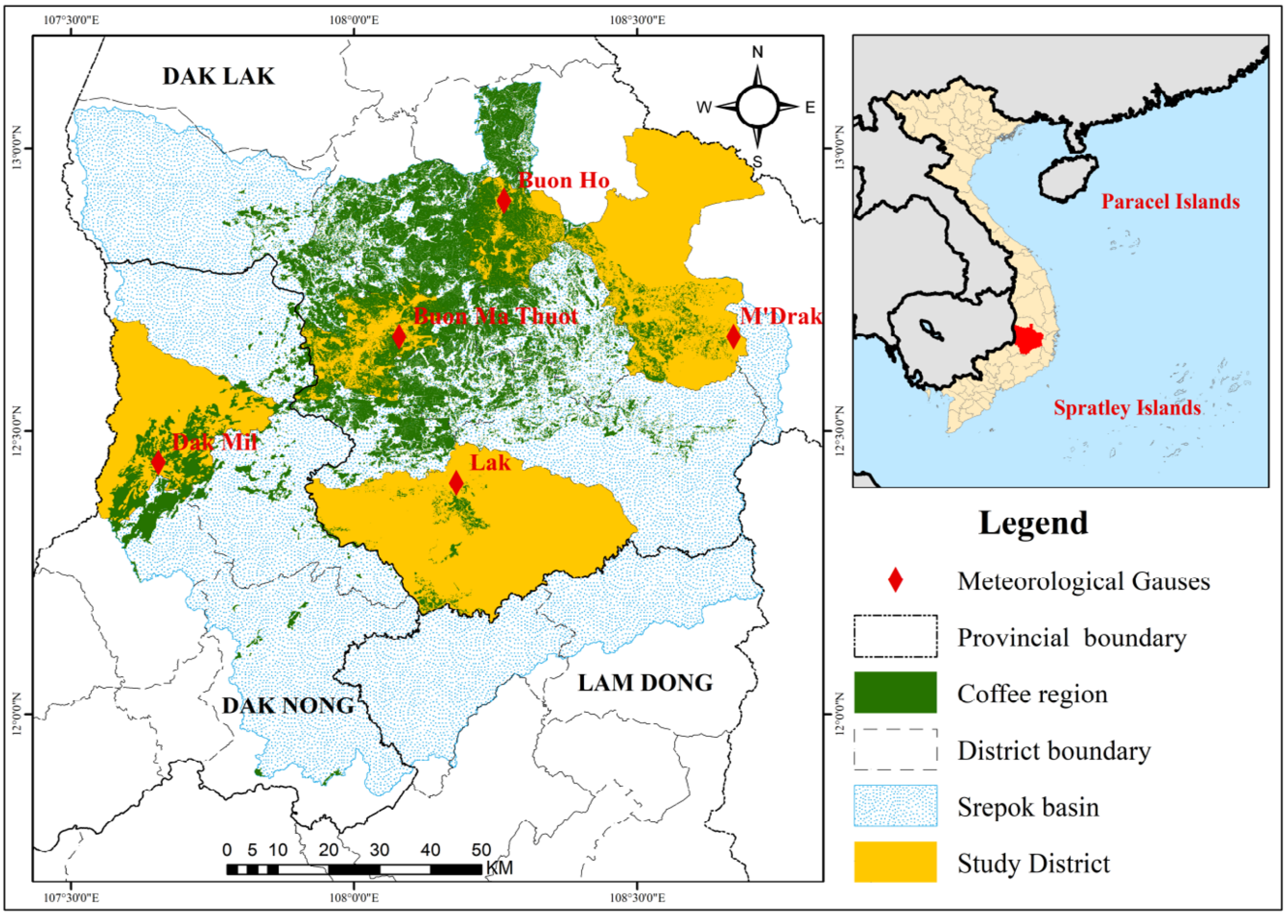

Figure 1. Study area.

spatial and temporal correspondence between the two datasets enables the establishment of quantitative relationships between climatic factors and coffee yield in the study area.

Water balance indices (PET, DEF, SUR) were calculated at the point scale of each meteorological station. Spatial interpolation was not applied; each station represents the agroclimatic conditions of the corresponding administrative district from which coffee yield statistics were sourced. Future water balance indices were derived from SDSM-downscaled daily climate series at each station location.

Three CMIP6 General Circulation Models were selected for future climate projections: CanESM5 (Canada), MPI-ESM1-2-HR (Germany), and NorESM2-MM (Norway). These models were chosen based on: (i) their demonstrated skill in simulating Southeast Asian monsoon dynamics in CMIP6 evaluations (Do et al., 2024); (ii) their representation of a range of climate sensitivities – CanESM5 (high), NorESM2-MM (moderate), and MPI-ESM1-2-HR (low) – ensuring a spread of projections that bounds scenario uncertainty; and (iii) the availability of daily output variables required for SDSM downscaling. Four SSP scenarios (SSP1-1.9, SSP1-2.6, SSP2-4.5, SSP5-8.5) were applied to represent the full range from strong mitigation to high-emission pathways.

2.1.2. Water balance indices

Based on the collected meteorological data, this study calculated three additional water balance indices crucial for analyzing climate impacts on coffee yield: potential evapotranspiration (PET), water deficit (DEF), and water surplus (SUR) (Jayakumar et al., 2017).

PET was estimated using the FAO Penman–Monteith method, the standard procedure recommended by the Food and Agriculture Organization (FAO) for calculating reference evapotranspiration (Allen et al., 1998). DEF was used to quantify crop water stress and AET. SUR was defined as the amount of water remaining after crop evapotranspiration requirements were satisfied (P – AET), representing excess water available for soil moisture recharge and potential runoff generation. These indices provide an integrated representation of water availability conditions affecting coffee growth and productivity. All calculations were performed on a monthly basis according to Equations (1)–(6).

$$\text{If } (P - PET)i < 0 = \begin{cases} NAC_i = NAC_{i-1} + (P\text{-}PET)_i \\ STO_i = WC.e^{\frac{NAC_i}{WC}} \end{cases} \tag{1}$$

$$\text{If } (P - PET)i \geq 0 = \begin{cases} STO_i = STO_{i-1} + (P\text{-}PET)_i \\ NAC_i = WC.ln\frac{STO_i}{WC} \end{cases} \tag{2}$$

$$ATL_i = STO_i - STO_{i-1} \tag{3}$$

$$AETi = \begin{cases} P + |ATL_i| \text{ , } if\, ATL < 0 \\ PET_i, \ if\, ATL \geq 0 \end{cases} \tag{4}$$

$$DEF = PET - AET \tag{5}$$

$$SURi = \begin{cases} 0 \text{ , } if\, WC < 0 \\ (P\text{-}PET)_i - ALT_i, \ if\, WC = 0 \end{cases} \tag{6}$$

where (Pi) is monthly precipitation (mm), (PETi) is monthly potential evapotranspiration (mm), (AETi) is monthly actual evapotranspiration (mm), (DEFi) is monthly water deficit (mm), and (SURi) is monthly water surplus (mm).

2.2. Methodology

2.2.1. LASSO-Based variable selection

This study examined 72 meteorological variables classified into three groups: (i) 8 annual variables, (ii) 16 variables corresponding to four coffee phenological stages (flowering, fruit development, ripening, and harvest), and (iii) 48 monthly variables (Table 1). The simultaneous inclusion of multiple correlated meteorological variables introduces the risk of multicollinearity, which compromises the accuracy and stability of conventional regression models. Therefore, this study employed the Least Absolute Shrinkage and Selection Operator (LASSO) regression method proposed by Tibshirani (1996) to select the set of variables genuinely influencing coffee yield.

LASSO is a regularization technique that operates by shrinking the regression coefficients of less important variables toward zero, thereby retaining only variables with non-zero coefficients in the final model. The objective function of LASSO is expressed as follows:

$$\widehat{\beta_{\text{LASSO}}} = \arg\min_{\beta \in R^p} \left\{ \frac{1}{2} \sum_{i=1}^{n} \left(Y_i - \left(\beta_0 + \sum_{j=1}^{p} X_{ji} \beta_j \right) \right)^2 + \lambda \sum_{j=1}^{p} |\beta_j| \right\} \tag{7}$$

where:

y_i is the observed value of the dependent variable at observation i

x_{ij} is the value of the j-th independent variable at observation i

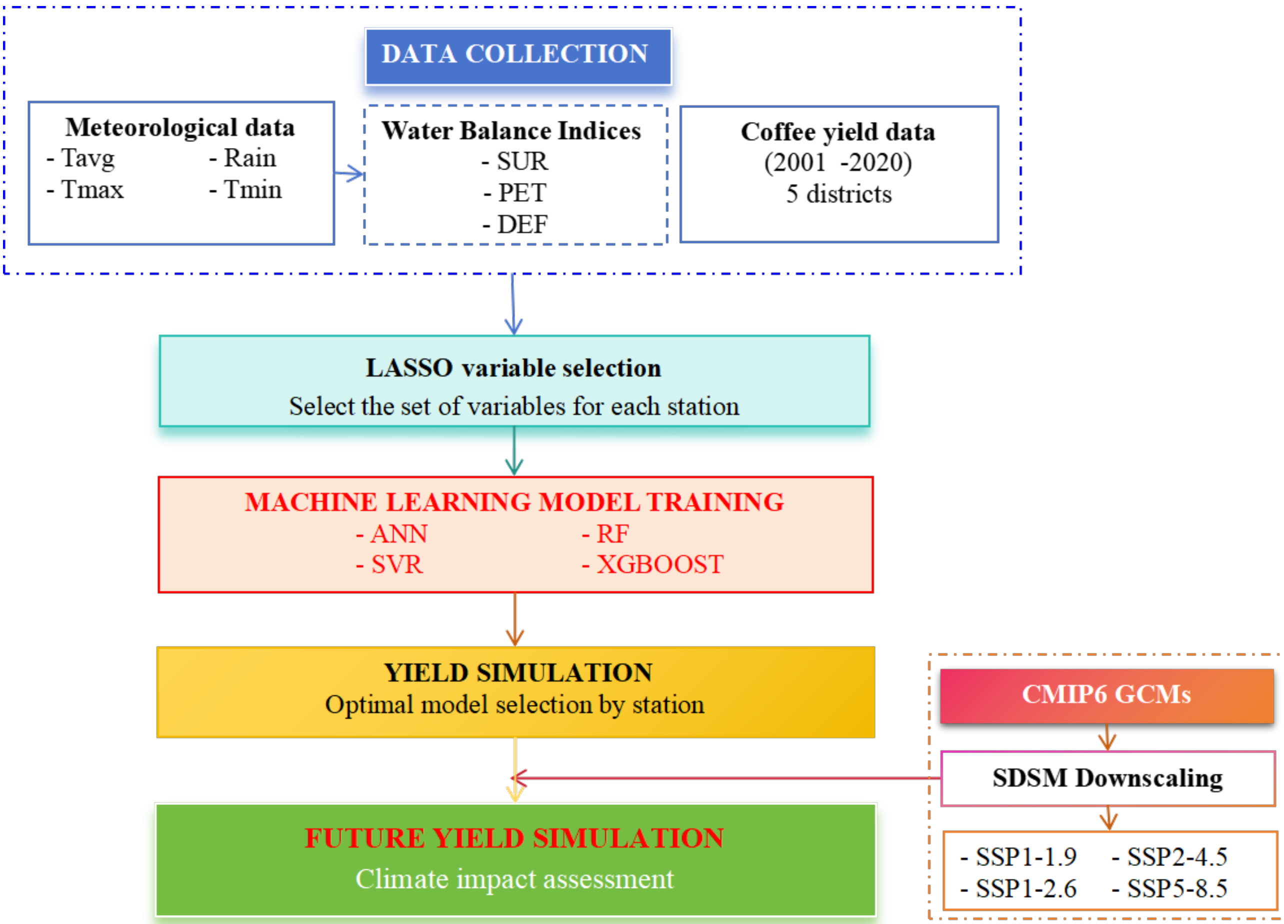

Figure 2. Research framework diagram.

β_j is the regression coefficient of the j-th variable
n is the number of observations
p is the number of input variables
λ is the regularization parameter controlling the shrinkage intensity

The component $\lambda \Sigma|\beta_j|$ (L1 penalty) plays a critical role in forcing the coefficients of less important variables toward zero. As λ increases, the shrinkage intensity intensifies, reducing the number of retained variables. Conversely, when $\lambda = 0$, the LASSO model reverts to ordinary linear regression (James et al., 2013).

In this study, LASSO was applied separately to each observation station to assess the local specificity of climate-yield relationships within the Srepok River Basin. The optimal λ value was selected through 10-fold cross-validation to ensure optimal model generalization capability (Hastie et al., 2009). LASSO analysis results identified the most important meteorological variables genuinely affecting coffee yield, eliminating statistically insignificant variables and those exhibiting multicollinearity, thereby providing a foundation for subsequent quantitative analyses in the next research steps.

2.2.2. Climate scenario development using SDSM

To assess future climate change impacts on coffee yield, this study employed the Statistical DownScaling Model (SDSM) (Wilby et al., 2002) to downscale climate information from General Circulation Models (GCMs) to the local scale at observation stations. This method establishes statistical relationships between large-scale atmospheric variables (predictors) and local climate variables (predictands) through a transfer function:

$$R = F(L) \tag{8}$$

The implementation procedure comprises five steps: (i) quality control and data transformation; (ii) predictor selection based on correlation analysis between NCEP/

Table 1. List of 72 meteorological variables used in LASSO analysis.

No.	Symbol	Description	Unit
I	Annual variables (8 variables)		
1	DayR	Number of rainy days per year	days
2	R	Annual total rainfall	mm
3	Tmax	Annual mean maximum temperature	°C
4	Tmin	Annual mean minimum temperature	°C
5	Tavg	Annual mean temperature	°C
6	PET	Annual potential evapotranspiration	mm
7	DEF	Annual water deficit	mm
8	SUR	Annual water surplus	mm
II	Growing season variables (16 variables)		
9-12	RS1, RS4, RS9, RS11	Rainfall in flowering (Jan-Mar), fruit development (Apr-Aug), ripening (Sep-Oct), harvest (Nov-Dec) stages	mm
13-16	TxS1, TxS4, TxS9, TxS11	Maximum temperature in each growing stage	°C
17-20	TmS1, TmS4, TmS9, TmS11	Minimum temperature in each growing stage	°C
21-24	TaS1, TaS4, TaS9, TaS11	Mean temperature in each growing stage	°C
III	Monthly variables (48 variables)		
25-36	R1 - R12	Monthly rainfall from January to December	mm
37-48	Tx1 - Tx12	Monthly maximum temperature from January to December	°C
49-60	Tm1 - Tm12	Monthly minimum temperature from January to December	°C
61-72	Ta1 - Ta12	Monthly mean temperature from January to December	°C

NCAR reanalysis data and station observations; (iii) model calibration; (iv) model validation; and (v) future climate scenario generation. SDSM simulation results were compared with observed data using three statistical indicators: coefficient of determination (R^2), root mean square error (RMSE), and Nash-Sutcliffe Efficiency (NSE) (Moriasi et al., 2007).

Following validation, future climate scenarios (2026-2100) were developed using three CMIP6 GCMs under four SSP scenarios described in Section 2.1.1

To quantify uncertainty in climate projections, this study applied a multi-model ensemble approach, which enables quantification of the range of climate projections arising from differences in GCM structure and parameterization (Tebaldi & Knutti, 2007). The ensemble mean (μ) represents the central tendency of climate change, while the dispersion among models is quantified through standard deviation (σ) and coefficient of variation (CV). The coefficient of variation is calculated as:

$$CV = (\sigma/\mu) \times 100\%$$

where μ is the mean value of simulations from the three GCMs and σ is the corresponding standard deviation. Higher CV values indicate greater uncertainty among climate models for specific scenarios and projection periods. This multi-model ensemble approach minimizes bias associated with reliance on any single climate model while providing a comprehensive picture of the uncertainty range in climate projections, thereby establishing a robust foundation for subsequent assessments of climate change impacts on coffee yield.

2.2.3. Machine learning models

To quantify the impacts of climate change on coffee yield, this study applied machine learning (ML) models to establish nonlinear relationships between the climate variables selected through LASSO and actual coffee yield at five observation stations during the 2001-2020 period. Climatic factors often interact in nonlinear and interdependent ways; consequently, traditional linear regression methods may inadequately capture these complex relationships. In recent years, machine learning models have demonstrated high effectiveness in crop yield forecasting due to their capacity to process multidimensional data and identify nonlinear patterns within datasets (Jeong et al., 2016; Khaki & Wang, 2019). The dataset was divided into training (70%) and testing (30%) subsets. Hyperparameter optimization for all models was conducted using grid search combined with five-fold cross-validation. Model performance was evaluated using Nash–Sutcliffe efficiency (NSE), coefficient of determination (R^2), root mean square error (RMSE), and mean absolute error (MAE). The best-performing model at each station was subsequently used for future coffee yield simulations under climate change scenarios.

Four machine-learning algorithms were evaluated, including Artificial Neural Network (ANN), Random Forest (RF), Support Vector Regression (SVR), and eXtreme Gradient Boosting (XGBoost). ANN was selected for its capability to approximate complex nonlinear relationships between climate variables and crop yield (Cybenko, 1989). RF is an ensemble tree-based method that improves predictive accuracy through bootstrap aggregation and random feature selection (Breiman, 2001). SVR constructs nonlinear regression functions using kernel transformations and has proven effective for environmental and agricultural applications with limited datasets (Smola & Schölkopf, 2004). XGBoost is a gradient-boosting algorithm that combines high predictive performance with built-in regularization to reduce overfitting (Chen & Guestrin, 2016).

Model hyperparameters were optimized using grid search and cross-validation. The algorithm with the highest predictive performance for each station was selected for subsequent climate impact simulations.

Water balance calculations and LASSO were performed in R v4.2.1. Climate downscaling used SDSM v5.3 (Wilby et al., 2002). Machine learning models (ANN, RF, SVR, XGBoost) were developed in RapidMiner Studio 10.3 . Summary figures were created in Microsoft Excel. Maps were produced using QGIS v3.28 LTR.

3. RESULTS

3.1. Historical climate and water balance conditions (2001–2020)

The baseline period (2001–2020) revealed substantial climatic and hydrological heterogeneity across the five stations (Table 2). Mean annual potential evapotranspiration (PET) ranged from 1,113 mm yr^{-1} at Dak Mil to 1,344 mm yr^{-1} at Lak, while annual water deficit (DEF) varied between 45 and 137 mm yr^{-1}. M'Drak recorded the highest annual precipitation (2,135 mm yr^{-1}) and surplus water (SUR; 862 mm yr^{-1}), whereas Lak exhibited the highest mean annual temperature (24.7°C) and water deficit. Despite relatively low annual DEF values, monthly deficits during the dry season (November–April) frequently exceeded 80–150 mm $month^{-1}$, indicating substantial seasonal water stress and irrigation demand for coffee cultivation. These baseline differences highlight the spatial variability in climatic and water-balance conditions across the Srepok River Basin and provide the reference for interpreting future climate and yield projections.

3.2. Projected climate change in the Srepok River Basin (2026-2100)

The constructed future climate scenarios (2026-2100) reveal increasing trends in both precipitation and temperature across all projection periods. Annual precipitation exhibits an increasing tendency under all scenarios, with changes ranging from 0.09% to 20.4% relative to the baseline period. Under the low-emission SSP1-1.9 scenario, precipitation increases by 4.8% to 6.9% by the end of the century. The SSP1-2.6 scenario shows more modest increases (0.09-6.2%), with the NorESM2-MM model projecting a slight decrease of 1.1% during 2026-2050. Under medium and high emission scenarios, precipitation increases are more pronounced: SSP2-4.5 projects increases of 2.0-12.6%, while SSP5-8.5 projects increases of 2.7-20.4% (Figure 3). The strongest increases occur in the late-century period (2076-2100) and are consistently associated with the CanESM5 model.

Similar to precipitation, mean annual temperature shows increasing trends across all scenarios. Temperature increases range from 0.3°C to 3.2°C depending on scenario and period. Under SSP1-1.9, temperatures increase by 0.8-1.3°C. The SSP1-2.6 scenario projects increases of 0.3-1.0°C. Under the medium-emission SSP2-4.5 scenario, temperatures rise by 0.3-1.5°C, while the high-emission SSP5-8.5 scenario records the most substantial increases of 0.5-3.2°C by the end of the century (Figure 4). Warming rates vary among models, with

Table 2. Baseline water balance and climate summary (2001–2020 annual averages).

Station	PET ($mm \cdot yr^{-1}$)	DEF ($mm \cdot yr^{-1}$)	SUR ($mm \cdot yr^{-1}$)	P ($mm \cdot yr^{-1}$)	Tmax (°C)	Tmin (°C)	Tavg (°C)
Buon Ho	1,137	57	499	1,595	27.4	19.6	22.8
BMT	1,270	93	654	1,825	29.8	20.9	24.1
Dak Mil	1,113	45	690	1,764	27.1	19.8	22.7
M'Drak	1,314	55	862	2,135	29.0	21.3	24.3
Lak	1,344	137	699	1,907	29.8	21.1	24.7

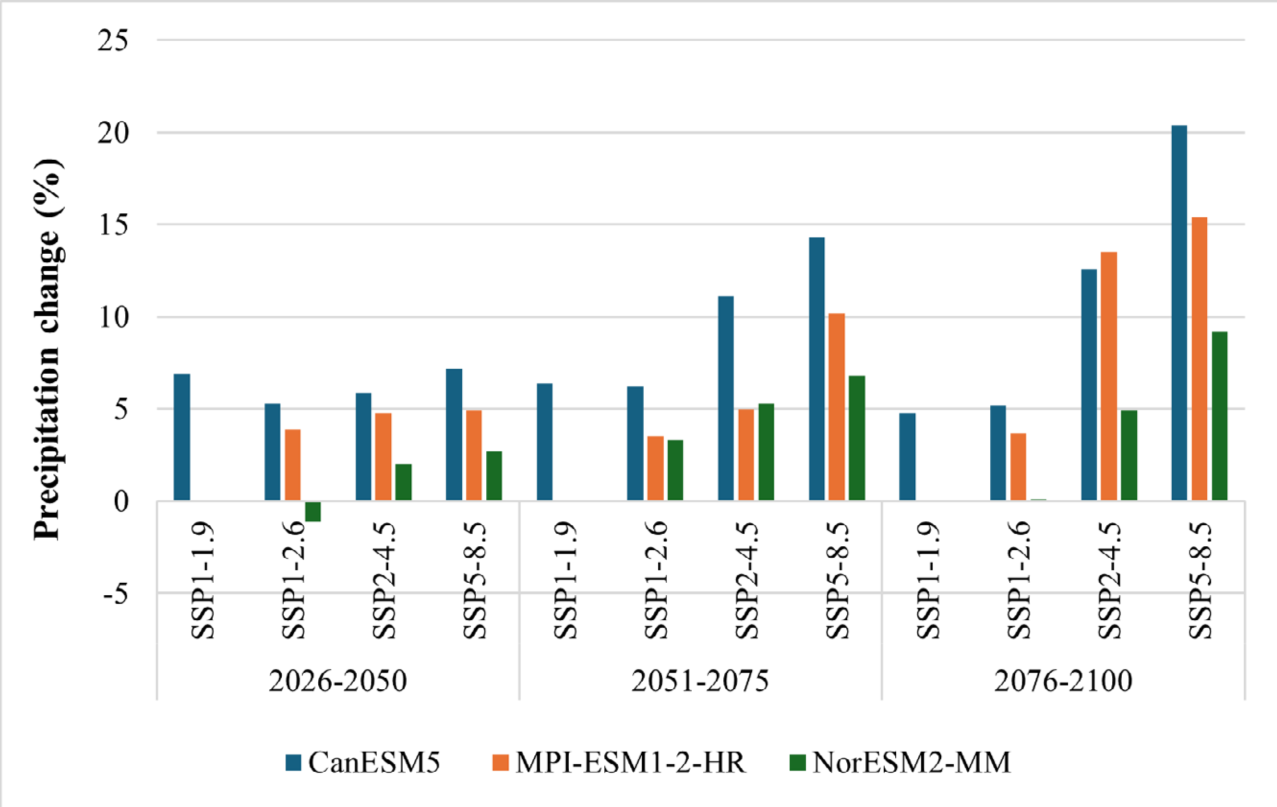

Figure 3. Projected changes in precipitation

CanESM5 consistently projecting the highest temperature increases.

Uncertainty analysis reveals distinctly different structures among climate variables, as detailed in Table 3. For precipitation, scenario uncertainty dominates (46.04%), followed by internal variability (34.47%), indicating that future precipitation regimes are highly sensitive to greenhouse gas emission assumptions. For temperature variables, scenario uncertainty also plays a dominant role. Notably, Tmin exhibits the highest scenario uncertainty proportion (56.59%), while internal variability is minimal (1.16%), suggesting that minimum temperatures primarily respond to large-scale climate forcing. In contrast, Tmax and Tavg display more balanced uncertainty structures among sources, with scenario contributions of 33.34% and 43.73%, respectively, reflecting simultaneous influences from emission factors and internal climate system variability.

The dominance of scenario uncertainty across all variables has a critical practical implication: the future climate trajectory of the Srepok Basin will be determined primarily by global emission pathways rather than by internal climate variability or model selection. For Tmin – a key determinant of Robusta coffee flowering success – the near-complete dependence on emission trajectory (56.59% scenario contribution, only 1.16% internal variability) means that ambitious mitigation efforts could substantially reduce thermal stress on coffee cultivation, whereas high-emission pathways will drive near-deterministic warming of minimum temperatures through the end of the century.

3.3. Climate variable selection using LASSO

LASSO regression was applied separately to each station to identify the set of climatic factors significantly influencing coffee yield in each distinct study area. The variable selection results are presented in Table 4.

The results reveal substantial spatial heterogeneity in the selected variable sets across stations. At Buon Ho, four variables were selected (PET, Tx9, Tm8, TmS9), indicating the dominant role of water balance and thermal extremes during the fruit ripening period (September–October). At Dak Mil and M'Drak, PET and growing-season temperature variables (TaS4 at Dak Mil; TaS1 at M'Drak) were identified as dominant predictors,

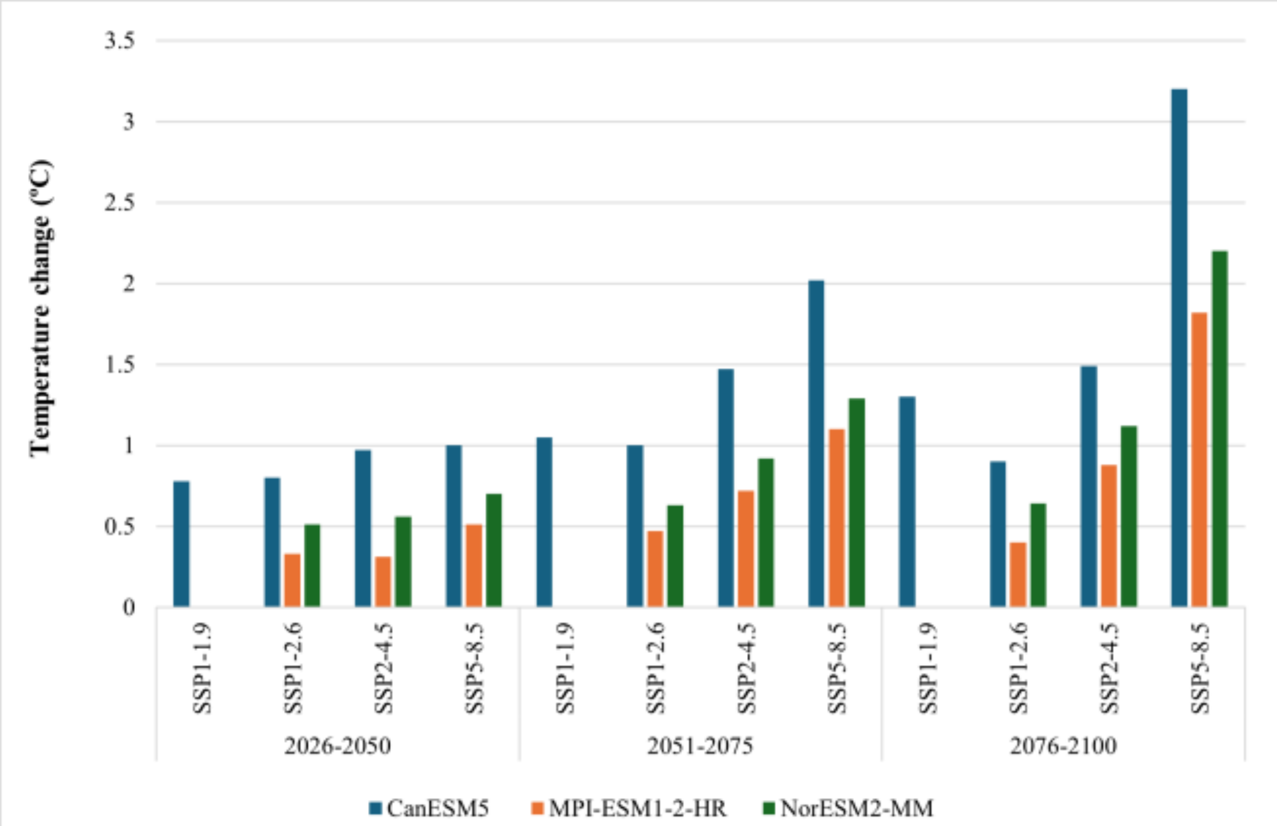

Figure 4. Projected changes in temperature.

Table 3. Uncertainty decomposition of climate change scenarios.

Component	Precipitation		Tmax		Tmin		Tavg	
	Variance	Contribution (%)	Variance	Contribution (%)	Variance	Contribution (%)	Variance	Contribution (%)
Model	14.16	6.63	0.08	12.10	0.13	22.68	0.10	16.83
Scenario	98.41	46.04	0.21	33.34	0.32	56.59	0.27	43.73
Period	27.49	12.86	0.14	22.40	0.11	19.57	0.15	23.93
Internal	73.67	34.47	0.20	32.15	0.01	1.16	0.09	15.51
TOTAL	213.73	100.00	0.62	100.00	0.57	100.00	0.61	100.00

reflecting the sensitivity of fruit development and flowering stages to thermal conditions at these stations. The selection of PET – rather than DEF – as the primary water balance predictor at Dak Mil and M'Drak is noteworthy: it indicates that the rate of evaporative demand, rather than the cumulative annual water deficit, governs yield variability at these stations, consistent with the relatively low baseline DEF values observed (45 and 55 mm·yr^{-1}, respectively; Table 2).

At Buon Ma Thuot and Lak, precipitation and water balance variables including SUR, RS4, and R9 appear alongside minimum temperature indices (Tmin, Tm1). Notably, RS4 – rainfall during the fruit development period (April–August) – was selected at both stations, demonstrating the crucial role of water availability during biomass accumulation and final yield formation. Furthermore, the presence of monthly extreme temperature variables (Tx and Tm) at most stations indicates that coffee is more sensitive to extreme temperature conditions than to annual mean values.

Overall, seasonal and monthly variables dominate over annual mean variables in the selected variable sets.

Table 4. LASSO regression results for variable selection by station.

	Buon Ho	Dak Mil	M'Drak	Buon Ma Thuot	Lak
Annual		DayR	Tmax	Tmin	R
	PET	PET	PET	SUR	SUR
Growing season	TmS9	TaS4	TaS1	RS4	RS4
Monthly		R3	R7	R9	R2
	Tx9	Tx2	Tx6		Tx5
	Tm8		Tm10	Tm1	Tm1
		Ta7		Ta7	Ta4

This indicates that "sensitive climate windows" within the coffee phenological cycle play a more important role in explaining yield variability. Concurrently, the differences in variable sets among stations confirm that climate-yield relationships exhibit local specificity, necessitating the development of separate predictive models for each region. The variables selected through LASSO analysis will serve as inputs for machine learning models (ANN, RF, SVR, and XGBoost) to simulate coffee yield under future climate change scenarios in the subsequent step.

3.4. Development and evaluation of coffee yield simulation models

Table 5 summarizes the performance of the optimal machine-learning models for each station. SVR achieved the highest predictive accuracy at Buon Ho, Dak Mil and M'Drak, whereas XGBoost performed best at Buon Ma Thuot and Lak. On the testing dataset, NSE values ranged from 0.783 to 0.850 and R^2 values ranged from 0.841 to 0.899, indicating very good model performance according to Moriasi et al. (2007). The similarity between training and testing statistics suggests that overfitting was effectively controlled despite the relatively limited sample size (n = 20 years). These results confirm that the selected climate variables successfully captured the major drivers of coffee yield variability and provide a reliable basis for future climate impact assessments.

3.5. Projected impacts of climate change on coffee yield

Projected climate change impacts on coffee yield exhibited strong spatial heterogeneity across the Srepok River Basin (Figure 5). Overall, yield losses intensified with increasing emission levels and toward the end of the century. Although future precipitation is projected to increase under most scenarios, rising temperatures and evapotranspiration demand offset these gains, resulting in increasing climatic stress on coffee production.

Dak Mil was identified as the most vulnerable area, with projected yield reductions ranging from 13.80% to 58.10% across scenarios and periods. Buon Ma Thuot also experienced substantial declines, ranging from 4.83% to 32.90%. In both locations, the combination of increasing temperature and changes in water-balance conditions contributed to significant reductions in productivity.

In contrast, M'Drak and Lak exhibited relatively stable responses to future climate change. Yield changes ranged from –11.76% to +2.43% at M'Drak and from –10.32% to +8.52% at Lak, indicating greater resilience under projected climate conditions. Buon Ho showed intermediate sensitivity, with maximum yield reductions reaching 10.73% under SSP5-8.5.

The increasing divergence among stations under higher-emission scenarios highlights the importance of local climate and water-balance conditions in determining coffee vulnerability. The difference between the most vulnerable and most resilient locations reached approximately 48 percentage points by the end of the century, emphasizing the need for location-specific adaptation strategies across the basin.

Table 5. Performance evaluation results of the best machine learning model by station.

Station	Machine Learning	Training				Testing			
		MAE	RMSE	NSE	R^2	MAE	RMSE	NSE	R^2
Buon Ho	SVR	0.05	0.053	0.878	0.887	0.059	0.059	0.783	0.841
Dak Mil	SVR	0.037	0.04	0.877	0.884	0.041	0.042	0.801	0.846
M'Drak	SVR	0.077	0.081	0.851	0.865	0.067	0.068	0.832	0.86
BMT	XGBoost	0.024	0.031	0.885	0.895	0.02	0.021	0.814	0.892
Lak	XGBoost	0.025	0.035	0.882	0.899	0.034	0.041	0.85	0.899

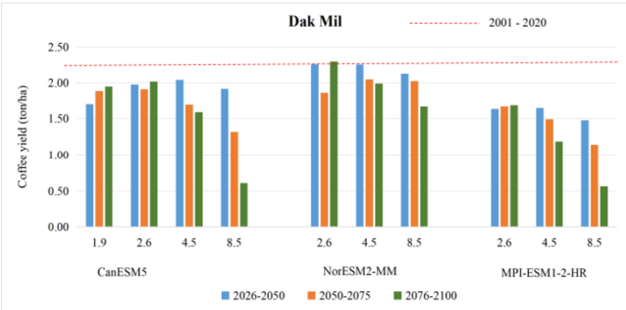

(a) Dak Mil

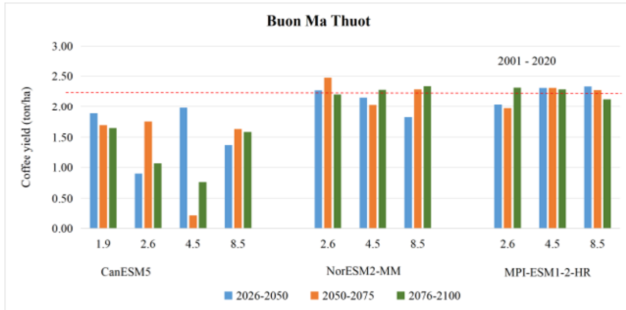

(b) Buon Ma Thuot

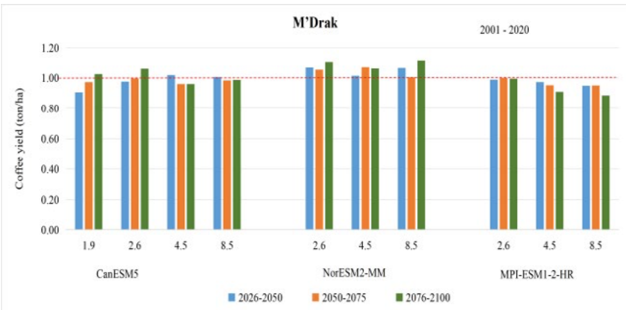

(c) M'Drak

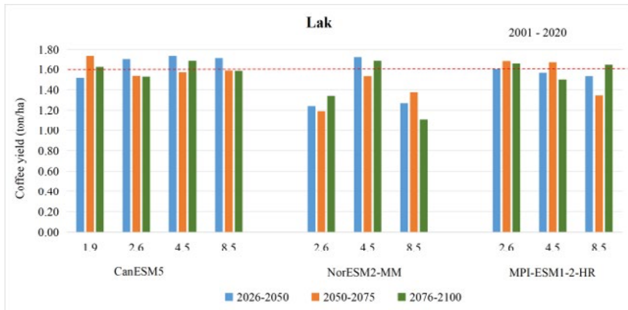

(d) Lak

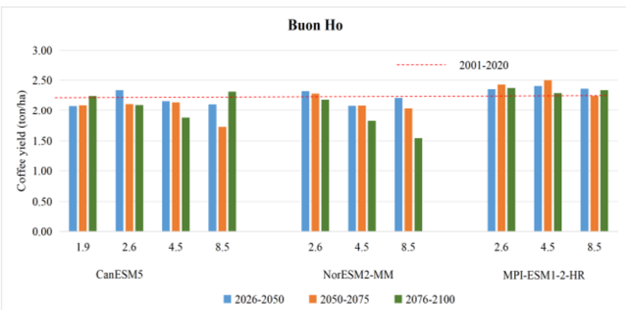

(e) Buon Ho

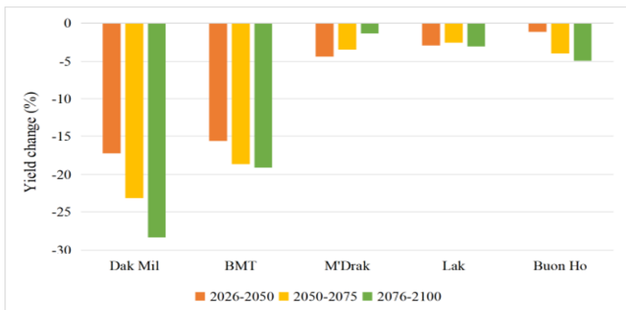

(f) Ensemble mean

Figure 5. Projected Robusta coffee yield change (%) for five stations (a–e) and multi-model ensemble mean (f) under climate change scenarios.

4. DISCUSSION

4.1. Role of water balance and climate-sensitive windows in determining yield

The dominance of PET and SUR among LASSO-selected predictors reflects the physiological reality of Robusta coffee cultivation in the Central Highlands dry season (November–April), when potential evapotranspiration routinely exceeds monthly precipitation by 80–180 mm. SUR – the residual water after evapotranspiration demand is met – functions as a direct proxy for soil water availability during the critical fruit development stage; its selection at Buon Ma Thuot and Lak confirms that water balance dynamics, not temperature alone, govern yield at low-elevation stations. This finding is consistent with Jayakumar et al. (2017), who demonstrated that growing-season water availability outperforms annual climatic means in explaining coffee yield variability in Kerala, India, and with Dinh et al. (2022), who identified the April–August water availability window as the principal determinant of Robusta yield formation in the Vietnamese Central Highlands.

The selection of monthly extreme temperature indices (Tx9, Tm8, Tmin) rather than annual mean values at most stations reflects the nonlinear physiological response of Robusta to thermal stress. Kath et al. (2020) demonstrated, using data from 798 farms across Vietnam and Indonesia, that each 1°C increase beyond optimal thresholds of 16.2/24.1°C for minimum/maximum temperature corresponds to an approximately 14% yield reduction. The projected temperature increases of 0.3–3.2°C documented in this study imply that stations whose baseline Tmax already approaches 29°C – particularly Lak (29.8°C) and Buon Ma Thuot (29.8°C) – may frequently exceed this threshold during flowering and fruit development under mid-to-high emission scenarios. At Dak Mil, where PET and growing-season temperature (TaS4) are the dominant LASSO predictors rather than DEF or SUR, projected increases in PET will progressively reduce water surplus availability (SUR), thereby creating an indirect water stress pathway during the fruit development window even though baseline annual DEF is the lowest among the five stations (45 mm·yr^{-1}). This distinction – between direct DEF-driven stress and indirect PET-driven SUR depletion – highlights the importance of using LASSO-identified predictors as the mechanistic basis for vulnerability explanation, rather than relying on annual deficit statistics that can be misleading in seasonally variable monsoon climates (Byrareddy et al., 2024).

4.2. Machine learning model performance and methodological contributions

SVR and XGBoost achieved NSE > 0.75 and R^2 > 0.84 across all five stations despite the limited 20-year training record, qualifying as “very good” performance under the Moriasi et al. (2007) criteria. This accuracy is comparable to studies using substantially larger datasets: Khaki & Wang (2019) reported R^2 > 0.85 for maize yield prediction in the United States using deep neural networks trained on thousands of farm records. The comparable accuracy achieved here reflects the efficiency of combining LASSO-based dimensionality reduction – which eliminates multicollinear variables before model training – with the built-in regularization properties of SVR (margin maximisation) and XGBoost (L1/L2 penalisation), both of which suppress overfitting under data-limited conditions.

The divergence in optimal algorithms may be related to differences in the dominant climate predictors among stations: SVR with the RBF kernel excelled at the three stations where temperature extremes dominate the predictor set (Buon Ho, Dak Mil, M’Drak), consistent with its ability to construct smooth nonlinear boundaries in high-dimensional feature spaces. XGBoost outperformed at Buon Ma Thuot and Lak, where precipitation-based predictors (SUR, RS4) drive yield variability and sequential error correction efficiently captures abrupt, threshold-like responses to rainfall anomalies. This pattern suggests that algorithm performance may depend on the dominant climate–yield relationships represented in the dataset.

4.3. Mechanisms underlying spatial heterogeneity in projected yield impacts

Projected climate change impacts exhibited pronounced spatial heterogeneity across the Srepok River Basin. M’Drak and Lak consistently showed lower vulnerability, whereas Dak Mil experienced the largest projected yield declines. These contrasting responses appear to be associated with differences in baseline water availability and projected changes in temperature and evaporative demand among stations.

M’Drak recorded the highest baseline surplus water (SUR = 862 mm yr^{-1}) and relatively small increases in projected water deficit, which may help maintain favorable moisture conditions during critical phenological stages. Consequently, yield changes remained relatively small and even showed slight increases under some low-emission scenarios.

In contrast, Dak Mil emerged as the most vulnerable station despite having the lowest baseline annual water deficit. LASSO identified PET and growing-season temperature (TaS4) as the dominant predictors at this location, indicating strong sensitivity to changes in atmospheric water demand and thermal conditions. Under future warming, increasing PET combined with higher temperatures during flowering and fruit development is likely to intensify both heat and water stress, resulting in substantial yield reductions. Notably, Dak Mil’s vulnerability arises from the projected rates of increase in PET and temperature, not from its current absolute PET value (1,113 mm·yr^{-1}), which is lower than at M’Drak (1,314 mm·yr^{-1}) and Lak (1,344 mm·yr^{-1}).

Lak provides an important example that annual water deficit alone does not fully explain climate vulnerability. Although Lak exhibited the highest baseline DEF, its relatively high precipitation and SUR values may help buffer future climatic stress. The selection of SUR and RS4 by LASSO further suggests that water availability during the fruit development period is more important than annual deficit statistics in determining coffee productivity.

These findings demonstrate that climate vulnerability is governed not only by changes in mean climate conditions but also by local water-balance characteristics and climate-sensitive growth stages. Consequently, adaptation planning should be tailored to the specific climatic drivers identified for each production area.

4.4. Comparison with other studies

The projected yield reductions at Dak Mil (–23.23% during 2050–2075) and Buon Ma Thuot (–18.65%) are broadly consistent with global projections for coffee under comparable emission scenarios. Della Peruta et al. (2025) project Arabica reductions of 23–35% in Latin America and 16–21% in Africa during 2036–2065; the comparable magnitude observed here for Robusta – a species generally considered more thermally tolerant than Arabica – reflects the amplifying role of simultaneous heat and water stress at vulnerable sites. At the regional scale, Sarvina (2021) documented 6–22% production losses due to seasonal climate variability in Indonesian Robusta, a range that overlaps with moderate-emission outcomes (SSP1-2.6, SSP2-4.5) at most stations during 2026–2050. Byrareddy et al. (2024) further demonstrated in Karnataka, India, that rainfall variability is the binding constraint at the district scale while temperature stress dominates at the regional scale – a scale-dependency consistent with the LASSO variable patterns observed across the five stations in this study.

4.5. Limitations and Future Research Directions

Four limitations should be acknowledged. First, the 20-year observational record constrains ML training, particularly for capturing decadal ENSO-related variability; the El Niño event of 2023–2024 was associated with a 20% decline in Vietnam's national coffee production – the lowest output in four years – with particularly severe impacts reported in the Central Highlands (USDA FAS, 2024) – an extreme not represented in the training period. Second, farm management variables (irrigation scheduling, fertilisation, shade-tree coverage) are excluded; since improved irrigation management can sustain yields above 3,000 kg·ha^{-1} with substantially reduced water inputs (Byrareddy et al., 2020), the projections here represent a no-adaptation baseline rather than inevitable outcomes. Third, district-level yield statistics aggregate heterogeneous management conditions and microclimates, limiting plot-scale validation. Fourth, the three-GCM ensemble does not capture the full CMIP6 spread; precipitation shows the highest inter-model variance in this study (46% scenario contribution), and future work should expand the ensemble and apply bias-correction to downscaled precipitation series.

Future priorities include: integrating satellite vegetation indices (NDVI, LAI) for continuous phenological monitoring; developing hybrid process–ML frameworks to improve extrapolation under unprecedented climate conditions; and extending the analysis to the full transboundary Srepok Basin including downstream Cambodia, where water allocation conflicts represent a growing climate-related risk for coffee-growing communities.

5. CONCLUSIONS AND RECOMMENDATIONS

This study assessed the impacts of climate change on Robusta coffee yield in the Srepok River Basin by integrating LASSO variable selection, machine learning models, and CMIP6 climate scenarios. The results indicate that water balance variables (PET, SUR) and extreme temperature indices play dominant roles in determining coffee yield, with seasonal and monthly climate variables accounting for 68% of selected predictors, demonstrating the existence of "sensitive climate windows" throughout the coffee phenological cycle. The developed machine learning models achieved high accuracy, with SVR and XGBoost exhibiting superior performance (NSE > 0.75; R^2 > 0.84). Simulation results reveal pronounced spatial heterogeneity in climate change impacts across the study basin. Dak Mil emerges as the most vulnerable area, with potential yield reductions reaching 58.10% by the end of the century, while M'Drak exhibits the smallest fluctuations. The findings are consistent with coffee yield reduction trends observed in major coffee-producing regions worldwide.

Based on the research findings, several adaptation strategies are proposed to mitigate climate change impacts on the coffee sector in the Srepok Basin. First, coffee production zoning should be reconsidered based on bioclimatic suitability, particularly in high-risk areas such as Dak Mil and parts of Buon Ma Thuot. Additionally, adaptive cultivation practices should be promoted, including adjusting planting calendars, implementing water-saving irrigation systems, enhancing shade tree coverage, and improving soil moisture retention capacity. Long-term priorities should include breeding programs for drought and heat-tolerant coffee varieties, along with developing monitoring and early warning systems based on key climatic factors. Furthermore, strengthening training and technology transfer to farmers regarding adaptive cultivation practices will contribute to enhancing the resilience of coffee production systems against future climate variability.

ACKNOWLEDGEMENTS

In memory of our supervisor, Associate Professor Dao Nguyen Khoi

REFERENCES

Allen, R. G., Pereira, L. S., Raes, D., & Smith, M. (1998). Crop evapotranspiration-Guidelines for computing crop water requirements-FAO Irrigation and drainage paper 56. Fao, rome, 300(9), D05109.

Arias, P., Bellouin, N., Coppola, E., Jones, R., Krinner, G., Marotzke, J., Naik, V., Palmer, M., Plattner, G.-K., & Rogelj, J. (2021). Climate Change 2021: the physical science basis. Contribution of Working Group I to the Sixth Assessment Report of the Intergovernmental Panel on Climate Change; technical summary.

Breiman, L. (2001). Random forests. Machine learning, 45(1), 5-32.

Byrareddy, V., Kouadio, L., Kath, J., Mushtaq, S., Rafiei, V., Scobie, M., & Stone, R. (2020). Win-win: Improved irrigation management saves water and increases yield for robusta coffee farms in Vietnam. Agricultural Water Management, 241, 106350.

Byrareddy, V. M., Kath, J., Kouadio, L., Mushtaq, S., & Geethalakshmi, V. (2024). Assessing scale-dependency of climate risks in coffee-based agroforestry systems. Scientific Reports, 14, 8028.

Chen, T., & Guestrin, C. (2016). Xgboost: A scalable tree boosting system. Proceedings of the 22nd acm sigkdd international conference on knowledge discovery and data mining.

Cybenko, G. (1989). Approximation by superpositions of a sigmoidal function. Mathematics of control, signals and systems, 2(4), 303-314.

Dak Lak Statistics Office, 2001–2021. Statistical Yearbooks of Dak Lak Province (2000–2020).

Dak Nong Statistics Office, 2001–2021. Statistical Yearbooks of Dak Nong Province (2000–2020).

Della Peruta, R., Mereu, V., Spano, D., Marras, S., Vezy, R., & Trabucco, A. (2025). Projecting trends of arabica coffee yield under climate change: A process-based modelling study at continental scale. Agricultural systems, 227, 104353.

Department of Natural Resources and Environment (DONRE) of Dak Lak Province. (2023). Meteorological dataset for Dak Lak Province (2001–2020) [Dataset]. Dak Lak, Vietnam.

Department of Natural Resources and Environment (DONRE) of Dak Nong Province. (2023). Meteorological dataset for Dak Nong Province (2001–2020) [Dataset]. Dak Nong, Vietnam.

Dinh, T. L. A., Aires, F., & Rahn, E. (2022). Statistical analysis of the weather impact on Robusta coffee yield in Vietnam. Frontiers in Environmental Science, 10, 820916.

Do, S. K., Nguyen, B. Q., Tran, V. N., Grodzka-Łukaszewska, M., Sinicyn, G., & Lakshmi, V. (2024). Investigating the future flood and drought shifts in the transboundary Srepok river basin using CMIP6 projections. IEEE Journal of Selected Topics in Applied Earth Observations and Remote Sensing, 17, 7516-7529.

Hastie, T., Tibshirani, R., Friedman, J. H., & Friedman, J. H. (2009). The elements of statistical learning: data mining, inference, and prediction (Vol. 2). Springer.

ICO (2023). Coffee Report and Outlook – December 2023. International Coffee Organization, London.

James, G., Witten, D., Hastie, T., & Tibshirani, R. (2013). An introduction to statistical learning: with applications in R (Vol. 103). Springer.

Jayakumar, M., Rajavel, M., Surendran, U., Gopinath, G., & Ramamoorthy, K. (2017). Impact of climate variability on coffee yield in India—with a micro-level case study using long-term coffee yield data of humid tropical Kerala. Climatic Change, 145(3), 335-349.

Jeong, J. H., Resop, J. P., Mueller, N. D., Fleisher, D. H., Yun, K., Butler, E. E., Timlin, D. J., Shim, K.-M., Gerber, J. S., & Reddy, V. R. (2016). Random forests for global and regional crop yield predictions. PloS one, 11(6), e0156571.

Kath, J., Byrareddy, V. M., Craparo, A., Nguyen-Huy, T., Mushtaq, S., Cao, L., & Bossolasco, L. (2020). Not so robust: Robusta coffee production is highly sensitive to temperature. Global Change Biology, 26, 3677–3688.

Kath, J., Byrareddy, V. M., Reardon-Smith, K., & Mushtaq, S. (2023). Early flowering changes robusta coffee yield responses to climate stress and management. Science of The Total Environment, 856, 158836.

Khaki, S., & Wang, L. (2019). Crop yield prediction using deep neural networks. Frontiers in plant science, 10, 621.

Moriasi, D. N., Arnold, J. G., Van Liew, M. W., Bingner, R. L., Harmel, R. D., & Veith, T. L. (2007). Model evaluation guidelines for systematic quantification of accuracy in watershed simulations. Transactions of the ASABE, 50(3), 885-900.

Bilen, C., El Chami, D., Mereu, V., Trabucco, A., Marras, S., & Spano, D. (2022). A systematic review on the impacts of climate change on coffee agrosystems. Plants, 12(1), 102.

Richardson, D., Kath, J., Byrareddy, V. M., Monselesan, D. P., Risbey, J. S., Squire, D. T., & Tozer, C. R. (2023). Synchronous climate hazards pose an increasing challenge to global coffee production. PLoS Climate, 2(3), e0000134.

Sam, T. T., Somura, H., & Moroizumi, T. (2025). Effects of different management approaches on unmet water demand in coffee-producing areas during wet and dry years: a case study of the Srepok River Watershed, Vietnam. Hydrological Research Letters, 19(2), 94-100.

Sarvina, Y., June, T., Sutjahjo, S. H., Nurmalina, R., & Surmaini, E. (2021). The impacts of climate variability on coffee yield in five indonesian coffee production centers.

Smola, A. J., & Schölkopf, B. (2004). A tutorial on support vector regression. Statistics and computing, 14(3), 199-222.

Tebaldi, C., & Knutti, R. (2007). The use of the multi-model ensemble in probabilistic climate projections. Philosophical transactions of the royal society A: mathematical, physical and engineering sciences, 365(1857), 2053-2075.

Thao, N. T. T., Khoi, D. N., Van Viet, L., Wellens, J., Lang, M., & Tychon, B. (2024). Comparing local people's perceptions of climate change and drought with scientific observations in the lower Mekong Basin: a case study in Dak Lak province, Vietnam. Environment, Development and Sustainability, 1-28.

Tibshirani, R. (1996). Regression shrinkage and selection via the lasso. Journal of the Royal Statistical Society Series B: Statistical Methodology, 58(1), 267-288.

USDA Foreign Agricultural Service. (2024). Vietnam: Coffee annual 2024 (GAIN Report No. VM2024-0012). United States Department of Agriculture.

Varma, V., Mosedale, J. R., Alvarez, J. A. G., & Bebber, D. P. (2025). Socio-economic factors constrain climate change adaptation in a tropical export crop. Nature Food, 6(4), 343-352.

Wilby, R. L., Conway, D., & Jones, P. (2002). Prospects for downscaling seasonal precipitation variability using conditioned weather generator parameters. Hydrological processes, 16(6), 1215-1234.

Italian Journal of Agrometeorology
Rivista Italiana di Agrometeorologia

Firenze University Press
https://riviste.fupress.net/index.php/IJAm

OPEN ACCESS

Citation: Alvar-Beltrán, J., Vallet, J., Kirungu, C., Soldan, R., Greenrod, S., Monzini, J. & Mottet, A. (2026). Direct and indirect effects of heat stress on cattle in East Africa. *Italian Journal of Agrometeorology* (1): 75-94. doi: 10.36253/ijam-3827

Received: November 5, 2025

Accepted: March 31, 2026

Published: September 15, 2026

Data Availability Statement: All relevant data are within the paper and its Supporting Information files.

Competing Interests: The Author(s) declare(s) no conflict of interest.

ORCID:
JAB: 0000-0003-2454-0629
JV: 0009-0008-5893-4419
CK: 0009-0008-9590-0402
RS: 0000-0003-2583-5840
AM: 0000-0003-4142-5171

Direct and indirect effects of heat stress on cattle in East Africa

Jorge Alvar-Beltrán[1,*], Julien Vallet[1], Caroline Kirungu[1], Riccardo Soldan[1], Samuel Greenrod[1], Jacopo Monzini[1], Anne Mottet[2]

[1] *Food and Agriculture Organization (FAO), Rome, Italy*
[2] *International Fund for Agricultural Development (IFAD), Rome, Italy*
*Corresponding author. Email: jorge.alvarbeltran@fao.org

Abstract. *Context*. East Africa has a heterogeneous climate, ranging from arid and semi-arid zones to humid highlands. This climate leads to diverse agroecological conditions and livestock production systems, from extensive pastoral and agro-pastoral systems in drier regions to intensive zero-grazing dairy systems. Climate-driven factors are anticipated to impact animal welfare, as well as reproduction and production parameters. Understanding the latter is paramount in a region where dairy production represents a lifeline for pastoral systems. *Objective*. Here we use state-of-the-art climate projections (CORDEX-CORE) across two representative concentration pathways (RCP) 2.6 and 8.5 to assess the direct (animal welfare) and indirect (fodder supply) effects of climate change on indigenous and climate resilient-breeds (Boran) in Tanzania, Kenya, Uganda, and Rwanda. *Methods*. Our approach involves applying the Temperature-Humidity Index (THI) and Milk Production Decline (MDEC) equations to assess heat stress on animal welfare and milk production, alongside evaluating the indirect effects on fodder supply, particularly maize and Napier grass through the Python Agroecological Zoning (AEZ) eco-physiological model. *Results*. Moderate stress ($81 < \text{THI} \le 91$) is likely to spread across the region under future climate, threatening milk production and reproductive performance. Boran daily milk yields losses may reach 0.45 kg/day (~14%) by 2070-2099 under RCP 8.5. Similarly, fodder shortages are anticipated in northern parts of Kenya and Uganda, threatening consistent animal fodder supply and affecting smallholder farmers dependent on rain-fed agricultural systems. *Conclusion*. The compounded effect of simultaneous weather hazards intensifies risks in vulnerable regions facing limited coping capacity. As demand for meat and dairy continues to rise in East Africa, immediate climate actions are essential to safeguard livestock productivity and to enhance food security in a region confronting the dire consequences of climate change. *Significance*. This comprehensive analysis is instrumental in guiding public and private investments aimed at fostering climate resilience and improving disaster risk management across livestock production systems in the region.

Keywords: THI, indigenous breeds, heat-tolerance, food security, climate resilience.

1. INTRODUCTION

1.1. Cattle: a lifeline for smallholder farmers in East Africa

About 19.6% of the 390 million cattle heads in Africa are found in the United Republic of Tanzania (9.7%), the Republic of Kenya (5.6%), Uganda (3.9%), and Rwanda (0.4%) (FAO, 2023a). While cattle production is crucial in the region, dairy farming is the lifeline for East African farmers, serving as a multifaceted cornerstone sustaining households and community livelihoods amid the challenges of climate change. In the diverse agricultural landscape of East Africa, where smallholder farming predominates, dairy farming not only provides income but also holds cultural significance, promotes social cohesion, and enhances resilience against economic shocks and environmental stresses. Dairy farming is, therefore, a primary source of income and wealth accumulation (Orodho, 2019; Rufino et al. 2013; Ngigi et al. 2010). Cattle, as the main source of dairy, provides a steady stream of milk that is processed and sold, contributing to household income generation and diversification. This additional income enables access to credit and financial services, empowering farmers to invest in agricultural inputs, education, and healthcare for their families. Beyond its economic importance, dairy farming is fundamental to food security and human nutrition due to its high-quality protein content, essential amino acids, vitamins, and minerals critical for health and growth, especially for vulnerable groups such as children and pregnant women (Beal, 2023; FAO, 2023b; Lokuruka, 2020).

Dairy production in East Africa is primarily smallholder and low-input systems. Three dairy production systems are typically identified: pastoralism, agro-pastoralism, and mixed crop-livestock (Hunt et al., 2019; Dawson et al. 2014). Production types vary based on the climatic conditions, the availability of fodder, access to land production resources, consumer demands, and market availability. Seasonal climatic variations, particularly rainfall and temperature, impact fodder and water availability, leading to detrimental effects on milk yields and reproductive performance of dairy animals (Ongadi et al. 2020). In a changing climate, rising temperatures, erratic rainfall patterns, and prolonged droughts, along with their complex interactions, are expected to further constrain water and fodder availability and quality (Trisos et al. 2022). Climate change may also influence the distribution and prevalence of livestock diseases and pests, which threaten fodder and dairy productivity, ultimately impacting food security and nutrition (Nalianya et al. 2020; Tadesse and Dereje, 2018).

1.2. Behavioral and physiological effects of heat stress on cattle

Climatic parameters such as air temperature, relative humidity, solar radiation, and rainfall patterns significantly impact livestock welfare, survival, disease, parasitism, and fodder availability and quality (Brychkova et al. 2022; Nardone et al. 2008). Among these climatic parameters, heat stress is the most critical factor affecting dairy production systems in the Horn of Africa (Rahimi et al. 2021). The normal temperature range, referred to as the thermoneutral zone (TNZ) (Ahmad et al. 2018), is the comfort zone at which dairy cows do not require additional energy to regulate their body temperature. TNZ is influenced by factors such as age, breed, feed intake, diet composition, prior temperature acclimatization, production levels, housing and stall conditions, tissue insulation (fat and skin), external insulation (coat), and animal behavior. Different dairy breeds exhibit varying abilities to maintain a constant internal body temperature, regardless of the external environmental conditions, due to various temperature-regulating physiological mechanisms (Gianone et al. 2023; Tao et al. 2020).

Heat stress is generally calculated using the Temperature Humidity Index (THI), with a value greater than 79 considered the onset of dairy cattle heat stress (see Table 1). However, the latter THI threshold can vary considerably depending on the breed. Heat stress arises when the animal's body temperature exceeds their normal range due to prolonged exposure to excessive heat and humidity (Becker et al. 2020). This condition occurs when an animal's ability to dissipate heat is compromised, leading to physiological and behavioral changes. Some physiological responses to heat stress in dairy cattle include sweating, elevated respiration rates, vasodilation with increased blood flow to the skin surface, higher rectal temperatures, reduced metabolic rates, decreased dry matter intake, diminished feed utilization efficiency, and altered water metabolism (Ganaie, 2013). These responses can adversely affect the productivity and health of dairy animals. Specifically, heat stress leads to decreased feed intake, lower milk yields, and changes in milk quality (Tao et al. 2020; Kumar et al. 2020; Smith et al. 2013). Heat stress exerts strong and well-documented constraints on livestock reproductive parameters, such as reduced fertility and conception rates (Dovolou et al. 2023; Ahmad et al. 2018), with critical implications for long-term sustainability of pastoral systems. These reproductive challenges arise from various physiological effects, including reduced blood flow to the uterus, altered hormone levels, and reduced quality of oocytes and embryos (Dovolou et al. 2023; Thatcher et al. 2010). Elevated thermal load also disrupts endocrine regulation and directly impairs ovarian and testicular function, leading to reduced conception and pregnancy rates, extended service and calving intervals, and increased early embryonic loss (Marai et al. 2007; Thornton et al. 2021). Female fertility is particularly vulnerable because the follicle-enclosed oocyte is highly sensitive to hyperthermia, while heat stress in males reduces spermatogenesis and semen quality, further constraining herd fertility. These reproductive impacts translate into cumulative demographic and economic consequences for pastoral herds, including lower replacement rates and reduced productivity over successive seasons.

Breed-specific differences strongly mediate reproductive resilience under heat stress. Tropically adapted *Bos indicus* cattle consistently exhibit greater reproductive tolerance than *Bos taurus* breeds, with experimental evidence showing higher embryo survival and developmental competence under elevated temperatures (Silva et al. 2013). Heat stress also impairs immune function, increasing disease susceptibility and compounding reproductive losses, particularly in pastoral systems with limited veterinary and nutritional buffering (Renaudeau et al. 2012). Together, these interactions highlight reproductive capacity and immune robustness as key traits underpinning heat tolerance and long-term adaptation in climate-stressed livestock systems. Heat stress is also linked to metabolic disorders through dysbiosis of rumen and hindgut microbiota (doi: 10.1128/spectrum.03312-23; doi: 10.3389/fmicb.2025.1724640). Several hormonal responses, triggering immune reactions are activated during heat stress (Cartwright et al. 2023; Bagath et al. 2019), leading to increased incidences of intramammary infections among heat stressed animals (Rakib et al. 2020).

1.3. Study rationale

In the Horn of Africa, recent failures in rainy seasons from 2020 to 2023, intensified by inter-annual rainfall variability associated with El Niño Southern Oscillation, have led to significant declines in crop yields and milk production. Insufficient water and fodder availability has resulted in the loss of over 9 million livestock heads (NASA, 2023). Such alarming statistics underscore the urgent need for the Food and Agriculture Organization (FAO) to broaden its understanding of heat stress on animal's welfare in a region where livelihoods are increasingly compromised, and food security is under severe threat. While literature on this topic is emerging (Rahimi et al. 2021; Ekine-Dzivenu et al. 2020), this study aims to build on the existing foundational work by exploring the dual effects (direct impacts on animal welfare and productivity and indirect effects on animal food supply) of heat stress on livestock. Given the complex interactions between climate variables and the physiological responses of livestock, this research is both timely and necessary.

To achieve this objective, we apply advanced climate projections from the Coordinated Regional Downscaling Experiment (CORDEX) and the Coordinated Output for Regional Evaluations (CORE). Additionally, we adopt well established scientific analytical frameworks such as the THI and Agroecological Zoning (AEZ) eco-physiological model to assess the evolving situation in a holistic manner. By linking climate science with impacts and actions, our goal is to provide evidence-based insights for decision-makers, agricultural extension workers, and researchers. This research also aims to equip pastoral communities with the knowledge and strategies necessary to tackle the increasing challenges posed by climate change, thereby enhancing resilience and promoting sustainable livelihoods.

2. MATERIALS AND METHODS

2.1. Climatic and ecosystem characterization

A tropical savannah climate covers the four countries, interrupted by a corridor of arid steppe and desert climates along the Indian Ocean coastline and across northwest Kenya and central Tanzania. Tropical rainforest conditions are found in the Lake Victoria Basin, while temperate climates occur in the high-altitude regions of the Great Rift Valley. Kenya is the driest among the four countries, with a total annual precipitation ranging from 400 to 600 mm near Lake Turkana and in areas bordering Somalia. In contrast, southern parts of Uganda and Rwanda receive an annual rainfall between 1,000 and 1,600 mm. These climatic conditions create a mosaic of environments, resulting in a diverse range of agroecological zones and livestock production systems across East Africa (Fig. 1).

2.2. Livestock production systems

2.2.1. Livestock density

Before characterizing the livestock production systems in East Africa, it is essential to have an overview of livestock density in Kenya, Rwanda, Tanzania, and Uganda. Although disaggregated values specifically for cattle are not available, Fig. 2 illustrates the number of livestock units per km^2. Regions approximately 150 km

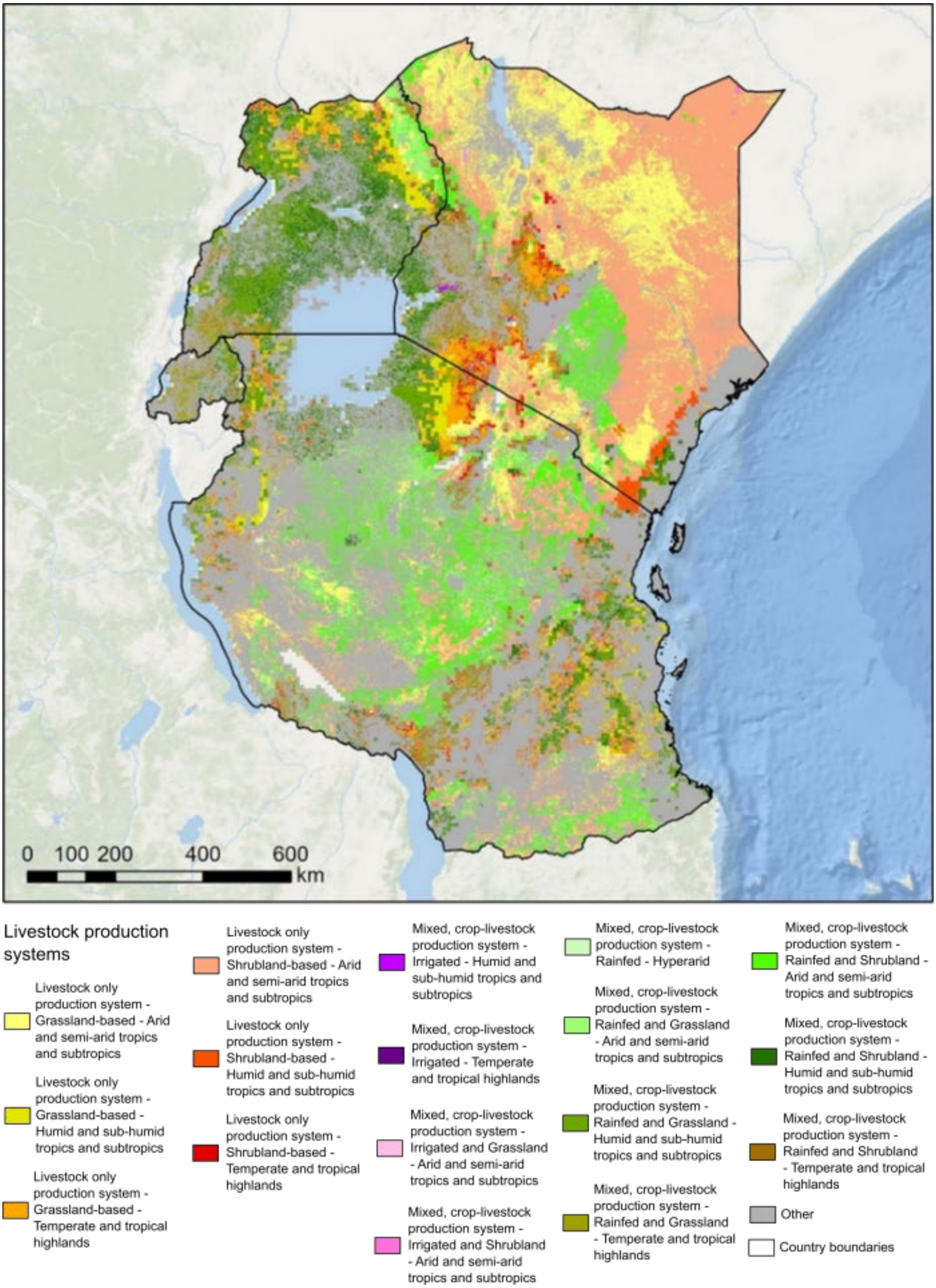

Figure 1. Livestock production systems in East Africa. Source: Robinson et al. (2011).

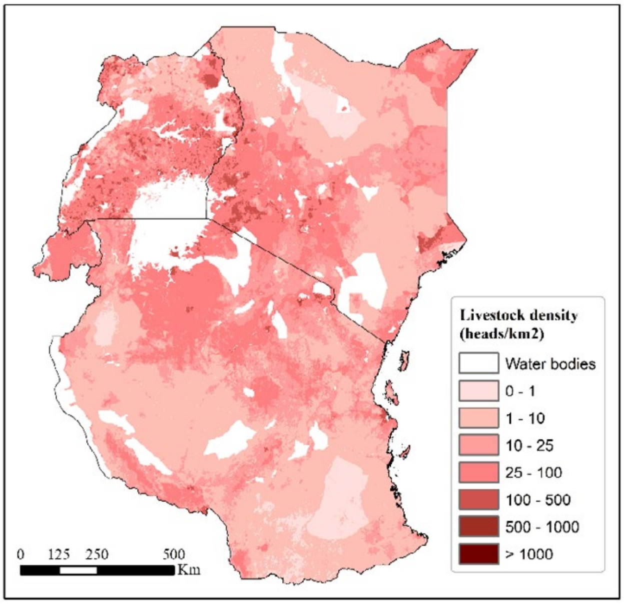

Figure 2. Livestock density (heads/km2) in East Africa. Figure adapted from Global Livestock of the World (GLW3) distribution dataset per km² for buffaloes, cattle, chicken, ducks, goats, horses, pigs and sheep (Gilbert et al. 2018).

from Lake Victoria exhibit the highest livestock density, 25-100 heads per km², along with areas in northeastern Kenya. In contrast, southeastern Tanzania and the Lake Turkana region have densities of less than one animal per km².

2.2.2. Kenya

The livestock production landscape in Kenya is categorized into three main systems (intensive, semi-intensive, and extensive) based on herd size, management practices, and inputs (FAO, 2018a). About 39% of the country's milk is produced by intensive systems, known as zero-grazing, while 43% is produced by semi-intensive, and 18% by extensive systems (FAO, 2022). In the Kenyan highlands, for example, over three-quarters of the smallholder dairy farms already fall under semi-intensive or intensive systems (Paul et al. 2022). Extensive farming systems relying on pasture are typically adopted by farms with larger herds, whereas agro-pastoral systems are key to livelihoods in arid regions.

2.2.3. Rwanda

Rwanda's livestock production systems include intensive or zero-grazing, pastoral or open grazing, and semi-grazing (Habiyaremye et al. 2021). Notably, 94% of dairy animals are raised on zero-grazing farms and produce 93% of national milk (FAO, 2022). The zero-grazing systems consist of feeding cut-and-carry fodder, mostly Napier grass and crop residues to animals kept in sheds (Eugene, 2018). Semi-grazing systems involve feeding cattle a mix of grass and fodder, combining elements of both zero and open grazing, with only 4% of Rwandan dairy cows categorized as semi-grazing. Only 2% of national dairy herd is kept under open grazing, contributing to 3% of the national milk production.

2.2.4. Tanzania

Tanzania's traditional pastoralist system focuses on the production of meat and milk while managing large cattle herds grazing on natural pastures. These herds may be family-owned or part of commercial operations, with large-scale production concentrated in the northern and western regions, while smallholders dominate the southern highlands (FAO and NZAGGRC, 2019a). Traditional pastoral systems produce 91% of national milk, whereas intensive dairy systems produce 9% of national milk and keep 2% of the dairy herd (FAO, 2022).

2.2.5. Uganda

Uganda's dairy industry is primarily led by traditional systems (extensive, agro-pastoral, and pastoral), accounting for 86% of the country's milk production (FAO and NZAGGRC, 2019b). Extensive systems keep around 18% of the herd and produce 24% of national milk (FAO, 2022). Agro-pastoral systems are mainly managed using family labor and few purchased inputs, keeping around 54% of the herd and producing 53% of the national dairy milk. Lastly, pastoral and semi-nomadic pastoralists keep about 27% of the herd and produce 9% of national milk.

2.3. Livestock breeds

In East Africa, livestock breeds can be categorized into three genetic groups: indigenous breeds (e.g., Boran, Kenyan Sahiwal, Maasai Zebu, Bahima, Chagga, Iringa Red, Kigezi, Mpwapwa, Ruzizi, Watusi, and Winam), exotic breeds (e.g., Holstein-Friesian, Jersey, Guernsey, Ayrshire, Brown Swiss, and Milking Shorthorn), and crossbreeds between indigenous and exotic breeds (Kambal et al. 2023; Rege, 1999). Indigenous breeds generally yield lower milk quantities and are kept for dual purposes, such as meat and milk production (Akinsola et al. 2023). Indigenous breeds are highly adapted to harsh environmental conditions and tolerant to endemic diseases. Indigenous cattle groups in Kenya, Tanzania, and Uganda include large and small East African Zebu, Zenga, and Sanga, whereas Rwanda mostly has the Sanga breed (Mwai et al. 2015).

In this work, we assessed the effects of heat stress on Boran's welfare and production. Boran cattle (*Bos indicus*) possess a combination of morphological, structural, and physiological traits that confer high tolerance to heat stress in East African pastoral systems (Haile, 2011) and are more productive than other indigenous breeds (Cossins et al. 1998). They can survive and reproduce under high ambient temperatures while utilizing low-quality fodder resources and enduring water shortages and long watering intervals (Bayssa et al. 2021). Boran cows in, for example, Ethiopia can produce 843 kg of milk over a 36-week lactation period (about 3.3 kg/day) under the pastoralist system in the Borana rangelands. Morphologically, they typically have a light grey to fawn coat that reflects solar radiation, along with a short hair coat and thin, highly pigmented, and motile skin that enhances convective and evaporative heat loss while protecting underlying tissues from ultraviolet radiation. Structurally, long legs elevate the body above hot ground surfaces, reducing conductive heat gain and enabling long-distance trekking, while large dewlaps and wide ears increase surface area for metabolic heat dissipation. Physiologically, Boran cattle exhibit low maintenance energy requirements, efficient fat mobilization, and adaptive water-conservation mechanisms, allowing sustained productivity and reproductive performance under high temperatures, feed scarcity, and limited water availability (Bayssa et al. 2021).

2.4. Historical and future climate data

The W5E5 dataset for the 1980-2009 period, which is an observational gridded dataset with global coverage at a 0.5º spatial resolution, was adopted in this study due to its strong performance ratings for temperature and precipitation variables (Cucchi et al. 2020). The W5E5 dataset is derived from the ERA5 dataset and adjusted using global observational datasets such as CRU TS4.03 and GPCCv2018 (Harris et al. 2020; Schneider et al. 2018). It provides daily information for twelve climatic variables and is the reference dataset by the Inter-Sectoral Impact Model Intercomparison Project (ISIMIP) for impact assessment studies such as this one.

For future climate projections, this study embraces CORDEX-CORE, which aims to establish a common climate modeling framework globally (Giorgi et al. 2021a). The CORDEX-CORE initiative provides consistent regional climate projections across most inhabited land regions using nine CORDEX domains at a 0.22º spatial resolution (~25 km). The reason for selecting three specific GCMs in this work is that, on the one hand, these GCMs (Global Climate Models) have a high (HadGEM2-ES), medium (MPI-ESM-MR), and low (NorESM1-M) equilibrium climate sensitivity within the Coupled Model Intercomparison Project-5 (CMIP5) ensemble; and, on the other hand, they perform reasonably well over most of the CORDEX-CORE domains (Elguindi et al. 2014; McSweeney et al. 2025). Future simulations were run for two climate change scenarios: Representative Concentration Pathway (RCP) 2.6 and 8.5, which correspond to approximately 490 and 1370 ppm CO_2 equivalent by 2100, respectively (Van Vuuren et al. 2011; Clarke et al. 2007; Riahi et al. 2011). The selection of RCPs 2.6 and 8.5 covers the Intergovernmental Panel on Climate Change (IPCC) range of greenhouse gas concentration pathways for the 21st century. Therefore, projected changes under the intermediate scenario (RCP 4.5), aiming to stabilize global temperature increases at 2 to 3 °C, are considered to fall within the simulation range of RCPs 2.6 and 8.5. Outputs from the GCMs are dynamically downscaled using the Regional Climate Model (RCM) REMO2015 at a 0.22º spatial resolution (Giorgi et al. 2021b). REMO2015 is selected because it has completed the full set of CORDEX-CORE experiment simulations (Giorgi et al. 2022; Jacob et al. 2012). Although RCMs can effectively represent regional climates, they often suffer from systematic biases that may limit their usefulness in impact assessment studies. To address these biases and correct climate projections, we applied bias-correction with Empirical Quantile Mapping using the period running from 1976 to 2005 as the overlapping timeframe between the W5E5 reanalysis dataset and the CORDEX-CORE historical simulation runs, concluding in 2005.

2.5. Direct effects of climate change

The analytical framework used to assess the effects of heat stress on dairy animals was based on the THI formula (Eq. 1) adopted in Sub-Saharan Africa by Ekine-Dzivenu et al. (2020), slightly differing from that of Hahn et al. (2009). However, a cross-validation of both formulas yielded nearly identical THI results (results not shown for brevity). After computing the THI units for each day using temperature and relative humidity data from CORDEX-CORE simulation runs, the THI units were categorized into four THI classes using the thresh-

Table 1. Degree of heat stress on beef cattle in East Africa.

THI category	THI units	Animal's responses
None	THI ≤ 75	– Both productive and reproductive performance are optimum.
Mild	75< THI ≤ 81	– Livestock body can control heat stress by chemical and physical means. – Livestock seeks shade. – Rectal temperature and respiration rates increase. – Dilation of blood vessels.
Moderate	81< THI ≤ 91	– Body temperature increases and productive and reproductive are severely affected. – Respiration rates significantly increase. – Dry matter intake and ratio of forage to concentrate intake decreases. – Water intake significantly increases.
Severe/Danger	THI >91	– Respiration and excessive saliva production increases. – Productive and reproductive performance significantly decrease. – Rumination and urination decrease. – Livestock may die under extreme stress conditions.

olds (Table 1) proposed by Rahimi (2020) for beef cattle in East Africa. Lastly, the THI daily data was aggregated into 30-year periods: 1980-2009 for the historical period and 2010-2039, 2040-2069, and 2070-2099 for future periods.

$$THI=(1.8 \times Tmax + 32) - [(0.55 - 0.0055 \times RH) \times (1.8 \times Tmax - 26.8) \quad (1)$$

where Tmax is the maximum daily temperature in °C and RH the daily relative humidity in %.

The increase in air temperature and relative humidity can result in a significant milk production decline (MDEC). From a quantitative perspective, Bernabucci et al. (2010) reported a daily milk loss of 0.27 kg for each THI unit increase. In this study, changes in milk production were calculated using the formula (Eq. 2) proposed by Berry et al. (1964) and extensively applied in literature (see, for example, Hammami et al. 2013):

$$MDEC\ (kg/day) = -1.075 - (1.736 \times NL) + (0.02474 \times NL \times THI) \quad (2)$$

where NL is the normal level of daily milk production (kg/day) for Boran (3.3 kg/day) under TNZ.

In Eq. 2, the baseline net lactation yield (NL = 3.3 kg/day) for Boran cattle represents an average daily milk yield under extensive pastoral conditions, derived from published estimates for indigenous cattle in East African arid and semi-arid systems. This value reflects a long-term mean across the lactation period, rather than peak yield, and implicitly integrates seasonal variability in feed and water availability characteristic of pastoral production systems. The baseline is, therefore, intended as a reference production level under non-intensive management, suitable for use in comparative and climate-sensitivity analyses rather than as a stage-specific or high-input performance estimate.

2.6. Indirect effects of climate change

Climate change may affect the availability and quality of fodder indirectly. It can result in feed shortages and decline in livestock productivity. To gain a better understanding of fodder changes, we estimated the impacts of climate change on potential yields using the AEZ method developed by the FAO and the International Institute for Applied Systems Analysis (IIASA) for land evaluation (FAO and IIASA, 2000). AEZ integrates crop simulation models with land management decision analysis to capture changes in agroclimatic resources over time (Fischer et al. 2021). To simplify the application of AEZ, a Python package (referred to as PyAEZ) is used to encapsulate the complex calculations involved in AEZ.

PyAEZ includes six main modules: (i) climate regime, (ii) crop simulations, (iii) climate constraints, (iv) soil constraints, (v) terrain constraints, and (vi) economic suitability analysis. All the climate data generated during the historical (W5E5) and future (CORDEX-CORE) simulation runs were used as data input in module 1. PyAEZ calculates biomass based on an eco-physiological model (Deshapriya et al. 2020). Constraint-free crop biomass accumulates throughout the growing season, driven mainly by incoming solar radiation, temperature, and crop-specific characteristics (e.g., crop cycle length, maximum photosynthesis rate, leaf area index at full development, harvest index, and crop sensitivity to heat). To maximize yields, PyAEZ automatically determines the optimal start of the growing season. Here, simulations are conducted under rain-fed conditions and yield projections are bias-corrected based on historical simulations and by using the differences between simulated yields in the first projected year and those of the last historical year (2010). The results are then averaged by administrative boundaries, as PyAEZ produces outputs at the same spatial resolution as the climate models. Yield results from different climate models are ensembled for various periods (2031-2060 and 2061-2090) and analyzed for two RCPs (2.6 and 8.5).

To assess the indirect impacts of climate change on livestock production, we selected maize (*Zea mays*) and Napier grass (formerly *Pennisetum purpureum*, now *Cenchrus purpureus*). Maize is commonly used as a basal feed and a source of fiber, carbohydrates, and protein in the form of silage, stover (residues), and grain (Nyokabi et al. 2022; Maleko, 2018). Maize starch provides a combination of rumen-fermentable energy, fueling the microbial population, and rumen bypass starch, which is then converted into glucose that the animal absorbs and utilizes. On the other hand, Napier grass is a fast-growing perennial grass native to Sub-Saharan Africa and serves as a multipurpose fodder crop, primarily used for feeding cattle in cut-and-carry production systems (Islam et al. 2024). Napier grass is used by East African smallholder farmers for cattle fattening and obtaining higher milk yields (Islam et al. 2023). Given that most smallholder farmers own small and fragmented land parcels, Napier grass represents an ideal alternative to other feed options due to their high yield, low input requirements, and minimal acreage needed for cultivation.

3. RESULTS

3.1. Effects of climate change on animal welfare

3.1.1. Historical THI analysis

Annual-averaged THI historical (1980-2009) results show moderate stress (81 < THI ≤ 91) conditions across Uganda, Kenya, and the eastern region of Tanzania (Fig. 3a). In these areas, moderate THI has already affected milk production (see Table 1) and reproductive parameters. Conversely, in high-altitude areas of south-west Kenya, Tanzania, and Rwanda the level of THI stress was either mild (75 < THI ≤ 81) or none (THI ≤ 75). In areas experiencing mild stress, heightened animal respiration rates have been noted, though the impact of heat on milk yields was minimal. Historical THI trends also reveal statistically significant differences ($p < 0.05$)

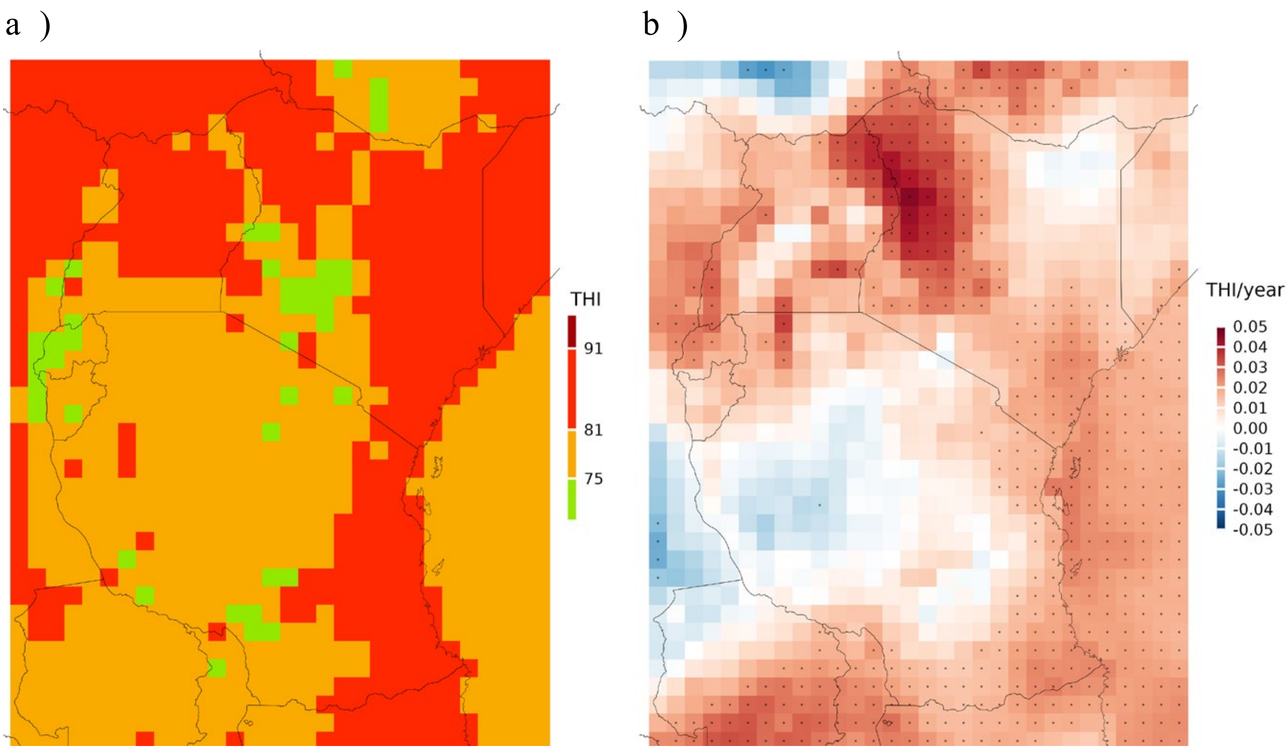

Figure 3. (a) Annual-averaged THI classes and (b) yearly change (THI units/year) over 1980-2009. Pixels with a black dot in Fig. 1b show statistically significant differences ($p < 0.05$) over the historical period.

across the arid and semi-arid zones of Kenya, including Uganda's Karamoja drylands and the coastal and southern regions of Tanzania (Fig. 3b). In these areas, THI units have risen at a rate of 0.02 to 0.04 units per year, totaling an increase of 0.70 to 1.40 since 1980. In contrast, THI units in central Tanzania and northeast Kenya have remained unchanged or slightly decreased since 1980.

Fig. 4 displays the annual count of days with above mild (THI > 75, Fig. 4a), moderate (THI > 81, Fig. 4b),

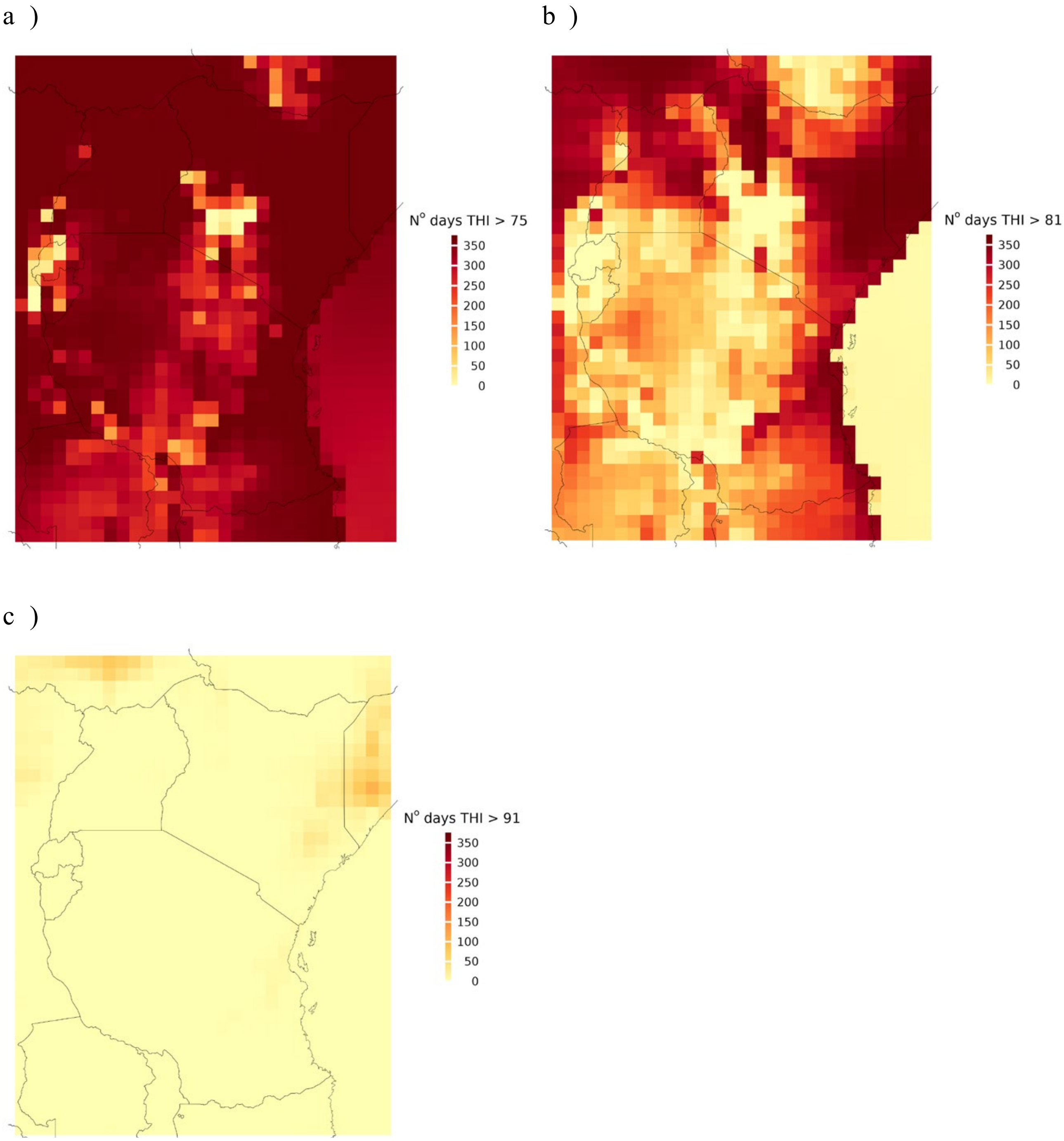

Figure 4. Annual-averaged count of days under (a) mild (THI >75), (b) moderate (THI >81), and (c) severe/danger (THI >91) heat stress over 1980-2009.

and severe/danger (THI > 91, Fig. 4c) heat stress conditions during the historical period from 1980 to 2009. Year-round (>300 days/year) mild stress conditions were observed in most regions, with exceptions in the mountainous south-western parts of Kenya, Rwanda, and south-western Tanzania (Fig. 4a). Additionally, the highest (300 days/year) annual count of days with above moderate stress conditions were reported in central parts of Uganda, areas around Lake Turkana and eastern parts of Kenya, as well as the coastal areas of Tanzania (Fig. 4b). Lastly, severe/danger (~50 days/year) conditions were only observed in small pockets of eastern Kenya (Fig. 4c). However, short-duration extreme (THI > 91) conditions fatal to animals may have occurred but are not detectable in annual averages.

3.1.2. Future THI analysis

Climate change is expected to increase Boran's exposure to heat stress (Fig. 5a). Under RCP 2.6, areas under moderate (81< THI ≤ 91) stress rise slightly until mid-century and then remain constant. In contrast, under RCP 8.5, moderate stress expands across all territories, particularly by mid- to late-century. Only a few areas will experience mild (75 < THI ≤ 81) stress whereas areas under no stress (THI < 75) vanish completely under both RCPs. Fig. 5b illustrates the incremental change in THI units for both RCPs throughout the century relative to 1976-2005. THI units are projected to increase by 1 to 2 units under RCP 2.6, and by 3 to 4 and 5 to 6 units by the mid and end of the century, respectively, under RCP 8.5. In the southern regions of Uganda and along the Tanzanian coastline, the THI increase could reach 6 to 7 units by 2070-2099 under RCP 8.5.

Fig. 6 depicts the change in the annual average number of days when specific THI conditions are met across the century for different RCPs relative to 1976-2005. Fig. 6a shows a year-round and widespread increase in mild (75 < THI ≤ 81) stress conditions across all countries, throughout the century and under both RCPs. Moderate (81 < THI ≤ 91) stress, characterized by substantial milk yield losses and reduced reproductive rates, further increase (250-350 days/years) in coastline areas by 2070-2099 under RCP 8.5 (Fig. 6b). Under the worst-case scenario, recurrent fatal conditions (THI > 91) for animals may increasingly occur (0-50 days/year under RCP 2.6 and 100-150 days/year under RCP 8.5), particularly along the Tanzanian and Kenyan coastlines (Fig. 6c).

3.2. Effects of climate change on milk production

3.2.1. Historical milk yield analysis

Fig. 7 illustrates the annual average milk losses (kg/day) for the Boran breed from 1980 to 2009. Since 1980, areas along Lake Turkana have experienced a statistically significant ($p < 0.05$) decrease in milk yield losses of 0.002 kg/day per year. This decline corresponds to a total daily milk reduction of 0.6 kg/day from a baseline of 3.3 kg/day under TNZ. Coastal regions of Tanzania and Kenya have also reported a statistically significant decline in milk yields, although these reductions are less pronounced (0.001 kg/day per year) than those observed along Lake Turkana. In contrast, in central and south-

a)

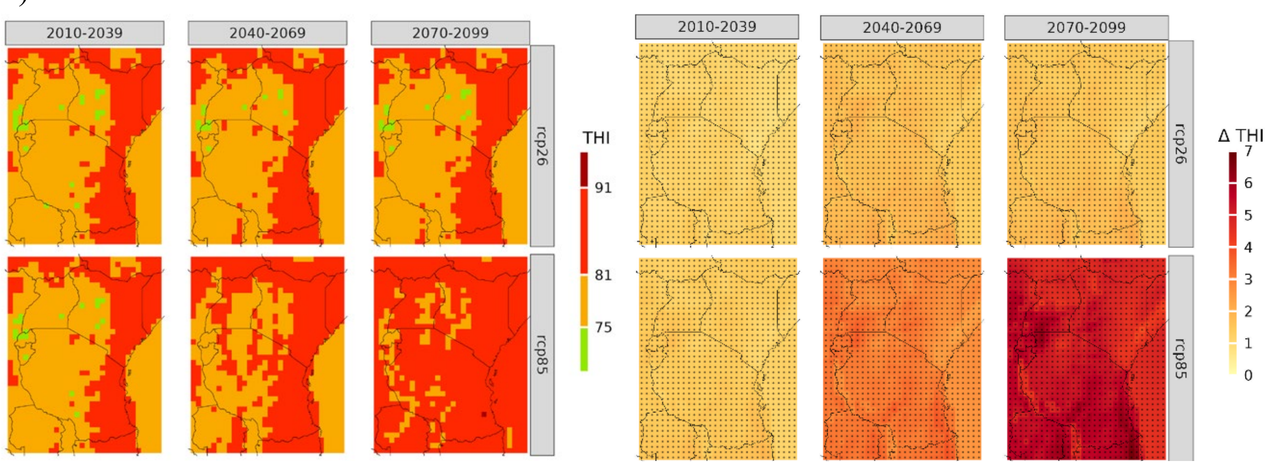

Figure 5. Projected (a) THI classes and (b) THI unit increase over the century for RCPs 2.6 and 8.5 relative to 1976-2005. A black-dot in Fig. 3b represents a high GCM agreement in the climate change signal.

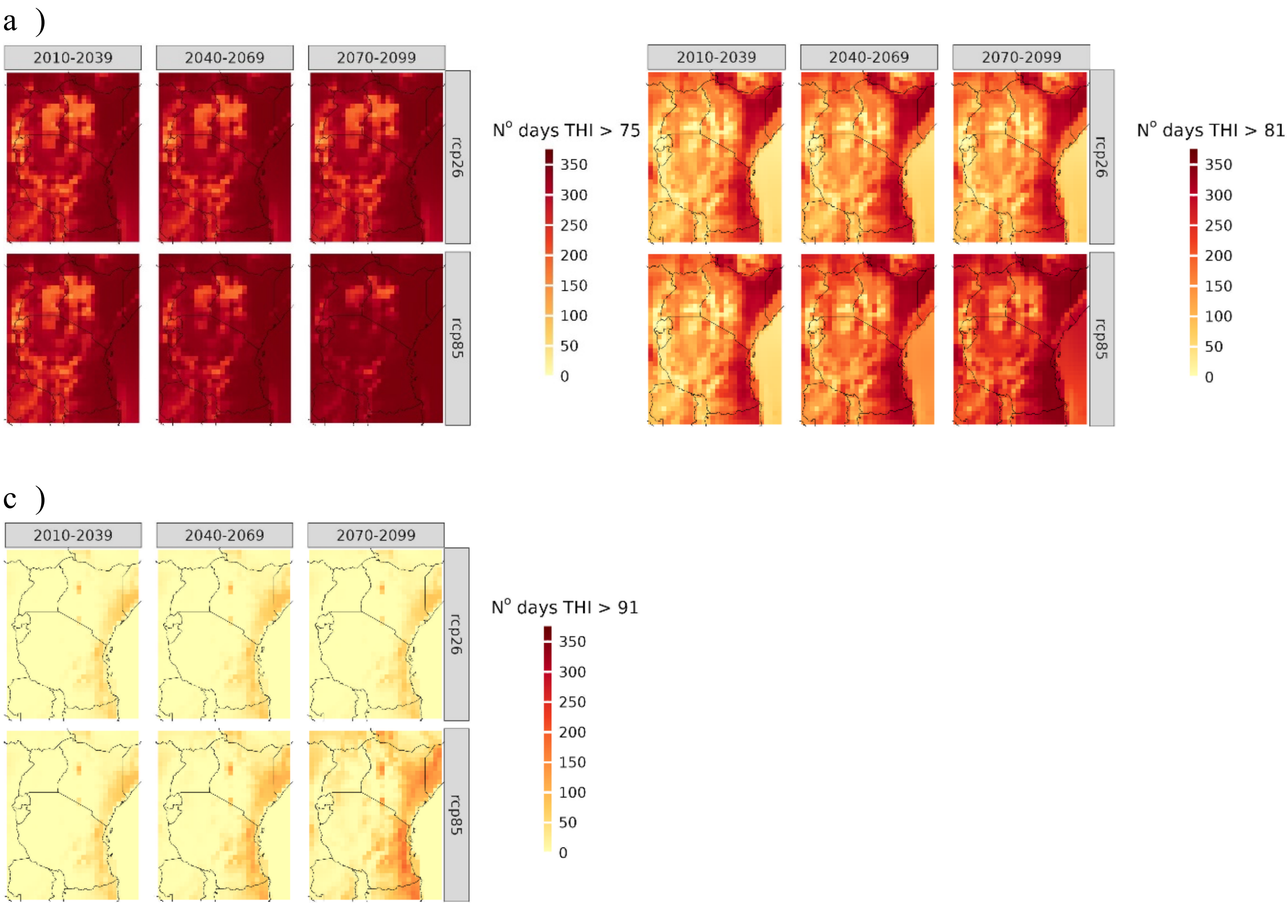

Figure 6. Change in the average count of days under (a) mild (THI >75), (b) moderate (THI >81), and (c) severe/danger (THI >91) heat stress over the century for RCPs 2.6 and 8.5 relative to 1976-2005. A black-dot represents a high GCM agreement in the climate change signal.

eastern areas of Tanzania milk yields have remained stable since 1980.

3.2.2. Future milk yield analysis

Future milk yield projections indicate strong GCM consensus regarding the impact of climate change. Under RCP 2.6, estimates suggest a slight loss of about 0.15 kg/day by 2070-2099 relative to 1976-2005 (Fig. 8). However, milk yield losses are intensified under RCP 8.5. For instance, along the Tanzanian coastline and northeastern parts of Kenya, milk yields are expected to decline by 0.30-0.45 kg/day by 2070-2099. Other areas in Uganda will see additional milk declines of about 0.15-0.25 kg/day by 2070-2099. Overall, Rwanda is the country that will experience the least declines in milk yields.

3.3. Effects of climate change on fodder resources

Fig. 9a illustrates the areas in East Africa with the highest potential to sustain maize yields under rain-fed conditions during the baseline period and across future timeframes (2031-2060 and 2061-2090). The highest yield potential during the baseline period is observed across the entirety of Rwanda, western Tanzania, the western and central regions of Uganda, and northwestern Kenya. Conversely, the eastern and southern parts of Tanzania and Kenya exhibit the lowest yield potential for maize in the baseline period. In the mid-term (2031-2060) and long-term (2061-2090), northern Kenya and Uganda are expected to experience the most significant changes in maize yields, with yield losses estimated at 5 to 10% under RCP 2.6 and 15 to 25% under RCP 8.5 by 2061-2090. On the other hand, in central, western, and eastern regions of Uganda, the entirety of Rwanda, and most of Tanzania (except for northern areas) maize yields are unaffected under both RCPs. Maize yield

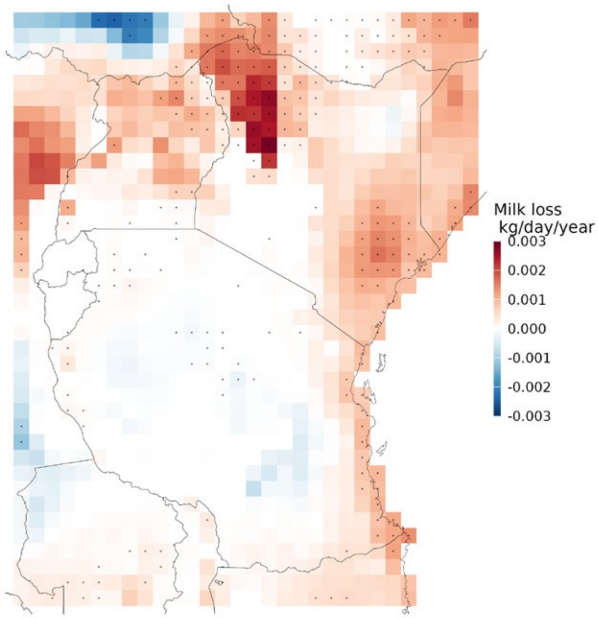

Figure 7. Annual-averaged daily milk losses (kg/day per year) for Boran over 1980-2009. Pixels with a black-dot show statistically significant differences (*p < 0.05*) over the historical period.

variations are primarily driven by changes in precipitation and temperature patterns, particularly pronounced under RCP 8.5 (results not shown for brevity).

Fig. 9b shows medium potential yield class for Napier grass in most parts of Uganda and Kenya in the baseline period, while high potential in Rwanda and southwestern Tanzania. Conversely, the eastern and northern parts of Tanzania are classified as low potential. Most areas are anticipated to experience yield declines ranging 0 to 10% in the mid-term (2031-2060) and further into the future (2061-2090) under RCP 2.6; except for southwestern Tanzania, which is expected to face minor yield losses. Under RCP 8.5, the most significant declines in Napier grass yields are anticipated in northern Uganda (30-35%), northern Kenya (30%), and southeastern Tanzania (20-30%).

Overall, livestock production systems in northern Kenya, which are predominantly extensive and heavily reliant on cultivated maize, may be at a higher risk compared to Rwanda, where maize yields are anticipated to remain unchanged. In northwestern Kenya and northern Uganda, animal feed shortages are likely to worsen due to a decline in Napier grass, primarily impacting the cut-and-carry fodder systems. Although southwestern Tanzania is not a livestock predominant area, the analysis shows rising yields for both maize and Napier grass, presenting a potential opportunity for enhancing livestock production systems across these areas.

4. DISCUSSION

4.1. Direct impacts on cattle

Heat stress is generally considered the most detrimental climate factor affecting cattle welfare and productivity (Carvajal et al. 2021; Rahimi et al. 2021; Thornton et al. 2021; Kadzere et al. 2002). Cattle exhibit various physiological responses to heat stress, including sweating, increased respiration rates, vasodilation that enhances blood flow to the skin's surface, elevated rectal temperature, reduced metabolic rate, decreased dry matter intake, lower feed utilization efficiency, and changes in water metabolism. Heat stress also negatively impacts reproduction, leading to diminished fertility and lower conception rates (Dovolou et al. 2023; Ahmad et al. 2018; Ganaie, 2013). Boran is recognized as one of the hardiest indigenous breeds for milk and meat production (Bayssa et al. 2021), whereas high-producing dairy cattle breeds are more susceptible to heat stress. Boran's ability to survive, produce, and reproduce under high ambient temperatures and water scarcity is attributed to a combination of morphological, physiological, biochemical, metabolic, cellular, and molecular adaptations (Bayssa et al. 2021). Some behavioral responses to climate stress observed in arid and semi-arid zones of East African rangelands is the reduction in feed intake and decreasing water excretion (Valente et al. 2015)

Our analysis indicates that Boran cattle is already experiencing some level (mild or moderate) of heat stress during the baseline period, except for high-altitude areas in the Great Rift Valley and the Buberuka Highlands in Rwanda, where heat stress is minimal (Fig. 3). These findings align with those of Rahimi et al. (2021), who reported a higher frequency of moderate THI stress across the four studied countries, excluding high-altitude regions in Kenya and Tanzania. Future climate scenarios suggest a widespread increase in moderate stress conditions, particularly by the end of the century and under RCP 8.5. The Tanzanian coastline is expected to experience severe/danger levels that could be fatal to animals (Figs. 5a, 6c), though these areas are not livestock predominant (Fig. 1). In contrast, northeastern and eastern Kenya, which are characterized by extensive livestock systems that rely on shrubland, are projected to see an increase in the annual average number of days with severe/danger (Fig. 6c) heat stress, particularly under RCP 8.5.

THI values are projected to rise by 1 to 2 units under RCP 2.6 and by 5 to 6 units under RCP 8.5. Bernabucci et al. (2010) noted a milk loss of 0.27 kg per day for each THI unit increase, highlighting the potential magnitude of milk losses in the region. Accord-

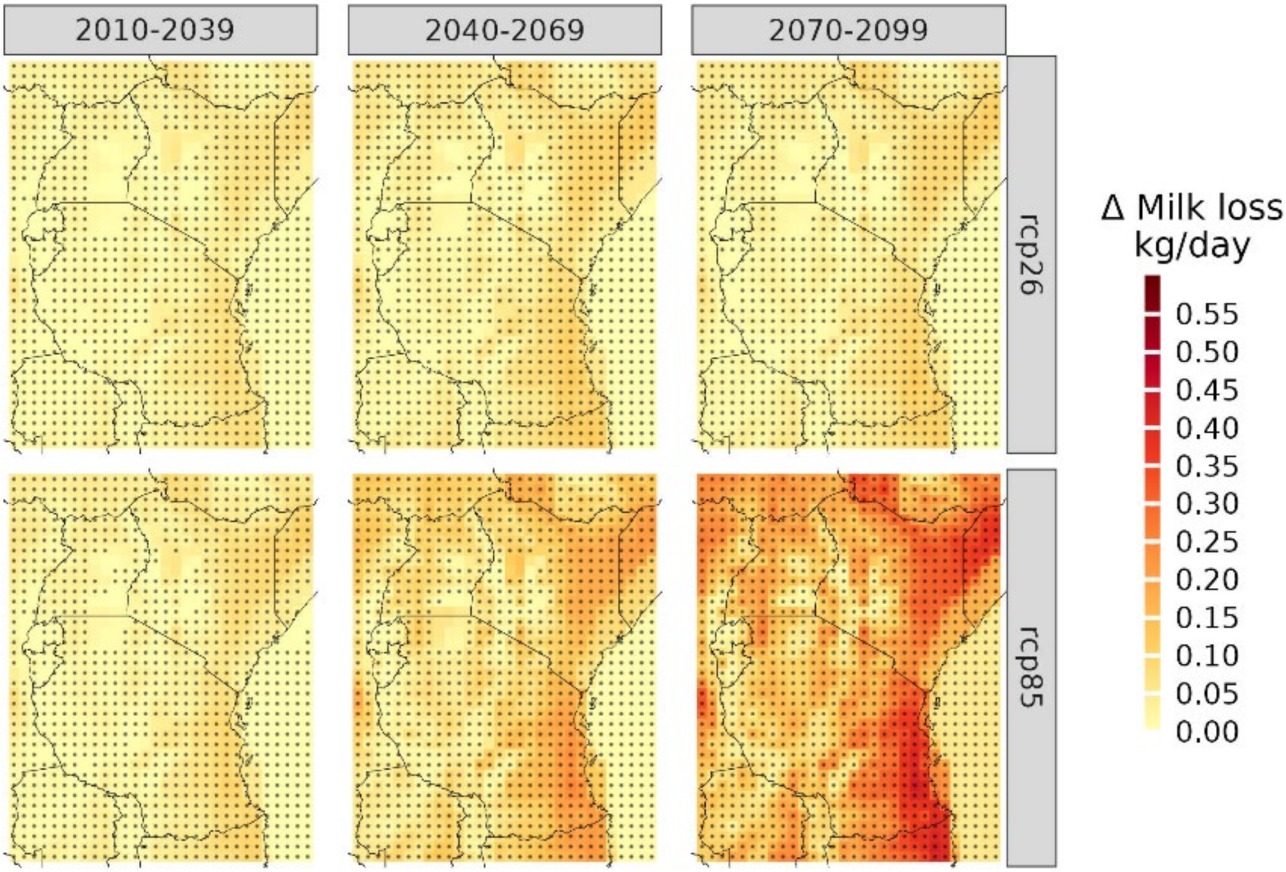

Figure 8. Projected daily average milk production losses (kg/day) for Boran breed over the century for RCPs 2.6 and 8.5. A black-dot represents a high GCM agreement in the climate change signal.

a)

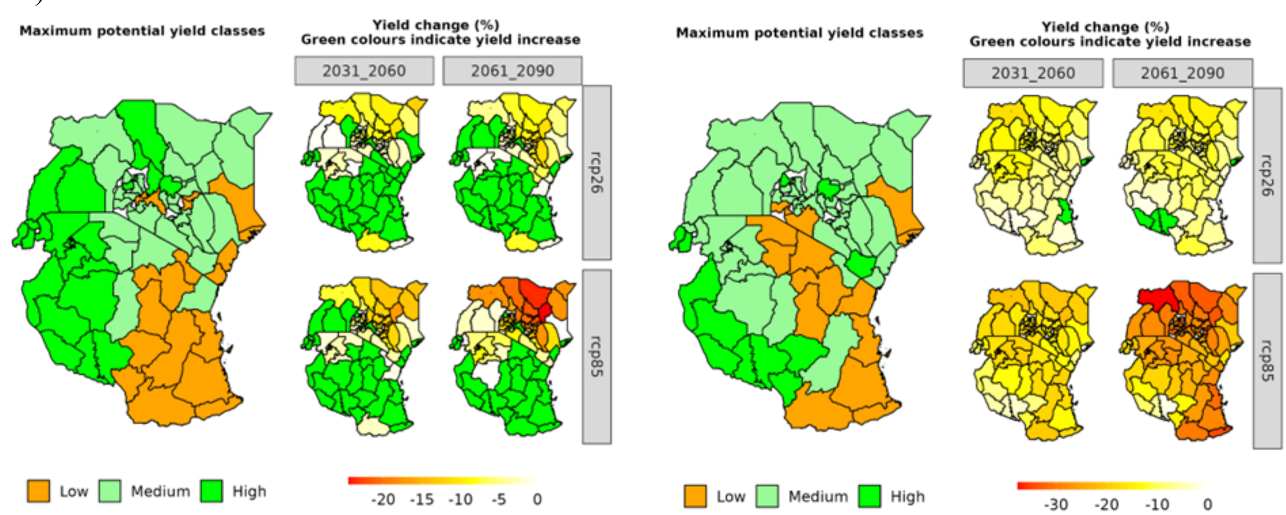

Figure 9. Maximum potential yield classes and yield change (%) for (a) maize and (b) Napier grass under rain-fed conditions over the century for RCPs 2.6 and 8.5. Yield results from different climate models are averaged (ensemble) for different time periods.

ing to Bernabucci et al. (2010) this is expected to result in an estimated milk production decline ranging from 0.54 to 1.62 kg/day. The latter per-unit THI loss rate was derived from high-producing Holstein cows and, as anticipated, exceeds our estimates (0.15-0.45 kg/day by 2070-2099) for the low-producing Boran breed, which shows lower absolute losses but potentially similar relative impacts on production capacity. The former represents a reduction of 4.5% to 14% for RCPs 2.6 and 8.5, respectively. Other regional studies (Rahimi et al. 2020) using three GCMs (GFDL-ESM2M, HadGEM2-ES, and MPI-ESM-MR) show milk production losses of 9%, 17%, and 35% under RCP 4.5 for the period 2071-2100 in West Africa.

4.2. Impacts on fodder supply

Feed shortage is a major constraint in dairy production systems in East Africa, leading to high milk production fluctuations due to pastoralists' dependence on precipitation for fodder production. Even during the wet season, there is not adequate fodder to be preserved and stored for use during the dry season (Ongadi et al. 2020). Climate-driven fluctuations in maize and Napier grass yields threaten consistent fodder supply, particularly for smallholders reliant on rain-fed systems. Additionally, reduced fodder quality (e.g. lower protein content in Napier grass) may decrease milk yields, especially for high-producing exotic breeds (Brychkova et al. 2022). Our findings on maize and Napier grass reveal even direr consequences for the dairy sector in East Africa, especially for extensive livestock production systems in the north of Uganda and Kenya. In these areas, smallholder dairy farms mostly rely on rain-fed production systems, though rainfall is erratic and sometimes inadequate.

The decline in maize yields is primarily driven by heat stress conditions reducing pollen viability, which subsequently affects kernel development (Lizaso et al. 2018). Additionally, water water deficit during the flowering and grain-filling stages can lead to significant yield penalties, particularly among non-drought-tolerant varieties (Sah et al. 2020). Stuch et al. (2021) estimate a decrease in maize yields of approximately 32% in East Africa between 1971-2000 and 2041-2070, with some exceptions in high-altitude areas where yields might increase as current cold related stress will diminish under future warmer conditions. Other regional studies, such as those conducted in Ethiopia, report declines in maize yields ranging from 24% to 43% in regions experiencing high rainfall variability and the greatest temperature increases (Abera et al. 2018). There are few studies addressing the impacts of climate change on forage grass species in East Africa; however, existing literature indicates that perennial C4 grasses may to benefit from rising ambient CO_2 levels (Brychkova et al. 2022). A study conducted in Ethiopia suggests that fodder demands of the dairy system could be met by the production of forage grasses under both current and future climate conditions. However, if land availability decreases and herd composition shifts towards higher-productivity exotic breeds, such as Holstein-Friesian, the forage resources may not be sufficient to meet cattle demand, even with improved agronomic management. Our findings contrast with those of Brychkova et al. (2022), likely because the PyAEZ model does not account for changes in atmospheric CO_2. PyAEZ predicts Napier grass yield losses of up to 10% under RCP 2.6 and between 20% and 30% under RCP 8.5 in northern Uganda and Kenya.

Overall, our study findings indicate a significant decrease in both maize and Napier grass yields along the Lake Turkana region in Kenya and in the Karamoja Drylands in Uganda. As cultivated fodder availability declines, livestock dependence on natural rangelands is likely to increase, intensifying grazing pressure in already fragile dryland ecosystems. In extensive livestock systems, this increased pressure often exceeds the regenerative capacity of native pastures, leading to reductions in perennial grass cover, increased bare soil exposure, and declining soil organic matter; key indicators of land degradation (Brychkova et al. 2022). These processes create a reinforcing feedback loop in which degraded rangelands further reduce forage availability, prompting wider herd movements and greater spatial concentration of grazing. Resulting feed shortages have already contributed to internal and cross-border competition over grazing and water resources among pastoral communities (Anno and Ameripus, 2022), a dynamic that is likely to intensify under projected climate change through increased rainfall variability and more frequent drought conditions.

4.3. Adaptation strategies

Effective adaptation to increasing heat stress in East African pastoral systems requires integrated strategies that operate at animal, herd, and rangeland levels and are aligned with local socio-ecological realities. Recent evidence from extensive livestock systems in East Africa indicates that relatively low-cost management interventions such as improved access to water, provision of shade (natural or artificial), and heat-aware grazing schedules can substantially reduce thermal load and productivity losses, making them economically feasible for pastoralists and smallholders with limited capital (Bashiru and Oseni, 2025). At the landscape scale, sustainable rangeland management practices, including controlled grazing, seasonal mobility, and restoration of degraded pastures, have shown to enhance forage availability, reduce land degradation, and strengthen ecosystem resilience under increasing climate variability (Njuguna, 2024).

Breed-based and system-level strategies are particularly important for long-term sustainability. The conservation and strategic use of heat-tolerant indigenous breeds, especially *Bos indicus* cattle, represent a cost-effective and climate-robust adaptation pathway compared with reliance on high-producing but heat-susceptible exotic breeds (Bashiru and Oseni, 2025). Complementary measures such as forage diversification, emergency feed reserves, and early warning systems that integrate climate and heat-stress indicators can further support anticipatory decision-making by policymakers and field operators (Njuguna, 2024). Indigenous adaptation practices, including seasonal herd mobility and local water-management strategies, remain central to sustaining livestock productivity in arid and semi-arid lands and should be strengthened rather than replaced by external interventions (Mungâ et al. 2019).

4.4. Uncertainties of this study and future research perspectives

Imprecise yield estimations are further exacerbated when simulating the impact of future climate on crop yields, particularly due to the use of inappropriate climate downscaling methods and a limited number of GCMs and RCMs. This study addresses these challenges by employing dynamic downscaling methods with RCMs, utilizing state-of-the-art reanalysis datasets (W5E5) for impact assessments, and selecting three GCMs with varying (high, medium, and moderate) equilibrium climate sensitivities. Furthermore, the causes of inaccurate yield gap estimations using top-down approaches, such as PyAEZ, have been thoroughly examined in literature (Alvar-Beltrán et al. 2023; Mourtzinis et al. 2017). Critical issues associated with these methods include reliance on secondary (unmeasured) gridded data, the coarse resolution of global soil maps, and insufficient ground data, which can result in inaccurate parameterization of cropping systems. These factors contribute to a misleading perception of data quality and availability in spatial grids. Additionally, since PyAEZ does not account for CO_2 fertilization, it may have led to an overestimation of yield losses.

THI is valuable because it provides a simple, actionable proxy for heat risk, but it is inherently an approximation – accurate assessment requires accounting for species, microclimate, physiology, and management. While the thermal categories for cattle are broadly recognized in literature, uncertainties emerge when evaluating the effects of heat stress on specific breeds, particularly heat-tolerant breeds like the Boran. Additionally, existing MDEC formulas lack correction factors tailored to individual cattle breeds, resulting in flexibility constraints that restrict their applicability.

Future research perspectives should focus on addressing the limitations of top-down approaches like PyAEZ through the incorporation of CO_2 fertilization effects on fodder resources. This will help improve future crop yield estimations. There is also a need for focused studies on the implications of heat stress on various cattle breeds, especially heat-tolerant breeds, to develop breed-specific correction factors for existing MDEC frameworks. This will allow for a quantitative assessment of the impact of THI stress on various cattle breeds, helping to identify those that are better suited for future climate conditions. Other heat-related factors such as accumulation of heat-load (balance of heat gained and lost by an animal during the day and night) could be further explored.

5. CONCLUSION

This research comprehensively evaluates the direct (animal welfare and production) and indirect (fodder availability) impacts of heat stress on the Boran breed, revealing the intricate repercussions faced by pastoral systems in East Africa. The escalating challenges to animal welfare and milk production, particularly in vulnerable pastoral regions, underscore a pressing need for intervention, except for certain areas in Rwanda and the high-altitude areas of Kenya and Tanzania. As critical issues such as livelihood loss, food insecurity, and conflicts over dwindling natural resources intensify in already food-insecure areas of northern Kenya and Uganda, our study illuminates current vulnerabilities and suggests adaptive solutions. Some of the actionable adaptation solutions (see also section 4.3) to modulate increasing heat stress conditions include: (i) livestock housing and climate-proofed processing plants; (ii) tree shelters in fields; (iii) animal bed and mattress cooling in barns; (iv) ventilation and evaporative cooling methods using fans and water misters/springs in barns; (v) timely and actionable agrometeorological services, including nearby suitable grazing areas and water points; (vi) heat index maps and transhumance corridors; (vii) risk transfer financial mechanisms; (viii) breeding heat-tolerant animal species; (ix) use of drought-tolerant crops and forages; and (x) dietary modifications, among many others.

Given the pivotal role of livestock research in supporting the livelihoods of dairy producers, agro-pastoralists, and farmers in mixed crop-livestock systems across East Africa, our work lays the foundation for future studies aimed at enhancing risk awareness. This study's strengths and limitations serve as both a benchmark and an invitation for further exploration into the impacts of climate change on other indigenous and improved exotic breeds across the region. Overall, the analysis provided here informs targeted investments in climate resilience and disaster risk management and empowers development agencies, research institutions, and national stakeholders to identify high-risk areas while evaluating the cost-effectiveness of implementing climate actions versus their anticipated benefits.

DECLARATION OF INTEREST STATEMENT

The authors declare that they have no known competing financial interests or personal relationships that could have appeared to influence the results reported in this research paper. The views expressed in this research paper are those of the author (s) and do not necessarily reflect the views of policies of FAO/IFAD.

ACKNOWLEDGEMENTS

The data collection and analysis was initiated during the design of a Programme led by the International Fund for Agricultural Development (IFAD) entitled "Dairy Interventions for Mitigation and Adaptation (DaIMA)" in Kenya, Rwanda, Uganda, and Tanzania submitted to the Green Climate Fund (GCF) and approved in July 2025 (https://www.greenclimate.fund/project/fp269). The authors recognize IFAD, FAO, GCF and the Global Dairy Platform (GDP) for committing funding for the overall Programme design process. The authors also recognize the invaluable support of Frans Goossens and Astrid Agostini (FAO) during the conceptualization of this work.

REFERENCES

Abera, K., Crespo, O., Seid, J. and Mequanent, F., 2018. Simulating the impact of climate change on maize production in Ethiopia, East Africa. Environmental Systems Research, 7(1), 1-12.

Ahmad, M., Bhatti, J.A., Abdullah, M., Javed, K., Ali, M., Rashid, G., Uddin, R., Badini, A.H. and Jehan, M., 2018. Effect of ambient management interventions on the production and physiological performance of lactating Sahiwal cattle during hot dry summer. *Tropical Animal Health and Production*, *50*, 1249-1254.

Akinsola, O.M., Musa, A.A., Muansangi, L., Singh, S.P., Mukherjee, S. and Mukherjee, A., 2024. Genomic insights into adaptation and inbreeding among Sub-Saharan African cattle from pastoral and agropastoral systems. Frontiers in Genetics, 15, 1430291.

Alvar-Beltrán, J., Soldan, R., Vanuytrecht, E., Heureux, A., Shrestha, N., Manzanas, R., Pant, K.P. and Franceschini, G., 2023. An FAO model comparison: Python Agroecological Zoning (PyAEZ) and AquaCrop to assess climate change impacts on crop yields in Nepal. Environmental Development, 47, 100882.

Anno, E.F. and Ameripus, M.E., 2022. Effects of internal and cross-border resource-based conflicts on livestock market performance in pastoral areas of Karamoja, Uganda and Turkana, Kenya. Am J Environ Resour Econ, 7, 87-96.

Bagath, M., Krishnan, G., Devaraj, C., Rashamol, V.P., Pragna, P., Lees, A.M. and Sejian, V., 2019. The impact of heat stress on the immune system in dairy cattle: A review. Research in veterinary science, 126, 94-102.

Bashiru, H.A. and Oseni, S.O., 2025. Simplified climate change adaptation strategies for livestock development in low-and middle-income countries. Frontiers in Sustainable Food Systems, 9, 1566194.

Bayssa, M., Yigrem, S., Betsha, S. and Tolera, A., 2021. Production, reproduction and some adaptation characteristics of Boran cattle breed under changing climate: A systematic review and meta-analysis. PloS one, 16(5), e0244836.

Beal, T., Gardner, C.D., Herrero, M., Iannotti, L.L., Merbold, L., Nordhagen, S. and Mottet, A., 2023. Friend or foe? The role of animal-source foods in healthy and environmentally sustainable diets. The Journal of nutrition, 153(2), 409-425.

Becker, C.A., Collier, R.J. and Stone, A.E., 2020. Invited review: Physiological and behavioral effects of heat stress in dairy cows. Journal of dairy science, 103(8), 6751-6770.

Bernabucci, U., Lacetera, N., Baumgard, L.H., Rhoads, R.P., Ronchi, B. and Nardone, A., 2010. Metabolic and hormonal acclimation to heat stress in domesticated ruminants. *Animal*, *4*(7), 1167-1183.

Berry, I.L., Shanklin, M.D. and Johnson, H.D., 1964. Dairy shelter design based on milk production decline as affected by temperature and humidity. *Transactions of the ASAE*, 7(3), 329-0331.

Brychkova, G., Kekae, K., McKeown, P.C., Hanson, J., Jones, C.S., Thornton, P. and Spillane, C., 2022. Climate change and land-use change impacts on future availability of forage grass species for Ethiopian dairy systems. Scientific Reports, 12(1), 20512.

Cartwright, S.L., Schmied, J., Karrow, N. and Mallard, B.A., 2023. Impact of heat stress on dairy cattle and selection strategies for thermotolerance: A review. Frontiers in veterinary science, 10, 1198697.

Carvajal, M.A., Alaniz, A.J., Gutiérrez-Gómez, C., Vergara, P.M., Sejian, V. and Bozinovic, F., 2021. Increasing importance of heat stress for cattle farming under future global climate scenarios. Science of The Total Environment, 801, 149661.

Clarke, L.E., 2007. *Scenarios of Greenhouse Gas Emissions and Atmospheric Concentrations: Report* (Vol. 2). US Climate Change Science Program.

Cossins, N.J. and Upton, M., 1988. The impact of climatic variation on the Borana pastoral system. Agricultural Systems, 27(2), 117-135.

Cucchi, M., Weedon, G.P., Amici, A., Bellouin, N., Lange, S., Müller Schmied, H., Hersbach, H. and Buontempo, C., 2020. WFDE5: bias-adjusted ERA5 reanalysis data for impact studies. *Earth System Science Data*, *12*(3), 2097-2120.

Dawson, I.K., Carsan, S., Franzel, S., Kindt, R., van Breugel, P., Graudal, L., Lillesø, J.P.B., Orwa, C. and Jamnadass, R., 2014. Agroforestry, livestock, fodder production and climate change adaptation and mitigation in East Africa: issues and options. World Agroforestry Center, Nairobi. Kenya.

Deshapriya, L., Thol, T., Gunasekara, K., Shrestha, R., Franceschini, G., Nachtergaele, F., Petri, M., and Damen, B., 2020. Python Package for Agro-ecological zoning (PyAEZ). GitHub repository. Available at: link

Dovolou, E., Giannoulis, T., Nanas, I. and Amiridis, G.S., 2023. Heat Stress: A Serious Disruptor of the Reproductive Physiology of Dairy Cows. Animals, 13(11), 1846.

Elguindi, N., Giorgi, F. and Turuncoglu, U., 2014. Assessment of CMIP5 global model simulations over the subset of CORDEX domains used in the Phase I CREMA. Climatic Change, 125(1), 7-21.

Ekine-Dzivenu, C.C., Mrode, R., Oyieng, E., Komwihangilo, D., Lyatuu, E., Msuta, G., Ojango, J.M. and Okeyo, A.M., 2020. Evaluating the impact of heat stress as measured by temperature-humidity index (THI) on test-day milk yield of small holder dairy cattle in a sub-Sahara African climate. Livestock science, 242, 104314.

Eugene, M., Ojok, L., Acai, J.O., Tukei, M. and Eugene, G.N., 2018. Prospects of Dairy Intensification and Commercialization in Eastern Province of Rwanda. Int J Anim Sci, 2(3), 1024.

FAO., 2023a. FAOSTAT. Crops and livestock products. Available online at: https://www.fao.org/faostat/en/#data/QCL

FAO., 2023b. Contribution of terrestrial animal source food to healthy diets for improved nutrition and health outcomes – An evidence and policy overview on the state of knowledge and gaps. Available online at: https://openknowledge.fao.org/server/api/core/bitstreams/0c1bfa99-18d4-42e4-b94f-27160126f826/content

FAO., 2022. Global Livestock Environmental Assessment Model (GLEAM) v.3 dashboard. Available online at: link

FAO and NZAGGRC., 2019a. Options for low emission development in the Tanzania dairy sector - reducing enteric methane for food security and livelihoods. Rome, Italy. Available online at: https://openknowledge.fao.org/server/api/core/bitstreams/8a3892bc-3daa-433e-9520-7ab86480dffd/content

FAO and NZAGGRC., 2019b. Options for low emission development in the Uganda dairy sector - reducing enteric methane for food security and livelihoods. Rome, Italy. Available online at: https://openknowledge.fao.org/server/api/core/bitstreams/fe65d8e4-9dca-4184-be89-f94f275512bb/content

FAO., 2018a. Africa Sustainable Livestock (ASL) 2050 Livestock and Environment Spotlight Kenya. Cattle and Poultry sectors. Nairobi, Kenya. Available online at: https://openknowledge.fao.org/server/api/core/bitstreams/c08cbc46-8987-4580-97cb-cb6cce290601/content

FAO and IIASA., 2000. Global Agro-Ecological Zones (GAEZ v1.0). CD-ROM Land and Water Media Series. Rome, Italy, Food and Agriculture Organization of the United Nations.

Fischer, G., Nachtergaele, F.O., van Velthuizen, H., Chiozza, F., Francheschini, G., Henry, M., Muchoney, D. and Tramberend, S., 2021. Global Agro-ecological Zones (GAEZ v4)-Model Documentation

Ganaie, A.H., Ghasura, R.S., Mir, N.A., Bumla, N.A., Sankar, G. and Wani, S.A., 2013. Biochemical and physiological changes during thermal stress in bovines: A review. Iranian Journal of Applied Animal Science, 3(3), 423-430.

Giannone, C., Bovo, M., Ceccarelli, M., Torreggiani, D. and Tassinari, P., 2023. Review of the heat stressinduced responses in dairy cattle. Animals, 13(22), 3451.

Gilbert, M., Nicolas, G., Cinardi, G., Van Boeckel, T.P., Vanwambeke, S.O., Wint, G.R. and Robinson, T.P., 2018. Global distribution data for cattle, buffaloes, horses, sheep, goats, pigs, chickens and ducks in 2010. Scientific data, 5(1), 1-11.

Giorgi, F., Coppola, E., Jacob, D., Teichmann, C., Abba Omar, S., Ashfaq, M., Ban, N., Bülow, K., Bukovsky, M., Buntemeyer, L. and Cavazos, T., 2022. The CORDEX-CORE EXP-I initiative: description and highlight results from the initial analysis. Bulletin of the American Meteorological Society, 103(2), E293-E310.

Giorgi, F., Coppola, E., Jacob, D., Teichmann, C., Abba Omar, S., Ashfaq, M., Ban, N., Bülow, K., Bukovsky, M., Buntemeyer, L. and Cavazos, T., 2021a. The CORDEX-CORE EXP-I initiative: description and highlight results from the initial analysis. *Bulletin of the American Meteorological Society*, 1-52.

Giorgi, F., Coppola, E., Teichmann, C. and Jacob, D., 2021b. Editorial for the CORDEX-CORE experiment I special issue. *Climate Dynamics*, *57*(5-6), 1265-1268.

Habiyaremye, N., Ouma, E.A., Mtimet, N. and Obare, G.A., 2021. A review of the evolution of dairy policies and regulations in Rwanda and its implications on inputs and services delivery. Frontiers in Veterinary Science, 8, 611298.

Hahn, G.L., Gaughan, J.B., Mader, T.L. and Eigenberg, R.A., 2009. Thermal indices and their applications for livestock environments. In *Livestock energetics and thermal environment management* (pp. 113-130). American Society of Agricultural and Biological Engineers.

Haile, A., 2011. Breeding strategy to improve Ethiopian Boran cattle for meat and milk production (Vol. 26). ILRI (aka ILCA and ILRAD).

Hammami, H., Bormann, J., M'hamdi, N., Montaldo, H.H. and Gengler, N., 2013. Evaluation of heat stress effects on production traits and somatic cell score of Holsteins in a temperate environment. Journal of dairy science, 96(3), 1844-1855.

Harris, I., Osborn, T.J., Jones, P. and Lister, D., 2020. Version 4 of the CRU TS monthly high-resolution gridded multivariate climate dataset. Scientific data, 7(1), 109.

Hunt, S., Eshete, G., Tadesse, M. and Eshetu, Z., 2019. Review of agricultural production systems in eastern Africa in relation to food and nutrition security and climate change.

Islam, M.R., Garcia, S.C., Islam, M.A., Bashar, M.K., Roy, A., Roy, B.K., Sarker, N.R. and Clark, C.E.F., 2024. Ruminant production from napier grass (Pennisetum purpureum Schum): A review. Animals, 14(3), 467.

Islam, M.R., Garcia, S.C., Sarker, N.R., Islam, M.A. and Clark, C.E., 2023. Napier grass (Pennisetum purpureum Schum) management strategies for dairy and meat production in the tropics and subtropics: yield and nutritive value. Frontiers in Plant Science, 14, 1269976.

Jacob, D., Elizalde, A., Haensler, A., Hagemann, S., Kumar, P., Podzun, R., Rechid, D., Remedio, A.R., Saeed, F., Sieck, K. and Teichmann, C., 2012. Assessing the transferability of the regional climate model REMO to different coordinated regional climate downscaling experiment (CORDEX) regions. Atmosphere, 3(1), 181-199.

Kadzere, C.T., Murphy, M.R., Silanikove, N. and Maltz, E., 2002. Heat stress in lactating dairy cows: a review. Livestock production science, 77(1), 59-91.

Kambal, S., Tijjani, A., Ibrahim, S.A., Ahmed, M.K.A., Mwacharo, J.M. and Hanotte, O., 2023. Candidate signatures of positive selection for environmental adaptation in indigenous African cattle: A review. Animal genetics, 54(6), 689-708.

Kumar, G., Devi, P., Sharma, N. and Somagond, Y.M., 2020. Impact of thermal stress on milk production, composition and fatty acid profile in dairy cows: A review. J. Entomol. Zool. Stud, 8(5), 1278-1283.

Lizaso, J.I., Ruiz-Ramos, M., Rodríguez, L., Gabaldon-Leal, C., Oliveira, J.A., Lorite, I.J., Sánchez, D., García, E. and Rodríguez, A., 2018. Impact of high temperatures in maize: Phenology and yield components. Field Crops Research, 216, 129-140.

Lokuruka, M.N., 2020. Food and nutrition security in East Africa (Kenya, Uganda and Tanzania): status, challenges and prospects. Food security in Africa.

Maleko, D., Msalya, G., Mwilawa, A., Pasape, L. and Mtei, K., 2018. Smallholder dairy cattle feeding technologies and practices in Tanzania: failures, successes, challenges and prospects for sustainability. International Journal of Agricultural Sustainability, 16(2), 201-213.

Marai, I.F.M., El-Darawany, A.A., Fadiel, A. and Abdel-Hafez, M.A.M., 2007. Physiological traits as affected by heat stress in sheep- a review. Small ruminant research, 71(1-3), 1-12.

McSweeney, C.F., Jones, R.G., Lee, R.W. and Rowell, D.P., 2015. Selecting CMIP5 GCMs for downscaling over multiple regions. Climate Dynamics, 44(11), 3237-3260.

Mourtzinis, S., Edreira, J.I.R., Conley, S.P. and Grassini, P., 2017. From grid to field: Assessing quality of gridded weather data for agricultural applications. European Journal of Agronomy, 82, 163-172.

Mungâ, H.G., Mbonile, M.J. and Maganga, F.P., 2019. Innovative pathways for enhancing climate change and variability resilience among agro-pastoral communities in semi-arid areas of Kiteto and Kilindi Districts, Tanzania. African Journal of Environmental Science and Technology, 13(5), 201-219.

Mwai, O., Hanotte, O., Kwon, Y.J. and Cho, S., 2015. African indigenous cattle: unique genetic resources in a rapidly changing world. *Asian-Australasian journal of animal sciences*, *28*(7), 911.

Nalianya, G.W., Wakhungu, J.W. and Nyandiko, N.O., 2020. Impacts of Climate Change and Variability on Smallholder Dairy Cattle Production in Bungoma, Kenya.

Nardone, A., Ronchi, B., Lacetera, N. and Bernabucci, U., 2006. Climatic effects on productive traits in livestock. Veterinary Research Communications, 30, 75.

NASA., 2023. NASA Earth Observatory. Deep Concern About Food Security in Eastern Africa. Available online at: link

Ngigi, M., Ahmed, M.A., Ehui, S. and Assefa, Y., 2010. Smallholder dairying in Eastern Africa. Successes in African Agriculture: Lessons for the Future, Johns Hopkins University Press, Baltimore MD, 209-61.

Njuguna, L., Biesbroek, R., Crane, T. and Tamás, P., 2024. Tracking climate change adaptation in Eastern Africa: integrating governmental and livestock keeper perspectives. Climate Policy, 24(4), 473-489.

Nyokabi, N.S., Luning, P.A., Phelan, J.E., Creemers, J., Lukuyu, B., Bebe, B.O. and Oosting, S.J., 2022. Intraannual variation in feed and milk composition in smallholder dairy farms in Kenya. NJAS: Impact in Agricultural and Life Sciences, 94(1), 137-155.

Ongadi, M., Mpolya, E., Gachuiri, C., Muyekho, F. and Lukuyu, A., 2020. Effects of season variation on water, feed, milk yield and reproductive performance of dairy cows in smallholder farms in eastern Africa.

Orodho, A.B., 2019. Intensive forage production for smallholder dairying in East Africa. In Grasslands (pp. 433-459). CRC Press.

Paul, B.K., Birnholz, C.A., Nzogela, B., Notenbaert, A.M.O., Herrero, M., Bwire, J., Groot, J.C. and Tittonell, P.A., 2021. Livestock feeding systems and feed gaps in East African smallholder farms.

Rahimi, J., Mutua, J.Y., Notenbaert, A.M., Marshall, K. and Butterbach-Bahl, K., 2021. Heat stress will detrimentally impact future livestock production in East Africa. Nature Food, 2(2), 88-96.

Rahimi, J., Mutua, J.Y., Notenbaert, A.M., Dieng, D. and Butterbach-Bahl, K., 2020. Will dairy cattle production in West Africa be challenged by heat stress in the future?. Climatic Change, 161(4), 665-685.

Rakib, M.R.H., Zhou, M., Xu, S., Liu, Y., Khan, M.A., Han, B. and Gao, J., 2020. Effect of heat stress on udder health of dairy cows. Journal of Dairy Research, 87(3), 315-321.

Renaudeau, D., Collin, A., Yahav, S., De Basilio, V., Gourdine, J.L. and Collier, R.J., 2012. Adaptation to hot climate and strategies to alleviate heat stress in livestock production. animal, 6(5), 707-728.

Riahi, K., Rao, S., Krey, V., Cho, C., Chirkov, V., Fischer, G., Kindermann, G., Nakicenovic, N. and Rafaj, P., 2011. RCP 8.5—A scenario of comparatively high greenhouse gas emissions. *Climatic change*, *109*, 33-57.

Robinson, T.P., Thornton, P.K., Franceschini, G., Kruska, R.L., Chiozza, F., Notenbaert, A., Cecchi, G., Herrero, M., Epprecht, M., Fritz, S. and You, L., 2011. Global livestock production systems. FAO and ILRI.

Rufino, M.C., Thornton, P.K., Mutie, I., Jones, P.G., Van Wijk, M.T. and Herrero, M., 2013. Transitions in agro-pastoralist systems of East Africa: impacts on food security and poverty. Agriculture, ecosystems & environment, 179, 215-230.

Sah, R.P., Chakraborty, M., Prasad, K., Pandit, M., Tudu, V.K., Chakravarty, M.K., Narayan, S.C., Rana, M. and Moharana, D., 2020. Impact of water deficit stress in maize: Phenology and yield components. Scientific reports, 10(1), 2944.

Schneider, U., Becker, A., Finger, P., Meyer-Christoffer, A. and Ziese, M., 2018. GPCC full data monthly product version 2018 at 0.25: monthly land-surface precipitation from rain-gauges built on GTS-based and historical data. Global Precipitation Climatology Centre.

Silva, C.F., Sartorelli, E.S., Castilho, A.C.S., Satrapa, R.A., Puelker, R.Z., Razza, E.M., Ticianelli, J.S., Eduardo, H.P., Loureiro, B. and Barros, C.M., 2013. Effects of heat stress on development, quality and survival of Bos indicus and Bos taurus embryos produced in vitro. Theriogenology, 79(2), 351-357.

Smith, D.L., Smith, T., Rude, B.J. and Ward, S.H., 2013. Comparison of the effects of heat stress on milk and component yields and somatic cell score in Holstein and Jersey cows. Journal of dairy science, 96(5), 3028-3033.

Stuch, B., Alcamo, J. and Schaldach, R., 2021. Projected climate change impacts on mean and year-to-year variability of yield of key smallholder crops in Sub-Saharan Africa. Climate and Development, 13(3), 268-282.

Tadesse, G. and Dereje, M., 2018. Impact of climate change on smallholder dairy production and coping mechanism in Sub-Saharan Africa-review. Climate Change, 4(15), 299-313.

Tao, S., Rivas, R.M.O., Marins, T.N., Chen, Y.C., Gao, J. and Bernard, J.K., 2020. Impact of heat stress on lactational performance of dairy cows. Theriogenology, 150, 437-444.

Thatcher, W.W., Flamenbaum, I., Block, J., and Bilby, T.R., 2010. Interrelationships of heat stress and reproduction in lactating dairy cows. In High plains dairy conference (pp. 45-60).

Thornton, P., Nelson, G., Mayberry, D. and Herrero, M., 2021. Increases in extreme heat stress in domesticated livestock species during the twenty-first century. Global Change Biology, 27(22), 5762-5772.

Trisos, C.H., I.O. Adelekan, E. Totin, A. Ayanlade, J. Efitre, A. Gemeda, K. Kalaba, C. Lennard, C. Masao, Y. Mgaya, G. Ngaruiya, D. Olago, N.P. Simpson, and S. Zakieldeen, 2022: Africa. In: Climate Change 2022: Impacts, Adaptation and Vulnerability. Contribution of Working Group II to the Sixth Assessment Report of the Intergovernmental Panel on Climate Change [H.-O. Pörtner, D.C. Roberts, M. Tignor, E.S. Poloczanska, K. Mintenbeck, A. Alegría, M. Craig, S. Langsdorf, S. Löschke, V. Möller, A. Okem, B. Rama (eds.)]. Cambridge University Press, Cambridge, UK and New York, NY, USA, pp. 1285–1455. https:doi.org/10.1017/9781009325844.011

Valente, É.E.L., Chizzotti, M.L., de Oliveira, C.V.R., Galvão, M.C., Domingues, S.S., de Castro Rodrigues, A. and Ladeira, M.M., 2015. Intake, physiological parameters and behavior of Angus and Nellore bulls subjected to heat stress. Semina: Ciências Agrárias, 36(6 Suppl 2), 4565-4574.

Van Vuuren, D.P., Edmonds, J., Kainuma, M., Riahi, K., Thomson, A., Hibbard, K., Hurtt, G.C., Kram, T., Krey, V., Lamarque, J.F. and Masui, T., 2011. The representative concentration pathways: an overview. Climatic change, 109, 5-31.

Italian Journal of Agrometeorology
Rivista Italiana di Agrometeorologia

Firenze University Press
https://riviste.fupress.net/index.php/IJAm

OPEN ACCESS

Citation: Štrbanović, R., Šimić, B., Poštić, D., Tabaković, M., Mirjanić, D., Oro, V. & Stanisavljević, R. (2026). Relationship between agroclimatic conditions and seed quality and seedling growth of crimson clover. *Italian Journal of Agrometeorology* (1): 95-104. doi: 10.36253/ijam-3512

Received: May 29, 2025

Accepted: January 9, 2026

Published: September 15, 2026

Data Availability Statement: All relevant data are within the paper and its Supporting Information files.

Competing Interests: The Author(s) declare(s) no conflict of interest.

ORCID:
RŠ: 0000-0001-6803-7035
DP: 0000-0002-4704-8613
MT: 0000-0002-4478-9088
DM: 0009-0002-9002-0015
RS: 0000-0003-2210-193X
VO: 0000-0002-0270-2458

Relationship between agroclimatic conditions and seed quality and seedling growth of crimson clover

Ratibor Štrbanović[1,*], Branimir Šimić[2], Dobrivoj Poštić[1], Marijenka Tabaković[3], Danijela Mirjanić[4], Violeta Oro[1], Rade Stanisavljević[1,*]

[1] *Laboratory for testing the quality of seeds and planting material, Institute for Plant Protection and Environment, 11040 Belgrade, Serbia*
[2] *Department of Seed Production and Processing, Agricultural Institute Osijek, 31000 Osijek, Croatia*
[3] *Department of Agroecology and Cropping Practices, Maize Research Institute, Slobodana Bajića 1, 11185 Zemun Polje – Beograd, Serbia*
[4] *Institute of Agricultural Economics, Volgina 15, 11060 Belgrade, Serbia*
*Corresponding authors. Email: ratibor.strbanovic@yahoo.com; stanisavljevicrade@gmail.com

Abstract. This study investigated the relationship between seed quality parameters (germination, dormancy, initial shoot and root growth) of crimson clover originating from six locations in eastern Serbia and the agroclimatic conditions over a three-year period. The results indicate significantly higher seed germination rates at temperatures of 20°C and 25 °C compared to 15 °C. A positive and statistically significant ($p \leq 0.05$) to very strong ($p \leq 0.001$) correlation was observed between mean monthly temperatures in May and seed dormancy. In contrast, a significant negative ($p \leq 0.05$) to strong ($p \leq 0.01$) correlation was found between total monthly precipitation in May and seed germination. No statistically significant correlations were identified between mean monthly temperatures in March and April and any of the seed quality parameters or seedling growth traits. Similarly, no statistically significant correlation was found between total precipitation in March and April and seed quality indicators. In light of global warming predictions and rising temperatures, these findings underscore the importance of adopting agronomic practices, such as seed treatment, to mitigate dormancy and increase germinable seed rates.

Keywords: mean monthly air temperature, monthly precipitation sum, seed germination and dormancy, shoot and root growth.

HIGHLIGHTS

- A significant positive to very strong correlation ($p \leq 0.05$ to $p \leq 0.001$) was observed between mean temperatures in May and seed dormancy.
- A significant negative correlation ($p \leq 0.05$ to $p \leq 0.01$) was identified between total precipitation in May and seed germination.

– There was no statistically significant correlation between seed germination or dormancy and either mean monthly temperatures or total precipitation during March and April.

1. INTRODUCTION

The genus *Trifolium* comprises approximately 250 species (Zohari and Heller, 1984), though only a few hold significant economic value as forage crops. White clover (*Trifolium repens* L.) is among the most widely cultivated species of the genus *Trifolium*. It is the most extensively distributed pasture legume across the temperate regions of Europe, western Asia, and northwestern Africa (Deng et al., 2025). Red clover (*Trifolium pratense* L.), a species of Mediterranean origin, has become cosmopolitan and is well-adapted to a wide range of edaphoclimatic conditions (Greveniotis et al., 2025).

Red clover is commonly grown for silage and hay in many temperate regions (Zupanič et al., 2025), and it naturally occurs in grasslands and pastures throughout Europe, western Asia, and northwestern Africa (Egan et al., 2021; Petrović et al., 2014). Grasslands and pastures in the Republic of Serbia account for 28.7% of the total agricultural land (Statistical Office of the Republic of Serbia, 2023), highlighting considerable potential for enhancing forage production. Compared to white clover and red clover, crimson clover (*Trifolium incarnatum*) is considerably less widespread. However, in eastern Serbia, it accounts for approximately 10% of pasture areas (Aćić et al., 2013), and up to 14% of pastures near the towns of Knjaževac and Zaječar (Petrović et al., 2007; Bogosavljević et al., 2007). Crimson clover can be cultivated similarly to other forage legumes (e.g., alfalfa and red clover), and in some regions, it produces satisfactory yields and forage quality (Zamanian et al., 2024; Peker et al., 2020).

Compared to monoculture of forage grasses, legume–grass mixtures – whether in pastures or sown forage systems – have been shown to enhance biological nitrogen fixation (requiring minimal nitrogen fertilization), improve soil quality, and increase both yield and forage nutritive value, particularly through higher protein content (Folina et al., 2025; Tomić et al., 2025). However, Velijević et al. (2018) reported that *Trifolium pratense* exhibits suboptimal germination rates under standard conditions, relative to its optimal sowing requirements, indicating that pre-sowing seed treatment is recommended to enhance germination performance. Similar germination challenges have been reported for *T. repens* (Chu et al., 2022). In *T. incarnatum*, the primary issue is a high proportion of dormant seed (around 50%), which results in lower overall germination of about 35% (Štrbanović et al., 2025). However, appropriate treatments can raise germination to as much as 60% (Štrbanović et al., 2025). Seed germination is influenced not only by genetic factors (Wawo et al., 2024), but also by the environmental conditions prevailing during seed development on the maternal plant (Donohue, 2009). Therefore, temperature and water availability directly impact seed development and subsequent germination (Bailly & Gomez Roldan, 2023). For this reason, investigating seed quality as a response to climate conditions and climate change is a step toward understanding their effects and proposing new agronomic approaches that provide future solutions (Bailly & Gomez Roldan, 2023).

The ability of seeds to overcome dormancy and successfully germinate is critical for all plant species (Willis et al., 2014) and this ability is strongly influenced by agroclimatic factors (Finch-Savage and Bassel, 2016). Despite its importance, there is a lack of studies directly examining the correlation between climatic conditions and seed quality. Crimson clover is a valuable species in eastern Serbia and many other regions globally, yet its germination performance under varying environmental conditions remains underexplored. The aim of this study was to investigate the relationship between agroclimatic conditions and seed quality – specifically germination and seedling growth – of crimson clover over a three-year period across six locations in eastern Serbia.

2. MATERIALS AND METHODS

Plant material and meteorological data

Based on previous studies by Petrović et al. (2007) and Bogosavljević et al. (2007), as well as our own research conducted on natural meadows and pastures across six locations in eastern Serbia, the presence of crimson clover (*Trifolium incarnatum* L.) was confirmed and geographical coordinates were recorded using a GPS device.

Seed harvesting was carried out at the end of May or during the first days of June each year, during 2021-2023 growing seasons (Table 1). Seeds were collected when the stems and inflorescences had turned brown. Inflorescences were collected manually, seeds were extracted by hand, and then naturally dried until seed moisture dropped below 13%. Seeds from all locations (I- VI) were stored in paper bags under ambient conditions in a seed storage facility, as described by Stanisavljević et al. (2020).

Identification of *T. incarnatum* was based on morphological characteristics of the stems, leaves, and, particularly, the inflorescences and seeds. Meteorological conditions were monitored during March, April, and

Table 1. Geographic origin and collection time of *T. incarnatum* seeds.

Locations	Latitude (N)	Longitude (E)	m a.s.l	Collection time -Year		
				2021	2022	2023
I (Bor)	43°54'15''	22°51'03''	199	27. 05	21.05	25. 05
II (Zaječar)	43°59'11''	22°20'18''	108	30. 05	29. 05	27. 05
III (Boljevac)	43°59'41''	21°57'14''	270	02. 06	05.06	02. 06
IV (Negotin)	44°13'16''	22°25'04''	223	26. 05	29. 05	29. 06
V (Knjaževac)	43°39'31''	22°14'58''	246	28. 05	01.06	01. 06
VI (Kladovo)	44°38'47''	22°33'17''	48	02. 06	29. 05	28. 06

May of 2021, 2022, and 2023, at six locations, in eastern Serbia. The parameters included mean monthly air temperatures (Table 2) and total monthly precipitation (Table 3).

After 3 to 4 months – coinciding with the autumn sowing season and/or pasture overseeding in Serbian agroclimatic conditions – seed samples were subjected to quality assessments and seedling growth testing.

Seed quality evaluation

Germinated seeds (GS) and **Dormant seeds (DS).** The experimental design comprised 450 seeds, arranged as 50 seeds per replication across three replications for each of three temperature regimes per each location and each year. Germinated and dormant seeds were assessed on the seventh day after placement in germination chambers, under dark conditions at 20 °C, in accordance with ISTA rules (ISTA, 2020). In addition to testing at 20°C, we also tested GS and DS seeds at 15°C and 25°C, to test the correlation between temperature and seed quality parameters.

When seed viability could not be clearly determined, a tetrazolium test was applied, which relies on the activity of certain dehydrogenase enzymes and indirectly

Table 2. Mean monthly air temperatures (T °C) during three years for months, March, April, and May.

Year	Month	Locations (I – VI)						$\bar{X}$	Min.	Max.	CV %
		I	II	III	IV	V	VI				
2021	March	6.2	4.8	3.6	5.6	3.9	5.1	4.9	3.6	6.2	20.37
	April	10.3	9.2	8.2	10.2	8.5	11.2	9.6	8.2	11.2	12.09
	May	15.3	16.1	15.6	17.6	15.9	18.3	16.5	15.3	18.3	7.29
2022	March	4.9	3.7	3.1	5.8	3.6	6.3	4.6	3.1	6.3	28.51
	April	11.4	11.8	11.2	12.2	11.8	13.2	11.9	11.2	13.2	5.96
	May	16.1	17.6	16.4	19.1	17.2	20.3	17.8	16.1	20.3	9.31
2023	March	8.3	8.8	8.1	7.6	7.9	9.1	8.3	7.6	9.1	6.77
	April	10.4	11.4	10.6	10.2	10.8	12.3	11.0	10.2	12.3	7.12
	May	14.9	16.7	14.8	15.2	15.2	17.6	15.7	14.8	17.6	7.28
$\bar{X}$		10.9	11.1	10.2	11.5	10.5	12.6				

Table 3. Average rainfall (mm) during three years for months, March, April, May.

Year	Month	Locations (I – VI)						Σ	Min.	Max.	CV %
		I	II	III	IV	V	VI				
2021	March	69.3	38.8	62.3	49.8	61.2	55.3	337	38.8	69.3	19.16
	April	59.3	49.8	59.6	56.0	66.3	61.2	352	49.8	66.3	10.38
	May	77.1	34.5	57.8	27.4	56.3	59.9	313	27.4	77.1	34.88
2022	March	61.2	17.4	68.4	70.2	59.3	55.3	332	17.4	70.2	35.07
	April	48.4	33.3	51.2	33.7	52.2	41.6	260	33.3	52.2	19.62
	May	30.5	52.1	34.3	61.3	44.6	56.3	279	30.5	61.3	26.41
2023	March	51.3	29.8	88.3	99.8	48.6	68.6	386	29.8	99.8	40.85
	April	49.6	62.4	61.2	67.9	59.3	51.3	352	49.6	67.9	11.88
	May	72.5	42.1	99.3	41.3	44.6	43.3	343	41.3	99.3	41.67
Σ		519	360	582	507	492	493				

measures the ability of living seed tissues to breathe (França-Neto and Krzyzanowski 2022).

Seedling growth

Shoot and root length (in cm), was measured on the same day as germination. This is the first time when the differences in the seedling growth can be observed. Shoot length was measured from the base of the shoot/root junction till the tip of the longest leaf with a gradual scale and expressed in cm. Root length was measured from the base of the shoot/root junction till the tip of the longest root (Stanisavljević et al., 2020; https://www.tropicalgrasslands.info/index.php/tgft/article/view/639/395).

Statistical analysis

Following ANOVA, Tukey's multiple range test was used to evaluate the statistical significance of treatment effects. Data were subjected to arcsine transformation. Standard error of the mean (SEM) and coefficient of variation (CV%) were calculated to express data variability. Data analysis was conducted using Minitab software, version 16.1.0 (Minitab Inc., State College, Pennsylvania, USA; https://www.minitab.com/en-us/, accessed November 25, 2023), and the R statistical computing environment (R Core Team, 2018), freely available from the R Foundation for Statistical Computing, Vienna, Austria.

3. RESULTS

During the three study years, the influence of location on variability in average monthly temperature was highest in March 2022 and March 2021 (CV=28.51% and CV=20.37%, respectively), and lowest in April 2022 (CV=5.96%) (Table 1).

The highest variability in monthly precipitation by location was observed in May 2023 (CV=41.67%), followed by March 2023 (CV=40.85%), March 2022 (CV=35.07%), and May 2021 (CV=34.88%). The lowest variability was recorded in April 2021 (CV=10.38%) and April 2023 (CV=11.88%) (Table 2).

Table 4. Germination (GS) and dormancy (DS) of seeds among different locations (I-VI) at different temperatures during 2021–2023.

Year	Locations	GS in Temperatures °C				DS in Temperatures °C			
		15	20	25	$\bar{X}$	15	20	25	$\bar{X}$
2021	I	28±0.28 bB	31±0.42 bA	32±0.61 bA	30.3	49±0.55 bA	50±0.55 bA	50±0.69 bA	49.7
	II	32±0.48 aB	35±0.48 aA	35±0.78 aA	34.0	50±0.36 bA	51±0.32 abA	51±0.36 bA	50.7
	III	31±0.36 aB	35±0.66 aA	34±0.45 aA	33.3	49±0.69 bA	51±0.48 abA	50±0.29 bA	50.0
	IV	32±0.71 aB	35±0.41 aA	35±0.52 aA	34.0	52±0.31 aA	52±055 abA	51±0.81 bA	51.7
	V	31±0.56 aB	34±0.77 aA	35±0.39 aA	33.3	49±0.49 bA	50±0.67 bA	50±0.55 bA	49.7
	VI	30±0.39 abB	33±0.81 abA	33±0.63 abA	32.0	52±0.55 aA	53±0.37 aA	53±0.29 aA	52.7
$\bar{X}$		30.7	33.8	34.0		50.2	51.2	50.8	
2022	I	35±0.49 aA	36±0.66 aA	36±0.29 aA	35.7	52±0.62 bA	53±0.42 cA	52±0.46 dA	52.3
	II	30±0.52 bcB	33±0.31 bA	34±0.32 abA	32.3	53±0.21 bA	55±0.36 bA	54±0.55 cAB	54.0
	III	34±0.64 aB	36±0.46 aA	37±0.68 aA	35.7	53±0.48 bA	52±0.45 cA	52±0.31 dA	52.3
	IV	31±0.72 bcA	32±0.52abA	32±0.55 bA	31.7	56±0.61 aAB	57±0.33 aAB	58±0.29 aA	57.0
	V	31±0.39 bcA	32±0.19abB	34±0.41 abA	32.3	54±0.54 abA	55±0.62 bA	56±0.21 bA	55.0
	VI	28±0.63 cB	31±0.39 cA	31±0.72 bA	30.0	52±0.42 bB	53±0.51 bcAB	54±0.44 cB	53.0
$\bar{X}$		31.5	33.3	34.0		53.3	54.2	54.3	
2023	I	30±0.39 abB	33±0.62 aA	33±0.28 abA	32.0	52±0.69cA	53±0.19dA	53±0.51deA	52.7
	II	31±0.64 abB	33±0.29 aA	34±0.55 aA	32.7	53±0.55bcB	55±0.66cA	54±0.43dAB	54.0
	III	29±0.48 bB	31±0.52 bA	32±0.48 bA	30.7	53±0.31bcA	52±0.43dA	52±0.62eA	52.3
	IV	32±0.51 aB	34±0.60 aB	34±0.32 aB	33.3	56±0.71aB	57±0.52bAB	58±0.55bA	57.0
	V	30±0.30 abB	33±0.68 aB	33±0.39 abB	32.0	54±0.41bB	55±0.61cAB	56±0.31cB	55.0
	VI	31±0.72 abB	34±0.36 aB	33±0.44 abA	32.7	58±0.33aB	59±0.72aAB	60±0.41aB	59.0
$\bar{X}$		30.5	33.0	33.2		54.3	55.2	55.5	

Tukey's multiple range test: p≤ 0.05, small letters a, b, c for the column, capital letters A, B, C for the row.

Table 5. Correlation coefficients (r) between mean monthly air temperatures and seed quality of six locations at three different temperatures – *T. incarnatum*.

Year	Mean monthly air temperatures	GS			DS		
		15 °C	20 °C	25 °C	15 °C	20 °C	25 °C
2021	March	-0.480 ns	-0.599 ns	-0.607 ns	0.652 ns	0.568 ns	0.720 ns
	April	-0.400 ns	-0.527 ns	-0.531 ns	0.726 ns	0.619 ns	0.737 ns
	May	0.269 ns	0.163 ns	0.092 ns	0.965 **	0.931 **	0.893 *
2022	March	0.134 ns	0.154 ns	-0.027 ns	0.755 ns	0.787 ns	0.628 ns
	April	0.521 ns	0.515 ns	0.359 ns	0.612 ns	0.699 ns	0.430 ns
	May	0.621 ns	0.619 ns	0.455 ns	0.965 **	0.975 ***	0.855 *
2023	March	0.034 ns	0.162 ns	-0.003 ns	0.237 ns	0.333 ns	-0.111 ns
	April	0.711 ns	0.458 ns	0.548 ns	0.378 ns	0.367 ns	0.617 ns
	May	0.468 ns	0.534 ns	0.339 ns	0.880 *	0.869 *	0.825 *

* p≤0.05, **p≤0.01, ***p≤0.001, ns not signifcant (p≥0.05).

Table 6. Correlation coefficients (r) between monthly amount of rainfall (mm) and seed quality of six locations at three different temperatures – *T. incarnatum*.

Year	Monthly amount of rainfall mm	GS			DS		
		15 °C	20 °C	25 °C	15 °C	20 °C	25 °C
2021	March	-0.770 ns	-0.652 ns	-0.648 ns	-0.489 ns	-0.417 ns	-0.415 ns
	April	-0.383 ns	-0.340 ns	-0.221 ns	-0.234 ns	-0.183 ns	-0.127 ns
	May	-0.899*	-0.819*	-0.860*	-0.352 ns	-0.176 ns	0.021 ns
2022	March	-0.051 ns	-0.094 ns	0.043 ns	-0.367 ns	-0.630 ns	-0.470 ns
	April	-0.571 ns	-0.605 ns	-0.401 ns	-0.367 ns	-0.630 ns	-0.470 ns
	May	-0.853*	-0.883*	-0.918**	0.526 ns	0.698 ns	0.778 ns
2023	March	0.119 ns	-0.059 ns	-0.233 ns	0.417 ns	0.122 ns	0.245 ns
	April	0.341 ns	-0.084 ns	0.400 ns	0.012 ns	-0.005 ns	-0.014 ns
	May	-0.823*	-0.873*	-0.815*	-0.541 ns	-0.800 ns	-0.739 ns

* p≤0.05, **p≤0.01, ***p≤0.001, ns not signifcant (p≥0.05).

Seed testing from six locations across all years showed that all locations had significantly higher germination (p≤0.05) at 20 °C compared to 15 °C, while no significant difference was observed between germination at 20 °C and 25 °C (p≥0.05) (Table 4).

For seeds collected between 2021 and 2023, dormancy and germination were tested at 15 °C, 20 °C, and 25 °C. Correlation analysis between mean monthly temperatures and seed germination at these test temperatures revealed no significant relationships (p ≥ 0.05) for any of the three months across the six locations (Table 5). However, seed dormancy assessed at the same temperatures showed a significant positive correlation with May temperatures across all locations and years, (r=p ≤ 0.05 to p ≤ 0.001. In contrast, no significant correlation was observed between dormancy and mean temperatures in March or April (p ≥ 0.05) (Table 5).

Over the three-year period, no significant correlation was observed between precipitation in March and April and seed germination at 15 °C, 20 °C, or 25 °C. In contrast, May precipitation showed a significant negative correlation with seed germination at all three temperatures (p ≤ 0.05 to p ≤ 0.01). Additionally, no significant relationship was found between precipitation in March, April, or May and seed dormancy at any of the tested temperatures (Table 6).

Shoot and root growth. For all seeds locations and all years, shoot and root growth were significantly higher (p≤0.05) following germination at 20 °C and 25 °C compared to 15 °C, while no significant difference was observed between growth after germination at 20 °C and 25 °C (p≥0.05) (Table 7).

No statistically significant difference (p≥0.05) was found between the relationship (r) of root and shoot

Table 7. Stem and root growth (cm) of seeds in six locations under different meteorological conditions (2021–2023).

Year	Locations	Stem cm				Root cm			
		15 °C	20 °C	25 °C	$\bar{X}$	15 °C	20 °C	25 °C	$\bar{X}$
2021	I	1.995 bB	2.167 bA	2.195bA	2.119	1.312 baB	1.365 bA	1.378 bA	1.352
	II	2.119 aB	2.195 abA	2.199bA	2.171	1.469 abB	1.489 abA	1.499 abA	1.486
	III	2.045 abB	2.189 abA	2.231abA	2.155	1.357 abB	1.371 bA	1.382 bA	1.370
	IV	2.121 abB	2.269 aA	2.286 aA	2.225	1.403 abA	1.452 abA	1.468 abA	1.441
	V	2.192 aB	2.239 abA	2.256a bA	2.229	1.504 aB	1.558 aA	1.562 aA	1.541
	VI	2.028 abB	2.198 abA	2.218abA	2.148	1.338 bB	1.368 bA	1.372 abA	1.359
$\bar{X}$		2,083	2.210	2.231		1.397	1.434	1.444	
2022	I	1.812 bB	1.993 bA	2.005 bA	1.937	1.267 abB	1.298 abB	1.299 abB	1.288
	II	2.037 aB	2.189 abA	2.297 abA	2.174	1.305 aB	1.351 aA	1.362 aA	1.339
	III	1.969 abB	2.195 abA	2.221 abA	2.129	1.304 aB	1.349 aA	1.354 aA	1.336
	IV	2.004 aB	2.362 aA	2.484 aA	2.283	1.294 abB	1.339 abA	1.342 abA	1.325
	V	1.903 abB	2.165 abA	1.192 b A	1.753	1.217 bB	1.263 abA	1.264 abA	1.248
	VI	1.838 abB	1.997 bA	2.011abA	1.949	1.209 bB	1.245 bA	1.248 bA	1.234
$\bar{X}$		1,927	2.150	2.035		1.266	1.308	1.312	
2023	I	2.074abB	2.275abA	2.312abA	2.220	1.465aB	1.489aA	1.496aA	1.483
	II	2.019abB	2.246abA	2.251abA	2.172	1.448abB	1.472aA	1.478abA	1.466
	III	2.006bB	2.256abA	2.272abA	2.178	1.455abB	1.469abA	1.470abA	1.465
	IV	2.119aB	2.289abA	2.342aA	2.250	1.451abB	1.473abA	1.478abA	1.467
	V	1.999bB	2.214bA	2.224bA	2.146	1.405bB	1.431bA	1.433bA	1.423
	VI	2.102bB	2.298aA	2.311abA	2.237	1.396bB	1.461abA	1.468abA	1.442
$\bar{X}$		2.053	2.263	2.285		1.437	1.466	1.471	

Tukey's multiple range test: p≤ 0.05, small letters a, b, c for the column, capital letters A, B, C for the row.

Table 8. Correlation coefficients (r) between mean temperatures and seedling growth of six locations at three different temperatures.

Year	Mean monthly air temperatures	Stem cm			Root cm		
		15 °C	20 °C	25 °C	15 °C	20 °C	25 °C
2021	March	-0.421	-0.325	-0.069	-0.503	-0.392	-0.402
	April	0.090	0.117	0.282	-0.037	0.064	0.031
	May	-0.594	-0.694	-0.531	-0.546	-0.481	-0.507
2022	March	-0.367	0.105	-0.100	-0.179	-0.195	-0.248
	April	-0.556	-0.417	-0.681	-0.375	-0.382	-0.408
	May	0.403	0.442	0.278	-0.117	-0.061	-0.039
2023	March	0.465	0.517	0.622	0.135	0.137	0.088
	April	-0.123	-0.222	-0.071	0.244	-0.147	-0.194
	May	-0.355	-0.037	-0.023	0.517	0.341	0.259

* p≤0.05, **p≤0.01, ***p≤0.001, ns not signifcant (p≥0.05).

growth and the monthly temperatures in March, April, and May over the three-year period (Table 8). Similarly, no significant correlation (p≥0.05) was found between root and shoot growth and monthly precipitation in March, April, and May from 2021 to 2023 (Table 9).

4. DISCUSSION

Many analyses indicate that we are experiencing a period of increased and variable average temperatures and irregular precipitation, often with extreme events, which inevitably impact agricultural production (Alvar-Beltrán & Franceschini, 2024; Messeri et al., 2024).

Table 9. Correlation coefficients (r) between monthly amount of rainfall (mm) and seedling growth of six locations at three different temperatures.

Year	Monthly amount of rainfall mm	Stem cm			Root cm		
		15	20	25	15	20	25
2021	March	-0.549	-0.238	-0.361	-0.579	-0.499	-0.506
	April	-0.489	-0.174	-0.290	-0.545	-0.461	-0.464
	May	0.007	0.219	0.171	-0.119	-0.117	-0.129
2022	March	-0.390	-0.190	0.278	-0.376	-0.428	-0.434
	April	-0.226	-0.191	0.029	-0.595	-0.586	-0.564
	May	0.009	0.070	0.210	-0.396	-0.373	-0.353
2023	March	-0.463	-0.565	-0.720	-0.784	-0.757	-0.711
	April	0.071	0.193	-0.140	-0.695	-0.235	-0.170
	May	0.264	0.326	0.029	-0.586	-0.095	-0.018

* p≤0.05, **p≤0.01, ***p≤0.001, ns not signifcant (p≥0.05).

Our research confirms this, showing high variability in both mean monthly temperatures and precipitation during March, April, and May across all years (2021, 2022, 2023) and six locations in Eastern Serbia (Table 1).

According to Willis et al. (2014), varying percentages of seed dormancy occur depending on climatic conditions and plant species, driven by complex physiological and biochemical mechanisms.

Over centuries, humans have domesticated plants and improved many traits – such as reduced seed dormancy and increased germination – to better align crop establishment with agroecological conditions (Purugganan, 2019). However, in species where breeding has been less intensive, dormancy levels remain similar to those of their wild relatives (Wen et al., 2024).

In legumes, water-impermeable seed coats prevent germination even under favorable agroecological conditions (Rezaei-Manesh et al., 2023; Fu et al., 2024).

According to Baskin and Baskin (2004), seed dormancy can be physiological, morphological, morphophysiological, physical, or a combination thereof. However, in legumes, physical dormancy is most common due to impermeable seed coats. Penfield & MacGregor (2017) note that seed coat structure is highly variable and strongly influenced by the environment, affecting seed dormancy depending on the species. The mechanisms regulating these processes primarily maintain a dynamic balance between abscisic acid and gibberellins (Nambara et al., 2010).

Baill & Gomez Roldan (2023) highlight that the seed-filling stage is critical, involving synthesis, mobilization, and transport of proteins, carbohydrates, lipids, and other compounds. This process is highly sensitive to environmental changes, which can cause both qualitative and quantitative shifts in seed traits.

In physically dormant seeds, such as those of many legumes, the seed coat prevents water uptake, thereby inhibiting embryo development (Bolingue et al., 2010). This physical dormancy, characteristic of Fabaceae (Leguminosae) family members – especially forage crops from the *Trifolium* (Štrbanović et al., 2025; Rezaei-Manesh et al., 2023; Can et al., 2009) and *Medicago* (Wu et al., 2023; Xie et al., 2023; Renziet al., 2020; Galussi et al., 2013) genera – is well documented.

According to Pawłowski at al. (2020) the dormancy cycling phenomenon has been widely studied, but the molecular mechanism responsible remains largely unknown. Seed dormancy breaking and germination is a multifaceted process, associated with changes in the gene expression, protein synthesis, and physiology, but also with organelle functioning (Née et al., 2017).

Our findings for *T. incarnatum* suggest that higher temperatures increase the synthesis of water-impermeable compounds in the seed coat, directly raising the percentage of dormant seeds. This is supported by positive correlation coefficients between mean monthly temperatures and seed dormancy (p≤0.05 to p≤0.001) (Table 5).

In contrast, higher May precipitation negatively affects seed germination, as indicated by significant negative correlations between rainfall amounts and germination percentages (p≤0.05 to p≤0.01) (Table 6).

According to Bailly & Gomez Roldan (2023), temperature and water availability directly influence seed development and germination. Therefore, examining seed quality in response to climate change is a step toward recommending new cultivars and agronomic practices to address future challenges.

5. CONCLUSION

These findings suggest that early spring precipitation (March and April) does not significantly influence the germination or dormancy of crimson clover seeds under given temperature conditions, indicating a degree of resilience in seed physiological development during this period.

In contrast, during the later stages of development (seed filling and ripening in May), increased rainfall has a significant negative effect on seed germination. During this same period, higher temperatures lead to an increased proportion of dormant seeds.

From an agricultural perspective, these results underscore the importance of monitoring and managing precipitation patterns during the late reproductive phase of crimson clover. Furthermore, site selection for seed production should consider agroclimatic conditions, especially during the seed-filling and maturation stages (May), to minimize the risk of impact of precipitation on seed quality. If climate change leads to higher May temperatures, it is realistic to expect increased seed dormancy, highlighting the need to implement new pre-sowing technologies to improve germination and early seedling growth.

Further studies are warranted to identify and optimize seed treatment methods that effectively break dormancy and improve germination performance in crimson clover, thereby supporting more consistent establishment in field conditions.

ACKNOWLEDGMENT

This research was financially supported by the Ministry of Science, Technological Development and Innovation of the Republic of Serbia, Projects No. 451-03-136/2025-03/ 200010, 451-03-136/2025-03/200040, 451-03-136/2025-03/200009 and 1377/24

REFERENCES

Aćić S., Šilc U., Vrbničanin S., Cupać S., Topisirović G., Stavretović N., Dajić-Stevanović Z. 2013. Grassland communities of Stol mountain (eastern Serbia): Vegetation and environmental relationships. Archives of Biological Sciences, 65: 211–227.

Alvar-Beltrán J., Franc-eschini G. 2024. Effect of future climate on crop production in Bhutan. Italian Journal of Agrometeorology (2): 101–119. https://doi.org/10.36253/ijam-2782

Bailly C. Gomez Roldan M.V. 2023. Impact of climate perturbations on seeds and seed quality for global agriculture. Biochemical Journal, 480: 177–196.

Baskin J.M., Baskin C.C. 2004. A classification system for seed dormancy. Seed Science Research 14: 1–16.

Bogosavljević S., Zlatković B., Ranđelović V. 2007. Flora klisure Svrljiškog Timoka/Abstract in English, Flora of the Svrljiski Timok Gorge in Eastern Serbia. In Proceedings of the 9th Symposium on flora of Southeastern Serbia and Neighbouring Regions, Nis, Serbia, 1–3 September, 41–54.

Bolingue W., Vu B.L., Leprince O., Buitink J. 2010. Characterization of dormancy behaviour in seeds of the model legume Medicago truncatula. Seed Science Research 20: 97–107.

Can E., Çeliktaş N., Hatpoğlu R., Avci S. 2009. Breaking seed dormancy of some annual *Medicago* and *Trifolium* species by different treatments. Turkish Journal Field Crops, 14: 72–78.

Chu L., Gao Y., Chen L., McCullough P.E., Jespersen D., Sapkota S., Bagavathiannan M., Yu J. 2022. Impact of Environmental Factors on Seed Germination and Seedling Emergence of White Clover (*Trifolium repens* L.). Agronomy, 12: 190. https://doi.org/10.3390/agronomy12010190

Deng X., Wang X., Yang Y., Li, J.; Gao Y., Huang H., Zhang Y., Du J., Wang P. 2025. Global Research Trends and Hotspots in White Clover (*Trifolium repens* L.) Responses to Drought Stress (1990–2024). Sustainability, 17, 1883. https://doi.org/10.3390/su17051883

Donohue K. 2009. Completing the cycle: maternal effects as the missing link in plant life histories. Philosophical Transactions of the Royal Society B: Biological Sciences, 364: 1059–1074 https://doi.org/10.1098/rstb.2008.0291

Egan L.M., Hofmann R.W., Ghamkhar K., Hoyos-Villegas V. 2021. Prospects for *Trifolium* Improvement Through Germplasm Characterisation and Pre-breeding in New Zealand and Beyond. Frontiers in Plant Science, 16: 12:653191. https://doi.org/10.3389/fpls.2021.653191

Finch-Savage W.E., Bassel G.W. 2016. Seed vigour and crop establishment: extending performance beyond adaptation. Journal of Experimental Botany, 67: 567–591 https://doi.org/10.1093/jxb/erv490

Folina A., Stavropoulos P., Mavroeidis A., Roussis I., Kakabouki I., Tsiplakou E., Bilalis D. 2025. Optimizing Fodder Yield and Quality Through Grass–Legume Relay Intercropping in the Mediterranean Region. Plants, 14: 877. https://doi.org/10.3390/plants14060877

França-Neto J., Krzyzanowski F.C. 2022. Use of the tetrazolium test for estimating the physiological quality of seeds. Journal of Seed Science, 50: 31–44.

Fu Y., Ma L., Li J., Hou D., Zeng B., Zhang L., Liu C., Bi Q., Tan J., Yu X., Bi J., Luo L. 2024. Factors Influencing Seed Dormancy and Germination and Advances in Seed Priming Technology. Plants, 13: 1319.

Galussi A.A., Argüello J.A., Moya M.E., Zuriaga F.D., Zimmermann L.R. 2013. Seed dormancy mechanism as a factor influencing seed physiological quality in alfalfa (*Medicago sativa*) cv. Baralfa 85. Seed Science and Technology, 41, 1: 50–59.

Greveniotis V., Bouloumpasi E., Skendi A., Korkovelos A., Kantas D., Ipsilandis C.G. 2025. Evaluation and Stability of Red and White Trifolium Species for Nutritional Quality in a Mediterranean Environment. Agriculture, 15, 391. https://doi.org/10.3390/agriculture15040391

International Seed Testing Association (ISTA). Rules for Testing Seeds; ISTA: Zurich, Switzerland, 2020.

Messeri A., Arcidiaco L., Bianca E., Tiako D., Orlandini S., Messeri G., Mancini, M. 2024. Effects of air temperatures on acacia and chestnut honey yields: case study in Italy. Italian Journal of Agrometeorology (1): 49–58. https://doi.org/10.36253/ijam-2296

Nambara E., Okamoto M., Tatematsu K., Yano R., Seo M., Kamiya Y. 2010. Abscisic Acid and the Control of Seed Dormancy and Germination. Seed Science Research, 20: 55–67.

Née G., Xiang Y., Soppe W.J. 2017. The release of dormancy, a wake-up call for seeds to germinate. Current Opinion in Plant Biology, 35: 8–14.

Pawłowski T.A., Bujarska-Borkowska B., Suszka J., Tylkowski T., Chmielarz P., Klupczyńska E.A., Staszak A.M. 2020. Temperature Regulation of Primary and Secondary Seed Dormancy in *Rosa canina* L.: Findings from Proteomic Analysis. International Journal of Molecular Sciences, 21: 7008. https://doi.org/10.3390/ijms21197008

Peker C., Ozkan U., Tansi V., Sevimay C.S. 2020. Ef-fects of mixture ratios and sowing methods on for-age yields of crimson clover (*Trifolium incarnatum* L.) and Italian ryegrass *Lolium multiflorum*) mixture under Ankara conditions. Fresenius Environmental Bulletin, 29: 1534–1541.

Penfield S., MacGregor D.R. 2017. Effects of environmental variation during seed production on seed dormancy and germination. Journal of Experimental Botany, 4:819-825. https://doi.org/10.1093/jxb/erw436

Petrović M., Dajić-Stevanović. Z., Sokolović D., Radović J., Milenković J., Marković J. 2014. Study of red clover wild populations from the territory of serbia for the purpose of pre-selection. Genetika, 46: 471–484.

Petrović B., Ranđelović V.; Zlatković B. 2007. Flora i vegetacija Krupačkog Blata kod Pirota u istočnoj Srbiji/Abstract in English, Flora and vegetation of Krupačko Blato swamp in eastern Serbia. In Proceedings of the 9th Symposium on Flora of Southeastern Serbia and Neighbouring Regions, Niš, Serbia, 1–3 September, 63–72.

Purugganan M.D. 2019. Evolutionary insights into the nature of plant domestication. Current Biology, 29: R705–R714. https://doi.org/10.1016/j.cub.2019.05.053

Renzi J.P., Duchoslav M., Brus J., Hradilová I., Pechanec V., Václavek T., Machalová J., Hron K., Verdier J., Smýkal P. 2020. Physical Dormancy Release in *Medicago truncatula* Seeds Is Related to Environmental Variations. Plants, 9: 503. https://doi.org/10.3390/plants9040503

Rezaei-Manesh H., Ghaderi-Far F., Nosratti I., Siahmarguee A.B.S., Chauhan B.S. 2023. Seed dormancy and germination ecology of several clover species. Seed Science and Technology, 51: 329–353.

Statistical Office of the Republic of Serbia 2023. - Statistical year books.

Stanisavljević R., Poštić D., Štrbanović R., Tabaković M., Jovanović S., Milenković J., Đokić D., Terzić D. 2020. Effect of seed storage on seed germination and seedling quality of *Festulolium* in comparison with related forage grasses. Tropical Grasslands-Forrajes Tropicales, 8: 125–132.

Štrbanović R., Šimić B., Stanišić M., Poštić D., Trkulja N., Oro V., Stanisavljević R. 2025. Seed Quality and Seedling Growth After Applying Ecological Treatments to Crimson Clover Seeds. Plants, 14: 839. https://doi.org/10.3390/plants14060839

Tejlor N.L., Smit R.R. 1979. Red clover breeding and genetics. In: Advances in Agronomy. Academic Press. New York In press.

Tomić D., Stevović V., Đurović D., Marjanović M., Madić M., Pavlović N., Lazarević Đ., Petrovic M. 2025. Perennial forage legumes as an element of sustainable systems. Notulae Botanicae Horti Agrobotanici Cluj-Napoca, 51: 1–16 13240.

Velijević N., Simić A., Vučković S., Živanović L.J., Poštić D., Štrbanović R., Stanisavljević R. 2018. Influence of different pre-sowing treatments on seed dormancy breakdown, germination and vigour of red clover and Italian ryegrass. International Journal of Agriculture and Biology, 20: 1548–1554.

Wawo A., Lestari P., Setyowati N., Syarif F., Juhaeti T., Kartika K. 2024. The influence of tem perature on germination and seedling growth of sorghum. Italian Journal of Agrometeorology 1: 95-107. https://doi.org/10.36253/ijam-1828

Wen Z., Lu X., Wen J., Wang Z., Chai M. 2024. Physical Seed Dormancy in Legumes: Molecular Advances and Perspectives. Plants, 13: 1473.

Willis C.G., Baskin C.C., Baskin J.M., Auld J.R., Venable D.L., Cavender-Bares J., Donohue K., Rubio de Casas R., NESCent Germination Working Group (2014) The evolution of seed dormancy: environmental cues, evolutionary hubs, and diversification of the seed plants. New Phytologist 203: 300–309. https://doi.org/10.1111/nph.12782

Xie J., Li Y., Jiang G., Sun H., Liu X., Han L. 2023. Seed color represents salt resistance of alfalfa seeds (*Medicago sativa* L.): Based on the analysis of germination characteristics, seedling growth and seed traits. Frontiers in Plant Science, 16. https://doi.org/10.3389/fpls.2023.1104948

Zamanian M., Golzardi F., Gitari H., Nungula E., Salehi F., Heydarzadeh S. 2024. Enhancing forage nutritional value in Persian clover (*Trifolium resupinatum*) and crimson clover (*Trifolium incarnatum*) through intercropping and optimized seeding rate. Cogent Food & Agriculture, 10. https://doi.org/10.1080/23311932.2024.2410459

Zohary M., Heller D. 1984. The Genus *Trifolium*. Jerusalem: Israel Academy of Sciences and Humanities.

Zupanič M., Žnidaršič T., Podvršnik M., Sem V., Kristan B., Rihter L., Kramberger B. 2025. Yield and Silage Quality of Winter Legume Cover Crop Mixtures Without Nitrogen Fertilization in Spring. Plants, 14: 726. https://doi.org/10.3390/plants14050726

RIGOROUS PEER REVIEW

Each submission to IJAm is subject to a rigorous quality control and peer-review evaluation process before receiving a decision. The initial in-house quality control check deals with issues such as competing interests; ethical requirements for studies involving human participants or animals; financial disclosures; full compliance with IJAm's data availability policy, etc.

Submissions may be returned to authors for queries, and will not be seen by our Editorial Board or peer reviewers until they pass this quality control check.

Each paper is subjected to critical evaluation and review by Field Editors with specific expertise in the different areas of interest and by the members of the international Editorial Board.

OPEN ACCESS POLICY

The Italian Journal of Agrometeorology provides immediate open access to its content. Our publisher, Firenze University Press at the University of Florence, complies with the Budapest Open Access Initiative definition of Open Access: By “open access”, we mean the free availability on the public internet, the permission for all users to read, download, copy, distribute, print, search, or link to the full text of the articles, crawl them for indexing, pass them as data to software, or use them for any other lawful purpose, without financial, legal, or technical barriers other than those inseparable from gaining access to the internet itself. The only constraint on reproduction and distribution, and the only role for copyright in this domain is to guarantee the original authors with control over the integrity of their work and the right to be properly acknowledged and cited. We support a greater global exchange of knowledge by making the research published in our journal open to the public and reusable under the terms of a Creative Commons Attribution 4.0 International Public License (CC-BY-4.0). Furthermore, we encourage authors to post their pre-publication manuscript in institutional repositories or on their websites prior to and during the submission process and to post the Publisher’s final formatted PDF version after publication without embargo. These practices benefit authors with productive exchanges as well as earlier and greater citation of published work.

COPYRIGHT NOTICE

Authors who publish with IJAm agree to the following terms:

Authors retain the copyright and grant the journal right of first publication with the work simultaneously licensed under a Creative Commons Attribution 4.0 International Public License (CC-BY-4.0) that allows others to share the work with an acknowledgment of the work's authorship and initial publication in IJAm.

Authors are able to enter into separate, additional contractual arrangements for the non-exclusive distribution of the journal's published version of the work (e.g., post it to an institutional repository or publish it in a book), with an acknowledgment of its initial publication in this journal.

Authors are allowed and encouraged to post their work online (e.g., in institutional repositories or on their website) prior to and during the submission process, as it can lead to productive exchanges, as well as earlier and greater citation of published work (See The Effect of Open Access).

PUBLICATION FEES

Unlike many open-access journals, the Italian Journal of Agrometeorology does not charge any publication fee.

WAIVER INFORMATION

Fee waivers do not apply at Firenze University Press because our funding does not rely on author charges.

PUBLICATION ETHICS

Responsibilities of IJAm's editors, reviewers, and authors concerning publication ethics and publication malpractice are described in IJAm’s Guidelines on Publication Ethics.

CORRECTIONS AND RETRACTIONS

In accordance with the generally accepted standards of scholarly publishing, IJAm does not alter articles after publication: "Articles that have been published should remain extant, exact and unaltered to the maximum extent possible". In cases of serious errors or (suspected) misconduct IJAm publishes corrections and retractions (expressions of concern).

Corrections

In cases of serious errors that affect or significantly impair the reader’s understanding or evaluation of the article, IJAm publishes a correction note that is linked to the published article. The published article will be left unchanged.

Retractions

In accordance with the "Retraction Guidelines" by the Committee on Publication Ethics (COPE) IJAm will retract a published article if:

- there is clear evidence that the findings are unreliable, either as a result of misconduct (e.g. data fabrication) or honest error (e.g. miscalculation)
- the findings have previously been published elsewhere without proper crossreferencing, permission or justification (i.e. cases of redundant publication)
- it turns out to be an act of plagiarism
- it reports unethical research.
- An article is retracted by publishing a retraction notice that is linked to or replaces the retracted article. IJAm will make any effort to clearly identify a retracted article as such.

If an investigation is underway that might result in the retraction of an article IJAm may choose to alert readers by publishing an expression of concern.

ARCHIVING

IJAm and Firenze University Press are experimenting a National legal deposition and long-term digital preservation service.

SUBMITTING TO IJAm

Submissions to IJAm are made using FUP website. Registration and access are available at: https://riviste.fupress.net/index.php/IJAm/submission

For more information about the journal and guidance on how to submit, please see https://riviste.fupress.net/index.php/IJAm/index

Principal Contact
Simone Orlandini, University of Florence
simone.orlandini@unifi.it

Support Contact
Alessandro Pierno, Firenze University Press
alessandro.pierno@unifi.it

GUIDE FOR AUTHORS

1. Manuscript should refer to original researches, not yet published except in strictly preliminary form.
2. Articles of original researches findings are published in Italian Journal of Agrometeorology (IJAm), subsequent to critical review and approval by the Editorial Board. External referees could be engaged for particular topics.
3. Three types of paper can be submitted: original paper, review, technical note. Manuscript must be written in English. All pages and lines of the manuscript should be numbered.
4. First Name, Last Name, position, affiliation, mail address, telephone and fax number of all the Co-Authors are required. Corresponding Authors should be clearly identified.
5. The abstract should be no longer than 12 typed lines.
6. Full stop, not comma, must be used as decimal mark (e.g. 4.33 and not 4,33).
7. Figures, tables, graphs, photos and relative captions should be attached in separate files. All images must be vector or at least 300 effective ppi/dpi to ensure quality reproduction.
8. Captions should be written as: Fig. x – Caption title, Tab. x – Caption title. Images should be referred to in the text as (Fig. x), (Tab. x).
9. Proof of the paper (formatted according to the Journal style) will be sent to the Corresponding Author for proof reading just one time. Corrections can be made only to typographical errors.
10. All the references in the text must be reported in the “References” section and vice-versa. In the text, only the Author(s) last name must be present, without the name or the first letter of the name (e.g. “Rossi, 2003” and not “Federico Rossi, 2003” or “F. Rossi, 2003”). If two authors are present, refer to them as: “Bianchi and Rossi, 2003” in the text (do not use “&” between the surnames). If more than two Authors are present, refer to them as: “Bianchi et al., 2003” in the text.

For journals, references must be in the following form:

Bianchi R., Colombo B., Ferretti N., 2003. Title. Journal name, number: pages.

For books:

Bianchi R., Colombo B., Ferretti N., 2003. Book title. Publisher, publishing location, total number of pages pp.

Manuscripts “in press” can be cited.

BECOME A REVIEWER

Peer review is an integral part of the scholarly publishing process. By registering as a reviewer, you are supporting the academic community by providing constructive feedback on new research, helping to ensure both the quality and integrity of published work in your field. Once registered, you may be asked to undertake reviews of scholarly articles that match your research interests. Reviewers always have the option to decline an invitation to review and we take care not to overburden our reviewers with excessive requests.

You must login before you can become a reviewer.

If you don't want to be a reviewer anymore, you can change your roles by editing your profile.

COMPETING INTERESTS

You should not accept a review assignment if you have a potential competing interest, including the following:

- Prior or current collaborations with the author(s)
- You are a direct competitor
- You may have a known history of antipathy with the author(s)
- You might profit financially from the work

Please inform the editors or journal staff and recuse yourself if you feel that you are unable to offer an impartial review.

When submitting your review, you must indicate whether or not you have any competing interests.

Italian Journal of Agrometeorology
Rivista Italiana di Agrometeorologia

n. 1 – 2026

Table of contents